Université de Montréal

Plasticité du cortex visuel: « homéodynamie » des connexions neuronales et modèle d'effets d'antidépresseurs

par Lyes Bachatene

Département des Sciences Biologiques

Faculté des arts et sciences

Thèse présentée
en vue de l'obtention du grade de Doctorat (Ph.D)
en Sciences Biologiques
option Neurophysiologie

Décembre 2015

Université de Montréal
Faculté des études supérieures

Cette thèse intitulée :
Plasticité du cortex visuel: « homéodynamie » des connexions neuronales et modèle d'effets d'antidépresseurs

présentée par :
Lyes Bachatene

a été évaluée par un jury composé des personnes suivantes :

Dre. Sophie Breton, président-rapporteur
Dr. Stéphane Molotchnikoff, directeur de recherche
Dr. Jean Rouat, membre du jury
Dr. Johannes Frasnelli, examinateur externe

Résumé

Les informations sensorielles sont traitées dans le cortex par des réseaux de neurones co-activés qui forment des assemblées neuronales fonctionnelles. Le traitement visuel dans le cortex est régit par différents aspects des caractéristiques neuronales tels que l'aspect anatomique, électrophysiologique et moléculaire.

Au sein du cortex visuel primaire, les neurones sont sélectifs à divers attributs des stimuli tels que l'orientation, la direction, le mouvement et la fréquence spatiale. Chacun de ces attributs conduit à une activité de décharge maximale pour une population neuronale spécifique.

Les neurones du cortex visuel ont cependant la capacité de changer leur sélectivité en réponse à une exposition prolongée d'un stimulus approprié appelée apprentissage visuel ou adaptation visuelle à un stimulus non préférentiel.

De ce fait, l'objectif principal de cette thèse est d'investiguer les mécanismes neuronaux qui régissent le traitement visuel durant une plasticité induite par adaptation chez des animaux adultes. Ces mécanismes sont traités sous différents aspects : la connectivité neuronale, la sélectivité neuronale, les propriétés électrophysiologiques des neurones et les effets des drogues (sérotonine et fluoxétine). Le modèle testé se base sur les colonnes d'orientation du cortex visuel primaire.

La présente thèse est subdivisée en quatre principaux chapitres. Le premier chapitre (A) traite de la réorganisation du cortex visuel primaire suite à une plasticité induite par adaptation visuelle. Le second chapitre (B) examine la connectivité neuronale fonctionnelle en se basant sur des corrélations croisées entre paires neuronales ainsi que sur des corrélations d'activités

de populations neuronales. Le troisième chapitre (C) met en liaison les aspects cités précédemment (les effets de l'adaptation visuelle et la connectivité fonctionnelle) aux propriétés électrophysiologiques des neurones (deux classes de neurones sont traitées : les neurones à décharge régulière et les neurones à décharge rapide ou burst). Enfin, le dernier chapitre (D) a pour objectif l'étude de l'effet du couplage de l'adaptation visuelle à l'administration de certaines drogues, notamment la sérotonine et la fluoxétine (inhibiteur sélectif de recapture de la sérotonine).

Méthodes

En utilisant des enregistrements extracellulaires d'activités neuronales dans le cortex visuel primaire (V1) combinés à un processus d'imagerie cérébrale optique intrinsèque, nous enregistrons l'activité de décharge de populations neuronales et nous examinons l'activité de neurones individuels extraite des signaux multi-unitaires. L'analyse de l'activité cérébrale se base sur différents algorithmes : la distinction des propriétés électrophysiologiques des neurones se fait par calcul de l'intervalle de temps entre la vallée et le pic maximal du potentiel d'action (largeur du potentiel d'action), la sélectivité des neurones est basée sur leur taux de décharge à différents stimuli, et la connectivité fonctionnelle utilise des calculs de corrélations croisées. L'utilisation des drogues se fait par administration locale sur la surface du cortex (après une craniotomie et une durotomie).

Résultats et conclusions

Dans le premier chapitre, nous démontrons la capacité des neurones à modifier leur sélectivité après une période d'adaptation visuelle à un stimulus particulier, ces changements aboutissent à une réorganisation des cartes corticales suivant un patron spécifique. Nous attribuons ce

résultat à la flexibilité de groupes fonctionnels de neurones qui étaient longtemps considérés comme des unités anatomiques rigides. En effet, nous observons une restructuration extensive des domaines d'orientation dans le but de remodeler les colonnes d'orientation où chaque stimulus est représenté de façon égale. Ceci est d'autant plus confirmé dans le second chapitre où dans ce cas, les cartes de connectivité fonctionnelle sont investiguées. En accord avec les résultats énumérés précédemment, les cartes de connectivité montrent également une restructuration massive mais de façon intéressante, les neurones utilisent une stratégie de sommation afin de stabiliser leurs poids de connectivité totaux. Ces dynamiques de connectivité sont examinées dans le troisième chapitre en relation avec les propriétés électrophysiologiques des neurones. En effet, deux modes de décharge neuronale permettent la distinction entre deux classes neuronales. Leurs dynamiques de corrélations distinctes suggèrent que ces deux classes jouent des rôles clés différents dans l'encodage et l'intégration des stimuli visuels au sein d'une population neuronale.

Enfin, dans le dernier chapitre, l'adaptation visuelle est combinée avec l'administration de certaines substances, notamment la sérotonine (neurotransmetteur) et la fluoxétine (inhibiteur sélectif de recapture de la sérotonine). Ces deux substances produisent un effet similaire en facilitant l'acquisition des stimuli imposés par adaptation. Lorsqu'un stimulus non optimal est présenté en présence de l'une des deux substances, nous observons une augmentation du taux de décharge des neurones en présentant ce stimulus. Nous présentons un modèle neuronal basé sur cette recherche afin d'expliquer les fluctuations du taux de décharge neuronale en présence ou en absence des drogues.

Cette thèse présente de nouvelles perspectives quant à la compréhension de l'adaptation des neurones du cortex visuel primaire adulte dans le but de changer leur sélectivité dans un

environnement d'apprentissage. Nous montrons qu'il y a un parfait équilibre entre leurs habiletés plastiques et leur dynamique d'homéostasie.

Mots-clés : Cortex visuel, Plasticité, Adaptation, Neurones, Sérotonine, Fluoxétine, Connectivité, Corrélation.

Abstract

Sensory informations are computed in the cortex by networks of co-activated neurons forming functional ensembles. Visual processing in the cortex underlies several aspects of neuronal characteristics such as anatomical, electrophysiological and molecular.

In the primary visual cortex, neurons display selectivity for stimulus features such as orientation, motion direction and spatial frequency. Each stimulus property elicits a maximal firing rate of specific neuronal populations.

Visual neurons display transient modifications of their response properties following prolonged exposure to an appropriate stimulus using visual learning or visual adaptation to a non-preferred stimulus.

The main objective of this thesis is to investigate the neuronal mechanisms underlying the visual processing during adaptation-induced plasticity in adult animals. These mechanisms are examined through different aspects: the neuronal connectivity, the neuronal selectivity, the electrical properties of neurons, and the effects of drugs (serotonin and fluoxetine). The tested model is the orientation columns of the primary visual cortex.

The present thesis is divided into four main chapters. The first chapter (A) focuses on the cortical reorganization following visual adaptation. The second chapter (B) examines the neuronal connectivity using pair-wise correlations and populational correlations of neuronal activities. The third chapter (C) further relate the previous aspects, *i.e.* the adaptation effects and the functional connectivity to the properties of neurons (two classes: regular-spiking and

fast-spiking neurons). Finally, the fourth chapter (D) investigates the coupling of visual adaptation with the local administration of drugs (serotonin and fluoxetine).

Methodology

Using in vivo extracellular recordings of the neural activity in the primary visual cortex (V1) combined with intrinsic optical brain imaging, we record the spiking activity of neuronal populations and examine, from the multi-unit activity, the activity of individual neurons. The analysis of brain activity uses different algorithms: the electrophysiological distinctions between neurons are based on the trough-to-peak time of each spike (spike-width), the selectivity of neurons is based on the firing rate at different stimuli, and the functional connectivity uses a crosscorrelation computation. The usage of drugs is performed locally on the visual cortex (after craniotomy and removing of the dura).

Results and conclusions

In the first chapter, we demonstrate the ability of neurons to modify their selectivity to the presented stimuli following visual adaptation, exhibiting a well-organized reprogramming of the orientation columns; we attribute this result to a flexibility of functional units rather than rigid anatomical structures. Indeed, we observe an extensive restructuring of the complete orientation domain in order to refine the columnar organization where every stimulus is equally represented. This is further confirmed in the second chapter where in this case, the connectivity maps are investigated. In concordance with the previous results, the connectivity maps also exhibit restructuring but interestingly, neurons use a summative strategy to stabilize their total connectivity weights. These connectivity dynamics are examined in the third chapter in relation to electrophysiological properties of neurons. Indeed, two differently firing

modes dissociate between two classes of neurons. Their distinct correlation dynamics point to the fact that they play different key roles in stimulus encoding within a neuronal population. Finally, in the last chapter, visual adaptation is coupled with the administration of serotonin and fluoxetine. Both drugs produce similar effects by facilitating the acquisition of the imposed stimulus. The non-preferred stimulus when adapted with the presence of the drug results in an increased firing rate of neurons at this particular stimulus. We present a neuronal model based on our findings to explain the fluctuations of firing with and without the drug.

This thesis provides new insights into how visual neurons adapt to change their selectivity in the interplay between their plastic ability and their homeostatic dynamic.

Keywords : Visual cortex, Plasticity, Adaptation, Neurons, Serotonin, Fluoxetine, Connectivity, Correlation.

Table des matières

Liste des figures

Liste des abréviations

CGL : Corps genouillé latéral

ISRS : Inhibiteur sélectif de recapture de la sérotonine

V1 : Cortex visuel primaire

MT : Aire temporale médiane

GABA : Acide γ-aminobutyrique

BDNF : Brain-derived neurotrophic factor

LTP : Potentialisation à long terme

LTD : Dépression à long terme

E-I : Excitation-Inhibition

À mes grands-parents Ammi et Djeddis …

Remerciements

La présente thèse est le fruit d'un travail acharné mais aussi d'un grand soutien de la part de gens présents tout au long de ce chemin fastidieux ou croisés occasionnellement.

Je remercie grandement tous ceux qui y ont contribué d'une façon ou d'une autre :

- Mon directeur de thèse : Dr Stéphane Molotchnikoff qui m'a accueilli dans son laboratoire, m'a transmis l'amour des neurosciences à ma première visite du labo, et a parfaitement dirigé mes travaux de recherche. Une mention spéciale pour les cafés autour de discussions passionnantes.
- Dr Jean Rouat dont les conseils et l'enseignement ont été très précieux.
- Mon équipe de laboratoire : Vishal, Sarah, Nayan et Faustin avec qui j'ai beaucoup appris scientifiquement et culturellement.
- Le groupe de recherche NECOTIS qui a fortement contribué à mon enrichissement en neurosciences computationnelles.
- Un chaleureux remerciement à Louise Pelletier dont le sourire radieux et les délicieux gâteaux ont égayé mon parcours.
- Hélène Lavigne et Josée Letellier avec qui les travaux pratiques ont enrichi mon parcours académique.
- Dre Sophie Breton, qui m'a permis d'avoir ma première charge de cours et qui a décuplé mon amour pour l'enseignement.
- Dr Johannes Frasnelli dont les conseils sont toujours si précieux.
- Le personnel du département des Sciences Biologiques.
- Ma fille IRIS, ma femme Sarah, mon frère Chafik, mes parents Samia et Khaled, ma belle-famille : Idriss, Mélissa, Amine et Nadia et mes meilleurs amis Milad et Jessy (sans oublier leur petite princesse Anastasia) pour leur soutien inébranlable.

1. Introduction

La vision harmonieuse intègre des mécanismes complexes depuis la rétine jusqu'aux différentes aires visuelles du cortex. Le système visuel est un système déterminant pour l'interaction avec le monde extérieur en particulier pour les carnivores aux yeux frontalisés (chasse, fuite et mobilité). Des millions de neurones corticaux sont impliqués dans le processus visuel et sont programmés spécifiquement pour la perception. Les neurones du cortex visuel répondent essentiellement aux variations de luminance se produisant au sein de leurs champs récepteurs où chaque neurone décharge de façon maximale agissant ainsi comme un filtre pour les propriétés du stimulus comme l'orientation, le mouvement, la fréquence spatiale... (Hubel and Wiesel, 1959; Hubel and Wiesel, 1968; Movshon, 1975; Martinez et al., 2005; Bishop and Henry, 1972).

Les recherches fructueuses de Hubel et Wiesel sur le cortex visuel du chat (Hubel and Wiesel, 1959; Hubel and Wiesel, 1968; Hubel and Wiesel, 1962; Hubel and Wiesel, 1963a; Hubel and Wiesel, 1963b) ont été fondamentales pour la compréhension des aspects anatomiques et physiologiques de la sélectivité des neurones corticaux. De nombreuses études se sont ensuite penchées sur ce sujet pour différentes espèces animales dans le but d'expliquer les mécanismes régissant les propriétés neuronales des différents cortex cérébraux en général et du cortex visuel en particulier. Néanmoins, les processus de traitement des informations visuelles et leur complexité restent des sujets fortement investigués, car encore largement incompris.

Le système visuel s'organise durant une période post-natale particulière nommée « période critique » (Tanaka et al., 2009) caractérisée par une plasticité cérébrale prononcée. Les réseaux neuronaux se remodèlent et les connexions inter-neuronales se renforcent et se maintiennent

facilitant ainsi les phénomènes d'apprentissage. Dans les récentes recherches, il est admis que ces réseaux neuronaux se reforment même après la période critique à un âge adulte (Chiu and Weliki, 2003; Southwell et al., 2010), spécialement sous l'effet de l'expérience, de la mémoire, et de l'apprentissage. Cette plasticité cérébrale permet donc aux sujets de s'adapter aux conditions de stimulation et de moduler le renforcement des connexions synaptiques qui se détériorent après des lésions cérébrales ou suite à des atteintes mnésiques comme dans la plupart des maladies cognitives dégénératives (maladie d'Alzheimer, Parkinson...).

Deux méthodes sont le plus souvent explorées afin d'aboutir à une plasticité induite dans le cas du système visuel, la privation oculaire et l'apprentissage visuel (ou adaptation visuelle). Ce dernier consiste en l'application forcée d'un stimulus sensoriel non préférentiel à un groupe de neurones qui, après cet apprentissage, changent leur sélectivité par acquisition du stimulus imposé ou d'un nouvel autre stimulus. Il est à noter également que de nombreuses recherches ont montré qu'au niveau du cortex visuel, l'administration de médicaments spécifiques potentialise ce type de plasticité (Maya-vetencourt et al., 2008; Maya-vetencourt et al., 2011). Ces processus sont réalisables grâce à des propriétés neuronales remarquables, notamment la dynamique de connectivité entre les neurones. En effet, le cortex est organisé de telle manière que le regroupement des cellules forme des régions spécialisées, dans le cortex visuel primaire des mammifères. Ces régions sont appelées colonnes. Les neurones au sein de ces colonnes partagent des propriétés de sélectivité aux stimuli et forment des connexions synaptiques entre eux.

Les objectifs majeurs de cette thèse de doctorat sont de comprendre les mécanismes qui régissent la plasticité cérébrale du cortex visuel primaire du chat (dont le cortex visuel est organisé en colonnes) sous trois aspects : les changements de propriétés neuronales, la

dynamique de connectivité (modulation des forces de connexions fonctionnelles de neurones et de réseaux neuronaux) ainsi qu'un aspect neuropharmacologique en étudiant les effets de la sérotonine et de la fluoxétine (ISRS, inhibiteur sélectif de recapture de la sérotonine).

Cette thèse se divise en 4 chapitres principaux :

Chapitre A: Réorganisation corticale (Article connexe : article A).

Chapitre B: Connectivité neuronale (Articles connexes : article Bi et Bii).

Chapitre C: Propriétés électrophysiologiques des neurones (Articles connexes : article Ci et Cii).

Chapitre D: Effets des antidépresseurs (Article connexe : Article D).

Articles connexes :

Article A :
Bachatene et al. Reprogramming of orientation columns in visual cortex: a domino effect. *Nature Sci Rep.* 2015 Mar 24;5:9436. doi: 10.1038/srep09436.

Article Bi :
Bachatene et al. Modulation of functional connectivity following visual adaptation: homeostasis in V1. *Brain Res.* 2015 Jan 12;1594:136-53. doi: 10.1016/j.brainres.2014.10.054. Epub 2014 Oct 31.

Article Bii :
Bachatene et al. Summation of connectivity strengths in the visual cortex reveals stability of neuronal microcircuits after plasticity. *BMC Neurosci.* 2015 Oct 9;16(1):64. doi: 10.1186/s12868-015-0203-1.

Article Ci :
Bachatene et al. Adaptation-induced plasticity and spike waveforms in cat visual cortex. *Neuroreport.* 2012 Jan 25;23(2):88-92. doi: 10.1097/WNR.0b013e32834e7e71.

Article Cii :
Bachatene et al. Electrophysiological and firing properties of neurons: Categorizing soloists and choristers in primary visual cortex. *Neurosci Lett.* 2015 Sep 14;604:103-8. doi: 10.1016/j.neulet.2015.07.049. Epub 2015 Aug 3.

Article D :
Bachatene et al. Fluoxetine and serotonin facilitate attractive-adaptation-induced orientation plasticity in adult cat visual cortex. *Eur J Neurosci.* 2013 Jul;38(1):2065-77. doi: 10.1111/ejn.12206. Epub 2013 Apr 15.

Le **chapitre A** explore l'effet de l'apprentissage visuel (adaptation visuelle) sur la sélectivité à l'orientation des neurones du cortex visuel primaire chez le chat adulte, c'est-à-dire comment les neurones changent leurs réponses en fonction des stimuli imposés ?

Le **chapitre B** se penche sur la connectivité neuronale entre paires cellulaires dont la sélectivité est homogène, ainsi que celle de réseaux de neurones (assemblées). Il s'agit là d'explorer l'effet de l'apprentissage visuel sur la modulation de la dynamique de connectivité entre ces cellules corticales par des analyses de corrélation croisée.

Le **chapitre C** montre que grâce à des critères bien spécifiques de discrimination électrophysiologiques, les neurones à différents taux de décharge peuvent avoir des propriétés distinctes durant la plasticité. Ainsi, le couplage populationnel (corrélation de l'activité d'un neurone avec celle du groupe auquel il appartient) a été examiné dans cette section.

Le **chapitre D** s'intéresse aux aspects pharmacologiques de ce type de plasticité des neurones corticaux, en effet, l'action d'un neurotransmetteur (la sérotonine) et d'un agent antidépresseur (la fluoxétine ou Prozac) a été investiguée et un modèle neuronal a été proposé.

1.1 Organisation du système visuel

1.1.1 Mise en contexte

Les aires visuelles constituent environ 25% du cortex humain comprenant approximativement 5 milliards de neurones. Les nombreuses recherches sur le cortex visuel ont pu révéler beaucoup de ces aires de la vision notamment les aires V1, V2, V3, V4 et MT; les mieux connues en terme de structure, de topographie et de propriétés physiologiques (Kujovic et al., 2012; Felleman and Van Essen, 1991). Ces régions sont impliquées dans le traitement d'une multitude d'informations visuelles telles que la forme, la couleur, l'orientation, la taille, le mouvement ...etc, résultant des diverses voies visuelles. La surface corticale des mammifères évolués comme les singes, les chats ou les humains est généralement divisée en modules de sélectivité, à titre d'exemple le cortex visuel primaire est subdivisé en colonnes de sélectivité appelées « colonnes d'orientation » (Hubel and Wiesel, 1959; Hubel and Wiesel,1962). Dans une colonne la majorité des cellules sont optimalement sensibles à la même orientation. Beaucoup de caractéristiques du système visuel des mammifères semblent communes à plusieurs espèces (Kaschube et al., 2010; Tyler et al., 1998). Il faut néanmoins souligner que des animaux moins évolués tels que les rats ou les souris possèdent un système d'organisation nommé «sel et poivre» en dépit de l'organisation en colonnes citée précédemment (Ohki et al., 2005; Van Hooser, 2007). Les recherches sur des modèles animaux sont donc utilisées à grande échelle pour investiguer les aspects structurel et fonctionnel notamment dans le cortex sensoriel. En général, les singes, les chats et les souris sont fréquemment utilisés dans des expérimentations électrophysiologiques au niveau cortical (Casagrande et Xu, 2004).

1.1.2 De la rétine aux aires visuelles

1.1.2.1 Rétine

La perception visuelle commence au niveau rétinien où la lumière est transformée en signal électrique par des cascades biochimiques se produisant dans les cônes et bâtonnets, photorécepteurs de la rétine (Cowan and Drisko, 1976). La rétine est constituée de neurones représentant le premier niveau de traitement de l'image. En plus des photorécepteurs, il existe des neurones interconnectés et qui sont: les cellules bipolaires, les cellules horizontales, les cellules amacrines et les cellules ganglionnaires. Dans les années 1950, Stephen Kuffler a effectué des enregistrements de l'activité de neurones ganglionnaires rétiniens, il a notamment montré que les champs récepteurs (voir aussi la section des champs récepteurs corticaux) des cellules bipolaires et ganglionnaires étaient concentriques avec une organisation centre pourtour (ON / OFF ou l'inverse).

Il est important de souligner qu'au niveau du système visuel, il existe un principe appelé: la rétinotopie. Deux régions contiguës de l'espace visuel vont stimuler deux cellules proches dans la rétine qui à leur tour vont projeter sur deux cellules adjacentes dans une aire corticale visuelle après un transfert via le noyau thalamique : le corps genouillé latéral . Cela aboutit à des représentations ordonnées du champ visuel dans les aires corticales visuelles, sous forme de cartes rétinotopiques.

1.1.2.2 Corps genouillé latéral

Le corps genouillé latéral (CGL) est une structure thalamique composée de six couches (Gilbert and Wiesel, 1979) numérotées de 1 à 6 à partir des couches les plus ventrales, cette

structure reçoit les signaux visuels des cellules ganglionnaires rétiniennes. Il envoie des projections vers le cortex visuel primaire. En effet, les couches 1, 4, 6 du CGL reçoivent l'information de l'œil controlatéral et les couches 2, 3, 5, celles de l'œil ipsilatéral (voir codes couleurs bleu et vert de la Figure 1). Les propriétés des champs récepteurs des neurones du corps genouillé latéral sont concentriques (centre / pourtour ON et OFF) comme ceux des neurones ganglionnaires rétiniens (Purves et al., 2004). Fondamentalement il y a peu de différence dans l'organisation des champs récepteurs entre le niveau rétinien et thalamique.

1.1.2.3 Cortex visuel primaire

Les influx nerveux émanant du corps genouillé latéral convergent vers des neurones du cortex visuel primaire. Les connexions cortico-corticales et les afférences du CGL confèrent aux cortex visuel le traitement de propriétés spécifiques de l'image visuelle. D'ailleurs, les cellules corticales forment des modules groupés selon les propriétés optimales pour lesquelles elles codent, par exemple l'orientation ou la fréquence spatiale. Ce sont les deux prix Nobel, Hubel et Wiesel qui ont, en 1959, montré la sélectivité des neurones du cortex visuel primaire à des barres lumineuses orientées de façon spécifique lorsque celles-ci étaient présentées dans leurs champ récepteur (voir section « notion de champs récepteurs »). En outre, les afférences du CGL conduisant à des formes allongées des zones ON / OFF du champ récepteur des neurones corticaux (V1), donnait lieu à des neurones simples et complexes ; les neurones simples codent les influx provenant du CGL, ce codage se renforce avec le traitement des signaux provenant des neurones simples par les neurones complexes.

En plus de ce traitement hiérarchique et ce regroupement de neurones selon leurs afférences genouillées latérales, il a été découvert par les mêmes auteurs (Hubel et Wiesel) qu'il existait une sélectivité importante des neurones de V1 à l'orientation des stimuli visuels. En effet, si l'on insère une électrode de manière oblique dans le cortex, les réponses neuronales optimales vont varier de façon méthodique (environ 16.5 degrés pour chaque 0.09 mm de cortex).

Les expériences de Hubel et Wiesel ont donné lieu à la proposition de l'organisation des neurones corticaux en colonnes d'orientation, puis en hypercolonnes où tous les angles sont représentés (Hubel & Wiesel, 1974). Les techniques avancées en électrophysiologie et en imagerie optique intrinsèque montrent donc qu'il existe des cartes de sélectivité neuronale dans le cortex visuel primaire, ce qui sous-entend l'existence de cartes de connectivité étant donné que les connexions locales des neurones leur confèrent ce regroupement selon leur sélectivité. En effet, le cortex visuel primaire (V1) se compose en majorité de cellules pyramidales (excitatrices) et de cellules étoilées lisses qui sont des interneurones locaux inhibiteurs, ou à épines (interneurones excitateurs, voir aussi section «types neuronaux»). Le cortex est divisé en six couches neuronales suivant le type, la taille des neurones et la densité de leur regroupement. La couche IV, appelée couche granulaire interne, est constituée d'un regroupement dense de cellules granulaires épineuses et lisses qui reçoivent des projections du corps géniculé latéral. Les neurones de chaque couche du cortex visuel primaire établissent des connexions inter-laminaires surtout dans l'axe «vertical» (Purves et al., 2004).

Figure 1 - Organisation du système visuel, de la rétine au cortex. De gauche à droite : Rétine ; les couches de cellules rétiniennes et des photorécepteurs captant la lumière. Corps genouillé latéral ; comprenant six couches, les deux codes couleurs correspondent aux afférences des yeux (l'œil ipsilatéral et contralatéral). Cortex visuel primaire ou V1 ; se compose de couches de neurones, la couche IV reçoit les afférences du CGL et les transmet aux autres couches. Il existe dans le cortex visuel différents types neuronaux (on voit que dans la couche IV, il y a des neurones étoilés par exemple).

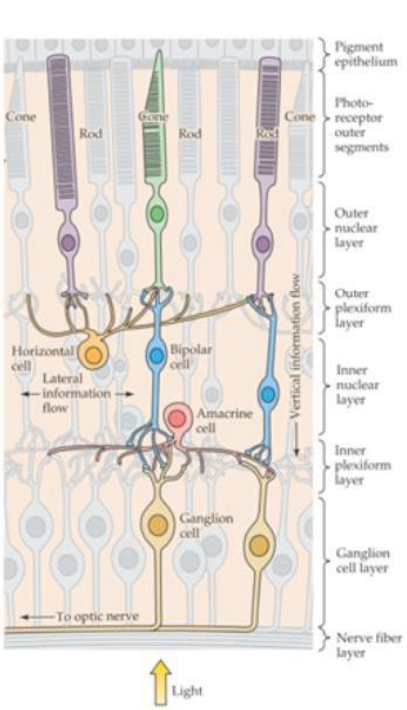

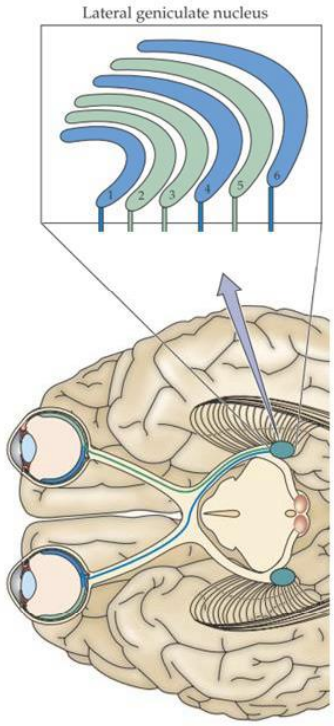

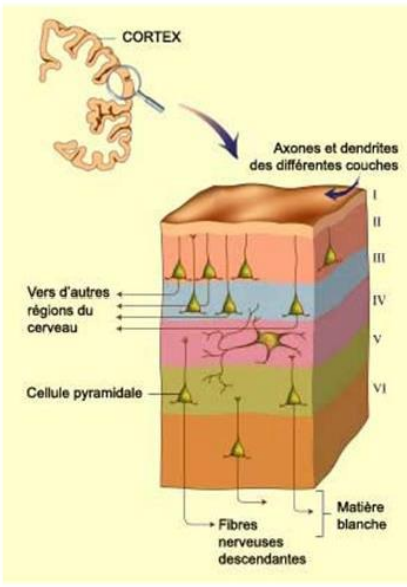

Adaptée de: Purves et al., 2004 et thebrain.mcgill.ca

1.1.2.4 Propriétés des neurones du cortex visuel : Sensibilité à l'orientation et colonnes de dominance oculaire

Au sein du cortex visuel primaire, il a été montré que certains neurones corticaux répondent fortement à des bords ou des barres de contraste, à condition qu'ils soient présentés dans le champ récepteur selon une orientation particulière. Chaque neurone est programmé à répondre à une «orientation optimale» pour laquelle son activité de décharge est maximale. Toutes les orientations d'un bord ou d'une barre sont représentées de façon à peu près égale dans le cortex. Les techniques d'études comme l'imagerie optique nous permettent aujourd'hui de construire des cartes corticales d'orientation (Figure 2), les « pinwheels » ou « moulinets » (le terme anglais pinwheel décrit le fait que les secteurs colorés semblent tourner autour d'un axe comme les ailes d'un moulinet) représentent les zones centrales où toutes les orientations se croisent (convergent). Ainsi, en enregistrant l'indice de sélectivité de neurones enregistrés de différentes régions de la carte corticale, cet indice varie de 0 à 1 selon que le neurone se trouve dans une zone d'iso-orientation (représentée par une couleur dans la carte corticale) ou un pinwheel (Figure 2).

Le cortex visuel primaire est caractérisé par un autre aspect d'organisation, la « dominance oculaire ». Ce terme désigne le fait que dans le cortex visuel primaire, l'hémisphère droit reçoit les signaux provenant du champ visuel gauche, captés par la rétine nasale de l'œil gauche et la rétine temporale de l'œil droit. Cette ségrégation des deux yeux s'observe dans le CGL, puisque les couches 1, 4, 6 du CGL reçoivent les axones de la rétine nasale controlatérale et

les couches 2, 3, 5 du CGL reçoivent les axones de la rétine temporale ipsilatérale (voir les projections bleues et vertes du CGL vers le cortex dans la Figure 1).

En effet, il a été démontré par l'injection au niveau d'un œil chez le singe d'un acide aminé radioactif que le cortex s'organise également en colonnes de dominance pour chaque œil notamment dans la couche IV (Purves et al., 2004).

Figure 2 - Carte de sélectivité à l'orientation et relation entre l'électrophysiologie et l'imagerie optique. A gauche et au milieu : fractions d'une carte (milieu) obtenue à partir de carte de sélectivité à l'orientation et les courbes de décharges (gaussiennes rouges) de neurones enregistrés de cette carte (points noirs). Les nombres à droite de chaque fraction correspondent aux indices de sélectivité à l'orientation de chaque neurone. A droite : courbe de décharge de population neuronale obtenue d'enregistrements électrophysiologiques. En bas est montrée la relation entre les résultats obtenus en imagerie optique et ceux obtenus en électrophysiologie, l'orientation optimale est sensiblement similaire dans les deux techniques.

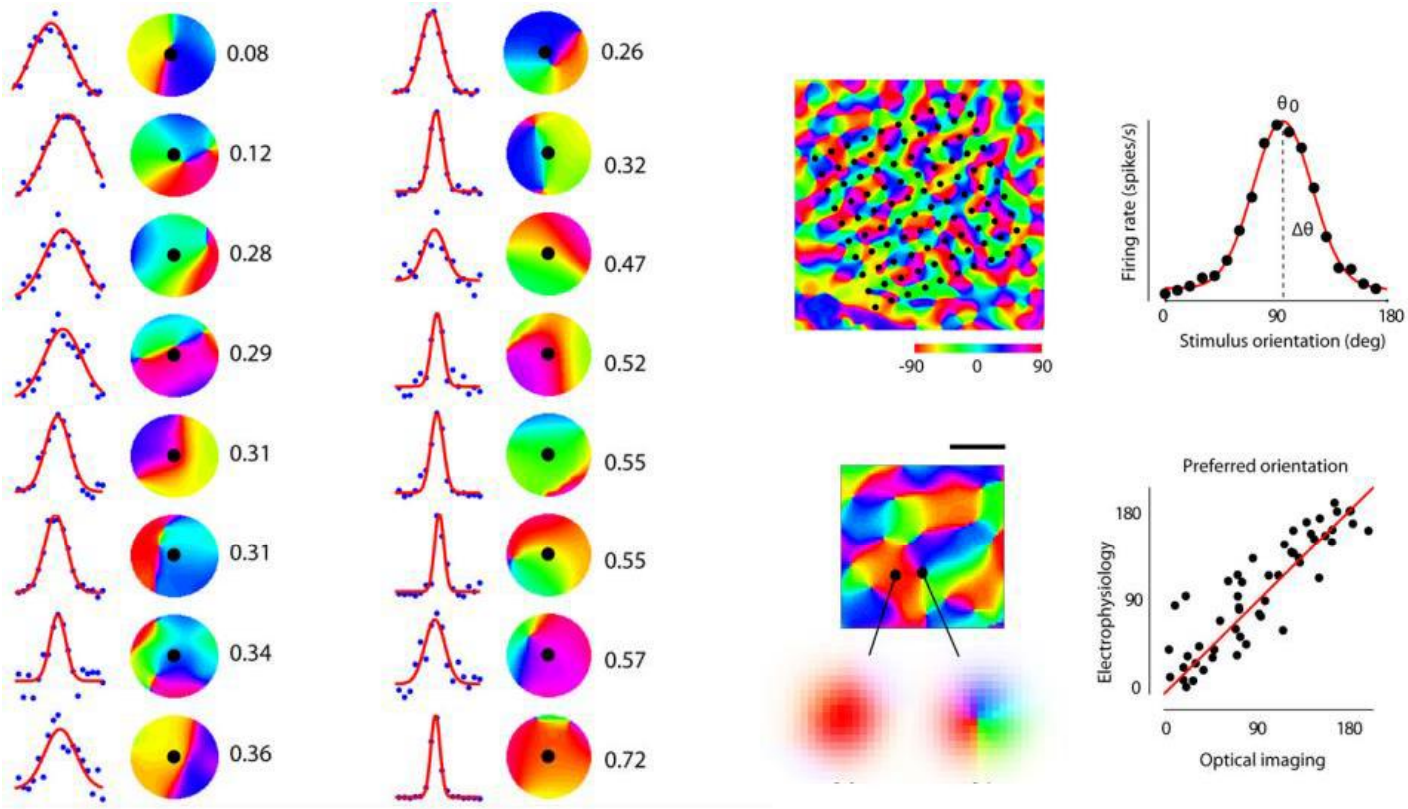

Adaptée de : Nauhaus et al., 2008

1.1.2.5 Aires visuelles associatives

En plus du cortex visuel primaire (aire V1), il existe de nombreuses aires visuelles extrastriées dont les fonctions sont cruciales dans le traitement visuel. Les neurones des aires visuelles V1 et V2 ont de petits champs récepteurs. Malgré la similitude des propriétés des neurones de V1 et V2 (Issa et al., 2000; Bonhoeffer and Grinvald, 1993), beaucoup de neurones de V2 répondent à des formes plus complexes. L'aire V3, détecte plus spécifiquement les formes des objets en mouvements (Braddick et al., 2001; Essen and Zeki, 1978). L'aire V4 contient les neurones traitant la couleur par exemple (Moran and Desimone, 1985). L'aire V5 (ou MT) est la région principale d'analyse du mouvement (Born and Bradley, 2005) (Figure 3). Ainsi, des projections neuronales peuvent être observées dans une aire corticale spécifique ou entre différentes aires.

Figure 3 - Aires visuelles associatives. Le cortex visuel primaire est représenté en vert. Les aires associatives reçoivent les afférences du cortex visuel primaire et traitent les images visuelles selon la propriété qu'elles codent. Ces aires ont un niveau de traitement plus global de l'information. Elles associent les signaux primaires pour faire émerger une représentation intégrée de l'image.

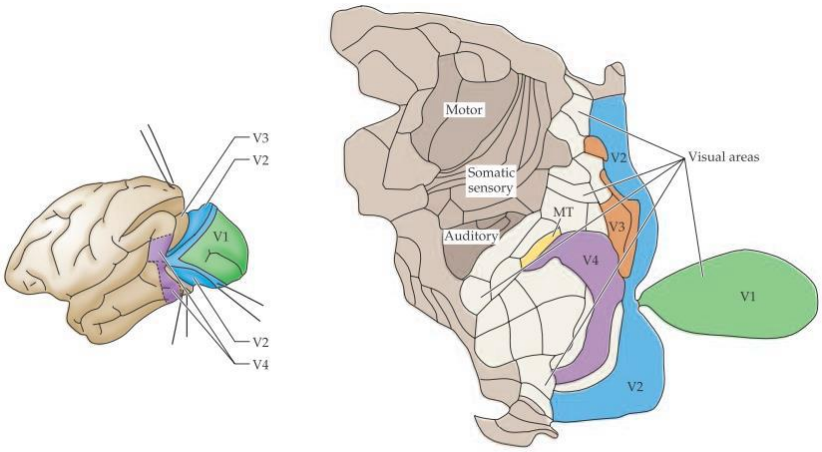

Purves et al., 2004

1.2 Notion de champs récepteurs

Les informations visuelles des cellules du CGL projettent vers les neurones récipients de la couche IV du cortex (V1), qui ont des champs récepteurs concentriques similaires à ceux des cellules du CGL. Les neurones de la couche IV projettent verticalement vers les autres couches corticales. Au niveau des couches II/III, les neurones possèdent une organisation différente des champs récepteurs. Au lieu d'être concentriques, les neurones ont tendance à répondre préférentiellement à des stimuli rappelant un rectangle tels des barres ayant des caractéristiques comme l'orientation, la fréquence spatiale, la direction, la longueur. Les neurones de ces couches sont classés en cellules simples, complexes et hypercomplexes selon les propriétés de leurs champs récepteurs.
Les cellules *simples* ont des champs récepteurs allongés. Elles répondent préférentiellement à des barres de lumière ayant une orientation spécifique.
Les cellules *complexes* ont des champs récepteurs plus larges et ne répondent que si un stimulus lumineux présente une orientation donnée et est en mouvement.
Les cellules *hypercomplexes* ne sont également sensibles qu'à des lignes en mouvement et de longueur bien limitée (Hubel and Wiesel, 1962; Gilbert and Wiesel, 1979).

1.3 Propriétés électrophysiologiques des potentiels d'action des neurones

Le cortex visuel se compose de six couches (nommées de 1 à 6) comprenant différents types neuronaux (Lin et al., 1979; Peters, 1984). Deux types majeurs de neurones sont généralement observés : les neurones pyramidaux et les interneurones, ces deux types sont

physiologiquement distincts. Chez la souris, les cellules pyramidales sont en général des neurones excitateurs qui projettent vers différentes régions cérébrales (González-Burgos, 2005; Povysheva et al., 2006), tandis que les cellules stellaires sont des neurones récipients des neurones relais du CGL, ce sont des cellules de nature inhibitrice en général mais il existe des interneurones locaux excitateurs (Markram et al., 2004). La couche IV du cortex contient de nombreux neurones stellaires.

De nombreux travaux de recherche ont démontré que les formes des spikes (potentiels d'action émis par les neurones) permettent la différenciation des deux types neuronaux (Bachatene et al., 2012; Ison et al., 2011, Wilson et al., 1994). D'un point de vue général, les cellules pyramidales déchargent de façon régulière en fonction du temps, la forme du spike est illustrée dans la Figure 4, tandis que les interneurones déchargent plus ou moins rapidement (appelés d'ailleurs fast spikes), la pente du potentiel d'action émis est abrupte (Figure 4) (Ison et al., 2011, Wilson et al., 1994) bien que chez le chat, ce paramètre (forme des potentiels d'action) n'est pas tout à fait valide car il existe des cellules pyramidales à décharge rapide (Nowak et al., 2003).

Figure 4 - Propriétés électrophysiologiques des neurones : formes des potentiels d'action. La forme des potentiels d'action émis donne lieu à une classification entre potentiels d'action à décharge régulière et potentiels d'action à décharge rapide. En haut à gauche : relation entre la forme du potentiel d'action et le cycle d'ondes gamma (Fries et al., 2007). En bas à gauche : superposition de neurones enregistrés de V1 chez le chat, la classification se fait selon la largeur du potentiel d'action sur l'échelle temporelle (Bachatene et al., 2012a). A droite : Relation entre la forme du potentiel d'action et le type neuronal. Les neurones pyramidaux ont un mode de décharge régulier alors que les interneurones ont un mode de décharge rapide (Bartho et al., 2004).

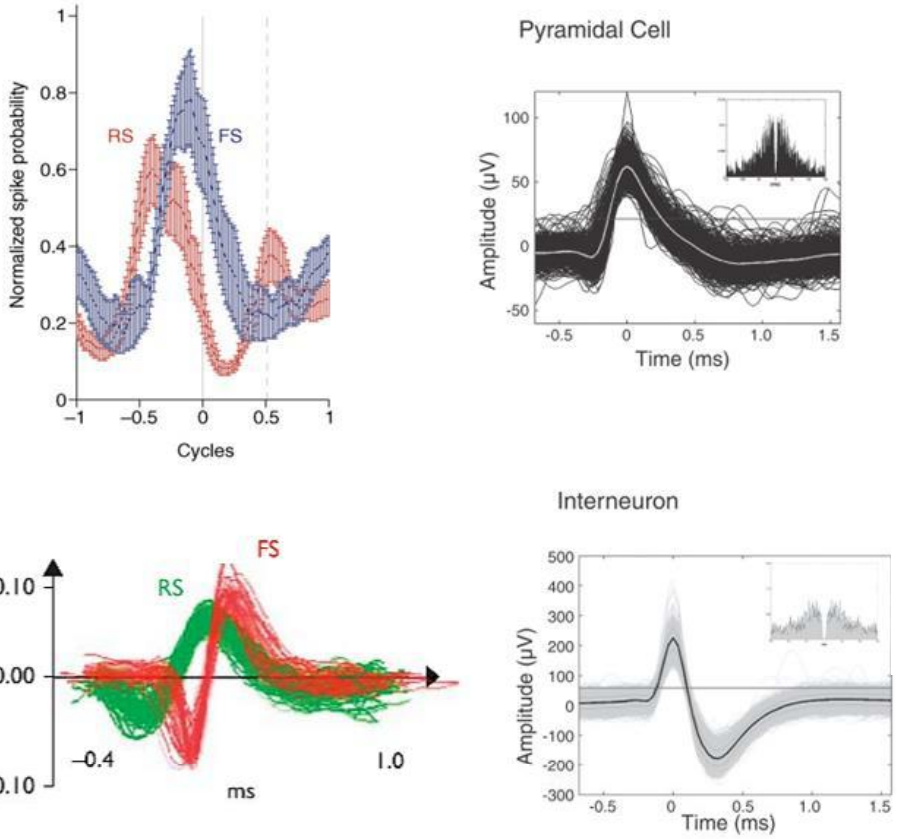

Fries et al., 2007, Bartho et al., 2004, Bachatene et al., 2012a

1.4 Plasticité corticale : divers modèles

1.4.1 Plasticité des domaines d'orientation

Les neurones dans le cortex visuel des mammifères sont programmés à répondre à différents paramètres des stimuli visuels tels que l'orientation, la fréquence spatiale, le contour, la vitesse... (Kohn and Movshon, 2003; Movshon, 1975; Hubel and Wiesel,1962; De Weerd et al., 1990, Marshansky et al., 2011). La sélectivité à l'orientation au sein des colonnes corticales est considérée comme stable dans le cortex visuel primaire, établie tôt dans la vie durant la «période critique» (Tanaka et al., 2009). Différentes études de divers laboratoires ont néanmoins montré que dans un cerveau mature adulte, le réseau neuronal se restructure même au-delà de la période critique suivant la naissance (Dragoi et al., 2000; Godde et al., 2002). De récentes investigations ont révélé la capacité des neurones visuels à répondre à des variations de condition de stimulation (privation monoculaire ou apprentissage visuel) en changeant leurs propriétés optimales acquises après la naissance (He et al., 2006; Tagawa et al., 2005; Maya-vetencourt and Origlia, 2012; Dragoi et al., 2000). Cette adaptabilité des neurones pour la perception visuelle suggère l'existence d'une plasticité neuronale chez les adultes ayant un cerveau mature. Dans le cortex visuel primaire de chats adultes, la plasticité induite par adaptation visuelle dans le cas de l'orientation est caractérisée par les auteurs comme une capacité des neurones corticaux de changer leur orientation préférentielle suivant une longue (Bachatene et al., 2012; Bachatene et al., 2013; Ghisovan et al., 2008; Nemri et al., 2009) ou une courte (Dragoi et al., 2000; Dragoi et al., 2001; Patterson et al., 2013) période d'exposition à une orientation non optimale, à titre d'exemple, une longue adaptation produit

un déplacement de la courbe d'accord à l'orientation des neurones enregistrés vers l'orientation imposée dans la majorité des cas. Les études par imagerie optique décrivent également les effets de l'adaptation visuelle sur les cartes polaires d'orientation (Dragoi et al., 2000; Godde et al., 2002, Cattan et al., 2014). Suivant une période d'adaptation visuelle à un stimulus non optimal, les cartes fonctionnelles d'orientation se reprogramment suivant un patron bien spécifique (voir détails dans la discussion). Ces changements ont été observés dans diverses parties des cartes (domaines d'iso-orientation et pinwheels). On pense que ces modifications seraient dues à des modulations de connectivité locale entre neurones ainsi qu'à des phénomènes de plasticité homéostatique permettant de réguler le niveau de chaque stimulus représenté dans la carte. D'ailleurs, il a été suggéré que les cellules appartenant à une même colonne d'orientation reçoivent des entrées d'autres cellules dans un volume cortical de 500 µm (Dragoi et al., 2001).

1.4.2 Plasticité dans d'autres aires corticales

En plus de la plasticité induite des cartes d'orientation et des colonnes de dominances oculaires, il a été démontré que les neurones d'autres aires cérébrales pouvaient également subir des changements de sélectivité suite à des périodes d'apprentissage visuel (période d'adaptation : 40 secondes), notamment dans l'aire temporale médiane ou MT chez le macaque (Kohn & Movshon, 2004).

Il semble donc y avoir des différences de réponses neuronales à l'adaptation visuelle d'une aire à une autre étant donné les effets absents d'une telle durée d'adaptation sur les neurones

du cortex visuel primaire. Cela est sans doute dû aux différences des fonctions attribuées à chacune de ces aires, l'aire MT étant principalement impliquée dans les mouvements.

Les changements de la sélectivité des neurones dépendant de l'expérience sensorielle ne sont pas spécifiques au cortex visuel. En effet, des changements de connectivité neuronale entre différentes aires auditives ont également été démontrés après une période de privation auditive par ablation cochléaire, stratégie similaire à la privation monoculaire qui induit des changements des colonnes de dominance oculaire (Hishida et al., 2007).

Il semble donc qu'il y ait une forte corrélation entre l'enrichissement environnemental (entrainement visuel ou auditif par exemple) et les changements de connectivité au sein des réseaux neuronaux. En effet, il a été observé qu'une augmentation de décharge de réseaux de neurones se manifestait durant des période d'entrainement visuel à un objet orienté spécifiquement (Furmanski et al., 2004) ou un entrainement à un instrument musical entrainant des changements au niveau du cortex auditif (Hyde et al., 2009).

La neurogenèse aurait également un rôle majeur pour la plasticité des réseaux neuronaux. La synthèse de nouvelles cellules neuronales renforceraient des circuits neuronaux et s'adapteraient à la fonction du réseau cible (Lledo et al., 2006).

1.5 Plasticité : entre période critique et âge adulte

De nombreuses études ont démontré une relation intime entre les phénomènes de plasticité cérébrale et l'inhibition corticale. En effet, le système GABAèrgique semble être crucial pour le déclenchement et la fin de la période critique (Huang et al., 1999; Hensch et al., 1998). Les auteurs ont confirmé cela en inactivant le GAD65 (enzyme de synthèse

GABAèrgique), ce qui a eu pour conséquence d'empêcher la période critique de commencer (Fagiolini & Hensch 2000, Hensch et al. 1998). Des souris avec surexpression de BDNF durant le développement montrent un déclenchement rapide de plasticité car le BDNF stimule le système GABAèrgique dans le cortex visuel (Huang et al., 1999). Durant la période critique, le système inhibiteur déclencheur et régulateur se fait par des interneurones. L'équilibre I/E devient donc crucial à l'établissement et à la fin de la période critique. Ainsi, La réduction de l'inhibition semble être une condition pour la plasticité adulte (Sale et al., 2007). À l'âge adulte, il est donc essentiel de favoriser la diminution de l'inhibition afin de récupérer des aptitudes de plasticité comme celles observées durant la période critique.

Figure 5 - Régulation de l'inhibition entre la période critique et l'âge adulte.
A la naissance, le système GABAèrgique permet la mise en place de la période critique où la plasticité cérébrale est forte, puis à l'âge adulte, l'augmentation de l'inhibition réduite les aptitudes plastiques du cerveau.

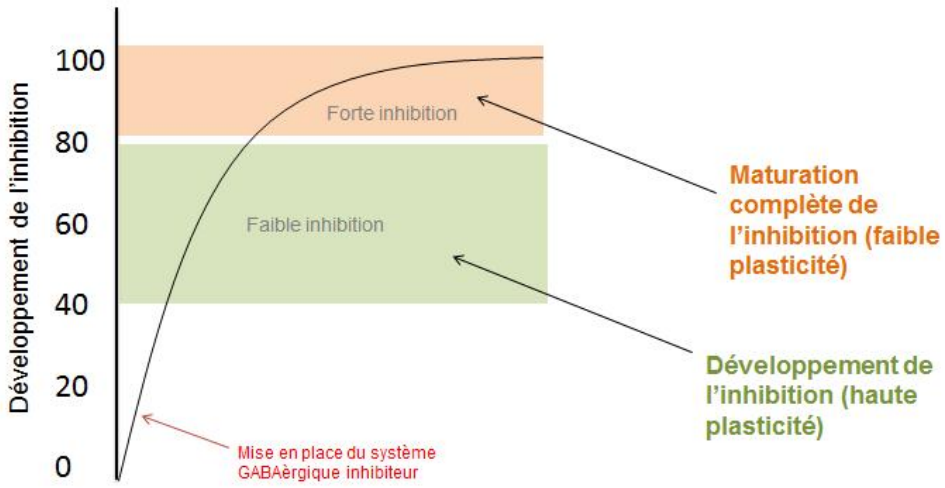

1.6 Connectivité neuronale

Les neurones du cortex visuel primaire sont connectés latéralement et verticalement. Les connexions horizontales sont des connexions longue distance entre différents domaines ou colonnes (Das and Gilbert, 1995; Sompolinsky et al., 1990), tandis que les connexions verticales sont des entrées de la couche IV vers les couches II/III (Yoshimura et al., 2000; Stratford et al., 1996) qui elles-mêmes projettent vers d'autres couches corticales. Comme modèle animal, les chats ont un système visuel performant proche de celui des primates, ce modèle fait l'objet de beaucoup de recherches dans le but de comprendre ses mécanismes fonctionnels. Les approches physiologiques d'étude du système visuel sont notamment l'électrophysiologie, l'imagerie optique intrinsèque, l'imagerie par résonnance magnétique (sur les sujets humains) et la tractographie.
A l'échelle neuronale, l'analyse par inter-corrélation (ou corrélation croisée) est un outil efficace qui révèle les relations fonctionnelles entre les neurones (Perkel et al., 1967). Beaucoup de travaux ont montré que la connectivité neuronale est reliée de façon importante aux propriétés de sélectivité des neurones aux stimuli, les projections neuronales étant de plus ample proportion (en terme de nombre de connexions et de force de connectivité) entre cellules ayant une sélectivité homogène, c'est-à-dire déchargeant de façon optimale à un même stimulus (Stepanyants et al., 2008; Ko et al., 2011). À titre d'exemple, les neurones ayant une sélectivité à l'orientation similaire sont groupés en colonnes (Hubel and Wiesel 1959; Alloway and Roy, 2002; Bartho et al., 2004; Yoshimura et Callaway, 2005; Csicsvari et al., 1998). À la suite de phénomènes de plasticité corticale, les neurones modifient leurs propriétés optimales et le cortex est ainsi réorganisé comme il est montré par les études

d'imagerie optique (Dragoi et al., 2000; Godde et al., 2002). Néanmoins, les mécanismes de dynamique de cette connectivité post-plasticité sont à explorer. Les analyses d'inter-corrélation fournissent un bon indice des relations fonctionnelles des activités de décharges coordonnées entre les neurones (Denman and Contreras., 2013; Perkel et al., 1967; Hata et al., 1991; Konig et al., 1995; Fujisawa et al., 2008; Bartho et al., 2004).

La Figure 6 montre un exemple de ce type d'analyse, deux cellules sont présentées, une représente le neurone référence et la seconde est la cellule cible. Les différentes combinaisons de corrélogrammes croisés sont illustrées ; la ligne rouge indique le degré de validité (95%) du corrélogramme croisé et les barres noires représentent les valeurs de probabilité de connexions fonctionnelles. Ces valeurs découlent de l'assimilation des valeurs des coefficients de corrélation aux probabilités d'avoir des projections entre neurones. Dans ce sens, plus le coefficient de corrélation est haut, plus la probabilité d'avoir une connexion fonctionnelle est haute (Perkel et al., 1967 ; Reid 2012).

Selon l'apparition des pics de part et d'autre du 0 (échelle temporelle de l'axe X), les projections entre ces deux neurones sont de sens opposé (voir «a» et «b»). Un événement plus rare est observé lorsque le pic coïncide avec le 0 (pic central) et est un indicateur d'une entrée commune aux deux cellules (voir «c») (Bachatene et al., 2012b; Denman and Contreras, 2013).

Figure 6 - Stratégie de corrélation croisée : divers cas possibles de connectivité fonctionnelle. ***a)*** Corrélogramme croisé entre deux neurones avec apparition du pic maximal dans une fenêtre temporelle de ±10 millisecondes ; le neurone cible projette sur le neurone référence. ***b)*** Similaire à A avec un pic central après le zéro de l'échelle temporelle ; le neurone référence projette sur le neurone cible. ***c)*** Corrélogramme croisé avec apparition de pic central sur l'échelle temporelle, cela correspond à une afférence commune et une synchronie de décharge des deux neurones.

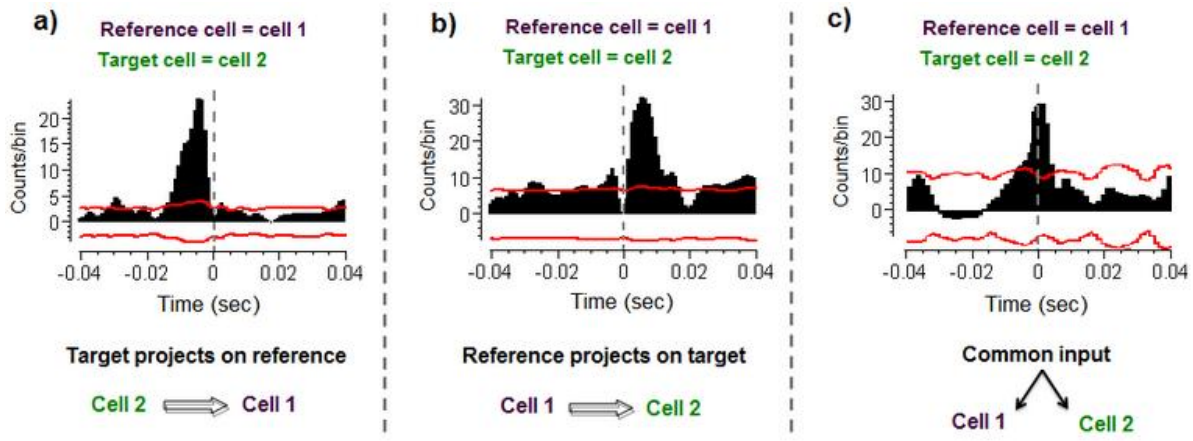

Bachatene et al., 2012b

1.7 Effets neuropharmacologiques

L'un des neurotransmetteurs du système nerveux central, la sérotonine (5-Hydroxytryptamine) a des fonctions majeures dans le développement du cerveau. Les quatorze sous-types de récepteurs dédiés à l'action de la sérotonine dans le système nerveux central en font un candidat idéal dans plusieurs fonctions sensorielles, cognitives et comportementales. Un certain nombre de recherches ont conclu que cette plasticité peut être modulée par différentes substances telles que l'acétylcholine et la noradrénaline (Bear and Singer, 1986) ou la sérotonine et son inhibiteur sélectif de recapture : la fluoxétine (Maya-vetencourt et al., 2008; Maya-vetencourt et al., 2011). Les récentes découvertes sur ces deux dernières

substances notamment la fluoxétine mieux connue sous le nom de *Prozac* et qui est prescrite dans des thérapies médicales contre les effets dépressifs (la dépression étant connue comme une débalance du niveau sérotoninergique), ouvrent de nouvelles perspectives quant aux effets de certains neuromédiateurs et de certaines substances médicamenteuses sur la plasticité corticale. L'équipe de Maya-vetencourt a montré que sur des rats adultes, la plasticité de la dominance oculaire se réinstalle suite à un traitement à la fluoxétine, il a été prouvé également que l'administration de cette dernière à des patients ayant été atteint d'accident vasculaire cérébral ischémique (causé par le blocage du débit sanguin vers le cerveau par un caillot de sang) améliore la récupération motrice de ces patients comparés à des patients traités au placebo (Chollet et al., 2011).

Sur des rats adultes privés de façon monoculaire (la privation visuelle consiste en obstruant un œil durant une certaine période), la plasticité de la dominance oculaire peut être récupérée pharmacologiquement par des régulations de la transmission neuronale (Harauzov et al., 2010).

De telles modifications des mécanismes physiologiques et moléculaires de plasticité cérébrale sont d'une importance fondamentale et thérapeutique dans certaines pathologies du système visuel comme l'amblyopie (Maya-vetencourt and Origlia, 2012).

1.8 Objectifs et hypothèses de recherche

1.8.1 Chapitre A : réorganisation corticale

L'organisation typique du cortex visuel suit un paradigme connu depuis les lois de Hebb (fire together, wire together). Ce principe veut que les neurones qui déchargent préférentiellement aux mêmes propriétés des stimuli soient co-localisés. En effet, dans le cortex visuel, les neurones sont organisés en colonnes d'orientation et colonnes de dominance oculaire. Dans une même colonne, la majorité des neurones répondent de façon optimale aux mêmes axes orientés dans l'espace visuel (orientation préférée). Cette sélectivité à l'orientation se fait dès la naissance et est malléable principalement durant la période critique. Cependant, dans un cerveau mature, il a été établi que les neurones changent leur sélectivité avec l'expérience sensorielle telle que l'apprentissage visuel. Dans ce chapitre, nous traitons de la réorganisation du cortex visuel primaire due à une adaptation visuelle dans une portion spécifique du champ visuel. Plus en détails, comment l'adaptation visuelle à un champ récepteur donné affecte les neurones avoisinants (donc des neurones non adaptés) ? L'hypothèse de ce travail est que les changements de propriétés de neurones adaptés par un stimulus forcé induisent des changements sous-jacents aux neurones voisins afin de maintenir la représentation sensorielle malgré un changement local des domaines d'orientations.

1.8.2 Chapitre B : connectivité neuronale

Le domaine des « connectomes » est un domaine émergent dans les neurosciences modernes, il permet notamment d'expliquer et de comprendre les relations fonctionnelles entre les zones cérébrales de façon générale, et entre les neurones de façon plus particulière. En mesurant l'activité de décharge des cellules enregistrées dans les couches II/III du cortex visuel primaire suite à des stimulations visuelles et à un entrainement visuel (adaptation) comme décrit précédemment, nous pouvons corréler ces trains de décharges à une échelle de temps suffisamment courte (5 à 10 millisecondes dans notre cas) afin de comprendre la modulation de la dynamique de connectivité dans ces deux conditions (pré et post-adaptation). Au cours de cette étude, nous avons investigué les relations inter-neuronales des décharges entre paires neuronales possédant des propriétés similaires de sélectivité à l'orientation, c'est-à-dire que les deux neurones de chaque paire partagent les mêmes stimuli optimaux avant et après le processus d'adaptation visuelle. La deuxième section a été faite sur des populations neuronales dont l'activité a été enregistrée par électrophysiologie et par imagerie optique intrinsèque afin d'explorer le rapport entre la sélectivité des neurones et leur connectivité avant et après plasticité. Notre hypothèse était que les neurones doivent conserver un certain ratio de connectivité fonctionnelle en fonction de leurs nouvelles propriétés acquises.

1.8.3 Chapitre C : Propriétés électrophysiologiques des neurones

Le traitement visuel dans le cortex implique de nombreux aspects de propriétés des neurones : aspects morphologiques, électrophysiologiques et moléculaires. En particulier, le patron de décharge neuronal et la forme du potentiel d'action sont d'importants indicateurs de la dynamique des circuits au sein d'une assemblée de neurones.

En effet, dans ces populations neuronales, les cellules peuvent agir en tant que solistes ou choristes au sein de l'orchestre neuronal. Ces deux comportements neuronaux diffèrent dans leur patron de corrélation avec la population neuronale à laquelle ils appartiennent. Dans la présente section, nous avons examiné la relation entre la forme du potentiel d'action de neurones visuels (activité enregistrée des couches 2/3 du cortex visuel primaire), leur niveau de décharge et leur tendance à agir en tant que solistes ou choristes. Notre hypothèse était qu'il devait y avoir des différences entre neurones possédant des modes de décharge distincts. Nous avons montré que, d'une part, les neurones à décharge rapide qui présentaient de plus hauts niveaux de décharge ont tendance à avoir un comportement choriste (forte corrélation entre leur activité et l'activité de la population de neurones). D'autre part, les neurones à décharge régulière présentant des faibles taux de décharges ont tendance à réagir de façon indépendante (solistes, faible corrélation entre leur activité et l'activité de la population de neurones). La conséquence majeure de cette étude est qu'en estimant la corrélation de l'activité de chaque neurone avec celle de l'assemblée à laquelle il appartient, nous pouvons prédire le type de décharge du neurone et ainsi la fréquence de décharge. Ces résultats donnent de nouvelles perspectives sur la relation entre le type neuronal et le traitement de l'information dans les

circuits complexes qui gouvernent la fonction corticale. L'effet de l'adaptation visuelle a également été traité.

1.8.4 Chapitre D : effets des antidépresseurs

L'objectif majeur de ce travail vise à étudier le rôle des antidépresseurs tels que la fluoxétine (Prozac) sur notre modèle de plasticité à l'orientation des neurones de V1 après adaptation visuelle. Aussi, l'utilisation de la sérotonine s'explique par le fait que les antidépresseurs sont prescrits suite à une déficience sérotoninergique dans le cerveau, ce sont des inhibiteurs sélectifs de la recapture de la sérotonine (ISRS). Il a été démontré qu'un traitement chronique de fluoxétine sur des rats réduit l'inhibition GABAèrgique et augmente l'expression du facteur de croissance BDNF, facilitant ainsi la récupération de la plasticité de dominance oculaire chez ces sujets adultes (Maya-vetencourt et al., 2008). De plus, la fluoxétine restructure les branches des extrémités dendritiques (Chen et al., 2011), un niveau élevé de transmission sérotoninergique augmente des cascades de signalisation du BDNF résultant par une potentialisation de la plasticité (Maya-vetencourt et al., 2011). Dans ce sens, nous avons émis l'hypothèse que la sérotonine et la fluoxétine pouvaient changer les propriétés neuronales du cortex visuel dans notre modèle de plasticité (colonnes d'orientation).

2. **Article intitulé:** Reprogramming of orientation columns in visual cortex: a domino effect

SCIENTIFIC REPORTS

OPEN

SUBJECT AREAS:
STRIATE CORTEX
CORTEX

Received
21 October 2014

Accepted
2 March 2015

Published
24 March 2015

Reprogramming of orientation columns in visual cortex: a domino effect

Lyes Bachatene[1,2], Vishal Bharmauria[1,2], Sarah Cattan[1,2], Jean Rouat[1,2] & Stéphane Molotchnikoff[1,2]

[1]Département de Sciences Biologiques, Université de Montréal, Montréal, QC, Canada, H3C 3J7, [2]Neurosciences Computationnelles et Traitement Intelligent des Signaux (NECOTIS, Département de Génie Électrique et Génie Informatique, Université de Sherbrooke, Sherbrooke, Québec, Canada, J1K 2R1).

Cortical organization rests upon the fundamental principle that neurons sharing similar properties are co-located. In the visual cortex, neurons are organized into orientation columns. In a column, most neurons respond optimally to the same axis of an oriented edge, that is, the preferred orientation. This orientation selectivity is believed to be absolute in adulthood. However, in a fully mature brain, it has been established that neurons change their selectivity following sensory experience or visual adaptation. Here, we show that after applying an adapter away from the tested cells, neurons whose receptive fields were located remotely from the adapted site also exhibit a novel selectivity in spite of the fact that they were not adapted. These results indicate a robust reconfiguration and remapping of the orientation domains with respect to each other thus removing the possibility of an orientation hole in the new hypercolumn. These data suggest that orientation columns transcend anatomy, and are almost strictly functionally dynamic.

Since the seminal investigations of Hubel and Wiesel in 1962[1], it has been extensively established that the visual cortex is organized for orientation selectivity in a columnar fashion from pial membrane to the white matter. That is, most neurons assembled in a vertical column are selective to the same axis of orientation in response to an edge presented within their respective receptive field (RF). Indeed, if an electrode penetrates the cortex in an oblique direction, the preferred neuronal orientation rotates in a methodical fashion by about 16.5° for every traveling step of 0.09 mm of the recording tip, as it crosses from one orientation column to the next. Such systematic progression implies that, once a few reference preferred orientations of neurons are determined, it is conceivable to predict the orientation sequence. This organization rests on the notion that columnar organization is an outcome of segregated architecture of inter-neuronal connections leading to a relatively inflexible layout of striate organization. For instance, LGN neurons aligned along an axis connect to a single cortical cell[2,3] giving rise to the orientation selectivity.

Yet, a few observations[4–6] have reported that these columnar organizations are highly variable, even in the same species.

Interestingly, recent experiments showed that following the continuous or frequent application of non-optimal stimuli, orientation in our case (called adapter to which neurons initially responded poorly), neurons change their stimulus selectivity[7–14]. For orientation, depending on the duration of adaptation, neurons in area 17 shift the peak of their orientation tuning curve either in the direction of the adapter (attractive shift) or away from the adapter (repulsive shift). Whatever the direction of the shift, the newly acquired optimal orientation presents a two-fold problem. The new selectivity following adaptation may be represented twice inside the hypercolumn, and alternatively, the emergence of a novel preferred orientation creates an orientation hole since the original axis is now deleted.

A basic question then arises: do cells in neighboring columns also shift their optimal orientation even if they were not exposed to the adapting stimulus, in order to restore the uniquely fashioned regularity of orientation processing? Heuristically, this invites another question: does the entire orientation hypercolumn exhibit an altered organization? In other words, are Hubel and Wiesel columns modifiable depending on the stimulation history or, in contrast, do orientation columns retain their original orientation selectivity in spite of the fact that the neighboring column changes its orientation-preference?

Our results allow us to argue that columnar organization is a processing unit rather than an anatomically based structure. The direct implication of our described investigations is that the orientation column organization classically supported by structural connections between neurons in V1 must be reassessed. We demonstrate that original preferred orientations of neurons are changed following local adaptation executed at some distance from tested cells.

Although shifts in orientation tuning of the adapted cells were described in previous reports[9–11], we were particularly interested in exploring what occurred in the non-adapted cells, i.e., if one group of cells changes its preferred orientation following adaptation, do the cells belonging to other and non-adapted orientation columns change their preferred orientation concurrently as well?

Results

Orientation preference and goodness of fits. In total, 266 cells were recorded in area 17 of anesthetized cats. Neurons were classified into two groups of cells on the basis of their orientation selectivity which was determined by the orientation selectivity index (OSI, see methods). In line with the previous reports[8,15–17], neurons having an OSI superior or equal to 0.4 are classified as sharply tuned cells. This classification led to 218 orientation-selective neurons while 48 cells were broadly tuned. In the present investigation, tuned neurons had an OSI of 0.5 ± 0.02 and 0.4 ± 0.02 for adapted and non-adapted sites respectively, whereas broadly tuned neurons exhibited an OSI of 0.08 ± 0.004 and 0.07 ± 0.005 for adapted and non-adapted sites, respectively (Fig. 1a). In addition, we computed the Gaussian fits from the raw tuning curves to precisely compute the preferred orientation (pre- and post-adaptation) thus allowing the calculation of shift of the peak of the orientation tuning curve. For both sites, i.e., adapted and non-adapted, significant differences were observed between tuned (mean $R^2 = 0.73 \pm 0.1$ for adapted sites, mean $R^2 = 0.76 \pm 0.1$ for non-adapted sites, Fig. 1b) and untuned neurons (mean $R^2 = 0.23 \pm 0.1$ for adapted sites, mean $R^2 = 0.26 \pm 0.1$ for non-adapted sites, Fig. 1b). Due to their poor orientation selectivity, all untuned cells were excluded from further analyses.

Comparison of the orientation selectivity index for all neurons from adapted and non-adapted sites before and after adaptation was performed. The values were respectively: $OSI_{pre\text{-}adaptation} = 0.44 \pm 0.01$ and $OSI_{post\text{-}adaptation} = 0.49 \pm 0.01$ (n = 218). The R-squared derived from the Gaussian fits were also computed for both conditions; the $R^2_{pre\text{-}adaptation} = 0.7 \pm 0.008$, the $R^2_{post\text{-}adaptation} = 0.7 \pm 0.01$ (n = 218).

Typical results. As expected from previous investigations, peaks of orientation tuning curves shift following visual adaptation in anesthetized cats that were conventionally prepared for recording neurons' electrical activity. Recorded unit activity was filtered, amplified and displayed on oscilloscope and computer screens. Figure 2 shows the typical results. Three receptive fields (RF) are displayed on the top left. In this example, the center to center distance was 4° between RF's A and B and 5° between RF's A and C. Only RF A was locally adapted (see methods for details), and all three fields were stimulated one-by-one with an identical drifting sine-wave grating patch positioned at the center of each excitatory field (stimuli properties were constant). RF's B and C are positioned on opposite sides relative to the adapted area. In the first stage, multi-unit orientation tuning curves were determined from recorded cumulative activities (multiunit responses) from all three areas. Each RF was stimulated in isolation, that is, gratings were applied alternatively in each field, and it is important to emphasize that we never stimulated excitatory fields simultaneously, in order to exclude direct cross talk between groups of cells. Additionally, the spontaneous activity of unstimulated cells remained unchanged when the companion field was excited (see example in Fig. 3c).

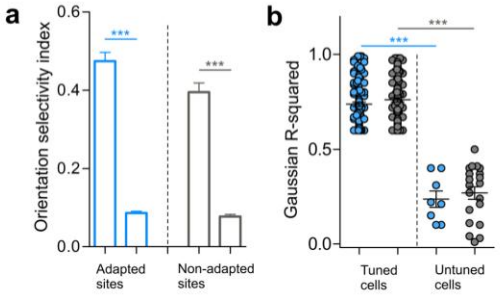

Figure 1 | Orientation selectivity and goodness of fits. (a) Histograms showing the mean values of orientation selectivity indices (OSI's) for both sites. Significant differences lead to the classification of cells into broadly tuned cells and orientation-selective neurons. (b) Differences of the Gaussian R-squared between tuned and untuned cells in both sites (adapted sites in blue, non-adapted sites in gray).

In the second phase, the adapting grating was placed within RF A at an orientation 45° off the optimal axis, as determined in the first phase, of this particular field. Other parameters of the sine-wave patch remained unchanged. The adaptation phase lasted 12 minutes without interruption and no stimulation was applied to companion RF's that remained dark. Single units were isolated from the multi-unit activity and Gaussian tuning curves were computed. The sorted waveforms at each site are displayed in the upper left part of the figure. The adaptation of RF A induced the classical shifts of the peak of the orientation tuning curves of cells belonging to this particular field. Trial-by-trial Pearson correlations of spike-counts (TC) between simultaneously recorded cells were computed in order to ascertain that cells are well isolated (Supplementary Fig. S1).

Figure 2 shows the classical attractive shifts in the adapted field for all three recorded units. This adaptation (adapting orientation indicated by downward red arrow head, in all figures; light colors in raw curves indicate error bars in all figures; Gaussian R-squared and OSI's are shown above each tuning curve) induced a roughly equal attractive displacement of the peak of the orientation tuning curves: 60.49°, 71.04°, and 96.22° for blue, green, and pink cells, respectively (first row, horizontal colored arrows in Fig. 2). However, and quite unexpectedly, neurons belonging to the non-adapted site B (located 4° away) also shifted their respective optimal orientation tuning curves. The orientation tuning curve of the orange neuron shifted in the repulsive direction (68.9°), while red and purple units displaced their respective optimal peaks towards the adapter (49.3° and 86.1° for red and purple neurons, respectively, middle row). Cells belonging to the third non-adapted site C (bottom row) also shifted their respective orientation tuning curves (22.1° for sky neuron, 38.3° for green neuron, and 27.4° for gray neuron) in the attractive direction, that is, the novel orientation approached the adapter. It is worthwhile to emphasize that, at this site the amplitude of the shift is smaller perhaps due to the larger distance separating both receptive fields (A and C, see Fig. 2 insert). Thus, in spite of the fact that cells excited within RF's B and C were not adapted, they reacted by showing new preferred orientations. Furthermore, the response magnitude of the novel optimal orientation was about equal to the strength of the original preferred orientation. Other examples are shown in a supplementary figure (Fig. S2).

Receptive-fields separation. The excitatory receptive field dimensions of the multi-unit activity extended from 2.5° to 4° (average = 3.8 ± 0.4°). All RF's were centrally located within a 15° radius from fovea (Fig. 3a). The adapting stimulus had equal dimensions and covered the excitatory receptive area. Measurements of receptive field size in area 17 as a function of eccentricity indicate that within a radius of 15° of fovea, RF dimensions rarely extend 5°[18,19]. The average distance separating the adapted and non-adapted fields was 8.0 ± 3.0° (histogram distribution shown in Fig. 3b, the downward triangle indicates the mean value). Most significantly, the absence of cross-influences between units excited through distant receptive fields was tested by measurement of spontaneous activity because the latter is weak and it readily fluctuates if a stimulus

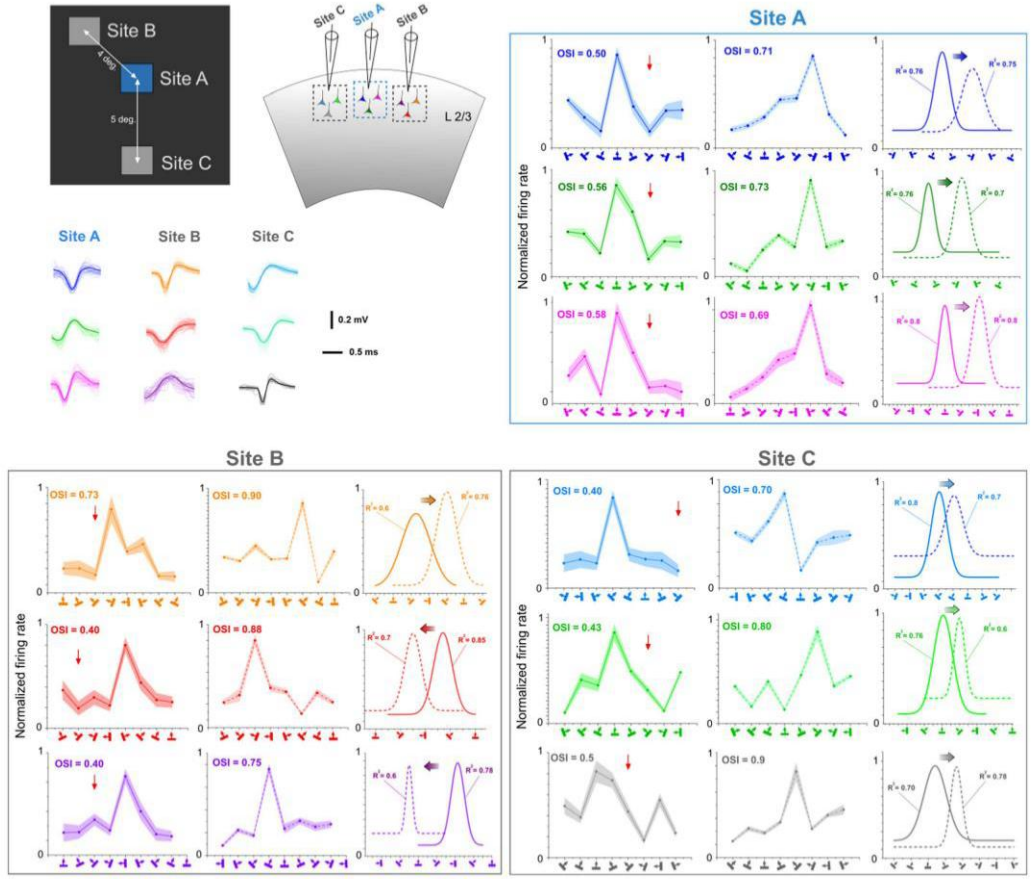

Figure 2 | **Typical examples of shifts of orientation tuning curve peaks.** Tuning shifts are underlined by horizontal colored arrows. The downward red arrow heads indicate the adapting orientation in this and all figures. Upper left insert shows the respective positions of three receptive fields. Only receptive field A was adapted. Waveforms of respective sorted out action potentials are shown below the insert. Tuning curves pre- and post-adaptation are illustrated for each stimulated site (Upper right row: site A, lower left row: site B, lower right row: site C). The curves represent raw data and Gaussian fits. Light colors indicate error bars. Orientations of gratings are depicted on X-axis. OSI's and R-squared are indicated for each tuning curve.

encroaches on the periphery of the companion receptive field. An example is displayed in Fig. 3c, indicating the levels of spontaneous firing while at the same time when the distant companion RF is stimulated with the selected range of orientations. In this example the distance separating both receptive fields was 6°. The spontaneous firing remained unchanged for all applied orientations (X-axis) and for every trial (a single dot stands for one trial presentation of the sine-wave grating applied for 4.1 s; one-way ANOVA: $p > 0.05$, Shapiro-Wilk normality test: $w = 0.9$, Bartlett's test for variances: $p = 0.8$). The average firing at spontaneous activity in control conditions was 15.8 Hz and in adaptation 15.76 Hz (t-test: $p > 0.05$, Shapiro-Wilk normality test: $w = 0.9$, $F = 1.2$). It must also be emphasized that RF's were never stimulated concurrently (see methods). Thus, RF's were sufficiently far apart in order to avoid overlapping surrounds. In addition, we observed non-significant differences of spontaneous activity across all the presented orientations within all RF's when stimulating the adjacent RF's pre- and post-adaptation (one-way ANOVA: $p > 0.05$, Shapiro-Wilk normality test: $w = 0.8$, Bartlett's test for variances: $p = 0.8$, Fig. 3d). Another example is illustrated in Fig. 3e. It shows the spiking activity of neurons from one RF (RF A, blue, *i.e.*, non-stimulated) during the stimulation of the adjacent RF (RF B, gray), and during the stimulation of the RF itself (RF A). Conversely, the activity was computed in a similar fashion for RF B when RF A was stimulated, and when RF B was stimulated.

We observed a significant difference between these two conditions for both RF's (unpaired t-test, $p < 0.05$, Shapiro-Wilk normality test: $w = 0.9$, $F = 1.7$, Fig. 3e). Furthermore, stimulating one RF did not modify the firing at spontaneous activity (red arrow, Fig. 3e). This is highly incompatible, had we encroached the boundaries of the companion RF.

Preferred orientation stability. It is important to confirm that optimal orientations do not fluctuate spontaneously. Many investigations have shown that for any given cell, although response magnitude varies, the preferred orientation remains remarkably

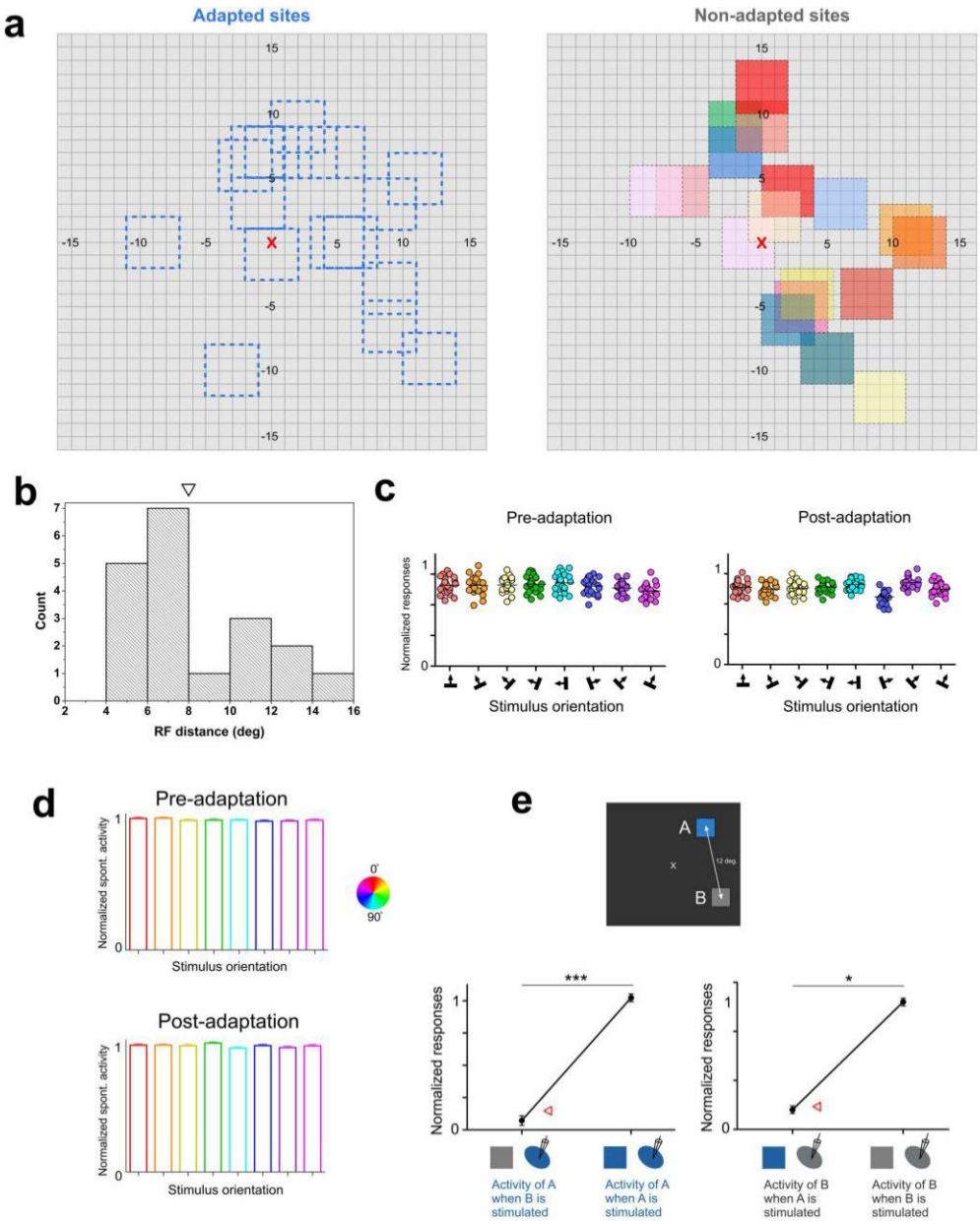

Figure 3 | Location of receptive fields and spontaneous activity. (a) Distribution of adapted (left) and non-adapted (right) receptive fields. Color codes of non-adapted sites correspond to colors of Figure 4a. The receptive field (RF) locations are relative to the fixation point which is underlined by the red cross. (b) Histogram distribution of RF-distances between adapted and non-adapted sites. The downward triangle represents the mean value of RF distance. (c) Absence of spontaneous activity (SA) modulations of one unit when the companion cell is stimulated within its RF at tested orientations. Distance between receptive fields: 6°. The total lack of modulation of SA suggests an absence of overlap between both RF's. (d) Global results of spontaneous activity of one site while stimulating the adjacent one in both pre- and post-adaptation conditions. (e) Example of multi-unit activity of one RF during the stimulation of the companion RF and during the stimulation of the RF itself. Statistical differences were observed between these conditions. Red triangles indicate the level of spontaneous activity of the RF of interest.

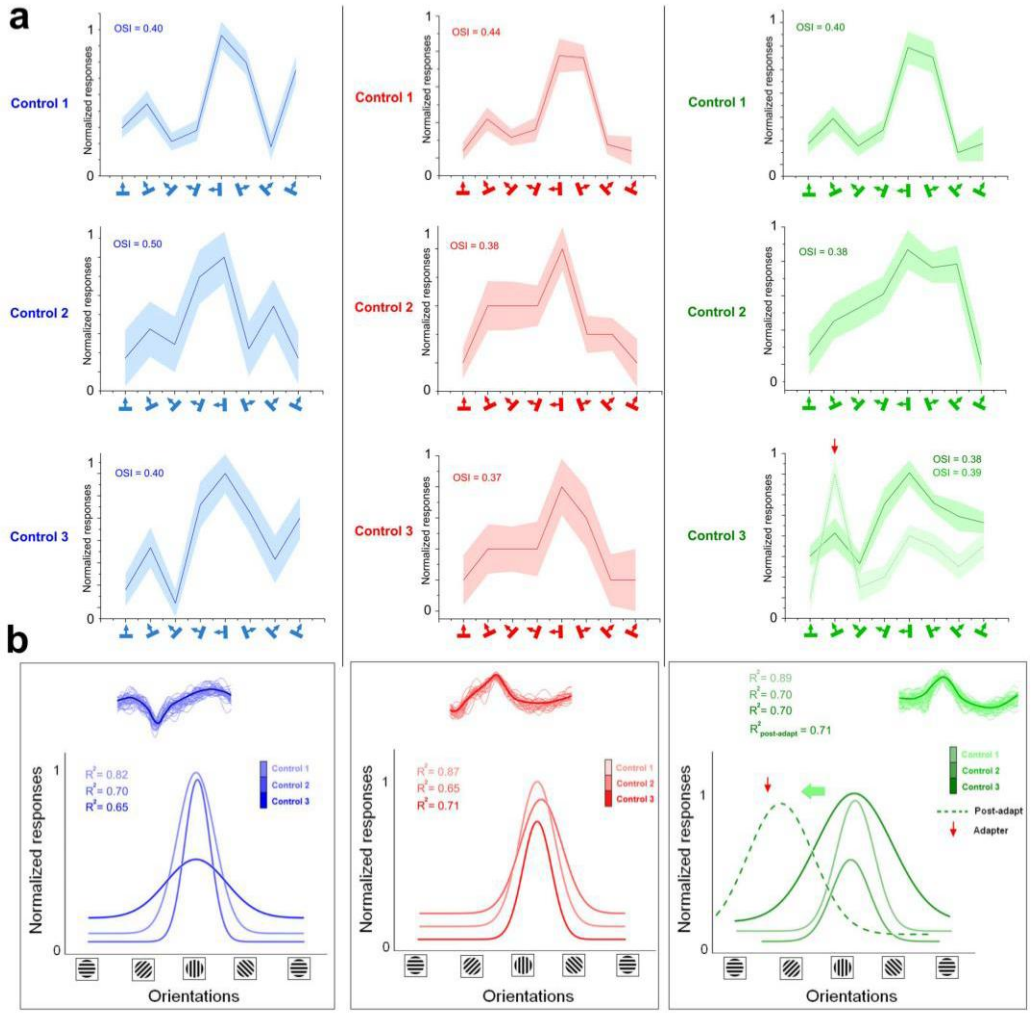

Figure 4 | **Tuning stability.** (a) Raw tuning curves of three neurons at different time-windows (90 min between control 1, control 2, and control 3). As an additional example, the green cell (right) shows the post-adaptation tuning curve (dashed tuning curve, red arrow head corresponds to the adapting orientation) demonstrating the classical observed tuning shift (horizontal green arrow); Y-axis is the normalized amplitude of the cell's firing. (b) Gaussian fits derived from raw data. Spike-waveforms for every neuron are shown above the Gaussian curves.

constant for several days[3,20,21]. Nevertheless, we proceeded with an additional control by measuring orientation tuning curves of three cells during a four hour period (about 90 min separated each recording session, Fig. 4). Raw responses are shown in Fig. 4a and Gaussian fits for each cell are illustrated in Fig. 4b. While the evoked firing rates vary in amplitude, the optimal response (normalized) is elicited by the same orientation in all three recorded neurons. Following these retests, adaptation (12 minutes) was carried out that resulted in a shift of the peak of the tuning curve (see example in Fig. 4, right, the green cell shifted by 45° in the attractive direction).

Shifts in non-adapted sites. Figure 5a illustrates the range of orientation shifts on a cell to cell basis (the short horizontal line indicates the average shifts for a particular cluster of cells). Clusters, *i.e.*, cells recorded from the same site, are identified on the X-axis and the Y-axis indicates shift-range of every unit belonging to non-adapted neurons. In total, 108 units were analyzed. Notice that the first two groups of neurons (labeled "LS1-135" and "Second attempt") are same units tested twice in order to ascertain the consistency of shifts in cells at the non-adapted locus. In this example, the mean magnitudes of shifts were 19.7° (first attempt) and 15.6° (second attempt). Therefore, it can be deduced that orientation shifts at non-adapted sites are the consequence of adaptation executed at some distance from the tested location. Although the average shift-magnitudes were about equal, it should be emphasized that within a single cluster (cells likely to be physically close to each other) some

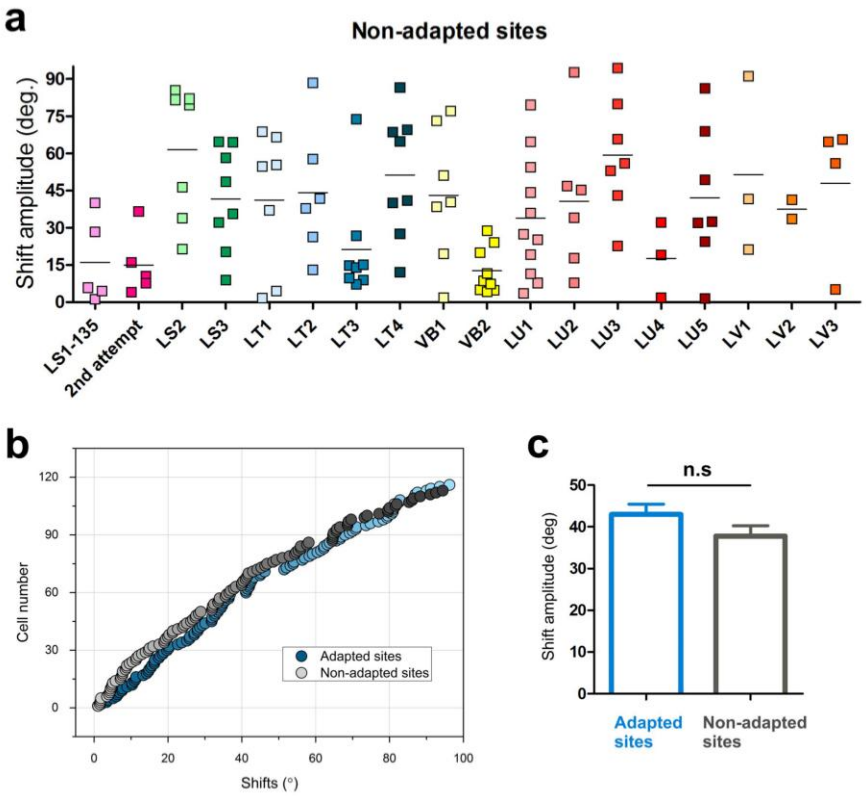

Figure 5 | General survey. (a) Shift-magnitude of every neuron in every cluster; Y-axis: shift amplitude, horizontal line: mean-shift for the corresponding cluster. Notice that the recording "LS1 135" is repeated (second attempt). X-axis: cluster code. For sake of clarity, cells recorded from closely positioned electrodes are grouped within one cluster. (b) Cumulative plots of orientation shifts, magnitudes in increasing order; the close parallelism between both curves suggests that in adapted (blue) and non-adapted (gray) cells, the shifts are comparable. (c) The equal average magnitude shifts confirm that there is no difference between adapted and non-adapted sites.

units significantly shifted their preferred orientation, whereas other neighboring cells failed to change their preferred orientation, hence suggesting that orientation changes are specific characteristics belonging to some neurons (cluster LU3 for instance). This last result indicates that changes of orientation may not be attributed to a general surge of excitation (see below). These results corroborate recent reports showing that within a large population of neurons in sensory cortices, there are embedded sub-networks of units whose selectivity is modifiable depending on a particular stimulus protocol[22]. Such a manifold potential for modification depending on groups of particular cells leads to the conclusion that within a pool of neurons, a class of cells maintains its initial property (original orientation); while another group of intermingled units has a potential to change its optimal stimulating feature to a newly acquired orientation. This heterogeneous organization echoed by dissimilar shifts following adaptation could allow the preservation of an overall stable network yet allowing adaptation to novel conditions of the visual environment.

In Fig. 5b, absolute orientation shifts' magnitudes are plotted in increasing order for every tested cell (cells are not paired, adapted site = 110; non-adapted site = 108). The very similar profiles of cumulative-type curves of shifts in adapted and non-adapted sites are indicative that in both sites the peaks of the orientation tuning curves are displaced with equal magnitude. Although the change of orientation in individual cells may vary, the overall mean shift-amplitude is about equal in adapted and non-adapted cells: 42.9° and 37.7°, respectively (Fig. 5c, t-test: $p > 0.05$, Shapiro-Wilk normality test: $w = 0.9$, $F = 1$). These data suggest that when a group of neurons modifies its orientation selectivity, some other cells follow the change in an equivalent magnitude. Analogously, it is like the domino effect: once the first block falls the other blocks tilt and fall accordingly. That is, a full set of orientation axes is represented with no orientation-hole. Alternatively, if such collective shifts were deficient, one orientation (shifted) would be represented twice since it would closely match an already present axis. Such double presentation of one axis of orientation appears incompatible with the notion that a single hypercolumn contains full range of orientations.

The above results along with data reported in the literature suggest that, following adaptation, the original equilibrium between multiple synaptic drives is ruptured. Consequently a novel optimal orientation arises[9,23]. In addition, we observed significant changes of another parameter: the tuning bandwidth. Indeed, the overall bandwidth at half magnitude is significantly narrower after adaptation for both sites (Control: 32.1 ± 1.7°; post-adaptation: 26.9 ± 1.4°, unpaired

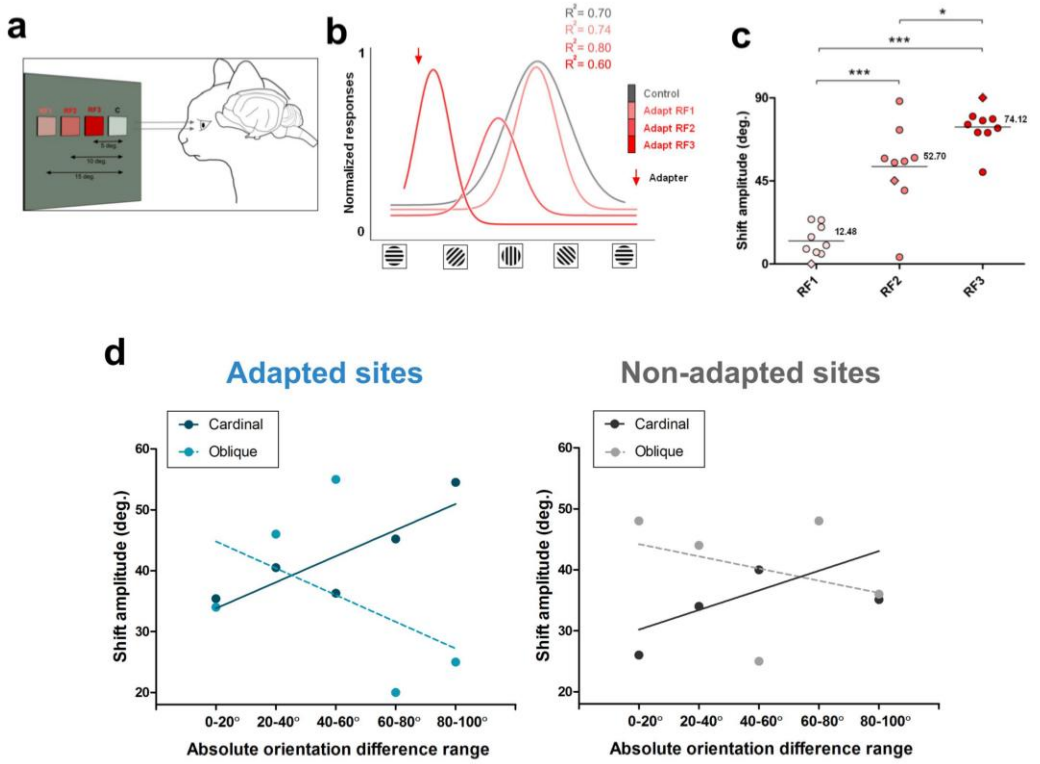

Figure 6 | Inter-receptive-field distances. (a) Experimental set up of stimulation and visual adaptation in relation to inter-RF distances. (b) Typical example of tuning curves of one neuron, responses normalized. The adapting site was approached in steps of 5° from 15° (RF1) — the largest distance separating both fields to the closest gap: 5° (RF3). The example shows that as the adapting field gets closer to the control receptive field, the stimulated neurons elicited larger shifts of the orientation tuning curve towards the adapter (downward red arrow). (c) Global distribution of the averaged shift-magnitudes in relation to inter-RF distances (same cells in all conditions). (d) Shift-amplitudes in adapted and non-adapted sites in relation to the original preferred orientation prior to adaptation, the broken line represents cells whose initial preferred orientation was oblique, while the solid line stands for units whose initial preferred orientations were cardinal (vertical or horizontal, see text for details). X-axis: absolute orientation differences between preferred orientation and the adapting orientation.

t-test: $p < 0.05$, Shapiro-Wilk normality test: $w = 0.8$, $F = 1.3$). This narrowing of the bandwidth following adaptation is coherent with the slight augmentation of the OSI after adaptation as described above.

Relationships between magnitude of shifts and inter-RF distance and orientation differences. We then examined the spatial extension of adaptation. We measured the amplitude of shifts in relation to the distance separating the two stimulated loci measured from center to center (Fig. 6a–c). The adapting grating was applied in steps at three distances: 5°, 10°, and 15° from the tested site (Fig. 6a, tested site identified by letter C). When both RF's were separated by 15°, the tuning curves of neurons were not modified in strong fashion, although the shifts were significant (average shift = 12.48°). Then, as the adapted field approached the tested field to 10° (RF2), the neurons shifted their optimal orientation with increased amplitude in the attractive direction (average shift = 52.70°). At the third adapted site (RF3) located 5° off the tested field (RF C), neurons showed an even larger shift, (average shift = 74.12°) (Fig. 6b, c). Figure 6c shows the distribution of shift amplitudes over a neuronal population ($n = 9$). It demonstrates the relationships between the distance separating both RF's and the shift amplitude (Shapiro-Wilk normality test: $w = 0.8$, t-test RF1-RF2, $p < 0.05$; t-test RF2-RF3, $p < 0.05$; t-test RF1-RF3, $p < 0.05$). Thus changes of orientation selectivity spread over a distance of up to 15°.

Previously[9] it has been reported that in adapted receptive fields cells tuned to cardinal orientations have larger shift-amplitudes when the orientation difference between the adapter and the original orientation increased. Conversely, cells tuned to oblique orientations exhibited larger shift amplitudes when the orientation difference was small, and shifts decreased as this gap increased. Figure 6d illustrates the shifts magnitudes between adapted and non-adapted sites when cells were grouped in relation to their initial optimal orientation. Thus cells with original cardinal orientations: 90° ± 22° and 0° ± 22° (solid line) were dissociated from cells with initial oblique orientation, 45° ± 22° (broken line). Furthermore, for these analyses, neurons were grouped into five 20° orientation classes (Fig. 6d). Interestingly, the same relationships were observed in both adapted and non-adapted sites. These data could signify that in order to maintain constancy of orientation organization following the shifts in the adapted and non-adapted sites, the cortical network rectifies its original orientation layout to maintain its orientation selectivity dis-

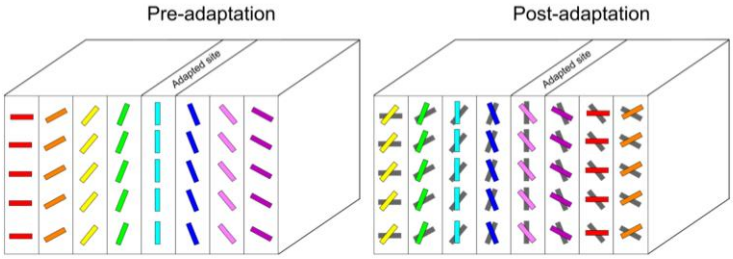

Figure 7 | Schematic model illustrating cortical reorganization following visual adaptation. "Ice cube" model exhibiting orientation columns. After adaptation, a tilt of orientation axis is displayed. Notice an absence of orientation hole.

tribution. In other words, a group of neurons in area 17 displaces the peaks of its orientation tuning curve in relation to the orientation of the neighboring neurons as reference axis.

Discussion

The results demonstrate that preferred orientation of neurons in the visual cortex changes following a relatively short period (12 min) of localized adaptation taking place remotely from the tested (non-adapted) receptive field. Data from our experiments have the following implications: (1) selectivity of orientation organization in area 17 is not attributed to a determined anatomically based and/or ontogenetic layout of a neuronal network. Rather, orientation column design appears to be a labile formation changing its selectivity depending on the history and more generally stimuli conditions exciting neighboring neurons; in other words, local persistent stimulus leads to unmapping and remapping of cortical orientation domains (Fig. 7). Thus, a cross-mutual influence may redraw what has been thought to be an immutable organization of the orientation layout. (2) It appears that orientation columns are a functional construction rather than strictly anatomical, one based on parallel segregation of input fibers emanating from the retina, and then from the lateral geniculate nucleus (LGN). These results may appear astonishing since orientation columns in the visual system are thought to be rather stable after the critical period that follows birth because coding visual trigger features necessitates highly discriminatory neuronal properties[24].

Methodological considerations. It may be argued that shifts in orientation are the consequences of spontaneous fluctuations of levels of firing rates. Although such a hypothesis may not be rejected, nonetheless, numerous experimental results argue against this eventuality. Recently, it has been shown that orientation selectivity in identified units remains stable over several days[20]. In addition, it is unlikely that response-changes may be ascribed to random fluctuations of cellular excitability. Several authors have demonstrated that orientation selectivity is invariant[3], as the jitter of the optimal orientation is small ($<5^{\circ}$). Finally, the response modulations of cells in the adapted and non-adapted sites are constrained roughly to the adapter and the initial preferred orientations. For instance, evoked responses close to the adapter are augmented while, in parallel, responses to the original preferred orientation are weakened[9]; such dual modulations in opposite directions cannot be reconciled with global fluctuations of excitability. Collectively, all of these arguments indicate that it is very unlikely that the described specific discharge modulations are due to spontaneous surges of excitability. Moreover, anesthesia eliminates the impact of attention. Imposing an orientation to a particular neuron for twelve minutes while the animal is paralyzed and anaesthetized is a situation that clearly does not replicate natural conditions. This is a compromise needed to induce neurons to change their preferred orientation. In many reports, it has been shown that imposing a sensory or appropriately timed electrical stimulus induces neuronal property changes within minutes[25–29], which is a time scale congruent with adaptation duration of the described experiments. Although the change in preferred orientation may last for many minutes[30] and may be ten times longer than adaptation duration[7], data suggest that the brain's network is dynamic as it is attuned to the environmental conditions. This may imply that functional column changes are transient yet lasting for many minutes.

Twelve minutes of continuous adaptation may raise the question of the duration of recovery. Literature reports that even after two hours following adaptation; only half of the neurons recover their original selectivity[7,27,30]. Indeed, while capturing the activity of both sites (adapted and non-adapted) post-adaptation; we started first with the adapted site by presenting it the grating corresponding to the original optimal orientation, thereafter, showing the grating corresponding to the original optimal of non-adapted site. In a systematic fashion, after the presentation of these gratings corresponding to the original optimal controls in both sites, we presented the adapter-grating alternatively to both sites (adapted then non-adapted). As evident from our data that most of the neurons exhibited shifts of the tuning curves superior to 10 degrees (both sites) post-adaptation (90% from the adapted sites, 80% from the non-adapted sites, Fig. 5a), thus indicating that they are indeed the result of the adaptation process.

Another methodological aspect may be clarified. In order to avoid surround cross-influence between the receptive fields, neurons stimulated by each site were never excited simultaneously (see Fig. 8). In this study, the average distance separating the adapted and non-adapted fields was $8.0 \pm 3.0^{\circ}$. It has been shown that far-surround radius in V1 averaged $5.5 \pm 2.64^{\circ}$[31]. This reduces the probability of extensive overlapping of both RF's. To our knowledge, no study has demonstrated that stimulating the surround of RF affects the orientation selectivity of neurons. Rather, the stimulation of the periphery results in the modulation of the firing rate (see Fig. 6b). Furthermore, as mentioned above, the spontaneous activity of each RF was never affected by the stimulation of the companion RF.

Mechanisms. Our results are supported by several recent reports. In mouse it has been demonstrated that a single dendritic branch exhibits, over a short distance, synaptic inputs with a large spectrum of orientation channels allowing mutual influences[32]. Whole-cell recording in rodent V1 shows large sub-threshold depolarization evoked by non-preferred orientations[33–35]. After adaptation, the impact of an applied orientation takes over the cell's excitability causing the emergence of a novel optimal orientation due to a specific excitatory drive, wherein one input dominates over other inputs, thus, driving the synaptic strength above threshold that provides the cell its orientation selectivity. Recently in human, it was demonstrated that when the neuronal processing is disturbed,

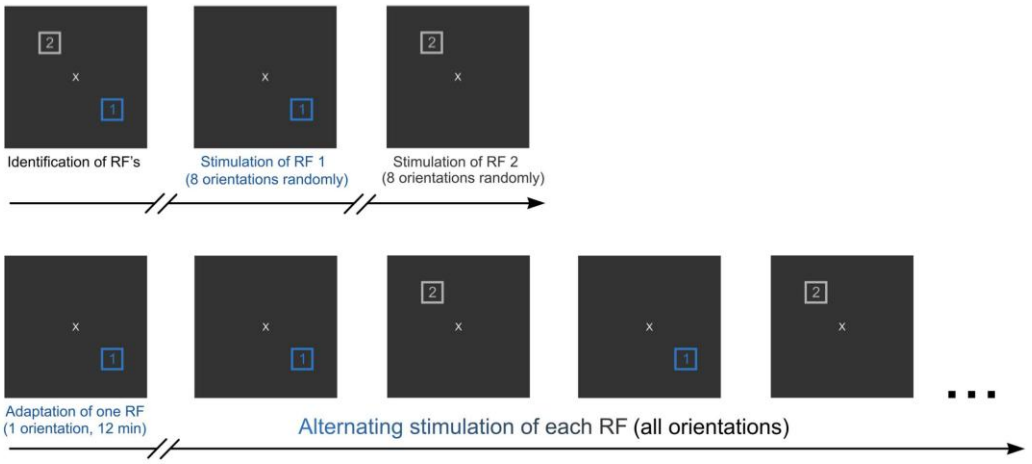

Figure 8 | **Visual stimulation and adaptation protocols.** Upper part: initial stimulation (control). Lower part: adaptation process and post-adaptation recordings.

another cortical area takes over the task to maintain subject performance[36]. These investigations, although at different levels, suggest that single cells or cortical areas may modify their destined commitment to specific functions or tasks following changing conditions, and thus shift the responses to new stimulating environments[37]. The above assumptions are supported by recent reports describing "classes of neurons that accumulate information from an entire cortical column and broadcasts outputs to distant targets"[22].

Neurons in the primary visual cortex receive polysynaptic inputs not only from neighboring cells, but also from a network of distal cortical sites. Indeed, feed-forward and feedback connections are extensive. Thus, area 17 neurons' preferred orientations are not exclusively resulting from feed-forward inputs originating from aligned lateral geniculate nucleus cells[2], since elicited responses are also influenced by long-range connections[38,39]. In particular, the cat's secondary visual cortex (area 18) exhibits strong reciprocal relations with area 17[40], which relays parvocellular inputs to area 18. Monier et al.[25] demonstrated by recording membrane potentials intracellularly that a single cortical cell is receiving inputs from a large variety of synaptic inputs. They came to the conclusion that the diversity of input combinations may be reflected in homogeneities of intra-cortical patterns of connectivity leading to changeable properties. It is to be expected that once the adaptation modifies the balance between inputs and specifically the gradient between excitatory and inhibitory synaptic weights, the neurons become susceptible to exhibit a novel optimal orientation. Because of the extensive intra-cortical network a particular neuron that modifies its selectivity influences other cells with which it is directly or indirectly connected, thus contributing to modifications of the orientation selectivity of an entire network (Fig. 7). Such neuronal dynamics have been described in the auditory cortex[41].

In conclusion, our results strongly suggest that orientation selectivity is a rapidly modifiable characteristic that is adjusted by specific neurons depending on the behavior of cells surrounding the tested neurons. Thus, orientation columns transcend anatomy, and are functionally dynamic entities.

Methods

Ethical approval. Animal surgery and electrophysiological procedures followed the guidelines of the Canadian Council on Animal Care and were approved by the Institutional Animal Care and Use Committee of the University of Montreal. Animals were supplied by the Division of Animal Resources of the University of Montreal.

Animal preparation. Electrophysiological recordings were performed using multielectrodes within area 17 of adult domestic cats. Adult cats (2.5–3.5 kg, age 12–24 months) of either sex, sedated with acepromazine maleate (Atravet, Wyeth-Ayerst, Guelph, ON, Canada; 1 mg kg^{-1}, intramuscular) and atropine sulfate (ATRO-SA, Rafter, Calgary, AB, Canada; 0.04 mg kg^{-1}, intramuscular), were anaesthetized with ketamine hydrochloride (Rogarsetic, Pfizer, Kirkland, QC, Canada; 25 mg kg^{-1}, intramuscular) maintained with 0.3% isoflurane (AErrane, Baxter, Toronto, ON, Canada). Lidocaine hydrochloride (Xylocaine, AstraZeneca, Missis-sauga, ON, Canada; 2%) was injected subcutaneously as a local anaesthetic during surgery. A tracheotomy was performed for artificial ventilation, and one forelimb vein was cannulated to administer a nutritive solution containing a paralyzing agent. Animals were then placed in a stereotaxic apparatus. Xylocaine gel (Astra Pharma, Mississauga, ON, Canada; 5%) was applied on the pressure points. For the remaining preparations and recording, paralysis was induced with 40 mg and maintained with 10 mg kg^{-1} h^{-1} gallaminetriethiodide (Flaxedil, Sigma Chemical, St. Louis, MO, USA; intravenous) administered in 5% dextrose lactated Ringer's nutritive solution. General anaesthesia was maintained by artificial ventilation with a mixture of N_2O/O_2 (70 : 30) supplemented with 0.5% isoflurane (AErrane, Baxter, Toronto, ON, Canada) for the duration of the experiment. Proper depth of anaesthesia was ensured throughout the experiment by monitoring the EEG, the electrocardiogram and expired CO_2. In addition the heart rate remained unmodified after skin stimulation. The end-tidal CO_2 partial pressure was kept constant between 25 and 30 mmHg. A heating pad was used to maintain a body temperature of 37.5°C. Tribrissen (Schering-Plough, Pointe-Claire, QC, Canada; 30 mg kg^{-1} per day, subcutaneous) and Duplocillin (Intervet, Withby, ON, Canada; 0.1 ml kg^{-1}, intramuscular) were administered to the animals to prevent bacterial infection. The pupils were dilated with atropine sulfate (Isopto-Atropine, Alcon, Mississauga, ON, Canada; 1%) and the nictitating membranes were retracted with phenylephrine hydrochloride (Mydfrin, Alcon, Mississauga, ON, Canada; 2.5%). The loci of the area centrales were inferred from the positions of the blind spots, which were ophthalmoscopically focused and back projected onto a translucent screen. Plano contact lenses with artificial pupils (5 mm diameter) were placed on the cat's eyes to prevent the cornea from drying (University of Montréal, PQ, Canada).

At the end of each experiment, euthanasia was achieved with a lethal dose of pentobarbital sodium (Somnotol, MTC Pharmaceuticals, Cambridge, ON, Canada; 100 mg kg^{-1}) by intravenous injection.

Electrophysiology and visual stimulation. Neurons from several recording sites in layers 2/3 were simultaneously recorded. Electrodes were lowered either tangentially (with a 20–30° angle, tetrode arrangements) or vertically (four electrodes, inter-electrode separation: 400 µm, Frederick Haer & Co, Bowdoinham, ME, USA; 2–10 MΩ at 1 kHz). The signal from the microelectrodes was amplified, band-pass filtered (300 Hz–3 kHz), digitized, and recorded with a 0.05 ms temporal resolution (Spike2, CED, Cambridge, England). In all cases at least two excitatory receptive fields were outlined. We paid particular consideration that surrounds of receptive fields were not overlapping.

Firstly, in order to minimize direct cross-influence between both sites, respective cells were never stimulated at the same time (Fig. 8). Secondly, the spontaneous spiking activity of each neuronal population belonging to one RF was recorded during the stimulation of the adjacent RF (see results). Finally, the surround influence in

responses evoked from excitatory area could modulate the magnitude of responses but the neuronal selectivity remained unaffected (see Fig. 6b).

Each site was stimulated with drifting sine-wave grating patches covering the excitatory fields (Spatial Frequency = 0.24 cycle/°, Temporal frequency = 1.0–2.0 Hz, Contrast = 80%). Cells were sequentially stimulated in pseudorandom presentation of gratings. The grating was placed in the center of the aggregate RF of the sampled units. We measured tuning with eight equally spaced orientations (22.5° interval) of the drifting sinusoidal grating. It is to be underlined that the gratings were presented only for one direction. Stimuli were presented in each receptive field in isolation, thus each group of cells was stimulated alternatively in order to eliminate direct cross influence between neurons (Fig. 8). Adapting and stimulating gratings were identical in size and characteristics. Prior to adaptation, respective tuning curves were obtained revealing the preferred orientation in each site that elicited the maximal firing rates. In the following step, only one site was adapted by applying a non-preferred orientation up to 90° off the initial preferred orientation of the neurons (usually evoking a weak response) continuously for twelve minutes. While the adaptation happened over one site, the second site was unstimulated. After adaptation, orientation tuning curves were re-investigated in the same manner as before adaptation.

Cell isolation. Given that the multi-unit activity was recorded concurrently from the same tips using multi-electrodes, it was essential to ascertain that cells were well isolated, because the same unit may exhibit sufficiently different waveforms (for instance, magnitude in relation to distance between recording tip), and thus belong to different clusters in principal component analysis.

Cell-separation was based on spike-waveforms, cluster-isolation using first principal components analyses, autocorrelograms, and trial-count correlation (TC). No more than 5 cells were recorded from the same electrode tip. TC denotes the trial by trial Pearson correlation-coefficient between simultaneously recorded firing of two neurons in response to the presentation of an identical stimulus. In response to the presentation of the same stimulus, the same unit fires identically, regardless of spike amplitude. In order to eliminate such occurrences we correlated neural activities of every cell-pair for every applied trial (25 trials, same stimulus, duration 4.1 s). Since optimal orientations eliciting maximal firing rates were chosen for this computation, and considering a relatively long time-window of analyses (4.1 s), we should expect a high value for correlation if it were the same unit, because such time windows of analyses are sufficiently large to capture the full strength of correlation. Indeed, correlations are underestimated if the counting window is too short. In all analyzed cells the TC was extremely weak (TC < 0.3). Such extremely feeble TC establishes that both spike trains do not originate from the same neuron (see Supplementary Fig. S1). Autocorrelograms preclude contamination by spikes of other units. Anesthesia and paralysis of animals reduced the possibility of similar modulations of firing patterns in cells of the same clusters due to rapid eye motion or attention.

Data analysis. Once single cells were sorted out off-line from multi-unit spike trains accumulated during data acquisition, Gaussian tuning curves were constructed from raw data. We fitted our raw data with the Gaussian function to determine with precision the preferred orientation of neurons and then measured shifts in orientation preference. We used the following Gaussian function:

$$y = y0 + \left(\frac{A}{w\sqrt{\pi/2}}\right) \cdot e^{-2\left(\frac{x-Xc}{w}\right)^2} \qquad \text{(Equation1)}$$

where y0 is the offset, Xc is the center, w is the width, and A represents the area under the Gaussian fit.

The shifts of peaks of tuning curves between pre- and post-adaptation conditions were calculated from the Gaussian fits using the following formula:

$$Shift = |Xc\ post - Xc\ pre| \qquad \text{(Equation2)}$$

where Xc is the central value derived from the Gaussian fit.

Orientation selectivity index (OSI) was calculated from data as the difference between firing rate (FR) at preferred and orthogonal orientations as follows:

$$OSI = \frac{FR\ pref - FR\ ortho}{FR\ pref + FR\ ortho} \qquad \text{(Equation3)}$$

The closer the OSI is to one, the stronger the orientation selectivity (see results).

It has been shown previously that averaged shifts inferior to 5° were not significant[9], however we consider all the shifts in the present investigation.

One-way ANOVA (95% confidence limit) statistical tests were used to compare the spontaneous firing activity between all presented stimuli. Statistical comparisons were performed using unpaired sample two-tailed t-test (95% confidence limit) for unpaired data. Shapiro-Wilk normality test (significance threshold = 0.05) was used for the normal distribution of data, and Fisher test to compare variances for all student tests.

Bartlett's test was performed to compare variances for ANOVA tests.

1. Hubel, D. H. & Wiesel, T. N. Receptive fields, binocular interaction and functional architecture in the cat's visual cortex. *J Physiol.* **160**, 106–154 (1962).
2. Jin, J., Wang, Y., Swadlow, H. A. & Alonso, J. M. Population receptive fields of ON and OFF thalamic inputs to an orientation column in visual cortex. *Nat Neurosci.* **14**, 232–238 (2011).
3. Henry, G. H., Bishop, P. O., Tupper, R. M. & Dreher, B. Orientation specificity and response variability of cells in the striate cortex. *Vision Res.* **13**, 1771–1779 (1973).
4. Horton, J. C. & Adams, D. L. The cortical column: a structure without a function. *Philos Trans R Soc Lond B Biol Sci.* **360**, 837–862 (2005).
5. Kaas, J. H., Krubitzer, L. A. & Johanson, K. L. Cortical connections of areas 17 (V-I) and 18 (V-II) of squirrels. *J Comp Neurol.* **281**, 426–446 (1989).
6. Swindale, N. V., Shoham, D., Grinvald, A., Bonhoeffer, T. & Hubener, M. Visual cortex maps are optimized for uniform coverage. *Nat Neurosci.* **3**, 822–826 (2000).
7. Dragoi, V., Sharma, J. & Sur, M. Adaptation-induced plasticity of orientation tuning in adult visual cortex. *Neuron* **28**, 287–298 (2000).
8. Dragoi, V., Rivadulla, C. & Sur, M. Foci of orientation plasticity in visual cortex. *Nature* **411**, 80–86 (2001).
9. Ghisovan, N., Nemri, A., Shumikhina, S. & Molotchnikoff, S. Long adaptation reveals mostly attractive shifts of orientation tuning in cat primary visual cortex. *Neuroscience* **164**, 1274–1283 (2009).
10. Ghisovan, N., Nemri, A., Shumikhina, S. & Molotchnikoff, S. Visual cells remember earlier applied target: plasticity of orientation selectivity. *PloS one* **3**, e3689 (2008).
11. Kohn, A. Visual adaptation: physiology, mechanisms, and functional benefits. *J Neurophysiol.* **97**, 3155–3164 (2007).
12. Kohn, A. & Movshon, J. A. Adaptation changes the direction tuning of macaque MT neurons. *Nat Neurosci.* **7**, 764–772 (2004).
13. Krekelberg, B., van Wezel, R. J. & Albright, T. D. Adaptation in macaque MT reduces perceived speed and improves speed discrimination. *J Neurophysiol.* **95**, 255–270 (2006).
14. Hietanen, M. A., Crowder, N. A., Price, N. S. & Ibbotson, M. R. Influence of adapting speed on speed and contrast coding in the primary visual cortex of the cat. *J Physiol.* **584**, 451–462 (2007).
15. Atallah, B. V., Bruns, W., Carandini, M. & Scanziani, M. Parvalbumin-expressing interneurons linearly transform cortical responses to visual stimuli. *Neuron* **73**, 159–170 (2012).
16. Ringach, D. L., Shapley, R. M. & Hawken, M. J. Orientation selectivity in macaque V1: diversity and laminar dependence. *J Neurosci.* **22**, 5639–5651 (2002).
17. Denman, D. J. & Contreras, D. The structure of pairwise correlation in mouse primary visual cortex reveals functional organization in the absence of an orientation map. *Cereb Cortex.* **24**, 2707–2720 (2014).
18. Freeman, J. & Simoncelli, E. P. Metamers of the ventral stream. *Nat Neurosci.* **14**, 1195–1201 (2011).
19. Orban, G. A., Kennedy, H. & Bullier, J. Velocity sensitivity and direction selectivity of neurons in areas V1 and V2 of the monkey: influence of eccentricity. *J Neurophysiol.* **56**, 462–480 (1986).
20. Lutcke, H., Margolis, D. J. & Helmchen, F. Steady or changing? Long-term monitoring of neuronal population activity. *Trends Neurosci.* **36**, 375–384 (2013).
21. Frenkel, M. Y. *et al.* Instructive effect of visual experience in mouse visual cortex. *Neuron* **51**, 339–349 (2006).
22. Harris, K. D. & Mrsic-Flogel, T. D. Cortical connectivity and sensory coding. *Nature* **503**, 51–58 (2013).
23. Bachatene, L., Bharmauria, V., Cattan, S. & Molotchnikoff, S. Fluoxetine and serotonin facilitate attractive-adaptation-induced orientation plasticity in adult cat visual cortex. *Eur J Neurosci.* **38**, 2065–2077 (2013).
24. Shtoyerman, E., Arieli, A., Slovin, H., Vanzetta, I. & Grinvald, A. Long-term optical imaging and spectroscopy reveal mechanisms underlying the intrinsic signal and stability of cortical maps in V1 of behaving monkeys. *J Neurosci.* **20**, 8111–8121 (2000).
25. Monier, C., Chavane, F., Baudot, P., Graham, L. J. & Fregnac, Y. Orientation and direction selectivity of synaptic inputs in visual cortical neurons: a diversity of combinations produces spike tuning. *Neuron* **37**, 663–680 (2003).
26. Fregnac, Y. *et al.* A Re-Examination of Hebbian-Covariance Rules and Spike Timing-Dependent Plasticity in Cat Visual Cortex in vivo. *Front Synaptic Neurosci.* **2**, 147 (2010).
27. Godde, B., Leonhardt, R., Cords, S. M. & Dinse, H. R. Plasticity of orientation preference maps in the visual cortex of adult cats. *Proc Natl Acad Sci U S A.* **99**, 6352–6357 (2002).
28. Schuett, S., Bonhoeffer, T. & Hubener, M. Pairing-induced changes of orientation maps in cat visual cortex. *Neuron* **32**, 325–337 (2001).
29. Yao, H., Shi, L., Han, F., Gao, H. & Dan, Y. Rapid learning in cortical coding of visual scenes. *Nat Neurosci.* **10**, 772–778 (2007).
30. Nemri, A., Ghisovan, N., Shumikhina, S. & Molotchnikoff, S. Adaptive behavior of neighboring neurons during adaptation-induced plasticity of orientation tuning in VI. *BMC Neurosci.* **10**, 147 (2009).
31. Shushruth, S., Ichida, J. M., Levitt, J. B. & Angelucci, A. Comparison of spatial summation properties of neurons in macaque V1 and V2. *J Neurophysiol.* **102**, 2069–2083 (2009).
32. Jia, H., Rochefort, N. L., Chen, X. & Konnerth, A. Dendritic organization of sensory input to cortical neurons in vivo. *Nature* **464**, 1307–1312 (2010).
33. Lien, A. D. & Scanziani, M. Tuned thalamic excitation is amplified by visual cortical circuits. *Nat Neurosci.* **16**, 1315–1323 (2013).

34. Li, Y. T., Ibrahim, L. A., Liu, B. H., Zhang, L. I. & Tao, H. W. Linear transformation of thalamocortical input by intracortical excitation. *Nat Neurosci.* **16**, 1324–1330 (2013).
35. Van Hooser, S. D., Heimel, J. A., Chung, S. & Nelson, S. B. Lack of patchy horizontal connectivity in primary visual cortex of a mammal without orientation maps. *J Neurosci.* **26**, 7680–7692 (2006).
36. Zanto, T. P., Chadick, J. Z., Satris, G. & Gazzaley, A. Rapid functional reorganization in human cortex following neural perturbation. *J Neurosci.* **33**, 16268–16274 (2013).
37. Reid, R. C. From functional architecture to functional connectomics. *Neuron* **75**, 209–217 (2012).
38. Ringach, D. L. Haphazard wiring of simple receptive fields and orientation columns in visual cortex. *J Neurophysiol.* **92**, 468–476 (2004).
39. Gilbert, C. D. & Wiesel, T. N. Columnar specificity of intrinsic horizontal and corticocortical connections in cat visual cortex. *J Neurosci.* **9**, 2432–2442 (1989).
40. Bullier, J., McCourt, M. E. & Henry, G. H. Physiological studies on the feedback connection to the striate cortex from cortical areas 18 and 19 of the cat. *Exp Brain Res.* **70**, 90–98 (1988).
41. Froemke, R. C., Merzenich, M. M. & Schreiner, C. E. A synaptic memory trace for cortical receptive field plasticity. *Nature* **450**, 425–429 (2007).

Acknowledgments

This study was supported by grants to S.M. (NSERC, FQRNT).

Author contributions

L.B., V.B. and S.C. contributed equally to this work. S.M. designed the study, contributed to data analyses and wrote the manuscript. J.R. contributed to data analyses.

Additional information

Supplementary information accompanies this paper at http://www.nature.com/scientificreports

Competing financial interests: The authors declare no competing financial interests.

How to cite this article: Bachatene, L., Bharmauria, V., Cattan, S., Rouat, J. & Molotchnikoff, S. Reprogramming of orientation columns in visual cortex: a domino effect. *Sci. Rep.* **5**, 9436; DOI:10.1038/srep09436 (2015).

3. **Article intitulé:** Modulation of functional connectivity following visual adaptation: homeostasis in V1

BRAIN RESEARCH 1594 (2015) 136–153

Available online at www.sciencedirect.com

ScienceDirect

www.elsevier.com/locate/brainres

Brain Research

Research Report

Modulation of functional connectivity following visual adaptation: Homeostasis in V1

L. Bachatene[a,b], V. Bharmauria[a,b], S. Cattan[a,b], J. Rouat[a,b], S. Molotchnikoff[a,b,*]

[a]Laboratoire de Neurosciences de la Vision, Département de Sciences Biologiques, Université de Montréal, C.P. 6128, Succursale Centre-ville, Montréal, QC, Canada H3C 3J7

[b]Neurosciences Computationnelles et Traitement Intelligent des Signaux—NECOTIS, Université de Sherbrooke, Sherbrooke, QC, Canada

ARTICLE INFO

Article history:
Accepted 26 October 2014
Available online 31 October 2014

Keywords:
Cortical plasticity
Crosscorrelation
Functional connectivity
Visual adaptation
Neuronal network
Homeostasis

ABSTRACT

Sensory neurons exhibit remarkable adaptability in acquiring new optimal selectivity to unfamiliar features when a new stimulus becomes prevalent in the environment. In conventionally prepared adult anesthetized cats, we used visual adaptation to change the preferred orientation selectivity in V1 neurons. Cortical circuits are dominated by complex and intricate connections between neurons. Cross-correlation of cellular spike-trains discloses the putative functional connection between two neurons. We sought to investigate changes in these links following a 12 min uninterrupted application of a specific, usually non-preferred, orientation. We report that visual adaptation, mimicking training, modulates the magnitude of crosscorrelograms suggesting that the strength of inter-neuronal relationships is modified. While individual cell-pairs exhibit changes in their response correlation strength, the average correlation of the recorded cell cluster remains unchanged. Hence, visual adaptation induces plastic changes that impact the connectivity between neurons.

1. Introduction

The brain has a remarkable capacity for plastic modifications where cortical areas are able to switch to a new selection-preference in relation to the stimulus. For instance, V1 neurons are selective for stimuli features such as orientation, spatial frequency, direction and speed (Dragoi et al., 2000; Hubel and Wiesel, 1959; Hubel and Wiesel, 1968; Kohn and Movshon, 2004; Marshansky et al., 2011; Movshon, 1975), but can modify their selectivity in order to functionally reorganize the visual cortex as an "adapted cortex" to altered stimulation. Primary visual neurons are organized into cortical domains exhibiting specific connections (Hubel and Wiesel, 1959, 1968; Stratford et al., 1996; Yoshimura et al., 2000).

Visual training impinges upon the spiking activity of neuronal populations (Bachatene et al., 2012, 2013; Dragoi

Abbreviations: CCG, crosscorrelogram; OSI, orientation selectivity index; RF, receptive field; TC, trial-count correlation; V1, primary visual cortex

http://dx.doi.org/10.1016/j.brainres.2014.10.054
0006-8993/

et al., 2000; Ghisovan et al., 2009; Kohn and Movshon, 2004; Patterson et al., 2013), hence it may influence the dynamic modulation of functional relationships between cells. Indeed, the primary visual cortex recalibrates its inputs to reconfigure information processing which results in modified neuronal connectivity after plasticity phenomenon (Fahle, 2004).

Many studies have shown that neuronal connectivity is related to the stimuli preference of neurons; cellular projections are higher between neurons sharing similar preferred features (Ko et al., 2011; Stepanyants et al., 2008). For example, cells exhibiting similar orientation selectivity are grouped into orientation columns (Alloway and Roy, 2002; Bartho et al., 2004; Csicsvari et al., 1998; Hubel and Wiesel, 1959, 1968; Yoshimura et al., 2005). Following cortical plasticity, the neurons change their selectivity (Bachatene et al., 2012; Dragoi et al., 2000; Ghisovan et al., 2009) and the cortex is reorganized (Dragoi et al., 2000; Godde et al., 2002), however, the mechanisms conferring a novel circuitry on cortical neurons are as yet unknown. Here, we seek to examine the impact of adaptation on connectivity between V1 neurons. Crosscorrelation computations signify inter-neuronal relationships that are indicative of functional connections emerging from coordinated neural activities of involved neurons (Bartho et al., 2004; Denman and Contreras, 2013; Fujisawa et al., 2008; Hata et al., 1991; Konig et al., 1995; Perkel et al., 1967). Moreover, crosscorrelograms (CCG) calculate a peak-strength which yields an index of connectivity between neurons (Alloway and Roy, 2002; Wise et al., 2010). Significant peaks within a short time-window in the CCG's are indicative of putative functional linkages between units (Bartho et al., 2004; Denman and Contreras, 2013; Fujisawa et al., 2008; Kara and Reid, 2003; Perkel et al., 1967). In the present investigation, we used crosscorrelation analyses to examine connection probabilities between V1 neuronal pairs sharing similar pre- and post-adaptation orientation-selectivity in order to reveal plastic changes in dynamic functional connectivity. In other words, how is the neural coding altered after experience-dependent plasticity? We report that visual adaptation considerably modulates the peaks-strengths among individual neuron-pairs, however, on average, peaks-strengths are not significantly different pre- and post-adaptation. Such adjustments involving cell-pairs in V1 while preserving the global time relationships between neuronal spikes allow constancy within neuronal properties of an assembly of cells and at the same time adaptability to visual stimuli modifications (Benucci et al., 2013).

2. Results

We measured extracellular spiking activity of V1 neurons in response to visual orientation gratings after spike sorting protocol within layers II/III. The current investigation was focused on how visual adaptation (prolonged presentation of a non-preferred orientation stimulus within the receptive field of neurons) affects this functional dynamic. In total, 166 cells were recorded, and 105 pairs were selected based on the similarity of orientation-preference pre- and post-adaptation.

2.1. *Peaks-strengths pre- and post-adaptation: A typical cell-pair example*

The computations in Fig. 1 display a typical example of CCG analysis for a cell-pair (both cells exhibited $\pm 22^{\circ}$ similar pre- and post-adaptation selectivity). We first isolated single units from multi-unit spiking activity (see methods). Fig. 1A illustrates two simultaneously recorded cells sorted by spike wave-shapes (top), cluster distribution derived from principal component analysis (below) and autocorrelograms (right), the latter showing an absence of event (refractory period) at 0 on the time-scale.

The raster plots and peri-stimulus time histograms are shown in Fig. 1B. The inserted histograms (on the right) display the push-pull effect at both orientations of interest, the spiking activity at the initial optimal orientation declines post-adaptation, and the firing rate at the new preferred orientation (evoking weak responses pre-adaptation) increases after visual adaptation. This is demonstrated by the respective tuning curves for both neurons (Fig. 1C). The raw orientation tuning curves revealed that both cells had $\pm 22^{\circ}$ similar preferred orientation (pink neuron: 3.9 ± 2.06 Hz at 67.5°, blue neuron: 3.19 ± 1.21 Hz at 90°). After 12 min of visual adaptation to a non-preferred orientation (indicated by the downward black arrows), both tuning curves shifted their peaks to 157.5° and 0° for pink and blue neurons, respectively (pink neuron: 3.7 ± 1.65 Hz at 157°, blue neuron: 1.6 ± 0.94 Hz at 0°). Thereafter, shift-corrected CCG's were computed to reveal the dynamic functional links between cell-pairs (see methods for details). Fig. 1D represents the CCG's analysis for neurons shown in Fig. 1A at similar original and novel preferred orientations (pre-adaptation condition is displayed on the left and post-adaptation on the right). In this example, neuron 1 (pink unit) was set as the reference neuron and neuron 2 (blue unit) as the target unit. The peaks-strengths at the original optimal orientation decreased from 0.040 to 0.015 after adaptation with a large decorrelation (see also next section for general distribution). However, for the new optimal orientation, we observed a decrease from 0.040 to 0.034 and the correlation was maintained (significant peak). This reflects the dynamic functional linkage due to visual adaptation. It is to be mentioned that the aim of this study was to investigate direct functional relationships between specific neurons. Therefore, the analyses were focused on significant peaks offset from zero mark in the CCG, such analysis is a useful method to interpret the putative functional links between neurons (Bartho et al., 2004; Csicsvari et al., 1998; Denman and Contreras, 2013; Fujisawa et al., 2008).

2.2. *Adaptation influences the correlation between units*

The next figure illustrates on a global scale the changing strength of connectivity (as reflected from the peaks-strengths) for all neuronal pairs sharing the same pre- and post-adaptation orientation-selectivity. Fig. 2A shows, on a cell-pair basis, the correlation of the peaks-strengths for the highest bins (>95%, time-window ± 5 ms) in the CCG's prior and post-adaptation, at original optimal orientation (left graph) and new optimal orientation (right graph). For the original optimal orientation, we obtained 87 cases of significant CCG's (peaks above 95% of the confidence line) before and/or after adaptation. At the new optimal orientation, 75 significant cases were obtained.

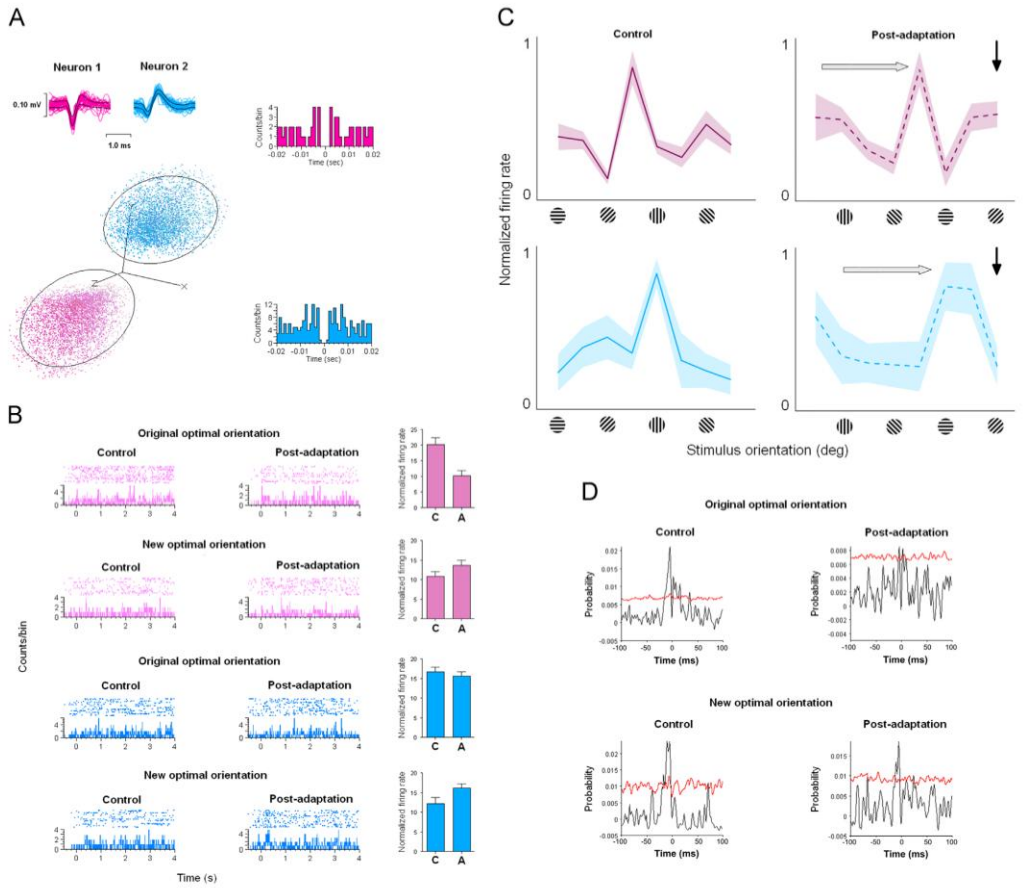

Fig. 1 – Typical example. (A) Two neurons (pink and blue units) sorted using spike waveforms, principal component analyses, and autocorrelograms. (B) Raster plots and peri-stimulus time histograms for both cells (at the initial optimal orientation and the new optimal orientation). The values of the mean firing activity are displayed in the histograms (on the right, C for control and A for adaptation). (C) Orientation tuning curves of both neurons for control (solid lines) and post-adaptation (dashed lines) conditions, corresponding lighter colors represent error bars. Horizontal gray arrows show the direction of shifts of tuning curves and the black downward arrows represent the adapting orientation. The two neurons are tuned to a $\pm 22^{\circ}$ similar oriented stimulus. (D) Shift-corrected crosscorrelograms of both neurons for their similar original optimal and new optimal gratings (left: control, right: post-adaptation). (For interpretation of the references to color in this figure legend, the reader is referred to the web version of this article.)

Thereafter, we correlated the peaks-strengths of neuronal pairs pre- and post-adaptation for both orientations (original and new optimal). The resultant linear regression analysis is shown in Fig. 2A. The dotted line in each graph represents the best-fit 45° line passing through the origin. The peak-strength before adaptation is indicated on the X-axis, whereas the Y-axis shows the peak-strength following adaptation. The solid black line in each graph corresponds to the linear regression trend with the value of the coefficient of determination (R^2). R^2 equals 0.17 and 8.10^{-5} for the original optimal orientation (left) and the new optimal orientation (right), respectively. Such a wide distribution of dots points to the fact that adaptation redistributes (decrease or increase of the peaks-strengths) the time-relationship between spiking activities of neuronal pairs, even though the cells are sharing the same orientation-selectivity following adaptation. We suggest that adaptation disturbs the original inter-neuronal relationships, thereby either erasing or establishing new functional connections to frame novel connectomes as a result of the emergence of newly acquired firing patterns of involved neurons.

The number of cases for diminution and augmentation of the peaks-strengths are as follows: at original optimal orientation,

we found 49 cases (56%) of diminution and 38 cases (44%) of augmentation ($n=87$), whereas, for new optimal orientation, a decrease was observed in 45 cases (60%), versus 30 cases (40%) of increase ($n=75$) (see next section for details).

Fig. 2B represents the total distribution of the peaks-strengths for all cell-pairs pre- (green) and post-adaptation (orange) at the original optimal orientation (left) and the newly acquired orientation (right). Below are shown the respective non-linear regression curves with the relative coefficients of determination (Original optimal: $R^2_{control}=0.99$, $R^2_{post\text{-}adaptation}=0.99$, New optimal: $R^2_{control}=0.97$, $R^2_{post\text{-}adaptation}=0.97$).

In spite of the decorrelation following adaptation on cell-pair basis as evident from Fig. 2A, we note that in Fig. 2B, the very close superposition of the cumulative distribution of dots and curves indicates an absence of difference in global modification of the peaks-strengths in both conditions (control and post-adaptation) at each orientation of interest (original optimal and new optimal), thus suggesting that even though functional connections may change at the cell-pair basis, it is, however, likely on a populational scale that there is an inherent stability (homeostasis) to the network. Furthermore, we compared the functional connectivity between neurons sharing a $\pm 22^\circ$ orientation-preference-range and between differently tuned neurons (superior to 22° of orientation-preference-range, Fig. 2C). We found a significant difference between these two groups (two-tailed t-test, $p<0.05$). These results suggest that even though visual adaptation modifies the peaks-strengths of crosscorrelograms that may reflect the functional connections between neurons, cells that exhibit newly similar orientations remain more strongly connected in comparison to differently tuned cells. In addition, we calculated the peaks-strengths at the adapting orientation. Overall, the modulations of the peaks-strengths set the latter at about the same average values (Fig. 2D).

2.3. *Modulation of peak-strengths*

Fig. 3 shows the population analysis of the peaks-strengths for both orientations of interest (original optimal and new optimal). We averaged the peaks-strengths for all neuronal pairs in pre-adaptation condition, and thereafter, the increase and decrease post-adaptation. Fig. 3A displays all cellular pairs showing a decline of the peaks; the mean probabilities pre- and post-adaptation were 0.029 and 0.011 respectively for the original optimal orientation ($n=49$, left, significant decrease of 0.018, two-tailed t-test, $p<0.05$). The same tendency is observed for the new optimal orientation ($n=45$, right), i.e., a significant decline of 0.019 from 0.032 to 0.013 (paired two-tailed t-test, $p<0.05$). Fig. 3B displays the group of pairs reacting with an increase in probability following adaptation (significant two-tailed paired t-tests for augmentation of the peaks-strengths for both original and new optimal orientations). Interestingly, the enhancement of the peak-strength for the new optimal orientation (right) is superior to the enhancement of the peak for the original optimal orientation (left); these increases are 0.027 and 0.015, respectively (one-tailed unpaired t-test, $p<0.05$). This is the highest modulation for this group of cells that acquire a new optimal orientation.

These sets of data and particularly the regression analysis (Figs. 2 and 3) suggest that even after visual adaptation, on average, the peaks-strengths are altered, yet, the constant application of the grating influences the time correlation of individual pairs of neurons in a flexible fashion. These computations suggest a lack of uniformity which, in turn, points toward the fact that adaptation adjusts the functional relationship between involved neurons. We suggest that such versatility in inter-neuronal relationships promotes flexibility, and, consequently, plasticity. To test whether these variations were due to spontaneous fluctuations of firing, peaks-strengths were compared for original orientations prior to, post-adaptation, and subsequently 1 h after adaptation (recovery). An example of crosscorrelograms between two cells is illustrated in Fig. 3C (left). It shows the effect of adaptation on the correlation between spike trains of these two neurons and the recovery of the magnitude level 1 h after adaptation. The maximal peaks of CCG's in this example were 0.06, 0.013 and 0.061 for control, post-adaptation and recovery, respectively. Other examples in Fig. 3C (right, upper part) show the variability of correlation due to adaptation process as the peak strength values return to control levels after recovery. These examples indicate that visual adaptation modulates the magnitude of the peak strength between correlated neuronal spike trains.

Globally, the average values were 0.022 ± 0.003, 0.019 ± 0.002, 0.022 ± 0.003 for control, post-adaptation and recovery, respectively (Fig. 3C right, lower part, random sample, $n=41$).

Additionally, we compared the CCG-magnitudes between the stimulus-condition and the non-stimulus-condition (spontaneous activity of the recorded neurons), and found a significant difference (two-tailed t-test, $p<0.05$). Crosscorrelogram-magnitudes during spontaneous activity were very low, suggesting that connectivity-strength is due to the presentation of stimulus rather than spontaneous neuronal firing (Fig. 3D). Moreover, stimulation was repeated in order to compare the CCG-values at different times. Fig. 3E shows an example of two CCG's between two neurons at time t_1 (attempt 1) and t_2 (attempt 2); the time-laps between both attempts was 1 h. The values of the CCG-peaks were 0.040 and 0.039, respectively. Taken together, these results demonstrate that the CCG's remain constant.

2.4. *Dynamics of correlation*

Firing rate of neurons pre- and post-visual adaptation is changed mostly for two main orientation classes: the original optimal orientation and the new acquired optimal orientation. It is changed in such a way that we generally notice a decline of evoked firing activity for the original preferred stimulus and an increase of elicited discharges for the new preferred stimulus by an already described push-pull mechanism, therefore leading to the observed shifts after the adaptation process (Bachatene et al., 2012, 2013; Ghisovan et al., 2009). We thus calculated a Fano factor ($F=\sigma^2/\mu$) by dividing the variance (σ^2) by the mean firing rate (μ) of every neuron from each pair; we then compared these factors in pre- and post-adaptation conditions. Fig. 4A shows the modulation of the Fano Factor for original (top) and new optimal (bottom) orientations. This factor increased from 0.49 to 0.57 for the original preferred orientation (paired two-tailed t-test, $p<0.05$) and decreased from 0.58 to 0.48 for the new preferred orientation (paired two-tailed t-test, $p<0.05$). These reverse trends show that spike patterns are more variable for the original optimal orientation and steadier for the new preferred

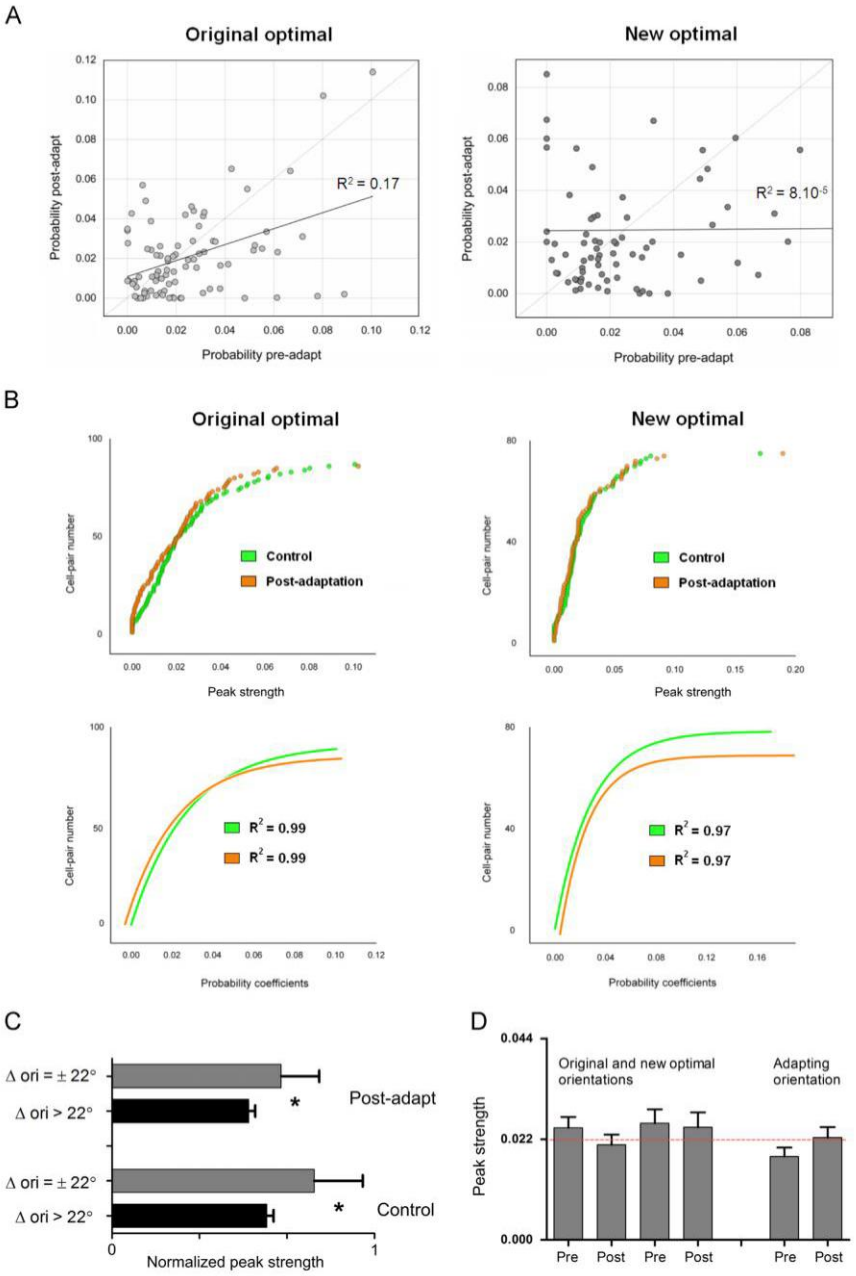
A
Original optimal
New optimal
Probability post-adapt
Probability pre-adapt
R² = 0.17
R² = 8.10⁻⁵
B
Original optimal
New optimal
Cell-pair number
Peak strength
Control
Post-adaptation
R² = 0.99
R² = 0.97
Probability coefficients
C
Δ ori = ± 22°
Δ ori > 22°
Post-adapt
Control
Normalized peak strength
D
Original and new optimal orientations
Adapting orientation
Peak strength
Pre
Post

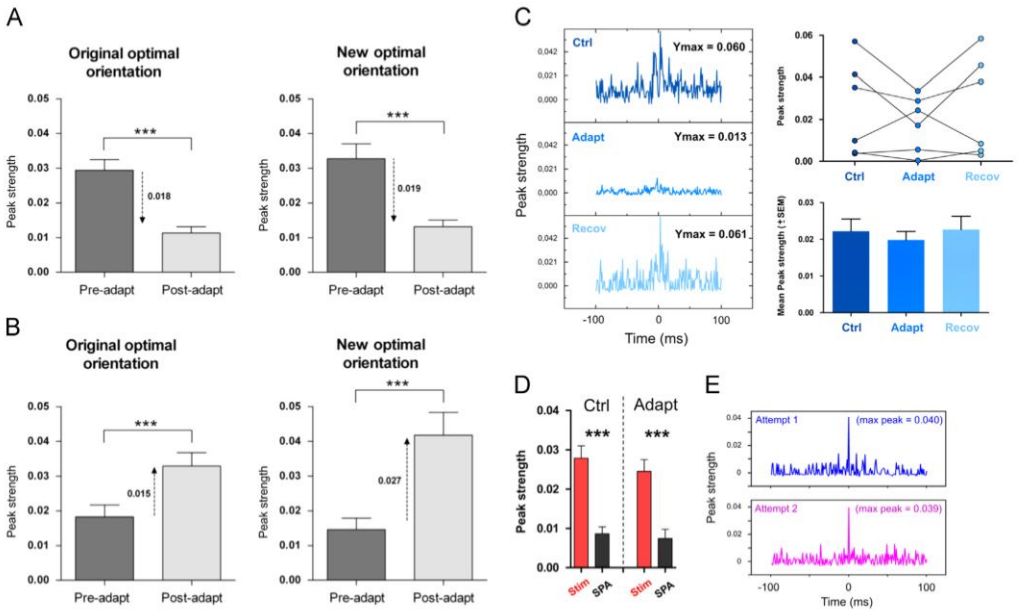

Fig. 3 – Population analyses of the modulation of peaks-strengths and spontaneous activity. (A) Cases of diminution of the mean peaks-strengths post-adaptation for the original optimal orientation (left) and the new optimal orientation (right), significant declines of 0.018 (two-tailed t-test, $p<0.05$) and 0.019 (two-tailed t-test, $p<0.05$) were observed for both orientations, respectively. (B) Cases of augmentation of the mean peaks-strengths following adaptation for both orientations (original and new optimal), the increase of mean peak-strength for the new optimal orientation is almost 50% superior to the increase for the original optimal (0.027 and 0.015, respectively). (One-tailed unpaired t-test, 95% significance level, $p=0.03$). (C) Left: example of CCG's between spike trains of two neurons. The peak magnitudes were 0.06, 0.013 and 0.061 for control, post-adaptation and recovery (1 h after adaptation process), respectively. Right, upper: other examples of correlation variability for these three conditions. Right, lower: random sample test of averaged peaks strengths ($n=41$) between control, post-adaptation and recovery period. Error bars in the histogram indicate the standard error of the mean. The observed peaks were 0.022 ± 0.003, 0.019 ± 0.002, 0.022 ± 0.003, respectively. (D) Averaged peak-strength (control and post-adaptation) for two conditions: during visual stimulation (red histograms) and during spontaneous activity (black histograms). Significant difference was observed for both conditions. (E) Example of two CCG's at two different times (two attempts separated by 1 h). This example shows the stability of the peak-strength over a period of time. (For interpretation of the references to color in this figure legend, the reader is referred to the web version of this article.)

Fig. 2 – Correlation of peaks-strengths pre- and post-adaptation. (A) Linear regression analyses of the peaks-strengths for the original optimal orientation (left, 87 significant cases found, $n=105$) and for the new acquired optimal orientation (right, 75 significant cases found, $n=105$). The dotted line indicates best-fit 45° line passing through the origin. X-axis and Y-axis show the peaks-strengths pre- and post-adaptation, respectively. Solid black line in each graph displays the linear regression trend ($R^2=0.17$ for the original optimal orientation, $R^2=8.10^{-5}$ for the new optimal orientation). (B) Total distribution of peaks-strengths for all cell-pairs, green dots and curves represent pre-adaptation condition, orange dots and curves show post-adaptation condition. Results for the original optimal orientation are on the left and for new optimal orientation on the right. Below are illustrated the respective non-linear regression curves (original optimal: $R^2_{control}=0.99$, $R^2_{post\text{-}adaptation}=0.99$, new optimal: $R^2_{control}=0.97$, $R^2_{post\text{-}adaptation}=0.97$). (C) Difference of connectivity strength between closely tuned neurons (gray bars) and differently tuned neurons (black bars) for control and post-adaptation. The peak-strength is significantly higher for closely tuned neurons in both conditions. (D) Averaged peak-strength at all orientations of interest (original and new optimal orientations on the left, adapting orientation on the right). The red dashed line represents the mean peak-strength (0.022) which is maintained post-adaptation. (For interpretation of the references to color in this figure legend, the reader is referred to the web version of this article.)

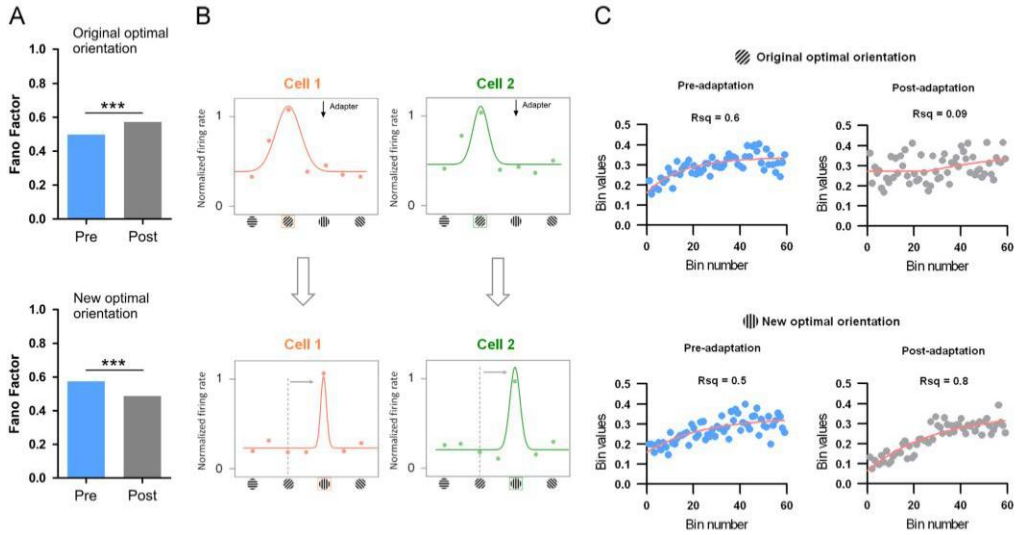

Fig. 4 – Variability of firing-responses. (A) Fano factors were calculated by dividing the variance (σ^2) by the mean firing rate (μ) of every neuron from each pair at original (left) and new optimal (right) orientations. This factor increased from 0.49 to 0.57 for the original preferred orientation (paired two-tailed *t*-test, $p<0.05$) and decreased from 0.58 to 0.48 for the new preferred orientation (paired two-tailed *t*-test, $p<0.05$). (B) Gaussian orientation tuning curves plotted from raw data of two neurons. (C) Probabilities values within each bin (7 ms) during the stimulus period of presentation (4.1 s) for the same neurons. We observed a large decorrelation for the original orientation ($R^2_{\text{pre-adaptation}}=0.6$, $R^2_{\text{post-adaptation}}=0.09$, top) whereas the correlation is stable for the new optimal orientation ($R^2_{\text{pre-adaptation}}=0.5$, $R^2_{\text{post-adaptation}}=0.8$, bottom).

orientation after adaptation. A typical example of response variability is shown in Fig. 4B and C; Gaussian tuning curves of two neurons are illustrated in Fig. 4B, the common preferred orientation for both cells is a 45° angle prior to adaptation. The new optimal orientation coincides with a vertically oriented angle (90°, which corresponds to the adapting orientation indicated by a black arrow in the plot) for both units post-adaptation. Probability values within each bin (7 ms) are plotted along the stimulus period of presentation (4.1 s) in Fig. 4C. These plots illustrate the large decorrelation for the original orientation ($R^2_{\text{pre-adaptation}}=0.6$, $R^2_{\text{post-adaptation}}=0.09$, top), whereas the correlation is conserved (stable) for the new optimal orientation ($R^2_{\text{pre-adaptation}}=0.5$, $R^2_{\text{post-adaptation}}=0.8$, bottom).

2.5. *Relationship with neuronal behavior*

Adapting neurons to a non-preferred stimulus leads to two major effects on the orientation tuning curves. Neurons acquire a new optimal orientation close to the adapter in an attractive shift. The second effect is a shift away from the adapter. Despite the fact that adaptation maintains the functional connectivity by rebalancing the excitation–inhibition and maintaining this ratio, we observed significant differences between attracted and retracted conditions (Fig. 5). Indeed, for the original optimal orientation (Fig. 5A), the new optimal orientation (Fig. 5B), and the adapting orientation (Fig. 5C), the CCG-magnitude was superior for attracted neurons (paired two-tailed *t*-test, $p<0.05$). This result may indicate a predictive effect of the neuronal behavior by estimating the strength of connectivity between neurons.

2.6. *Spike waveforms and tuning bandwidth*

Cortical processing involves a necessary interplay between different neuronal types. Two major classes of neurons are classically distinguished: regular-spiking and fast-spiking cells (Bachatene et al., 2012; Bortone et al., 2014). Fast-spiking neurons were identified by a narrow spike waveform (trough-to-peak time less than 0.5 ms, Fig. 6A) whereas regular-spiking neurons had a longer trough-to-peak interval (greater than 0.5 ms, Fig. 6A) (Bortone et al., 2014). An example of two neurons is shown in Fig. 6B indicating the respective spike wave-shapes of each neuron. The crosscorrelation computations were carried out between regular spiking neurons, between fast spiking neurons, and between both types of neurons. No significant difference was observed between cell types, that is, visual adaptation rebalances the functional connectivity strength among neurons by maintaining the global connectivity strength within neuronal networks made of regular-spiking and fast-spiking neurons (Fig. 6C).

Neurons in area 17 are remarkably selective for orientation (Hubel and Wiesel, 1959). The sharpness of orientation selectivity can be gauged by measuring the bandwidth at half height of the orientation Gaussian tuning curve (Moore et al., 2005;

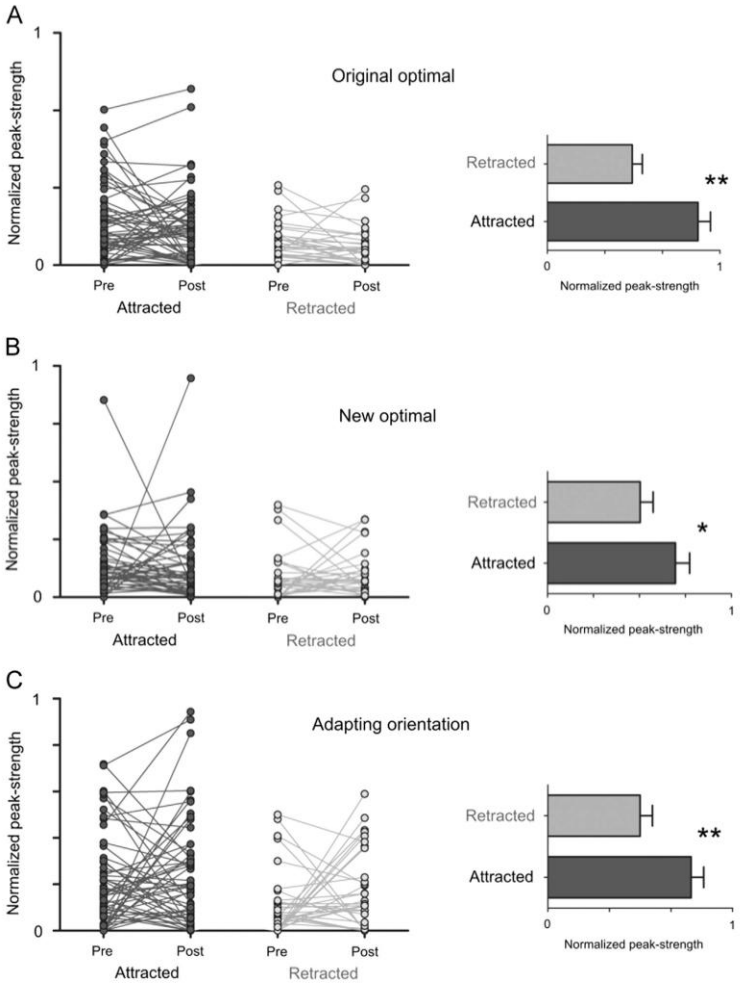

Fig. 5 – Relationship to neuronal behavior. (A) Differences of peak-strength pre- and post-adaptation between attracted and retracted neurons at the original optimal orientation. Histograms on the right side represent the average. The results demonstrate significant differences between attracted and retracted neurons (higher peak-strength for attracted neurons). (B and C) Similar to A for new optimal orientation and adapting orientation, respectively.

Ringach et al., 2002). In the next analyses, we compared the peak-strength-modulation in relation to the tuning bandwidth. Fig. 6D shows the changes in the latter before and after adaptation. Cell-classes are grouped depending on whether, following adaptation, the peak-strength decreased (red dots) or increased (green dots). Note that original and new optimal orientations are used as peak markers for tuning curves. Overall, the tuning bandwidth at half magnitude (FWHM: full width at half magnitude) is slightly diminished. Interestingly, the narrowest bandwidth belongs to a particular group of neurons exhibiting the largest augmentation in the peaks-strengths (bandwidth values: green dots, original preferred orientation, non-significant from 29.41 to 21.20, new optimal orientation significant from 26.47 to 17.33, non-parametric Mann–Whitney test, $p<0.05$, see Fig. 6D, right, green dots). Such a decrease strongly implies that adaptation induces the development of a jointly novel preferred orientation with a finer tuning curve. In addition, this specific group of cells exhibited the strongest enhancement of the peak-strength suggesting a closer time relationship between spike trains of involved cells.

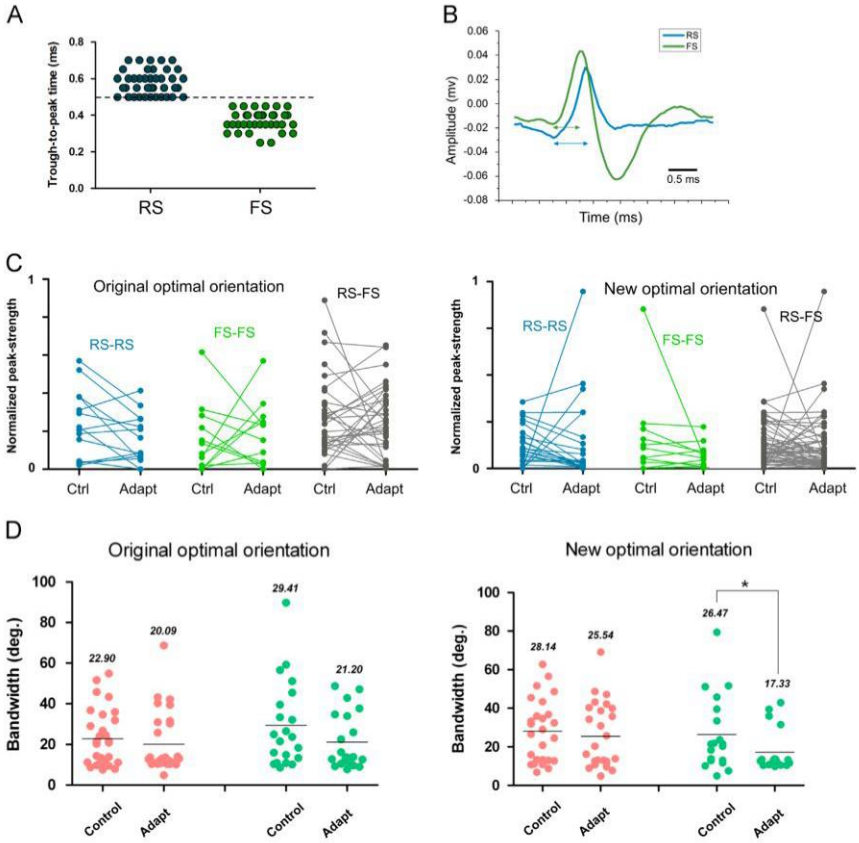

Fig. 6 – Spike wave-forms and tuning bandwidth. (A) Separation of spikes based on trough-to-peak time, regular spikes had a trough-to-peak time greater than 0.5 ms (blue dots) and fast spikes had a smaller value (inferior to 0.5 ms, green dots). (B) Example of two neurons with two different spike-shapes (blue unit: regular-spiking cell, green unit: fast-spiking cell). (C) Peak-strength modulation of all possible groups (RS–RS: blue plots, FS–FS: green plots, RS–FS: gray plots). No significant difference was observed between these spike-types. (D) Connection probability and tuning bandwidth. Tuning bandwidths measured (full width at half magnitude) for the original and the new optimal orientations. Neuronal pairs were classified in relation to the augmentation (green dots) or the diminution (red dots) of the peaks-strengths post-adaptation. The higher decrease of bandwidth is occurring for new optimal orientation (26.4° to 17.3°, Mann–Whitney test, 95% significance level, $p<0.05$). (For interpretation of the references to color in this figure legend, the reader is referred to the web version of this article.)

2.7. *Dynamics of a microcircuit: Restructuring the neuronal assembly by adaptation*

In previous sections, we demonstrated that the relationships between cells are modulated by adaptation. Indeed, some functional connections are strengthened while others are weakened, as revealed by CCG analyses. These modifications occur while both cells shift their preferred orientation to exhibit an almost identical new optimal orientation.

In the next section, we expand our analysis by constructing a peak-strength-matrix in a homogenous population, i.e., a group of simultaneously recorded neurons responding to the same original preferred stimulus and shifting their tuning curves after adaptation to the same new preferred orientation. Fig. 7 illustrates a typical example of a cluster of five cells recorded simultaneously and constituting a microcircuit with putative projections corresponding to the strength of connectivity as derived by crosscorrelation data. In Fig. 7A, orientation tuning curves (error bars indicate the standard error of the mean) and Gaussian fits of all cells are shown with their respective spike-waveforms (color codes apply to all the parts of this figure, where the black lines of spike waveforms specify the template window of spike sorting). All five cells responded similarly to the same optimal orientation (45° angle) before adaptation. After adaptation (orientation of the adapter equals 90°), a 90° oriented angle eliciting the highest discharge rate

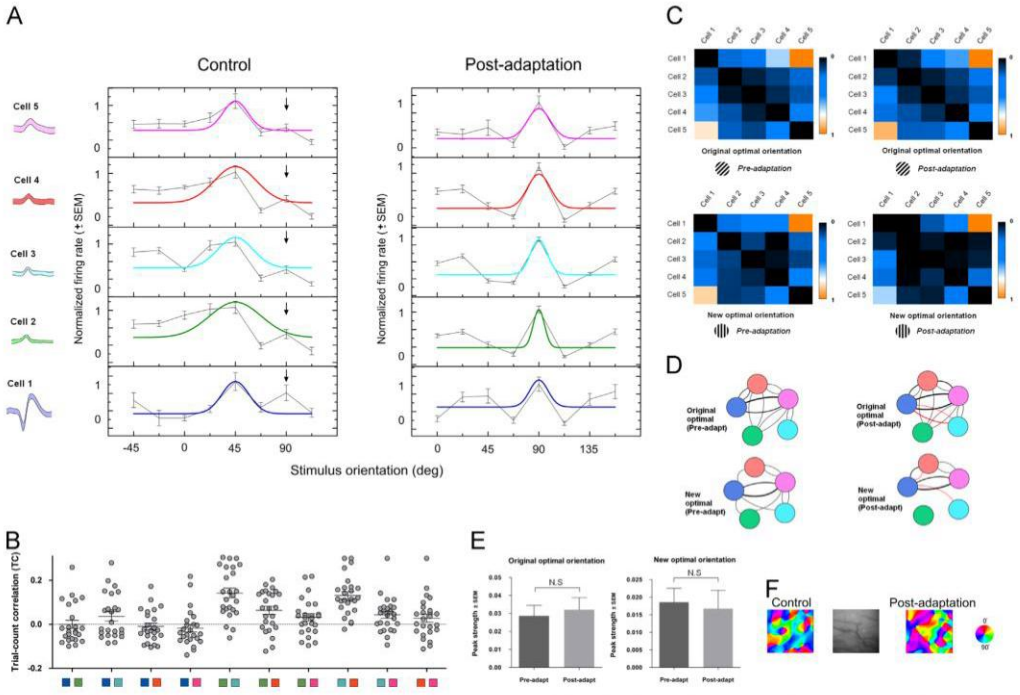

Fig. 7 – Cell-assembly computations. (A) Orientation tuning curves and Gaussian fits of five neurons (respective waveforms shown on the left) recorded simultaneously and responding preferentially to 45° grating before adaptation. All neurons shifted their original optimal orientation to reach 90° grating (corresponding to the adapter, downward black arrow in the plots), error bars in the tuning curves indicate standard error of the mean. (B) Cluster separation of all five neurons using the Trial-count correlation (*TC*), scatter plots are displayed for each neuronal pair of the entire group, mean *TC*'s values are indicated by the horizontal bars. (C) Connectivity matrices of peak-strengths for original optimal orientation at control condition (top left) and post-adaptation (top right), and for the new optimal orientation at control (bottom left) and post-adaptation (bottom right). Colored scale indicates the normalized peaks-strengths. (D) Putative connections plotted from the matrices indicating the strength of connectivity (thickness of projections); red lines indicate newly formed connections after adaptation. (E) Comparative histograms of averaged peaks-strengths for the entire matrices between both conditions for original optimal orientation (top) and new optimal orientation (bottom). (F) Example of an orientation-map generated using optical imaging. It shows the changes of the entire map post-adaptation. (For interpretation of the references to color in this figure legend, the reader is referred to the web version of this article.)

corresponds to the new acquired preferred orientation. Fig. 7B illustrates the trial-count correlation computations (*TC*) for all possible pairs among the cluster, the mean *TC* values are indicated by horizontal bars. The exceedingly weak values indicate that spike trains originate from distinct cells (see methods for details). The matrices comparing the peaks-strengths are displayed in Fig. 7C. Adaptation modified the structure of the matrices; some connections are strengthened while others are weakened, and few remain unchanged (for example, cell 1–cell 5 pair, see Fig. 7C; cell 1 projects on cell 5 almost with equal peak-strength pre- and post-adaptation, whereas cell 5 reverse projects with varying peak-strength before and after adaptation). The values of probabilities are indicated by the color scale on the right of each matrix. These matrices allowed plotting cell-assemblies for each case and each orientation of interest. Indeed, the linkage between similarly selective neurons within a group is modified as some connections emerge, while others are inhibited and some cells were functionally disconnected, for instance the green cell. Fig. 7D shows a microcircuit of the presented neurons putatively connected, red lines represent the newly formed projections after adaptation (in the displayed network, the red connection indicated the change of direction from cyan cell to blue cell) and the thickness of lines highlights the strength of projections between units.

Furthermore, for the same cell-assembly, we averaged the peaks-strengths of all connections for both orientations, in order to compare the global strength of functional connectivity between the same assembly prior to and post-adaptation (Fig. 7E). The mean values for the peaks-strengths of matrices

were not significant for both orientations (paired two-tailed *t*-test, $p=0.21$ and 0.39 for original optimal and new optimal orientations, respectively).

This analysis underscores the following: adapting cells to a non-preferred orientation induces two major effects; first there is a change of the preferred orientation and second there is a modification of the connectivity of the neuronal network and consequently its dynamics. Overall, connectivity strength is maintained and redistributed to different neurons for the broadcast of the learned feature. An example of changes of an orientation polar map is shown in Fig. 7F with a new orientation-configuration established post-visual adaptation (Cattan et al., 2014).

3. Discussion

We examined functional time-relationships between spike trains of primary visual cortical neurons by computing cross-correlation analyses for specific pairs of cells stimulated visually. Pairs of neurons were selected on the basis of their similar orientation-selectivity axis and post-adaptation behavior which lead to acquiring of same preferred orientation (for both neurons) after we imposed a visual "training" to non-preferred grating for 12 min. Crosscorrelogram data processing is a powerful in-situ tool for establishing the functional interactions between cells within sensory systems by indicating time-delay spiking activity between two neurons, where one neuron's spikes are set as reference to another neuron's spikes (target); therefore, it indicates putative functional projections between cells when it displays significant peaks within a short time-window reflecting direct functional relationships (Bartho et al., 2004; Denman and Contreras, 2013; Fujisawa et al., 2008; Konig et al., 1995; Perkel et al., 1967). In this report, we aimed to investigate the linkage dynamics between neuron-pairs prior and post-visual adaptation to a non-preferred oriented grating in order to reveal the extent of changes in neuronal connectivity after cells adopted new orientation-selectivity. Adaptation induced the following main results: the peaks-strengths that reflect cellular connectivity are disturbed and recalibrated after adaptation. Furthermore, the highest increase of the peak-strength belonged to cells that exhibited the sharpest bandwidth. In conclusion, there is an emergence of a novel sub-network after adaptation.

3.1. *Methodological considerations*

It was important to ask whether the disclosed functional connections were due to some physiological parameters such as anesthesia or attention. The brain state of an anesthetized animal might control the number of responsive neurons and the magnitude of the firing rate. Rhythmic oscillations which permit the synchronization of neuronal population may also be recorded in an anesthetized state (Poulet and Petersen, 2008). Moreover, the sequence of stimuli presentations is unrelated to the spontaneous oscillatory activity of cortical rhythms of the anesthetized animals (Xing et al., 2012). Furthermore, the stimuli were applied in a random fashion with inter-stimulus time intervals varying from 1 to 3 s. Since the recordings were done in the anesthetized cats, the response output of the cells for the presented stimulus cannot be attributed to the attention parameters (de Kock and Sakmann, 2009).

Time-relationships between action potentials of neurons in the circuits may go undetected due to low firing rates of neurons; however, this does not necessarily mean that temporal locking of neurons cannot be elicited with low firing rates of neurons. It has been demonstrated that the firing rates and peaks in CCG's are unrelated (Duret et al., 2006; Rolls and Treves, 2011; Shumikhina et al., 2004).

In addition to the classical cells' isolation using spike waveshapes, principal component analyses, and autocorrelation, it was important to ascertain that the isolated cells emerged from distinct templates; therefore we performed trial-count-correlation (*TC*) between every possible pair of neurons in order to compare the firing pattern between cells. To this aim, we used a 1 ms resolution. All correlations had a value inferior to 0.25 which ascertains that spike-trains emerged from different cells. Furthermore, we carried out these count correlations on a time-window of 4.1 s across all trials that corresponded to the presentation of the stimuli. Given that we divided the 4.1 s epoch into 1 ms time-bins (1 ms resolution), the probability of synchronous spikes in the same template within this short time-window is exceedingly low.

3.2. *Crosscorrelation and functional connections*

Crosscorrelation computations have been used in neurophysiological analyses in order to reveal functional linkages between spike trains of two neurons recorded simultaneously (Perkel et al., 1967). A synaptic connection can be attributed to correlation only under certain circumstances (Reid, 2012), however, a time-relationship between the firing activity two neurons may be considered as a clue to temporal projections between two cells as the temporal delay in the crosscorrelograms may suggest modifications in wiring. Temporal connections can be demonstrated by an increase in the firing probability of the postsynaptic neuron (Bharmauria et al., 2014; Reid, 2012).

A typical CCG is generated with the aim of disclosing the significance level and strength of connectivity between two cells within a specific time-frame. Depending on the peak-position in the CCG's, the analyses revealed the spike timing of both neurons in relation to each other. However, it is worth noting that a typical CCG may lead to biased significant peaks due to the co-stimulation of both neurons at each trial of the stimulus cycle. In order to circumvent and lessen this potential bias, we employed the shuffling minus subtraction algorithm based on neuron firing rates, and subtracted it from the raw CCG's which eliminated evoked firing (Dong et al., 2008).

We examined neuronal connectivity between cell-pairs within a time-window of ± 5 ms primarily to unveil putative direct synaptic connections between cells. It has been demonstrated in the macaque MT area that neuronal crosscorrelation between pairs of cells is mostly short-termed within a time-window of 10–100 ms (Bair et al., 2001). Though in several investigations various time-windows have been taken into consideration ranging from 3 ms to 10 ms (Bartho et al., 2004) to reveal the functional connections between the involved neurons, nonetheless a time window of ± 5 ms is most frequently used and is reasonably short.

In addition to disclosing functional projections between neurons, the crosscorrelation technique allows for the evaluation of the strength of neuronal connectivity (through peak-strength) as it is significant in understanding variations of cell-assemblies in response to experience (Bock et al., 2011). We investigated the changing of probability-indices prior to and after visual adaptation in order to uncover the modulation mechanisms of neuronal relationships (see next section for details). Indeed, this adaptation process leads to modifications of neural spiking activity attributed to push-pull mechanisms (Bachatene et al., 2012; Bachatene et al., 2013; Ghisovan et al., 2009; Kohn and Movshon, 2004). It has been demonstrated previously that long adaptation of neurons to a non-preferred stimulus, which is orientation in our experiments, for the most part leads to a decrease in firing activity for the original optimal orientation, and in contrast, a firing increase for the new preferred orientation (Bachatene et al., 2012, 2013; Ghisovan et al., 2009). It was relevant to explore whether the probability modulation of neuronal connectivity is related to the firing rates of neurons, as previously shown. However, we found no significant correlation between the peak-strengths and the firing rates in our results, as previously described (Duret et al., 2006; Ghisovan et al., 2008; Rolls and Treves, 2011). In addition, results indicated no relationship between spike waveforms which are attributed to specific putative cellular types, and peak strength fluctuations post-adaptation.

3.3. *Neuronal connectivity and orientation-selectivity*

Neurons within the primary visual cortex are "orientation-detectors", and respond maximally to a properly oriented stimulus presented in their receptive field (Hubel and Wiesel, 1959). Several studies have demonstrated the ability of V1 neurons to adjust their stimulus-selectivity in order to restructure the primary visual cortex as an "adapted cortex" to the imposed visual environment by a persistent adaptation to a specific stimulus. For instance, such modifications have been reported for orientation (Bachatene et al., 2012, 2013; Dragoi et al., 2000; Ghisovan et al., 2009; Kohn and Movshon, 2004), spatial frequency (Marshansky et al., 2011), direction of motion (Kohn and Movshon, 2004) and speed (Movshon, 1975). By changing their preferred features, neurons acquire new optimal properties for a short or long period of time depending on the visual training duration (Bachatene et al., 2013; Ghisovan et al., 2009; Patterson et al., 2013). In V1, cells are scattered within cortical domains and connected to each other laterally and vertically. Horizontal connections are characterized as long range connections between neurons preferring similar stimulus features (Das and Gilbert, 1995; Sompolinsky et al., 1990) which are functionally connected to each other at large distances (Hata et al., 1991; Ts'o et al., 1986). Vertical connections are described as inputs to layers II and III from layer IV of the visual cortex (Stratford et al., 1996; Yoshimura et al., 2000) which receives its inputs from LGN (Alonso et al., 1996). From layers II and III, the connections descend to layers V and VI (Stratford et al., 1996).

As suggested by crosscorrelogram analysis, neuronal connectivity has been reported to be high between cells with similar preferred parameters due in part to specific connections between cortical domains having similar tuning properties (Alloway and Roy, 2002; Alonso et al., 1996; Bartho et al., 2004; Csicsvari et al., 1998; Yoshimura et al., 2005). Indeed the correlation between neurons sharing reciprocal tuning properties is well established (Kohn and Smith, 2005; Zohary et al., 1994). Neuronal connections within the cortex are very specific, mostly depending on the properties of the responses of neurons (Alonso, 2002). For instance, in macaque visual cortex, it has been shown that correlation varies with stimulus condition and this variation is stronger between neurons sharing similar direction tuning curves (Bair et al., 2001). In mouse primary visual cortex, it has been reported that significant pair-wise synchrony is related to orientation preference between neurons (Denman and Contreras, 2013). Neuronal connectivity can also be related to specific stimulus preference; it has been demonstrated that in mouse visual cortex, the similarity of neuronal activity to a specific feature of the stimulus affects the connection-probabilities; for example, neurons sharing similar selectivity for oriented stimuli exhibit more connectedness with each other than neurons having orthogonal orientation selectivity (Ko et al., 2011).

These findings provide evidence that stimuli features influence the temporal pattern of neuronal activity (Gray et al., 1990). Nevertheless, following plastic modifications, connectivity patterns among neuronal pairs in V1 have yet to be explored. In the present paper, we sought to examine how the peaks-strengths calculated from crosscorrelation analyses between pair-wise neurons sharing stimulus-feature selectivity are modulated following a long duration visual "training."

Following the critical period, neurons programmed to connect to distinctive neurons that share homogenous orientation-selectivity start responding to a new acquired orientation after visual adaptation, and therefore switch on to connect a different neuronal population to participate in a different sub-network of cells. Indeed, some authors have demonstrated in mouse visual cortex a reorganization of the connectivity configuration. This is related to a higher proportion of links between neurons with similar visual responses, while connections were eliminated between visually unresponsive units, yet the overall connectedness remained unchanged (Ko et al., 2013).

Although peaks-strengths on average were not significantly different, individual pairs appeared to increase or decrease their respective peaks, suggesting that the adaptation process redeploys the strength of projections between neurons to restructure the entire linkage-dynamic of the neuronal population in response to the changing stimuli environment. For instance, the forceful presentation of a particular stimulus (a different orientation in our experiments) results in the disappearance of some relationships and the appearance of new projections. Understanding the temporal relations between neurons within sub-networks could help us to decipher how visual processing is altered under specific changes of environmental conditions and how the plastic capacity of neuronal networks lead to the acquisition of new features. Although our stimulation conditions are artificial (stimulus exposure), it still mimics training or forcing cells to respond to a particular trigger feature which in turn, may serve as basis for learning process.

An alternative possibility may be hypothesized. Neurons are connected with excitatory (*E*) and inhibitory (*I*) fibers and their spiking output is the net outcome of these antagonistic influences. Thus adaptation may strengthen and weaken excitatory and inhibitory connections, respectively, in order to unlock cellular time-relationships in involved cortical areas whereby a new *E–I* equilibrium might be considered as a possible scenario for the neuronal variability dynamic after visual adaptation. The fluctuations of neuronal alterability due to adaptation effects may rebalance the *E–I* ratio and contribute to the stability of the total inter-neuronal variability (Kasamatsu et al., 2001). It has been shown in layers 2/3 of the mouse visual cortex that *E–I* ratios are equalized across pyramidal cells (Xue et al., 2014). Our results are in concordance with the equalization of excitation–inhibition ratios after adaptation (Fig. 7D and E).

This is in line with recent findings which assign an important contribution of adaptation to neuronal homeostasis within a population of cells sharing neuronal response uniformity, as well as visual feature selectivity (Benucci et al., 2013). We reported that adaptation restructures the neural code following plasticity by maintaining the connectivity strength within the cellular network and redistributing this linkage to different neurons within the assembly (see Fig. 7D and E). In models of cross-orientation, feature-selectivity is induced by inhibitory connections between cells with different orientation preferences (Alonso, 2002). Furthermore, it has been shown that in relation to differences in orientation-selectivity between two neurons, excitatory, inhibitory and common input correlations occur mostly in neuronal pairs with a difference of orientation preference inferior to 45° (Hata et al., 1991). Moreover, adaptation may provide a 'window of opportunity' for recipient neurons to modify excitatory/inhibitory balance in order to reorganize the spiking cortical activity (Stanley, 2013). Indeed, complex feedforward-feedback mechanisms emerge within the primary visual cortex in order to reorganize the signal processing following plasticity (Fahle, 2004).

Therefore, we postulate that orientation-selective neuronal pairs modify the strength of connections following adaptation in order to recalibrate the neural code.

Such rapid changes may not be accounted by structural modifications, there are most likely due to modification of equilibrium between excitation and inhibition influences to a recorded cell which allows silent synapses to become effective. For instance, in mouse visual cortex, it has been demonstrated that a single dendritic branch receive synaptic drives from a large spectrum of orientations (Jia et al., 2010).

Excitatory and inhibitory cells coordinate time-related firing activity to maintain the neuronal population output during visual information processing.

4. Conclusion

Visual adaptation of neurons to non-optimal stimuli suggests the adaptability of neuronal code to visual stimuli. In the primary visual cortex, neurons respond in coordination with neighboring cells to the trigger features, and encode stimuli properties by constituting cell assemblies (Kampa et al., 2011; Lee and Reid, 2011; Wallace and Kerr, 2010) wherein cells are anatomically connected by forming synaptic contacts or by interacting through synchronous time-relationships. To reveal how this local circuitry of different neurons in the visual cortex is set up and modulated in response to different visual stimulation conditions is of prime importance to understanding the mechanisms of information processing.

5. Experimental procedures

5.1. *Ethical approval*

Animal surgery procedures and electrophysiological recordings followed the guidelines of the Canadian Council on Animal Care and were approved by the Institutional Animal Care and Use Committee of the University of Montreal. Animals were supplied by the Division of Animal Resources of the University of Montreal. The experiments were conducted in accordance with the Guide for Care and Use of Laboratory Animals of the National Institutes of Health (USA).

5.2. *Animal surgery*

Electrophysiological recordings were performed using multi-electrodes within V1 area of adult domestic cats (*Felis catus*). Eleven adult cats (2.5–3.5 kg, age 12–24 months) of either sex, sedated with acepromazine maleate (Atravet, Wyeth-Ayerst, Guelph, ON, Canada; 1 mg kg^{-1}, intramuscular) and atropine sulfate (ATRO-SA, Rafter, Calgary, AB, Canada; 0.04 mg kg^{-1}, intramuscular), were anesthetized with ketamine hydrochloride (Rogarsetic, Pfizer, Kirkland, QC, Canada; 25 mg kg^{-1}, intramuscular) maintained with 0.3% isoflurane (AErrane, Baxter, Toronto, ON, Canada). Lidocaine hydrochloride (Xylocaine, AstraZeneca, Missis-sauga, ON, Canada; 2%) was injected subcutaneously as a local anesthetic during surgery. A tracheotomy was performed for artificial ventilation, and one forelimb vein was cannulated. Animals were then placed in a stereotaxic apparatus. Xylocaine gel (Astra Pharma, Mississauga, ON, Canada; 5%) was applied on the pressure points. For the remaining preparations and recording, paralysis was induced with 40 mg and maintained with 10 mg kg^{-1} h^{-1} gallamine triethiodide (Flaxedil, Sigma Chemical, St. Louis, MO, USA; intravenous) administered in 5% dextrose lactated Ringer's nutritive solution. General anesthesia was maintained by artificial ventilation with a mixture of N_2O/O_2 (70:30) supplemented with 0.5% isoflurane (AErrane, Baxter, Toronto, ON, Canada) for the duration of the experiment. Proper depth of anesthesia was ensured throughout the experiment by monitoring the EEG, the electrocardiogram and expired CO_2. In addition the heart rate remained unmodified after skin stimulation. The end-tidal CO_2 partial pressure was kept constant between 25 and 30 mmHg. A heated pad was used to maintain a body temperature of 37.5 °C. Tribrissen (Schering-Plough, Pointe-Claire, QC, Canada; 30 mg kg^{-1} per day, subcutaneous) and Duplocillin (Intervet, Withby, ON, Canada; 0.1 ml kg^{-1}, intramuscular) were administered to the animals to prevent bacterial infection. The pupils were dilated with atropine sulfate (Isopto-Atropine, Alcon, Mississauga, ON, Canada; 1%)

and the nictitating membranes were retracted with phenylephrine hydrochloride (Mydfrin, Alcon, Mississauga, ON, Canada; 2.5%). The loci of the area centrales were inferred from the positions of the blind spots, which were ophthalmoscopically focused and back projected onto a translucent screen. In order to verify the stability of the eye this procedure was repeated at the end of tests. Plano contact lenses with artificial pupils (5 mm diameter) were placed on the cat's eyes to prevent the cornea from drying (University of Montréal, PQ, Canada).

At the end of each experiment, euthanasia was achieved with a lethal dose of pentobarbital sodium (Somnotol, MTC Pharmaceuticals, Cambridge, ON, Canada; 100 mg kg^{-1}) by intravenous injection.

5.3. *Electrophysiology*

Multi-unit activity in the primary visual cortex was carried out with tungsten microelectrode (Frederick Haer & Co, Bowdoinham, ME, USA; 2–10 MΩ at 1 kHz). Each set of electrodes, consisting of a four microelectrode in linear array (inter-electrode spacing of 400 μm) enclosed in stainless steel tubing, was controlled by a separate micromanipulator. The signal from the microelectrodes was amplified, band-pass filtered (300 Hz–3 kHz), digitized and recorded with a 0.05 ms temporal resolution (Spike2, CED, Cambridge, England). We recorded at an average of 400–500 μm cortical depth from two recording sites (Average of three neurons recorded per electrode per session). Action potentials were sorted out using a window discriminator for further off-line analyses. Multiunit signals from one electrode included well-isolated single units. The spike sorting method was based on cluster classification in reduced space (Spike2, CED). The stability of each cell's activity across conditions was verified qualitatively by visual control of the clusters disposition and of the waveforms shape. Autocorrelograms and principal component analysis were systematically performed to insure proper single cell capture (refractory period for autocorrelograms). Spike-count correlation was used to ascertain that spikes emerged from different neurons. 85% of neurons were included in the data analyses.

5.4. *Visual stimulation*

Stimulation was monocular (dominant eye, the opposite eye was shut). After clearly detectable activity was obtained, the multiunit receptive fields (RF) were mapped as the minimum response fields (Barlow et al., 1967) by using a hand-held ophthalmoscope. RF edges were determined by moving a light bar from the periphery toward the center until a response was elicited. Eye-screen distance was 57 cm. These preliminary tests revealed qualitative properties such as dimensions, velocity preference, orientation and directional selectivity. Visual stimuli were generated with a VSG 2/5 graphic board (Cambridge Research Systems, Rochester, England) and displayed on a 21-in. monitor (Sony GDM-F520 Trinitron, Tokyo, Japan) placed 57 cm from the cat's eyes, with 1024 × 768 pixel, running at 100 Hz frame refresh. Stimuli were drifting sine-wave grating patches (~2° to 5°) covering the excitatory RF (Maffei and Fiorentini, 1973). Patches characteristics were set to evoke optimal responses: contrast at 80%, mean luminance at 40 cd m^{-2}, optimal spatial and temporal frequencies set within the 0.1–0.5 cycles/deg. and 1.0–2.0 Hz range, respectively. The blank screen was uniformly gray (~35 cd m^{-2}). In all cases the above parameters were chosen with the aim of evoking the maximal discharges. V1 neurons are known to respond well to sine wave drifting gratings (Bardy et al., 2006). After manual RF characterization, nine oriented stimuli centered on the preferred orientation were selected and used for the rest of the experiment. With a 22.5° interval between orientations, tuning curves covered 180°. Test orientations were applied in random order. Each oriented stimulus was presented in blocks of 25 trials lasting 4.1 s each, with a random inter-trial interval (1.0–3.0 s) during which no stimuli were presented. Thus, a recording session lasted for 25–30 min. Peri-stimulus time histograms were recorded. Once control orientation tuning curves were characterized, an adapting non-preferred stimulus was presented continuously for 12 min. The adapting stimulus was a drifting grating whose orientation was randomly selected in the range 22.5 to 67.5° off of the neuron's preferred orientation (Fig. 8A). All other stimulus parameters were kept constant, at control values, throughout the recordings. During this adaptation period no recordings were performed. Immediately after adaptation, orientation tuning curves was measured starting with the adapting and control preferred orientations to prevent an unlikely premature recovery, as these two orientations were the center of interest, while the remaining orientations were recorded in random order.

5.5. *Cells' isolation*

Given that the multi-unit activity was recorded concurrently from same tips using multi-electrodes, it was essential to ascertain that cells were well isolated, because the same unit may exhibit sufficiently different waveforms (for instance magnitude in relation to distance between recording tip), and thus belong to different clusters in principal component analysis. Cell-separation was based on spike-waveforms, cluster-isolation using first principal components analyses, autocorrelograms and trial-count correlation (*TC*). Cluster analysis was performed using Spike2 (CED, Cambridge, England) in a 3-dimensional plot. The isolation distance was calculated using the Mahalanobis distance; it defines boundaries of constant probability around the multi-dimensional center of the distribution. This estimation allows the separation of a cluster from the nearest cluster. All clusters within Mahalanobis distance of 2.5 were considered for analysis (Bharmauria et al., 2014).

Trial-count correlation (*TC*) denotes the trial by trial Pearson correlation-coefficient between simultaneously recorded firing of two neurons in response to the presentation of the identical stimulus. In response to the same grating, the same unit fires identically regardless of spike amplitude. In order to eliminate such occurrences, we correlated neural activities of each cell-pair for every applied trial (25 trials, same stimulus, duration 4.1 s). Given that optimal orientations eliciting maximal firing rates were chosen for this computation as well as a relatively long time-window analysis (4.1 s), we would have expected a high value for correlation if it had been the same unit, because such a time-window analysis is sufficiently large

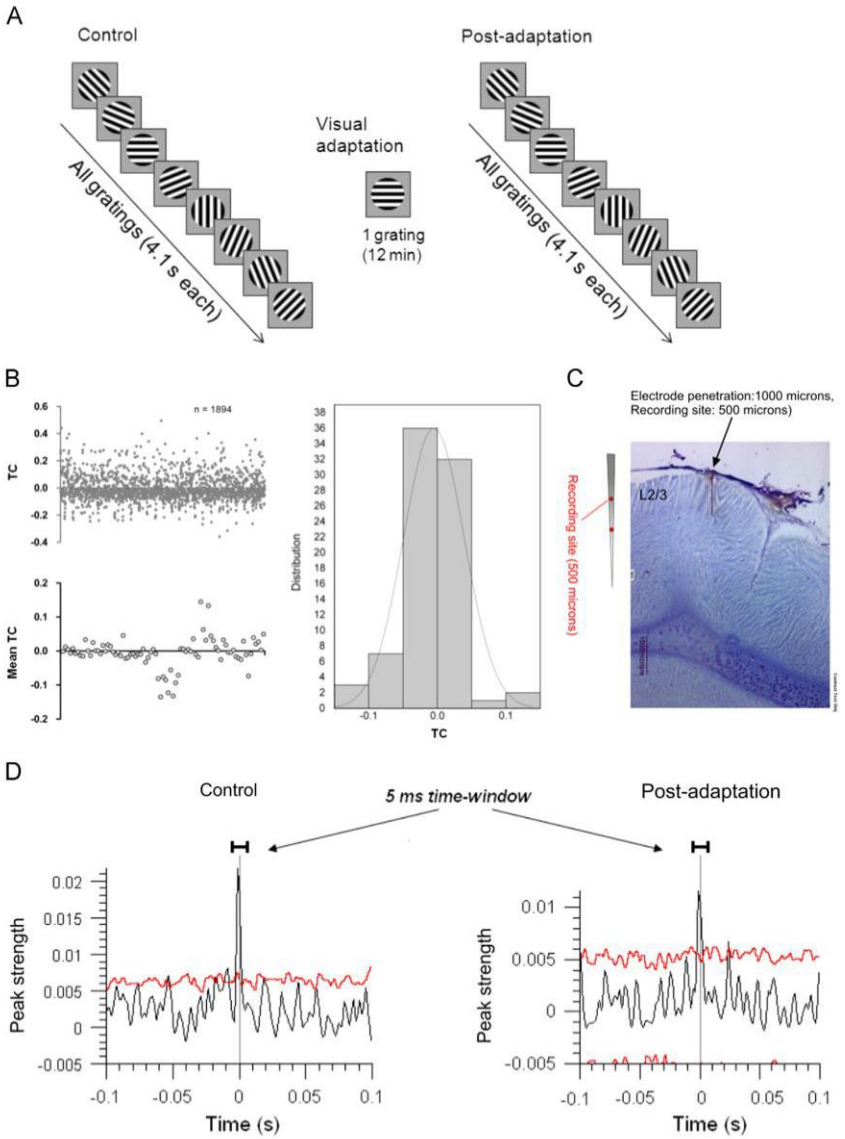

Fig. 8 – Visual stimulation, cell separation and crosscorrelation. (A) Time course stimulus. Left: control condition, 8 orientations presented in random order within the receptive fields of recorded neurons in 25 trials (4.1 s each trial, 1–3 s interval time). Middle: one grating (non-preferred orientation in control) is presented continuously (12 min). Right: post-adaptation condition, all orientations are projected as in the control step. (B) Trial-count correlation (*TC*). Upper left side: *TC* values for all trials ($n=1894$) accumulated over all selected neuron-pairs. Downer left side: averaged *TC* values for each cell pair ($TC=-0.005$). Right side: histogram-distribution of the averaged *TC* for each neuronal pair, gray curve represents the normal distribution curve. (C) Histological brain slice showing the electrode penetration and the recording site. (D) Examples of crosscorrelogram analyses indicating the ± 5 ms time range (time-delay of putative direct synaptic connections between cells). Red line indicates the 95% statistical threshold for the bin's significance; Y-axis shows the peak-strength computed from the counts/bin. (For interpretation of the references to color in this figure legend, the reader is referred to the web version of this article.)

to capture the full strength of correlation (Bair et al., 2001; Kohn and Smith, 2005; Reich et al., 2001). Indeed correlations would be underestimated if the counting window is too short (Cohen and Kohn, 2011). In spite of such conditions, the found correlations were exceedingly low (average $TC = -0.005$, see Fig. 8B). Pairs exhibiting correlations superior to 0.25 were eliminated from further analyses (as a general rule). This very weak correlation in spike response patterns (close to zero) indicates that the spikes arise from different units, hence the cells fire in an independent fashion. Fig. 8B illustrates the trial-count correlation analysis performed for the cells and recorded from the same electrode tip within each group.

Fig. 8B depicts the *TC* values for all trials ($n = 1894$) accumulated over all selected neuron-pairs (the average *TC* value for each cell pair equals to -0.005). The distribution of the average *TC* for each neuronal pair is shown in the figure (gray curve represents the normal distribution curve). The correlation values are clustered around zero and never exceed 0.25, which is in agreement with earlier published data (Cohen and Kohn, 2011; Ecker et al., 2010; Maruyama and Ito, 2013). This ascertains that firing patterns of the two selected neurons are different and ensures the cells' isolation.

Autocorrelograms preclude contamination by spikes of other units. Anesthesia and animal paralysis reduce the possibility of similar modulations of firing patterns in cells of same clusters due to rapid eye motion or attention (de Kock and Sakmann, 2009).

5.6. Data analysis and statistical computations

Once single cells were sorted out off-line from multi-unit spike trains accumulated during data acquisition, orientation tuning curves were constructed from raw data. Because orientation tuning is best described by Gaussian-like functions, we fitted our raw data with the von Mises function (Swindale, 1998). This allowed us to determine with precision the preferred orientation of neurons and then measure shifts in orientation preference. The von Mises function is defined as:

$$M(\theta) = A \times e^{b[\cos(\theta - c)]} + d$$

where *A* is the value of the function at the preferred orientation, *c*, and *b* is a width parameter. An additional parameter, *d*, represents the spontaneous firing rate of the cell (Kohn and Movshon, 2004; Swindale, 1998). The above calculations are necessary because tuning curves derived from raw data may be imperfect in determining the preferred orientation since the interval between the stimulus orientations is relatively large, 22.5°. In the cat, over 90% of V1 neurons are well tuned to stimulus orientation (Bishop and Henry, 1972). It was, however, necessary to ensure that cells in our sample were properly tuned for orientation. We measured an orientation selectivity index (OSI) by dividing the firing rate at orthogonal orientations by the firing rate for the preferred orientation, and subtracting the result from one (Liao et al., 2004; Ramoa et al., 2001). The closer the OSI is to one, the stronger the orientation selectivity. Adaptation induced shifts were measured as the distance between peak positions of the fitted tuning curves before and after conditioning. To assess the statistical significance of tuning shifts, curve fits were generated separately for each of the 25 trials, and the mean difference was tested by a paired *t*-test. Shifts in preferred orientation larger than 5° were statistically significant (paired sample two-tailed *t*-test, $p < 0.05$). Tuning bandwidths were calculated based on the full width at half magnitude of the Gaussian tuning curves. Statistical analyses were performed with Graphpad Prism (GraphPad Software Inc., La Jolla, California, USA). Student's *t*-tests were computed to compare the peaks-strengths between control and post-adaptation conditions, and to compare bandwidths between different classes. Ninety-five percent confidence-interval was used. Gaussian curves were fitted using the following equation:

$$y = y0 + \left(A \div \left(w \times \sqrt{\left(\frac{\pi}{2}\right)}\right)\right) \times e^{(-2\times((x-xc)/w)^2)}$$

where *y0* is the offset, *xc* is the center, *w* is the width and *A* represents the area.

Non-linear regression analyses were computed using this equation:

$$y = y0 + A1 \times (1 - e^{(-x/t1)}) + A2 \times (1 - e^{(-x/t2)})$$

where *y0* is the offset, *A1* and *A2* are the amplitudes, *t1* and *t2* are the widths.

5.7. Crosscorrelograms, shift predictor and confidence limits

We generated CCG's between simultaneously recorded spike trains of cell-pairs at specific orientations, i.e., the original optimal orientation and the new optimal orientation of each pair of neurons. Cell-pairs were selected based on their similarity of spiking discharge for these two preferred orientations using an orientation range of ±22.5°.

CCG's were performed in order to compare the spike distribution of each neuron of the pair within a time-frame; one neuron is set as reference and the second as target; this allows us to show the firing of the target neuron at a specific time-spread in relation to the firing of the reference neuron.

Time axis is divided into bins. The first bin is defined as: XMin, XMin+Bin. The next bin is XMin+Bin, XMin+Bin × 2, etc. We calculated the distances from each spike to all spikes of the spike train as follows:

$$d[i] = ts[i] - ref[k]$$

where *ts*[i] represents the spike train, and *ref*[k] is each timestamp.

Bin counts were then divided by the number of reference events to normalize the counts per bin into probabilities. Fig. 8D illustrates the parameters of CCG's; the red line represents the 95% statistical threshold for the significance of the bins. Each bin-width was set at 1 ms, Y-axis corresponds to the peak-strength calculated from the counts/bin as follows:

$$P = F \times b$$

where *F* is the neuron frequency and *b* represents the bin size of the calculated firing of the neuron (Abeles, 1982).

The neuron frequency *F* was calculated as follows:

$$F = \frac{N}{T}$$

where *T* represents the total time interval and *N* the number of spikes within this interval.

The 95% confidence limit was calculated assuming that the expected bin count (C) has a Poisson distribution:

$$C = P \times Nref$$

where *Nref* is the number of reference events.

The 95% confidence limit is calculated as follows:

$$\text{Low Conf.} = x \text{ such that Prob}\,(S < x) = 0.005$$
$$\text{High Conf.} = y \text{ such that Prob}\,(S > y) = 0.005$$

where S represents a random variable which has a Poisson distribution with parameter C.

The bins which fit into the ±1 ms around the center were classified as synchrony events (putative common afferent input to both neurons). Raw CCG's were corrected by subtracting a shift-predictor algorithm in order to eliminate the putative significant peaks due to the simultaneous stimulation of both cells during each trial. We used linear regression analysis with 95% confidence interval for the entire population of the recorded neuron-pairs to determine the modulation of the peak-strength for the two major specific preferred stimuli (original and newly acquired orientations).

Acknowledgments

This work was supported by grants to S.M.

The Natural Sciences and Engineering Research Council of Canada (Grant no. 6943-2010RGPIN). Fonds québécois de la recherche sur la nature et les technologies.

REFERENCES

Abeles, M., 1982. Quantification, smoothing, and confidence limits for single-units' histograms. J. Neurosci. Methods 5, 317–325.

Alloway, K.D., Roy, S.A., 2002. Conditional cross-correlation analysis of thalamocortical neurotransmission. Behav. Brain Res. 135, 191–196.

Alonso, J.M., Usrey, W.M., Reid, R.C., 1996. Precisely correlated firing in cells of the lateral geniculate nucleus. Nature 383, 815–819.

Alonso, J.M., 2002. Neural connections and receptive field properties in the primary visual cortex. Neuroscientist 8, 443–456.

Bachatene, L., Bharmauria, V., Rouat, J., Molotchnikoff, S., 2012. Adaptation-induced plasticity and spike waveforms in cat visual cortex. Neuroreport 23, 88–92.

Bachatene, L., Bharmauria, V., Cattan, S., Molotchnikoff, S., 2013. Fluoxetine and serotonin facilitate attractive-adaptation-induced orientation plasticity in adult cat visual cortex. Eur. J. Neurosci. 38, 2065–2077.

Bair, W., Zohary, E., Newsome, W.T., 2001. Correlated firing in macaque visual area MT: time scales and relationship to behavior. J. Neurosci. 21, 1676–1697.

Bardy, C., Huang, J.Y., Wang, C., FitzGibbon, T., Dreher, B., 2006. 'Simplification' of responses of complex cells in cat striate cortex: suppressive surrounds and 'feedback' inactivation. J. Physiol. 574, 731–750.

Barlow, H.B., Blakemore, C., Pettigrew, J.D., 1967. The neural mechanism of binocular depth discrimination. J. Physiol. 193, 327–342.

Bartho, P., Hirase, H., Monconduit, L., Zugaro, M., Harris, K.D., Buzsaki, G., 2004. Characterization of neocortical principal cells and interneurons by network interactions and extracellular features. J. Neurophysiol. 92, 600–608.

Benucci, A., Saleem, A.B., Carandini, M., 2013. Adaptation maintains population homeostasis in primary visual cortex. Nat. Neurosci. 16, 724–729.

Bharmauria, V., Bachatene, L., Cattan, S., Rouat, J., Molotchnikoff, S., 2014. Synergistic activity between primary visual neurons. Neuroscience 268, 255–264.

Bishop, P.O., Henry, G.H., 1972. Striate neurons: receptive field concepts. Invest. Ophthalmol. 11, 346–354.

Bock, D.D., Lee, W.C., Kerlin, A.M., Andermann, M.L., Hood, G., Wetzel, A.W., Yurgenson, S., Soucy, E.R., Kim, H.S., Reid, R.C., 2011. Network anatomy and in vivo physiology of visual cortical neurons. Nature 471, 177–182.

Bortone, D.S., Olsen, S.R., Scanziani, M., 2014. Translaminar inhibitory cells recruited by layer 6 corticothalamic neurons suppress visual cortex. Neuron 82, 474–485.

Cattan, S., Bachatene, L., Bharmauria, V., Jeyabalaratnam, J., Milleret, C., Molotchnikoff, S., 2014. Comparative analysis of orientation maps in areas 17 and 18 of the cat primary visual cortex following adaptation. Eur. J. Neurosci. 40, 2554–2563.

Cohen, M.R., Kohn, A., 2011. Measuring and interpreting neuronal correlations. Nat. Neurosci. 14, 811–819.

Csicsvari, J., Hirase, H., Czurko, A., Buzsaki, G., 1998. Reliability and state dependence of pyramidal cell-interneuron synapses in the hippocampus: an ensemble approach in the behaving rat. Neuron 21, 179–189.

Das, A., Gilbert, C.D., 1995. Long-range horizontal connections and their role in cortical reorganization revealed by optical recording of cat primary visual cortex. Nature 375, 780–784.

de Kock, C.P., Sakmann, B., 2009. Spiking in primary somatosensory cortex during natural whisking in awake head-restrained rats is cell-type specific. Proc. Natl. Acad. Sci. U.S.A 106, 16446–16450.

Denman, D.J., Contreras, D., 2013. The structure of pairwise correlation in mouse primary visual cortex reveals functional organization in the absence of an orientation map. Cereb. Cortex.

Dong, Y., Mihalas, S., Qiu, F., von der Heydt, R., Niebur, E., 2008. Synchrony and the binding problem in macaque visual cortex. J. Vis. 8 (30), 1–16.

Dragoi, V., Sharma, J., Sur, M., 2000. Adaptation-induced plasticity of orientation tuning in adult visual cortex. Neuron 28, 287–298.

Duret, F., Shumikhina, S., Molotchnikoff, S., 2006. Neuron participation in a synchrony-encoding assembly. BMC Neurosci 7, 72.

Ecker, A.S., Berens, P., Keliris, G.A., Bethge, M., Logothetis, N.K., Tolias, A.S., 2010. Decorrelated neuronal firing in cortical microcircuits. Science 327, 584–587.

Fahle, M., 2004. Perceptual learning: a case for early selection. J. Vis. 4, 879–890.

Fujisawa, S., Amarasingham, A., Harrison, M.T., Buzsaki, G., 2008. Behavior-dependent short-term assembly dynamics in the medial prefrontal cortex. Nat. Neurosci. 11, 823–833.

Ghisovan, N., Nemri, A., Shumikhina, S., Molotchnikoff, S., 2008. Synchrony between orientation-selective neurons is modulated during adaptation-induced plasticity in cat visual cortex. BMC Neurosci 9, 60.

Ghisovan, N., Nemri, A., Shumikhina, S., Molotchnikoff, S., 2009. Long adaptation reveals mostly attractive shifts of orientation tuning in cat primary visual cortex. Neuroscience 164, 1274–1283.

Godde, B., Leonhardt, R., Cords, S.M., Dinse, H.R., 2002. Plasticity of orientation preference maps in the visual cortex of adult cats. Proc. Natl. Acad. Sci. U.S.A 99, 6352–6357.

Gray, C.M., Engel, A.K., Konig, P., Singer, W., 1990. Stimulus-dependent neuronal oscillations in cat visual cortex: receptive

field properties and feature dependence. Eur. J. Neurosci. 2, 607–619.
Hata, Y., Tsumoto, T., Sato, H., Tamura, H., 1991. Horizontal interactions between visual cortical neurones studied by cross-correlation analysis in the cat. J. Physiol. 441, 593–614.
Hubel, D.H., Wiesel, T.N., 1959. Receptive fields of single neurones in the cat's striate cortex. J. Physiol. 148, 574–591.
Hubel, D.H., Wiesel, T.N., 1968. Receptive fields and functional architecture of monkey striate cortex. J. Physiol. 195, 215–243.
Jia, H., Rochefort, N.L., Chen, X., Konnerth, A., 2010. Dendritic organization of sensory input to cortical neurons in vivo. Nature 464, 1307–1312.
Kampa, B.M., Roth, M.M., Gobel, W., Helmchen, F., 2011. Representation of visual scenes by local neuronal populations in layer 2/3 of mouse visual cortex. Front. Neural Circuits 5, 18.
Kara, P., Reid, R.C., 2003. Efficacy of retinal spikes in driving cortical responses. J. Neurosci. 23, 8547–8557.
Kasamatsu, T., Polat, U., Pettet, M.W., Norcia, A.M., 2001. Colinear facilitation promotes reliability of single-cell responses in cat striate cortex. Exp. Brain Res. 138, 163–172.
Ko, H., Hofer, S.B., Pichler, B., Buchanan, K.A., Sjostrom, P.J., Mrsic-Flogel, T.D., 2011. Functional specificity of local synaptic connections in neocortical networks. Nature 473, 87–91.
Ko, H., Cossell, L., Baragli, C., Antolik, J., Clopath, C., Hofer, S.B., Mrsic-Flogel, T.D., 2013. The emergence of functional microcircuits in visual cortex. Nature 496, 96–100.
Kohn, A., Movshon, J.A., 2004. Adaptation changes the direction tuning of macaque MT neurons. Nat. Neurosci. 7, 764–772.
Kohn, A., Smith, M.A., 2005. Stimulus dependence of neuronal correlation in primary visual cortex of the macaque. J. Neurosci. 25, 3661–3673.
Konig, P., Engel, A.K., Roelfsema, P.R., Singer, W., 1995. How precise is neuronal synchronization?. Neural Comput 7, 469–485.
Lee, W.C., Reid, R.C., 2011. Specificity and randomness: structure-function relationships in neural circuits. Curr. Opin. Neurobiol. 21, 801–807.
Liao, D.S., Krahe, T.E., Prusky, G.T., Medina, A.E., Ramoa, A.S., 2004. Recovery of cortical binocularity and orientation selectivity after the critical period for ocular dominance plasticity. J. Neurophysiol. 92, 2113–2121.
Maffei, L., Fiorentini, A., 1973. The visual cortex as a spatial frequency analyser. Vision Res. 13, 1255–1267.
Marshansky, S., Shumikhina, S., Molotchnikoff, S., 2011. Repetitive adaptation induces plasticity of spatial frequency tuning in cat primary visual cortex. Neuroscience 172, 355–365.
Maruyama, Y., Ito, H., 2013. Diversity, heterogeneity and orientation-dependent variation of spike count correlation in the cat visual cortex. Eur. J. Neurosci. 38, 3611–3627.
Moore, B.D.t., Alitto, H.J., Usrey, W.M., 2005. Orientation tuning, but not direction selectivity, is invariant to temporal frequency in primary visual cortex. J. Neurophysiol. 94, 1336–1345.
Movshon, J.A., 1975. The velocity tuning of single units in cat striate cortex. J. Physiol. 249, 445–468.
Patterson, C.A., Wissig, S.C., Kohn, A., 2013. Distinct effects of brief and prolonged adaptation on orientation tuning in primary visual cortex. J. Neurosci. 33, 532–543.
Perkel, D.H., Gerstein, G.L., Moore, G.P., 1967. Neuronal spike trains and stochastic point processes. I. The single spike train. Biophys. J. 7, 391–418.
Poulet, J.F., Petersen, C.C., 2008. Internal brain state regulates membrane potential synchrony in barrel cortex of behaving mice. Nature 454, 881–885.
Ramoa, A.S., Mower, A.F., Liao, D., Jafri, S.I., 2001. Suppression of cortical NMDA receptor function prevents development of orientation selectivity in the primary visual cortex. J. Neurosci. 21, 4299–4309.
Reich, D.S., Mechler, F., Victor, J.D., 2001. Independent and redundant information in nearby cortical neurons. Science 294, 2566–2568.
Reid, R.C., 2012. From functional architecture to functional connectomics. Neuron 75, 209–217.
Ringach, D.L., Shapley, R.M., Hawken, M.J., 2002. Orientation selectivity in macaque V1: diversity and laminar dependence. J. Neurosci. 22, 5639–5651.
Rolls, E.T., Treves, A., 2011. The neuronal encoding of information in the brain. Prog. Neurobiol. 95, 448–490.
Shumikhina, S., Guay, J., Duret, F., Molotchnikoff, S., 2004. Contextual modulation of synchronization to random dots in the cat visual cortex. Exp. Brain Res. 158, 223–232.
Sompolinsky, H., Golomb, D., Kleinfeld, D., 1990. Global processing of visual stimuli in a neural network of coupled oscillators. Proc. Natl. Acad. Sci. U.S.A 87, 7200–7204.
Stanley, G.B., 2013. Reading and writing the neural code. Nat. Neurosci. 16, 259–263.
Stepanyants, A., Hirsch, J.A., Martinez, L.M., Kisvarday, Z.F., Ferecsko, A.S., Chklovskii, D.B., 2008. Local potential connectivity in cat primary visual cortex. Cereb .Cortex. 18, 13–28.
Stratford, K.J., Tarczy-Hornoch, K., Martin, K.A., Bannister, N.J., Jack, J.J., 1996. Excitatory synaptic inputs to spiny stellate cells in cat visual cortex. Nature 382, 258–261.
Swindale, N.V., 1998. Orientation tuning curves: empirical description and estimation of parameters. Biol. Cybern. 78, 45–56.
Ts'o, D.Y., Gilbert, C.D., Wiesel, T.N., 1986. Relationships between horizontal interactions and functional architecture in cat striate cortex as revealed by cross-correlation analysis. J. Neurosci. 6, 1160–1170.
Wallace, D.J., Kerr, J.N., 2010. Chasing the cell assembly. Curr. Opin. Neurobiol.
Wise, A.K., Cerminara, N.L., Marple-Horvat, D.E., Apps, R., 2010. Mechanisms of synchronous activity in cerebellar Purkinje cells. J. Physiol. 588, 2373–2390.
Xing, D., Shen, Y., Burns, S., Yeh, C.I., Shapley, R., Li, W., 2012. Stochastic generation of gamma-band activity in primary visual cortex of awake and anesthetized monkeys. J. Neurosci. 32 (13873-80a).
Xue, M., Atallah, B.V., Scanziani, M., 2014. Equalizing excitation–inhibition ratios across visual cortical neurons. Nature 511, 596–600.
Yoshimura, Y., Sato, H., Imamura, K., Watanabe, Y., 2000. Properties of horizontal and vertical inputs to pyramidal cells in the superficial layers of the cat visual cortex. J. Neurosci. 20, 1931–1940.
Yoshimura, Y., Dantzker, J.L., Callaway, E.M., 2005. Excitatory cortical neurons form fine-scale functional networks. Nature 433, 868–873.
Zohary, E., Shadlen, M.N., Newsome, W.T., 1994. Correlated neuronal discharge rate and its implications for psychophysical performance. Nature 370, 140–143.

4. Article intitulé: Summation of connectivity strengths in the visual cortex reveals stability of neuronal microcircuits after plasticity

Bachatene *et al. BMC Neurosci (2015) 16:64*
DOI 10.1186/s12868-015-0203-1

BMC Neuroscience

RESEARCH ARTICLE Open Access

Summation of connectivity strengths in the visual cortex reveals stability of neuronal microcircuits after plasticity

Lyes Bachatene[1,2], Vishal Bharmauria[1,2], Sarah Cattan[1,2], Nayan Chanauria[1,2], Jean Rouat[1,2] and Stéphane Molotchnikoff[1,2*]

Abstract

Background: Within sensory systems, neurons are continuously affected by environmental stimulation. Recently, we showed that, on cell-pair basis, visual adaptation modulates the connectivity strength between similarly tuned neurons to orientation and we suggested that, on a larger scale, the connectivity strength between neurons forming sub-networks could be maintained after adaptation-induced-plasticity. In the present paper, based on the summation of the connectivity strengths, we sought to examine how, within cell-assemblies, functional connectivity is regulated during an exposure-based adaptation.

Results: Using intrinsic optical imaging combined with electrophysiological recordings following the reconfiguration of the maps of the primary visual cortex by long stimulus exposure, we found that within functionally connected cells, the summed connectivity strengths remain almost equal although connections among individual pairs are modified. Neuronal selectivity appears to be strongly associated with neuronal connectivity in a "homeodynamic" manner which maintains the stability of cortical functional relationships after experience-dependent plasticity.

Conclusions: Our results support the "homeostatic plasticity concept" giving new perspectives on how the summation in visual cortex leads to the stability within labile neuronal ensembles, depending on the newly acquired properties by neurons.

Keywords: Visual cortex, Plasticity, Summation, Correlation, Adaptation

Background

Visual processing in the brain highly depends on physiological connectivity of neurons to establish functional circuits in the visual cortex. Specific neuronal connections are framed between stimulus selective neurons (functional circuits) within cell-assemblies that process visual information [1]. These recruited functional circuits, when co-activated, encode the attributes of stimuli [2] and are believed to be crucial for visual perception [1]. It is well established that neurons sharing similar selectivity vigorously and strongly connect with each other in response to the visual stimulation [1, 3, 4].

In a recent report [5], we showed that neurons exhibit changes in the correlation-strength after adaptation for their original optimal and new acquired optimal orientations suggesting that adaptation impacts the strength of their functional connections. These previous data were investigated on cell-pairs basis and focused exclusively on cells sharing similar orientations before and after adaptation phase. Hence the previous report was not centered on the large spectrum of orientations. In the present paper, seeking a deeper understanding how connectivity-strength is modified, we further broadened analyses by investigating the connection strengths between cells selective to a wide range of orientations as revealed within a cluster of neurons. Thus, crosscorrelograms

were computed between all cells of a cluster irrespective of the axis of the preferred orientation. The magnitudes of the central pic were computed to derive the strength of inter-neuronal functional relationships and then we investigated the modulation of crosscorrelogram pics following adaptation. In addition, the present paper focuses on a summative model which explains how within cell-assemblies formed by similarly tuned and differently tuned neurons, the summed connectivity strength remained relatively unchanged during plasticity. We recorded visual responses from neuronal units and populations using extracellular electrophysiological recordings and intrinsic optical imaging. Brain plasticity is an inherent feature of cortical neurons that is inevitable for animals to adapt to the environment. The cortical organization is well known to be malleable mostly during early stages of life [6, 7]. For instance, visual neurons of animals raised in a forced, stripped environment exhibit orientation-preference shifts toward the imposed stimulus [7]. Such plastic changes have been widely observed at neuronal [8–11] and populational levels [10, 12, 13]. In principle, these changes are attributed to visual deprivation or visual training (adaptation).

Crosscorrelations have been widely employed to reveal the putative functional connections between neurons [14–16]. We crosscorrelated the spiking activity of simultaneously recorded neurons to reveal the functional relationships between them.

Our results are in line with the concept of homeostatic plasticity [17–19]. Indeed, a homeostatic process is established in order to stabilize the initial global connectivity strength of the neuronal group [19]. This regulatory activity is considered as a complementary process to the Hebbian plasticity wherein changes of synaptic strength are observed in order to redefine the properties of neuronal-assemblies [19–21].

Methods

Ethical approval

Animal surgery procedures and electrophysiological recordings followed the guidelines of the Canadian Council on Animal Care and were approved by the Institutional Animal Care and Use Committee of the University of Montreal. Animals were supplied by the Division of Animal Resources of the University of Montreal. The experiments were conducted in accordance with the Guide for Care and Use of Laboratory Animals of the National Institutes of Health (USA).

Animal surgery

Briefly, electrophysiological recordings and optical imaging were performed within layer II/III of V1 area of adult anaesthetized cats (Felis catus). Eight adult cats (2.5–3.5 kg, age 12–24 months) of either sex were used for this study. General anaesthesia was maintained by artificial ventilation with a mixture of N_2O/O_2 (70:30) supplemented with 0.5 % isoflurane (AErrane, Baxter, Toronto, ON, Canada) for the duration of the experiment. The following parameters were monitored throughout the experiment: the EEG, the expired CO_2, the temperature and the heart rate. At the end of each experiment, euthanasia was achieved with a lethal dose of pentobarbital sodium (Somnotol, MTC Pharmaceuticals, Cambridge, ON, Canada; 100 mg kg^{-1}) by intravenous injection. Details are described in Bachatene et al. [5].

Electrophysiology

Visual stimuli were generated with a VSG 2/5 graphic board (Cambridge Research Systems, Rochester, England) and displayed on a 21-in. monitor (Sony GDM-F520 Trinitron, Tokyo, Japan) placed 57 cm from the cat's eyes, with 1024 × 768 pixels, running at 100 Hz frame refresh. Stimuli were drifting sine-wave grating square patches (~2°–5°) covering the excitatory RF (unidirectional movement). Patches characteristics were set to evoke optimal responses: contrast at 80 %, mean luminance at 40 cd/m^2, optimal spatial and temporal frequencies set within the 0.1–0.5 cycles/deg. and 1.0–2.0 Hz range, respectively. In all cases the above parameters were chosen with the aim of evoking the maximal discharges. After manual RF characterization, nine oriented stimuli centered on the preferred orientation were selected and used for the rest of the experiment. Test orientations were applied in random order. Each oriented stimulus was presented in blocks of 25 trials lasting 4.1 s each, with a random inter-trial interval (1.0–3.0 s) during which no stimuli were presented. Thus, a recording session lasted for 25–30 min. Peri-stimulus time histograms were recorded. Once control orientation tuning curves were characterized, an adapting non-preferred stimulus was presented continuously for 3 or 12 min and 24 min in one experiment. The adapting stimulus was a drifting grating whose orientation was randomly selected in the range 22.5°–67.5° off of the neuron's preferred orientation. All other stimulus parameters were kept constant, at control values, throughout the recordings. Neurons were isolated from multi-unit activity using autocorrelograms, principal component analysis, spike wave-shapes and cluster separation. Details are described in Bachatene et al. [5].

Optical imaging

Detailed account of intrinsic optical imaging is available in Cattan et al. [12]. Intrinsic optical imaging allows assessment of the activity of a large population of cells.

Thus, we used this technique to visualize the range of shift propagation following adaptation.

After craniotomy, the dura mater was removed, a round chamber (15 mm in diameter) was fixed with dental cement above one hemisphere's area 17 and the chamber was filled with mineral oil and closed with a cover glass.

Achromatic gratings were to stimulate all cortical area within the imaging window to obtain orientation maps in control and post-adaptation sessions (contrast: 75 %; generated by VSG software; Cambridge Research Systems, Rochester, UK), presented randomly in order to avoid stimulus-order bias with rotation in eight different orientations from 0° to 157.5°, spatial frequency: 0.3 cycles/°, temporal frequency: 1 Hz). Each trial started with the presentation of a black screen for 15 s, and this was followed by the presentation of every orientation (12 s). For each presented orientation spanning 12 s, the grating was kept stationary during the first 6 s to remove the cortical activity resulting from the stimulus onset, and this was followed by drifts in one direction for the next 3 s and then in the reverse direction for 3 s to maximize cortical responses. The stimulation was full-screen. From these recordings, we generated control polar orientation maps. Then we presented a patch as an adapter for 12 min (full screen stimulus). Immediately after adaptation, we stimulated again all cortical area within the imaging window by presenting full screen stimuli as in the control phase. The polar map obtained post-adaptation was compared with the control map to evaluate the spatial spread of local adaptation.

Data acquisition and processing

The cortex was illuminated with 630-nm light. Cortex images were captured with a CCD camera (Dalsa 1 M60P; Dalsa, Waterloo, Ontario, Canada), composed of two 50-mm f1.2 lenses arranged in tandem, and focused 500 μm below the cortical surface. Images were digitised with Imager 3001 (Optical Imaging, Germantown, NY, USA), with a spatial resolution of 1024 × 1024 pixels (binned 2 × 2), and a temporal resolution of 20-ms frame duration. Image analysis was performed with MATLAB programs (MathWorks, Natick, MA, USA).

Thirty images were recorded for every orientation. As the last images showed more activity than the initial images, the average of the last 10 images (21–30) was divided by the average of the first 20 images (1–20). This calculation was performed to remove the non-specific activity in initial images, while preserving the specific activity recorded mostly in the last frames. Then, the generalised indicator function method [22] was applied. In short, this method extracts the frames that account for as much of the signal as possible by using principal component analysis, and optimises the differences between signal and noise.

Pixel shifts

To quantify changes in the orientation of pixels between control and post-adaptation polar maps, the amplitude of the shift in orientation was calculated from pairs of pixels located at the same position in the two maps.

$$s_{i,j} = \min\left(\left|p2_{i,j} - p1_{i,j}\right|, 180 - \left|p2_{i,j} - p1_{i,j}\right|\right)$$

where s is the shift-amplitude associated with the pair of pixels at the map position (i, j); p1 the pixel-orientation in the first map and, p2 the orientation of the same pixel in the second map. The shift-map comprised of all the shifts calculated for each position.

Connectivity strength, crosscorrelograms and shift predictor

Crosscorrelograms (CCG's) were performed in order to compare the spike distribution of each neuron of the pair within a time-frame; one neuron is set as reference and the second as target; this allows us to show the firing of the target neuron at a specific time-spread in relation to the firing of the reference neuron.

Time axis is divided into bins. The first bin is defined as: XMin, XMin + Bin. The next bin is XMin + Bin, XMin + Bin*2, etc. We calculated the distances from each spike to all spikes of the spike train as follows:

$$d[i] = ts[i] - ref[k]$$

where ts[i] represents the spike train, and ref[k] is each timestamp.

Bin counts were then divided by the number of reference events to normalize the counts per bin into probabilities. 95 % statistical threshold for the significance of the bins was used. Each bin-width was set at 1 ms. The connectivity strengths were calculated from the counts/bin as follows:

$$CS = F \times b$$

where F is the neuron frequency and b represents the bin size of the calculated firing of the neuron.

The neuron frequency F was calculated as follows:

$$F = \frac{N}{T}$$

where T represents the total time interval and N the number of spikes within this interval.

The 95 % confidence limit was calculated assuming that the expected bin count (EBC) has a Poisson distribution:

$$EBC = CS \times Nref$$

where Nref is the number of reference events.

The 95 % confidence limit is calculated as follows:

$$Low\ \ Conf. = x\ such\ that\ Prob(S < x) = 0.005$$

$$High\ Conf. = y\ such\ that\ Prob(S > y) = 0.005$$

where S represents a random variable which has a Poisson distribution with parameter EBC.

Raw CCG's were corrected by subtracting a shift-predictor algorithm in order to eliminate the putative significant peaks due to the simultaneous stimulation of both cells during each trial.

Results

To investigate the temporal relationships of spikes between cells of recorded assemblies, we performed optical imaging and extracellular electrophysiological recordings in V1 of adult anaesthetized cats based on an exposure-learning procedure (Fig. 1a). Optical imaging allows examining orientation shifts of a population of neurons [12] whereas electrophysiology permits recording a small number of neurons. Orientation preference maps were generated in order to compare the orientation layout before and after stimulus exposure: 3 or 12 min presentation of one particular orientation. An example of orientation maps is shown in Fig. 1b for both conditions (pre and post-adaptation periods). In addition to the optical imaging, electrophysiological recordings reveal, at the single cell scale, the orientation preference of cells and the changes of their selectivity after adaptation (orientation maps and neuronal tuning curves are shown in Fig. 1c, simulated data [23]). Colored dots within the circles depict orientation domains before (left) and following adaptation (right). Two orientation tuning curves are illustrated. Crosscorrelogram (CCG) analysis was used to unveil the putative inter-neuronal functional connections between neurons within a cell-assembly [15]. Raw CCGs were shift-corrected to eliminate the putative significant peaks due to the simultaneous stimulation of both cells (Fig. 1d). In this example, the CCG shows a significant peak within 10 ms time-window before zero mark. This suggests that cell A functionally projects onto cell B (cell B being the reference cell and cell A was set as a target neuron).

Stability of pixel proportion in orientation domains

In the following section, we examined the orientation selectivity on a populational level using intrinsic brain imaging. For this purpose, area 17 was probed in order to perform computations of pixel-changes of orientation and pixel-distribution in the region of interest.

To attribute the observed shifts in orientation maps to the effect of adaptation, we performed control tests of the stability of the maps over a period of time (1 h). From these maps, pinwheel spots and regions between two iso-orientation domains were identified and traced in both maps. An example of two generated maps is illustrated in Fig. 2a. A shift map was generated between test 1 and test

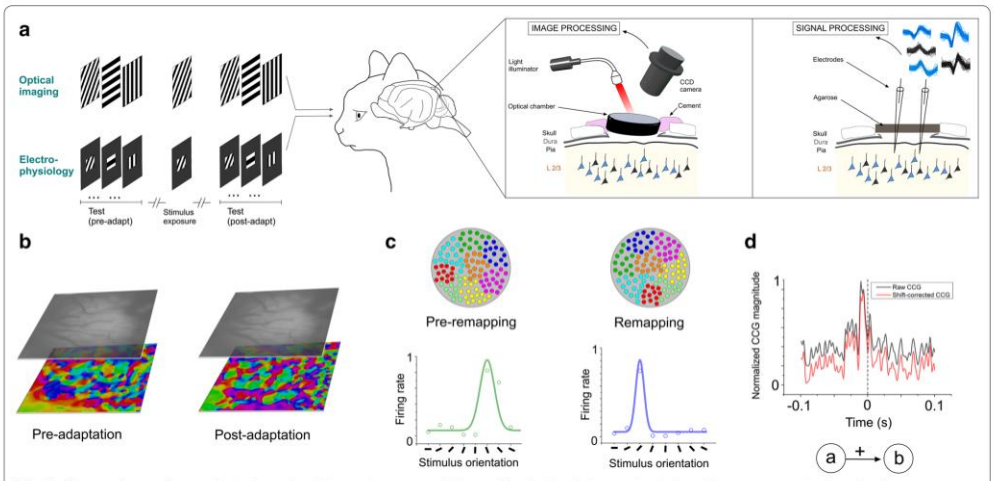

Fig. 1 Neuronal recordings, orientation selectivity and crosscorrelation. **a** Visual stimulations, oriented gratings are presented randomly; one non-preferred grating is used for stimulus-exposure as adaptation (duration: 12 min). Visual responses are measured using intrinsic optical imaging and electrophysiological recordings. **b** Examples of orientation maps pre- and post-adaptation. **c** Model of plasticity of orientation maps and tuning curves shifts of one neuron (simulated data). **d** Raw (*gray*) and corrected (*red*) crosscorrelograms showing a mono-projection from neuron "a" to neuron "b"

2. We observed small shifts in the frontiers between iso-orientation domains. This may be attributed to the small displacement of the pixels which may result from cortical movement, animal breathing…etc. However, in the shift map between pre- and post-adaptation, the shifts are more likely to happen in several regions of the map (see the description of Fig. 2d below).

As a further control of the stability of both maps, Pearson coefficient was computed between test 1 and test 2. We found a Pearson coefficient of 0.49 which is equivalent to a map similarity-index of 0.7 as previously shown [13, 43–45].

The spatial coordinates of each pinwheel was computed to test the stability of both orientation maps as shown in Fig. 2b for X-axis (red) and Y-axis (blue). The black dot represents the example shown in Fig. 2c (pinwheel 5). The similarity of both profiles is suggestive of the stability of the maps and thus the changes may be related to adaptation effect.

Following 12 min of stimulus exposure to one particular oriented grating (generally 90°), we observed a rearrangement of the orientation map characterized by pixel-shifts after adaptation. Figure 2d illustrates an orientation map generated from intrinsic optical imaging computations. In this investigation, we focused on the distribution of pixels for each orientation inside the region of interest for control and post-adaptation maps. This region of interest was selected based on pinwheel organization which is common to species such as cats and monkeys [24, 25].

To assess the magnitude of orientation shifts after visual adaptation, pixels were subtracted between the control and post adaptation steps. The result of this subtraction identified as pixel-shifts map is displayed in Fig. 2d (lower right); the color-scale represents the shift-intensity.

It is interesting to highlight that the global proportion of pixels is maintained, in other words, a new cortical map emerges following adaptation with a new distribution of pixels for each orientation, yet the proportion remained unchanged (One-way Anova test between pre- and post-adaptation, $p > 0.05$, Fig. 2e).

Functional connectivity modulation

The previous results indicate that following adaptation, neurons modified their original orientation selectivity;

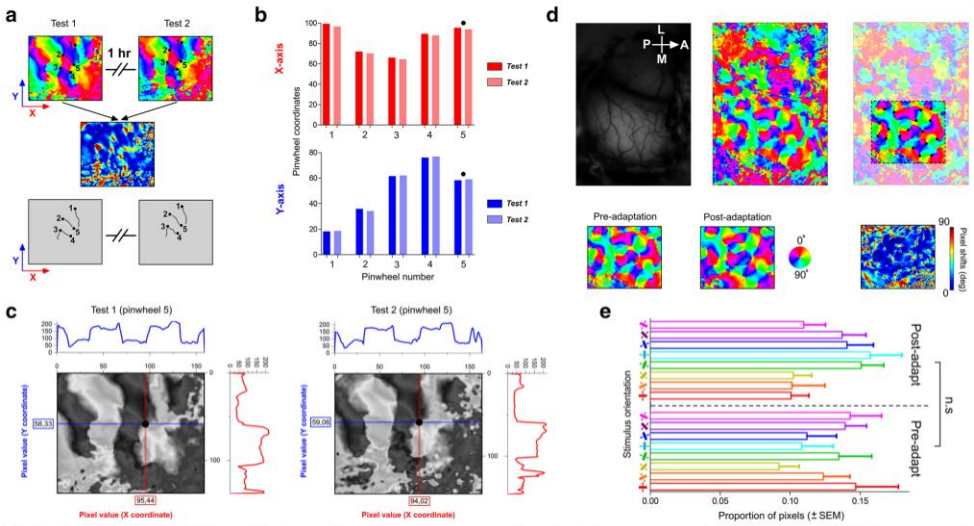

Fig. 2 Orientation maps stability and Pixel proportions in orientation maps. **a** Two orientation maps generated at two intervals (1 h). Pinwheels and zones separating iso-orientation domains were traced within each map. The shift map in illustrated below both orientation maps (test 1 and test 2). **b** Spatial coordinates (*x* and *y axes*) of each pinwheel during both tests. The *black dot* indicates the pinwheel presented in (**c**). **c** Profile plot of pinwheel 5 with its respective coordinates for both tests. **d** Orientation maps pre- and post-adaptation, each color represents one specific orientation. The *dashed rectangle* indicates the region of interest wherein each *black dot* represents a pinwheel. Pixel-shifts map generated using pixel-by-pixel subtraction between the two maps (pre- and post-adaptation) and is shown on the *lower right part*. **e** Pixel proportions of all orientations for both pre- and post-adaptation conditions

hence the pixel-distribution of each orientation was reorganized. However the global distribution of orientations remained unmodified which is in line with previous report [23]. This raises one question: how the relationships between cells are modulated to maintain the equal distribution of orientations? Therefore, it becomes interesting to investigate how time-relationships between spikes of recorded neurons are changed. For this, we investigated the functional connectivity between neurons regardless of their orientation selectivity within sub-networks in pre- and post-adaptation phases. We recorded simultaneously the extracellular activity of groups of cells around two distinct electrodes (400 microns). Six examples of neuronal responses are shown in Fig. 3a (three cells from each site). Orientation tuning curves of all cells obtained from the raw data (response matrices) before and after adaptation are shown. Neuronal firing activity was crosscorrelated for all the possible neuron-pairs between the recorded sites. Based on the highest significant peaks across the CCGs of all pairs (pairs are coded by colored squares, the first colored square in the CCG represents the reference neuron, Fig. 3b, in this example all reference neurons were from site 1), putative functional connections were revealed within the networks and are further described in the next section. The spike waveforms of each neuron are displayed in Fig. 3b (left).

Coordinated adjustment of synaptic weights in the circuits

We generated a connectivity circuit between the simultaneously recorded neurons shown previously (Fig. 4a). In the illustration, the value of CCG magnitude reflecting connection strength is indicated above each connecting-line, and is proportional to the thickness of the latter. The computations of CCG magnitudes of all summed pairs ($n = 7$) indicated a non-significant difference between the mean magnitude in pre- and post-adaptation conditions (paired two-tailed t test, $p > 0.05$, Fig. 4b). The sums (ΣP) of CCG magnitudes before and after visual adaptation were 0.14 and 0.13 respectively.

Another example is illustrated by a connectivity matrix (4×4 cells from two sites, Fig. 4c); it shows that the total connectivity strength remains unchanged following adaptation (the sums of CCG magnitudes were 0.11 and 0.10 before and after adaptation, respectively) despite the fact that functional connections are redeployed between different cells within the neuronal network (Fig. 4c). The connectivity matrices were found to be significantly different (Pearson coefficient = 0.11). Hence, there is an emergence of a new functional network within the same assembly that is characterized by the merging of both novel orientation selectivity's and new links between cells wherein the functional strengths may weaken or strengthen. This suggests that there is a coordinated adjustment of synaptic strengths within the circuits leading to a rearrangement of functional connectivity with a change of orientation selectivity. However and most importantly, the overall proportion of connections is stable (histogram in Fig. 4d, left). The total values in all experiments pre- and post-adaptation point toward such stability (the summed CCG magnitude remained same at both pre and post-adaptation conditions, $\Sigma P = 0.08$, $n = 135$ cells, histogram in Fig. 4d, right).

Interplay between selectivity and connectivity

Based on our findings, we propose a plastic neuronal network model which links the selectivity of neurons to their respective connectivity following plastic changes (Fig. 5). We found that the sum of the connectivity strength is equal at pre- and post-adaptation conditions. Mathematically, the total connectivity volume of a cell-assembly is the sum of all the individual contributions to the connectivity matrix; the connectivity strength is redistributed within the network following a "steady-selectivity-connectivity rule" so that the total connectivity volume of the entire assembly remains constant. This rule could be represented by the following equation:

$$W = \sum_{i=1}^{n} CSi$$

$$CS = \frac{N \times b}{t}$$

where W is the total connectivity weight within the network, CS is the measure of the individual Connectivity Strength for each cell-pair and n is the number of neuron-pairs, t represents the total time interval, N the number of spikes within this interval, and b represents the bin size of the calculated firing of the neuron (see "Methods").

Correlations as a function of adaptation-duration and distance between electrodes

Finally, the effect of the time of adaptation on the connectivity-strength summation was investigated. For this purpose, three adaptation-durations were used: 3 min, 12 min and 24 min (Fig. 6a–c, respectively). The results indicate that the summed connectivity strengths are maintained post-adaptation with no significant effect of the time of adaptation. The results were: $\Sigma P = 1.2$ pre-adaptation and $\Sigma P = 1.2$ post-adaptation for both 3 and 12 min adaptation-duration, and $\Sigma P = 1.1$ pre-adaptation and $\Sigma P = 1.08$ for 24 min adaptation. Another parameter which has been tested is the distance between the recorded neurons. Multi-channel electrodes allowed simultaneously recording locally clustered cells as well

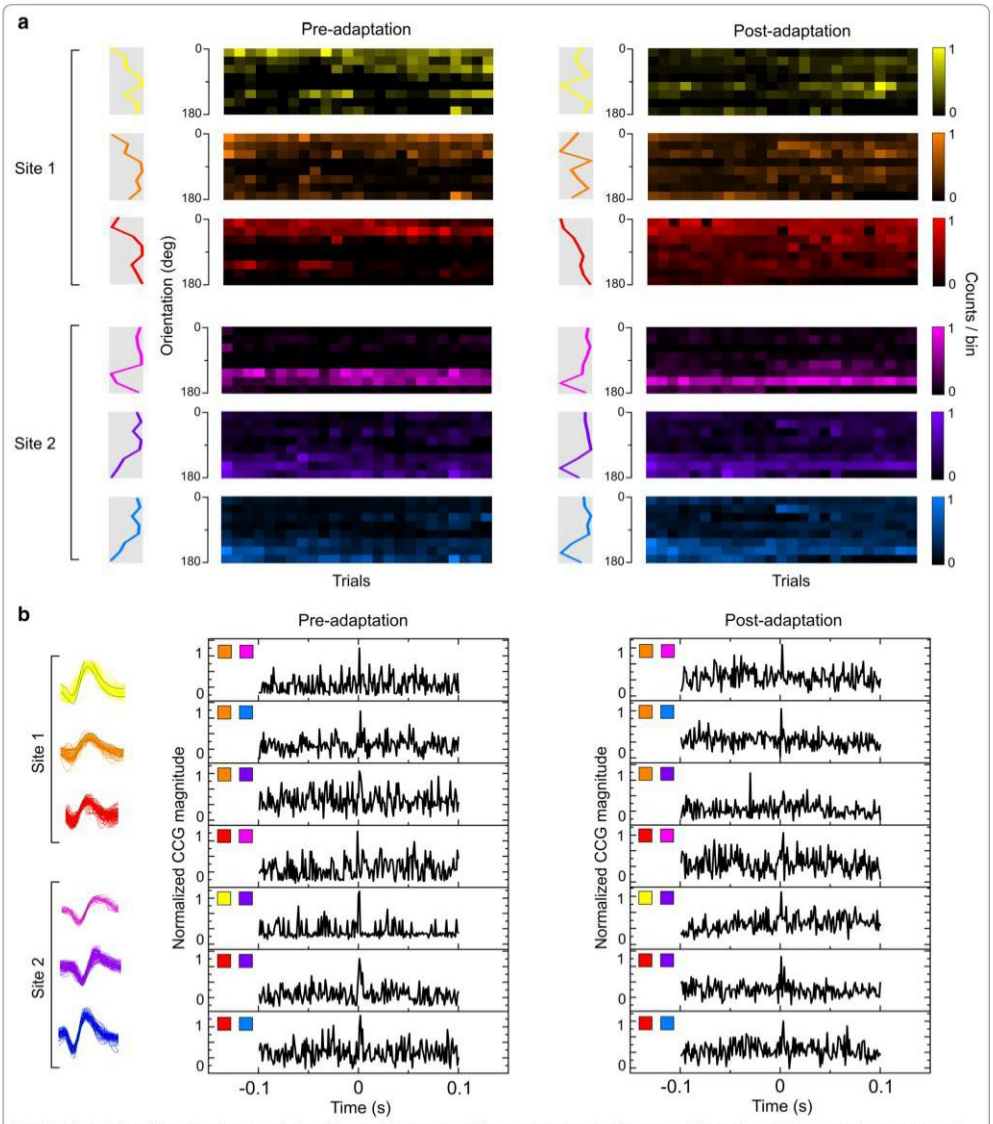

Fig. 3 Modulation of functional connectivity. **a** Neuronal responses of six neurons recorded from two different sites. Colored matrices correspond to the measured responses at each trial (*X-axis*) and at all presented orientations (*Y-axis*). On the *left* are shown the raw tuning curves of each neuron. **b** Significant CCG's between pairs of neurons from (**a**). The spike waveforms are displayed on the *left*

as cells separated by up to 800 microns. The correlation-strength was then examined between neurons recorded from the same electrode tip (local, Fig. 6d) and between neurons recorded from distinct electrodes (distal, Fig. 6d). The results show significant differences between the connectivity strength of locally recorded neurons and the

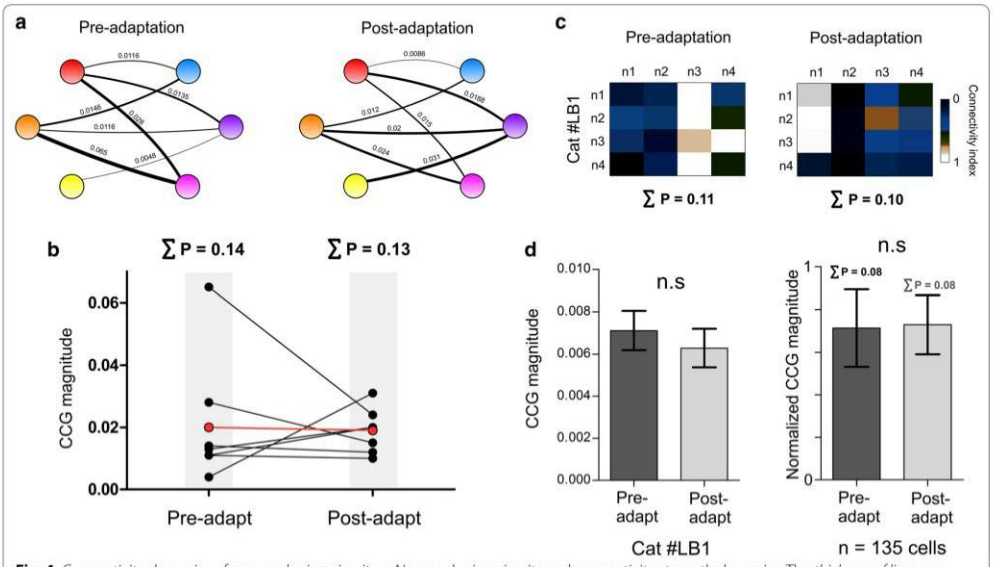

Fig. 4 Connectivity dynamics of neuronal microcircuits. **a** Neuronal microcircuits and connectivity strength dynamics. The *thickness of lines* corresponds to the connectivity level. **b** Comparison between connectivity indices pre- and post-adaptation conditions. *Red dots* represent the mean connectivity strength. *Sums* are indicated above each condition. **c** Connectivity matrix of a different neuronal group showing the connectivity strength between all pairs. **d** Comparative histograms of the previous example (*left*) and global results (*right*)

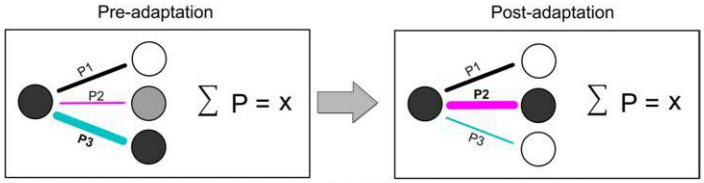

Fig. 5 Mathematical model of connectivity pattern suggesting the stability of neuronal connectivity-strength after orientation-induced plasticity (*P1*, *P2* and *P3* represent the connection probabilities of each neuronal pair, *X* represents the total connectivity weight of the microcircuit)

connectivity strength of distal neurons. These differences were observed for both pre- and post-adaptation phases (t-test, $p < 0.01$, Fig. 6d). Interestingly, for distal pairs, significant difference was also observed between pre- and post-adaptation phases with an increased average of the CCG magnitude (t-test, $p < 0.01$, Fig. 6d). This could be explained by an expansion of functional connections between neurons belonging to distinct microcircuits.

Discussion

Sensory systems are continuously affected by the external environmental attributes [26]. The visual system is highly altered by experience wherein neuronal properties and neuronal circuits undergo important changes during development [6, 7]. These modifications may persist during adulthood as a consequence of large panoply of strategies such as visual deprivation [27, 28], retinal lesions [29] or adaptive sensory experience (short, long or repetitive visual exposure) [9–12, 30–32]. It appears that visual stimulation recruits functional groups of neurons which, when co-activated, process the visual stimuli properties [2]. Thus, the visual input from one microcircuit may affect the information provided to different downstream cell-assemblies [12, 26].

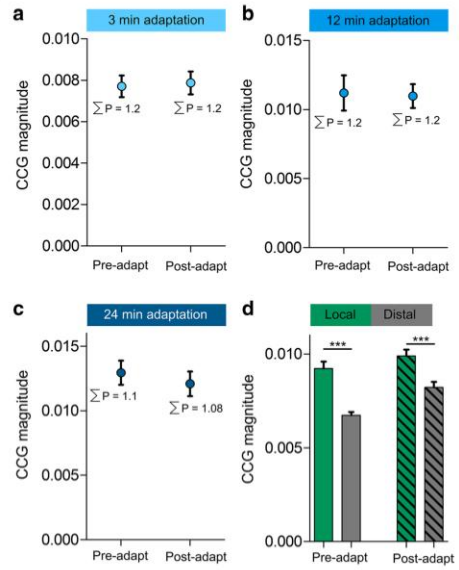

Fig. 6 Correlations as a function of adaptation-duration [3 min in (**a**), 12 min in (**b**) and 24 min in (**c**)] and distance between neurons (**d**). The results indicate no significant difference in the summed connectivity-strengths between different adaptation-durations. However, significant differences were observed between locally recorded neurons (higher CCG magnitude) and neurons recorded from distinct electrode tips (lower CCG magnitude)

Methodological considerations

From intrinsic optical imaging recordings, pixel-by-pixel subtraction computations allow the quantification of the difference between two orientation maps (in our case pre- and post-adaptation maps). It was thus important to test the stability of the maps as a control; indeed, the recorded signal may be contaminated by ambient noise due to breath-induced movement, light intensity change, cortical movement… etc. We have measured the light intensity of all generated images and found no difference between all animals as well as between all recording sessions. Despite the inherent presence of noise, the generated maps clearly contained well-organized regions with iso-orientation domains that converge at the center of pinwheels. This regular pattern cannot be attributed to random noise. In addition, orientation preference maps remained unchanged when tested twice (if no adaptation is applied) (Fig. 2a–c).

The dynamic of neuronal connectivity

Brain processing is intimately related to how important the dynamic of complexly connected microcircuits is. Visual neurons within layers 2/3 are selectively interconnected leading to the emergence of independent fine-scale circuits entrenched in the cortical architecture [1]. In line with our data, experience-dependent plasticity leads to modifications of the connectivity patterns within the neuronal network. However, it has been proposed that a homeostatic process is established in order to stabilize the global connectivity strength of the neuronal group [19]. This regulating activity is considered as a complementary process to the Hebbian plasticity where changes in synaptic strengths are observed after plasticity in order to refine the properties of neuronal-assemblies [19–21]. In young animals for instance, stimulus adaptation leads to the development of orientation maps. Exposing kittens to a single oriented environment shifted the optimal orientations of many neurons to the experienced orientation [7]. Hence, experience is a significant factor in determining the plastic changes operating in orientation maps [7]. In adulthood, there have been studies reporting the adapting ability of the visual cortex to external stimuli: orientation, contrast, motion, direction and spatial frequency [9–11, 30, 31, 33]. Stimulus exposure (adaptation) which mimics the learning process changes neuronal properties; this may be attributed to changes in dynamics of neuronal cell-assemblies wherein neurons acquire new optimal properties [8, 11, 32]. Recent findings assign a high contribution of adaptation to neuronal response uniformity within a population of cells sharing neuronal and feature selectivity [5, 34]. Moreover, it has been shown that adaptation enhances the spike-synchrony in the gamma frequency range in V4 [35] as well as in V1 [36]. This gamma-modulation of synchrony is coupled with an improvement of feature encoding [35, 36].

Functional cell-assemblies are newly formed wherein neurons sharing similar stimulus preference exhibit high connectivity profile [4, 37]. On the other hand, during the critical period and learning in adulthood, synaptic strengths have to be modified in order to regulate the neuronal properties changes due to multiple synaptic drives and maintain a stable level of firing [17]. In line with our findings, homeostatic scaling was proposed as a strategy to normalize the global synaptic connectivity strength to compensate the Hebbian plasticity which modifies the inter-cellular connectivity in relation to the neuronal selectivity [38]. Homeostatic plasticity prevents an over-increase or over-decrease of the firing activity levels due to long-term potentiation (LTP) or long-term depression (LTD) which modify the connectivity strength in order to change the neuronal selectivity features [39–41]. Another scenario would be the change in excitation-inhibition equilibrium that could lead to critical effects on neuronal spiking activity and information processing

[18, 42]. Maintaining stable excitation-inhibition ratio could thus prevent an exceeding augmentation or diminution of global strengths within networks allowing sensory processing to remain stable [18].

Conclusion

The concept of neuronal homeostasis implies that synaptic weights could be limited to an optimal level in order to regulate the total connectivity ratio within the assemblies. Indeed, the increase of synaptic strengths within a group of neurons may lead to the decrease of other connections as a trade-off allowing, therefore, the formation of new functional microcircuits after plasticity.

Abbreviations

OSI: orientation selectivity index; CS: connectivity strength; RF: receptive field; CCG: crosscorrelogram.

Authors' contributions

LB performed the experiments and analyzed the data including the statistical analyses. VB, SC and NC contributed to data analyses and writing of the paper. SM conceived the study and contributed to data analyses. LB and SM wrote the manuscript. JR contributed to data analyses. All authors read and approved the final manuscript.

Author details

[1] Laboratoire de Neurosciences de la vision, Département de Sciences Biologiques, Université de Montréal, CP 6128 Succ. Centre-Ville, Montréal, QC H3C 3J7, Canada. [2] Neurosciences Computationnelles et Traitement Intelligent des Signaux (NECOTIS), Département de Génie Électrique et Génie Informatique, Université de Sherbrooke, Sherbrooke, QC, Canada.

Acknowledgements

We thank Dr Milad Toubal and Simon Brodeur for their useful comments on the manuscript.

Competing interests

The authors declare that they have no competing interests.

Received: 22 May 2015 Accepted: 30 September 2015
Published online: 09 October 2015

References

1. Yoshimura Y, Dantzker JL, Callaway EM. Excitatory cortical neurons form fine-scale functional networks. Nature. 2005;433(7028):868–73. doi:10.1038/nature03252.
2. Miller JE, Ayzenshtat I, Carrillo-Reid L, Yuste R. Visual stimuli recruit intrinsically generated cortical ensembles. Proc Natl Acad Sci USA. 2014;111(38):E4053–61. doi:10.1073/pnas.1406077111.
3. Alloway KD, Roy SA. Conditional cross-correlation analysis of thalamocortical neurotransmission. Behav Brain Res. 2002;135(1–2):191–6.
4. Ko H, Hofer SB, Pichler B, Buchanan KA, Sjostrom PJ, Mrsic-Flogel TD. Functional specificity of local synaptic connections in neocortical networks. Nature. 2011;473(7345):87–91. doi:10.1038/nature09880.
5. Bachatene L, Bharmauria V, Cattan S, Rouat J, Molotchnikoff S. Modulation of functional connectivity following visual adaptation: homeostasis in V1. Brain Res. 2015;1594:136–53. doi:10.1016/j.brainres.2014.10.054.
6. Hensch TK. Critical period plasticity in local cortical circuits. Nat Rev Neurosci. 2005;6(11):877–88. doi:10.1038/nrn1787.
7. Sengpiel F, Stawinski P, Bonhoeffer T. Influence of experience on orientation maps in cat visual cortex. Nat Neurosci. 1999;2(8):727–32. doi:10.1038/11192.
8. Bachatene L, Bharmauria V, Cattan S, Molotchnikoff S. Fluoxetine and serotonin facilitate attractive-adaptation-induced orientation plasticity in adult cat visual cortex. Eur J Neurosci. 2013;38(1):2065–77. doi:10.1111/ejn.12206.
9. Bachatene L, Bharmauria V, Rouat J, Molotchnikoff S. Adaptation-induced plasticity and spike waveforms in cat visual cortex. NeuroReport. 2012;23(2):88–92. doi:10.1097/WNR.0b013e32834e7e71.
10. Dragoi V, Sharma J, Sur M. Adaptation-induced plasticity of orientation tuning in adult visual cortex. Neuron. 2000;28(1):287–98.
11. Ghisovan N, Nemri A, Shumikhina S, Molotchnikoff S. Long adaptation reveals mostly attractive shifts of orientation tuning in cat primary visual cortex. Neuroscience. 2009;164(3):1274–83. doi:10.1016/j.neuroscience.2009.09.003.
12. Cattan S, Bachatene L, Bharmauria V, Jeyabalaratnam J, Milleret C, Molotchnikoff S. Comparative analysis of orientation maps in areas 17 and 18 of the cat primary visual cortex following adaptation. Eur J Neurosci. 2014;40(3):2554–63. doi:10.1111/ejn.12616.
13. Godde B, Leonhardt R, Cords SM, Dinse HR. Plasticity of orientation preference maps in the visual cortex of adult cats. Proc Natl Acad Sci USA. 2002;99(9):6352–7. doi:10.1073/pnas.082407499.
14. Denman DJ, Contreras D. The structure of pairwise correlation in mouse primary visual cortex reveals functional organization in the absence of an orientation map. Cereb Cortex. 2014;24(10):2707–20. doi:10.1093/cercor/bht128.
15. Perkel DH, Gerstein GL, Moore GP. Neuronal spike trains and stochastic point processes. I. The single spike train. Biophys J. 1967;7(4):391–418. doi:10.1016/S0006-3495(67)86596-2.
16. Reid RC. From functional architecture to functional connectomics. Neuron. 2012;75(2):209–17. doi:10.1016/j.neuron.2012.06.031.
17. Surmeier DJ, Foehring R. A mechanism for homeostatic plasticity. Nat Neurosci. 2004;7(7):691–2. doi:10.1038/nn0704-691.
18. Turrigiano G. Homeostatic synaptic plasticity: local and global mechanisms for stabilizing neuronal function. Cold Spring Harb Perspect Biol. 2012;4(1):a005736. doi:10.1101/cshperspect.a005736.
19. Turrigiano GG. Homeostatic plasticity in neuronal networks: the more things change, the more they stay the same. Trends Neurosci. 1999;22(5):221–7.
20. Hebb DO. The organization of behavior: a neuropsychological theory. New York: Wiley and Sons; 1949.
21. Shatz CJ. Impulse activity and the patterning of connections during CNS development. Neuron. 1990;5(6):745–56.
22. Yokoo T, Knight BW, Sirovich L. An optimization approach to signal extraction from noisy multivariate data. NeuroImage. 2001;14(6):1309–26. doi:10.1006/nimg.2001.0950.
23. Bachatene L, Bharmauria V, Cattan S, Rouat J, Molotchnikoff S. Reprogramming of orientation columns in visual cortex: a domino effect. Sci Report. 2015;5:9436. doi:10.1038/srep09436.
24. Ohki K, Matsuda Y, Ajima A, Kim DS, Tanaka S. Arrangement of orientation pinwheel centers around area 17/18 transition zone in cat visual cortex. Cereb Cortex. 2000;10(6):593–601.
25. Okamoto T, Ikezoe K, Tamura H, Watanabe M, Aihara K, Fujita I. Predicted contextual modulation varies with distance from pinwheel centers in the orientation preference map. Sci Report. 2011;1:114. doi:10.1038/srep00114.
26. Patterson CA, Wissig SC, Kohn A. Adaptation disrupts motion integration in the primate dorsal stream. Neuron. 2014;81(3):674–86. doi:10.1016/j.neuron.2013.11.022.
27. He HY, Hodos W, Quinlan EM. Visual deprivation reactivates rapid ocular dominance plasticity in adult visual cortex. J Neurosci Off J Soc Neurosci. 2006;26(11):2951–5. doi:10.1523/JNEUROSCI.5554-05.2006.
28. Shibata K, Kawato M, Watanabe T, Sasaki Y. Monocular deprivation boosts long-term visual plasticity. Curr Biol CB. 2012;22(9):R291–2. doi:10.1016/j.cub.2012.03.010.
29. Keck T, Scheuss V, Jacobsen RI, Wierenga CJ, Eysel UT, Bonhoeffer T, et al. Loss of sensory input causes rapid structural changes of inhibitory neurons in adult mouse visual cortex. Neuron. 2011;71(5):869–82. doi:10.1016/j.neuron.2011.06.034.
30. Kohn A, Movshon JA. Adaptation changes the direction tuning of macaque MT neurons. Nat Neurosci. 2004;7(7):764–72. doi:10.1038/nn1267.

31. Nemri A, Ghisovan N, Shumikhina S, Molotchnikoff S. Adaptive behavior of neighboring neurons during adaptation-induced plasticity of orientation tuning in VI. BMC Neurosci. 2009;10:147. doi:10.1186/1471-2202-10-147.
32. Patterson CA, Wissig SC, Kohn A. Distinct effects of brief and prolonged adaptation on orientation tuning in primary visual cortex. J Neurosci Off J Soc Neurosci. 2013;33(2):532–43. doi:10.1523/JNEUROSCI.3345-12.2013.
33. Marshansky S, Shumikhina S, Molotchnikoff S. Repetitive adaptation induces plasticity of spatial frequency tuning in cat primary visual cortex. Neuroscience. 2011;172:355–65. doi:10.1016/j.neuroscience.2010.10.017.
34. Benucci A, Saleem AB, Carandini M. Adaptation maintains population homeostasis in primary visual cortex. Nat Neurosci. 2013;16(6):724–9. doi:10.1038/nn.3382.
35. Wang Y, Iliescu BF, Ma J, Josic K, Dragoi V. Adaptive changes in neuronal synchronization in macaque V4. J Neurosci Off J Soc Neurosci. 2011;31(37):13204–13. doi:10.1523/JNEUROSCI.6227-10.2011.
36. Hansen BJ, Dragoi V. Adaptation-induced synchronization in laminar cortical circuits. Proc Natl Acad Sci USA. 2011;108(26):10720–5. doi:10.1073/pnas.1102017108.
37. Ko H, Cossell L, Baragli C, Antolik J, Clopath C, Hofer SB, et al. The emergence of functional microcircuits in visual cortex. Nature. 2013;496(7443):96–100. doi:10.1038/nature12015.
38. Turrigiano GG, Nelson SB. Hebb and homeostasis in neuronal plasticity. Curr Opin Neurobiol. 2000;10(3):358–64.
39. Burrone J, O'Byrne M, Murthy VN. Multiple forms of synaptic plasticity triggered by selective suppression of activity in individual neurons. Nature. 2002;420(6914):414–8. doi:10.1038/nature01242.
40. Turrigiano GG, Leslie KR, Desai NS, Rutherford LC, Nelson SB. Activity-dependent scaling of quantal amplitude in neocortical neurons. Nature. 1998;391(6670):892–6. doi:10.1038/36103.
41. Turrigiano GG, Nelson SB. Homeostatic plasticity in the developing nervous system. Nat Rev Neurosci. 2004;5(2):97–107. doi:10.1038/nrn1327.
42. Nelson SB, Turrigiano GG. Strength through diversity. Neuron. 2008;60(3):477–82. doi:10.1016/j.neuron.2008.10.020.
43. Gödecke I, Bonhoeffer T. Development of identical orientation maps for two eyes without common visual experience. Nature. 1996;379(6562):251–4.
44. Chapman B, Stryker MP, Bonhoeffer T. Development of orientation preference maps in ferret primary visual cortex. J Neurosci. 1996;16(20):6443–53.
45. Schuett S, Bonhoeffer T, Hübener M. Pairing-induced changes of orientation maps in cat visual cortex. Neuron. 2001;32(2):325–37.

5. Article intitulé: Adaptation-induced plasticity and spike waveforms in cat visual cortex

Adaptation-induced plasticity and spike waveforms in cat visual cortex

Lyes Bachatene[a], Vishal Bharmauria[a], Jean Rouat[a,b] and Stéphane Molotchnikoff[a,b]

Orientation-selective neurons shift their preferred orientation after being adapted to a nonpreferred orientation. These shifts of the peaks of tuning curves may be in the attractive or repulsive direction in relation to the adapter orientation. In anesthetized cats, we recorded evoked electrical responses from the visual cortex in a conventional manner. The recorded spikes in cortex may present two typical waveforms: regular spikes or fast spikes. However, there is no evidence whether the shapes of spikes are related to the attractive or repulsive shifts of orientation tuning curves of cells. Our results show that after adaptation the recorded cells with both attractive and repulsive shifts display one or the other shape of spike. However, the magnitude of shifts is systematically higher for regular spikes, which is attributed to putative pyramidal cells, whereas tuning curves for fast spikes have smaller magnitudes and are evoked by putative interneurons. *NeuroReport* 23:88–92 © 2012 Wolters Kluwer Health | Lippincott Williams & Wilkins.

NeuroReport 2012, 23:88–92

Keywords: adaptation, fast spikes, interneurons, neurophysiology, pyramidal cells, regular spikes, visual cortex

[a]Department of Biological Sciences, University of Montreal, Montreal and [b]Department of Electrical and Computer Engineering, University of Sherbrooke, Sherbrooke, Quebec, Canada

Introduction

Neurons in the mammalian visual cortex are tuned to respond to visual stimuli such as contour orientation, motion direction, and speed [1–3]. In previous studies, it has been shown that it is possible to modify the preferred stimulus which optimally excites neurons by applying a nonpreferred adaptation stimulus [4,5] in adult visual cortex. Adaptation studies in recent years have presented a more complex picture where prolonged exposure to a nonpreferred orientation has shown modifications in neurons' preferred orientations [4,6,7]. Longer adaptation durations ($\geq$ 6 min) were shown to induce attractive shifts more frequently than repulsive shifts [6,8,9], but repeated or prolonged exposure to an adapter is also known to reduce neuronal responsiveness to that same stimulus, especially if it is the neuron's preferred stimulus [10].

Preference for orientation is considered relatively stable in the primary visual cortex (V1) as an emergent property that is established early in life following the so-called critical period [11]. Classically, spike waveforms allow dissociating two functional cell-groups into excitatory pyramidal cells and inhibitory interneurons [12,13]; hence, it is worth investigating how these two cell types react to adaptation. To this aim, we dissociated the recorded cells and analyzed their respective orientation tunings before and after adaptation to a nonpreferred orientation. This study deciphers whether after adaptation there is a relation between behaviour (attractive or repulsive) of cells and their respective waveforms. The most novel and interesting finding in our results was that the regular-spiking cells always shifted with higher magnitude than fast-spiking cells after adaptation. Furthermore, both types of cells shifted their peaks of orientations in either direction.

Methods

Animal preparation and electrophysiological recordings

Experiments were carried with the approval of Université de Montréal animal care committee following the guidelines of the Canadian Council on Animal Care. Anesthetized and paralyzed cats were prepared for electrophysiological recordings in upper layers of visual cortex (two to three, recording depths 250–1500 μm) in a conventional manner fully described previously [8,9,14]. A brief account is provided below.

Adaptation protocol

After manual receptive field characterization (all receptive fields were within 15° of area centralis), nine electrically generated, oriented drifting gratings were selected and centered on the preferred orientation for the entire experiment. Tuning curves covered 180° (22.5° intervals). Test orientations were presented in monocular manner in random order. Each oriented stimulus was presented in blocks of 25 trials (4.1 s each) with a random intertrial interval (1.0–3.0 s) during which no stimulus was presented. Once control orientation tuning curves were characterized, an adapting oriented stimulus was presented continuously for 12 min. The adapting stimulus was a drifting grating whose orientation was generally set within 22.5 to 67.5° of the neurons' preferred orientations. No recordings were performed during this

0959-4965 © 2012 Wolters Kluwer Health | Lippincott Williams & Wilkins

DOI: 10.1097/WNR.0b013e32834e7e71

adaptation period. Immediately after adaptations, orientation tuning curves were measured starting with the adapting and control preferred orientations, whereas the remaining orientations were recorded in random order.

Data analysis

Once single cells were sorted out offline from multiunit spike trains accumulated during data acquisition (Spike 2, Cambridge Electronic Design, CED Limited, Cambridge, England), orientation tuning curves were constructed from raw data and fitted with the Gaussian function. This allowed us to determine the preferred orientation of neurons with precision and then measure shifts in orientation preference. The Gaussian function is defined as

$$y = b + \mathrm{rmx} \times \exp\{-[(x-x0)^2] / 2s^2\},$$

where b is the baseline, rmx is max firing rate, x is used orientation, $x0$ is optimal orientation, and s is sigma.

In the present study, over 82% of V1 neurons were well tuned to stimulus orientation. However, it was necessary to ensure that cells in our sample were properly tuned for orientation. In our experiments, 25 consecutive measurements of a neuron's response to the same stimulus yielded 25 slightly different tuning curves. Adaptation-induced shifts were measured as the distance between peak positions of the fitted tuning curves before and after conditioning. To assess the statistical significance of tuning shifts, curve fits were generated separately for each of the 25 trials, and the mean difference was tested by a paired t-test. In all cases, shifts in preferred orientation greater than 5° are statistically significant (paired sample two-tailed t-test, $P < 0.01$) [9].

Cells were sorted out offline from multiunit activity of the recording site and were analyzed cell by cell (single-unit activity). We measured the degree of shift for each cell. This allowed us to classify the cells on the basis of their behavior: attractive or repulsive, or with no shift (preferred orientation remained within 5° of the initial optimal orientation). The spike waveforms were dissociated in the ascending phase of the action potential by measuring the slope (dv/dt) of each spike within an interval of 0.2 ms. This computation allowed us to separate the regular-spiking cells from the fast-spiking cells [15,16].

Polar plots that calculate the bandwidth of each cell were constructed on the basis of its response at all orientations. Chi-square test was done to estimate significance of difference between the bandwidth of fast spikes and regular spikes.

Results

We recorded the multiunit activity of cells for stimulations at nine orientations in the primary visual cortex of anesthetized cats before and after adapting the neurons for a period of 12 min. We analyzed the single-unit activity of cells by spike sorting and we sorted out 73 cells (Table 1).

Figure 1a shows the distribution of regular and fast spikes according to dv/dt (slope) calculations in a time window of 0.2 ms. Both groups are clearly distinguished. In Fig. 1b, waveforms of all 73 cells were overlaid illustrating the difference between spike shapes, wherein red waveforms stand for fast-spiking cells ($n = 23$), whereas green

Table 1 Classification of cells after adaptation

		Attractive	Repulsive	No shift
Total cells ↓ → n=73 cells		42 (57%)	18 (25%)	13 (18%)
Regular spikes	50 (68%)	30 (41%)	14 (19%)	6 (8%)
Fast spikes	23 (32%)	12 (16%)	4 (6%)	7 (10%)

Fig. 1

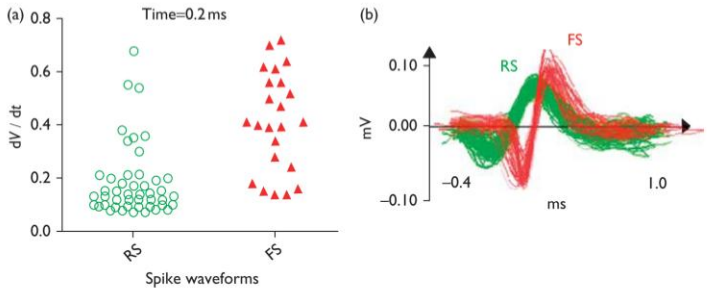

Comparison between regular spikes (RS) and fast spikes (FS). (a) Distribution of RS and FS based on dv/dt (slope) in a time window of 0.2 ms. (b) Superposition of RS and FS from all cells.

indicates regular-spiking cells ($n = 50$). Furthermore, we compared the distribution pattern of spikes for the rising phase of waveforms. We found that regular spikes and fast spikes were distinct by their ascending phase, that is, regular spikes always had a lesser slope than fast spikes (Fig. 1a and b). Also, after aligning the waveforms of fast spikes and regular spikes at the same origin we observed that regular spikes peak earlier than fast spikes by a phase difference of (almost) 0.1 ms (Fig. 1b).

We then classified neurons on the basis of their behavior (attractive, repulsive, no shift) and shape (regular or fast). Overall results are summarized in Table 1. Figure 2 illustrates a typical example. In Fig. 2a and b, Gaussian tuning curves are plotted for two individual cells for all 25 trials. Waveforms for these cells are illustrated in Fig. 2c and d. The cell in Fig. 2a shifted by 20°, whereas the cell in Fig. 2b shifted by 15°. Both units shifted in the attractive direction (t-test, $P < 0.05$), even though they belonged to different groups. Consistent with published data [4,5], regular-spiking cells had a sharper tuning curve for orientation, whereas fast-spiking cells exhibited a broader tuning curve. Indeed, both types of cells react in attractive or repulsive directions. The polar plot (Fig. 2e) exhibiting the bandwidth illustrates the representative difference characterizing both types of cells. Fast-spiking cells responded strongly to more orientations creating broadly tuned bandwidths than regular-spiking cells that responded strongly to a few orientations (roughly optimal) creating narrowly tuned bandwidths (Fig. 2e) because discharge rates declined rapidly as the angle of orientation tilted away from the preferred axis [1,2,9–11]. Chi-square tests compared the responses at every tested orientation and showed a significant difference between both bandwidths ($P < 0.0001$, $\alpha < 0.05$, $n = 8$ orientations).

Fig. 2

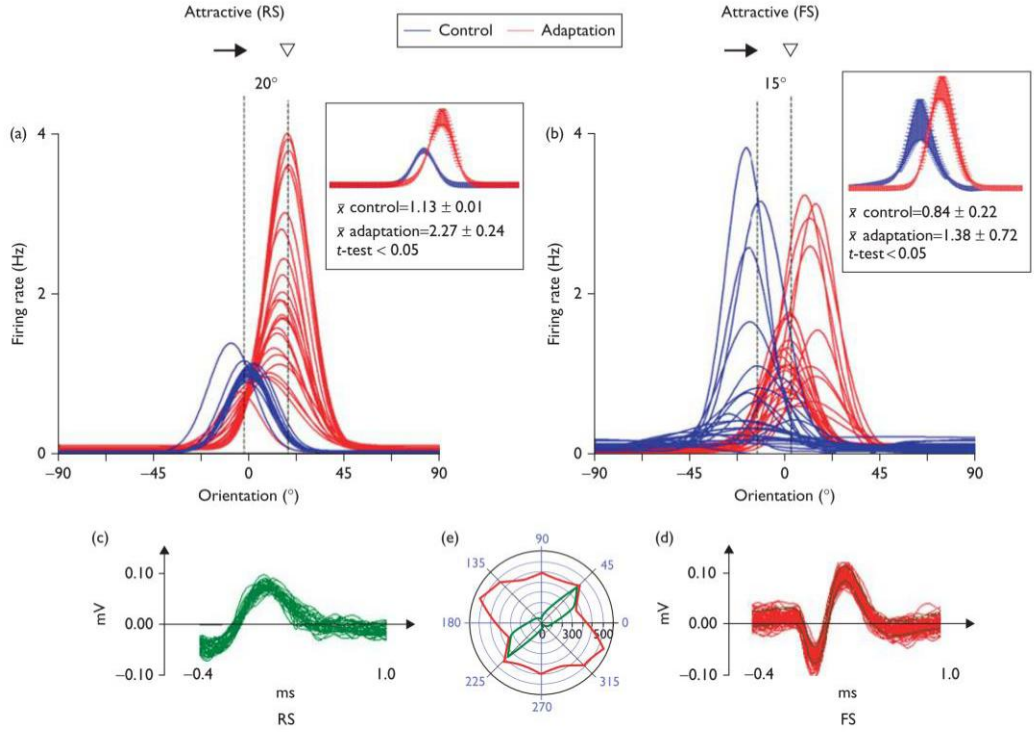

An example of an attractive orientation tuning shift for a fast-spiking (FS) cell and a regular-spiking (RS) cell. (a) Cell displayed a 20° attractive shift following adaptation in the case of a regular waveform of the spike. Downward triangle indicates the adapting orientation. (b) Cell displayed a 15° attractive shift following adaptation in the case of a fast waveform of the spike. Downward triangle indicates the adapting orientation. (c) Example of an RS waveform. (d) Example of an FS waveform. (e) Polar plots (fast and regular cell superimposed) of two cells: RS cell and FS cell.

Fig. 3

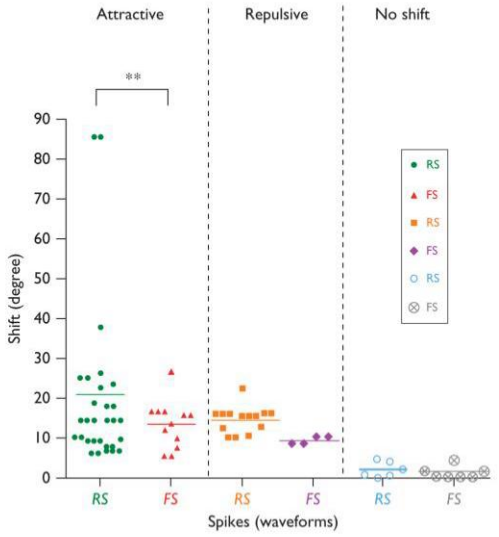

Distribution of two classes of spikes according to postadaptation shift of attractive, repulsive, and no shift cells. This figure demonstrates that magnitudes of attractive and repulsive shifts are higher in regular-spiking (RS) cells than the fast-spiking (FS) cells (Fisher test between RS attractive cells and FS attractive cells: *P*-value <0.05). The maximum value of the shift was 85.5° and 26.7°, respectively, for RS and FS cells. The small number ($n=4$) of FS cells with repulsive reaction precludes statistical computations, yet the trend appears clear that the peaks of the orientation tuning curves for RS cells in the repulsive direction were also displaced to a larger extent.

Moreover, as shown in Fig. 3, regular-spiking cells for attractive behavior shifted within a range of 5–85.5° (average shift 21°) and the fast-spiking cells shifted within a range of 6–27° (average shift 14°; Fisher test, $P < 0.05$). Similarly, regular-spiking cells for repulsive behavior shifted within a range of 10–23° (average shift 15°) and the fast-spiking cells shifted to 9°.

Discussion

The results of our study indicate that both types of functionally identified cells exhibit, following relatively long adaptation (12 min), shifts of their peaks of the orientation tuning curves in both directions, attractive and repulsive. The most interesting result that we found after induced adaptation to a nonpreferred orientation is that the regular-spiking cells and the fast-spiking cells shift in a consistent pattern with respect to each other, though to different degrees.

Therefore, directions of shifts are independent of types of waveforms. As expected from previous studies attractive shifts were more frequent [8]. Such common behavior suggests that neurons reacted collectively irrespective of the cell type. Our conclusion is in line with an earlier investigation showing that in most cases all cells recorded by a single electrode tip shift in the same direction [9]. These observations suggest that adaptation impacts a neuronal network, where a large proportion of cells change their preferred orientation jointly. However, fast-spiking units shift with a smaller magnitude than regular-spiking units. Various studies have indicated that fast-spiking cells are interneurons [17–21] with broader bandwidths of their tuning curves [15,22]. Their broader orientation tuning is a sign that these neurons are driven by a large spectrum of orientations with approximately equal strength. In that case, it is likely that each oriented input is contributing to the cell's response(s) with about comparable magnitude. Therefore, if one assumes that adaptation affects mostly the testing orientation, the other inputs maintain their excitatory drive producing relatively higher firing rates. The net result is a relatively lesser shift of the peak of the tuning curve.

On the other hand, the regular-spiking cells are pyramidal cells [21,23,24] with narrower bandwidths [15,22] exhibiting much sharper tuning curves. Consequently, the range of orientations generating higher firing rate is small, presumably due to a combination of inhibitory inputs [18] sharpening the bandwidths. Thus, optimal responses are produced by a smaller range of oriented input. Therefore, the modified equilibrium between excitation and inhibition that was induced by adaptation results in larger shifts because imposed orientation potentiate response, while remote orientations contribute less to the tuning curves. Indeed, in line with previous reports [4,8,9] responses evoked by flanked orientations did not change significantly.

Based on our findings, we hypothesize that in the primary visual cortex of cat after adaptation the pyramidal cells and interneurons interact and communicate with each other in an organized way to respond to orientation stimuli.

Conclusion

To our knowledge, this study is the first to show that the regular-spiking cells always shift more than the fast-spiking cells after adaptation to stimuli. We may conclude that in primary visual cortex of the cat, pyramidal cells and interneurons interact with each other in parallel to respond to induced adaptation stimuli. Pyramidal cells set the orientation selectivity and the interneurons regulate this selectivity.

Acknowledgements

Conflicts of interest

There are no conflicts of interest.

References

1 Hubel DH, Wiesel TN. Receptive fields of single neurones in the cat's striate cortex. *J Physiol* 1959; **148**:574–591.
2 Hubel DH, Wiesel TN. Receptive fields and functional architecture of monkey striate cortex. *J Physiol* 1968; **195**:215–243.

3 Movshon JA. The velocity tuning of single units in cat striate cortex. *J Physiol* 1975; **249**:445–468.
4 Dragoi V, Sharma J, Sur M. Adaptation-induced plasticity of orientation tuning in adult visual cortex. *Neuron* 2000; **28**:287–298.
5 Kohn A, Movshon JA. Neuronal adaptation to visual motion in area MT of the Macaque. *Neuron* 2003; **39**:681–691.
6 Ghisovan N, Nemri A, Shumikhina S, Molotchnikoff S. Visual cells remember earlier applied target: plasticity of orientation selectivity. *PLoS ONE* 2008; **3**:e3689.
7 Yap H, Dan Y. Stimulus timing-dependent plasticity in cortical processing of orientation. *Neuron* 2001; **32**:315–323.
8 Ghisovan N, Nemri A, Shumikhina S, Molotchnikoff S. Long adaptation reveals mostly attractive shifts of orientation tuning in cat primary visual cortex. *Neuroscience* 2009; **164**:1274–1283.
9 Nemri A, Ghisovan N, Shumikhina S, Molotchnikoff S. Adaptive behaviour of neighboring neurons during adaptation-induced plasticity of orientation tuning in V1. *BMC Neurosci* 2009; **10**:147.
10 Maffei L, Fiorentini A, Bisti S. Neural correlate of perceptual adaptation to grating. *Science* 1973; **182**:1036–1038.
11 Chiu C, Weliki M. The role of neural activity in the development of orientation selectivity. In: Chalupa LM, Werner J, editors. *The visual neurosciences.* Cambridge, MA: MIT Press 2003. pp. 117–125.
12 Ison MJ, Mormann F, Cerf M, Koch C, Fried I, Quiroga RQ. Selectivity of pyramidal cells and interneurons in the human medial temporal lobe. *J Neurophysiol* 2011; **106**:1713–1721.
13 Wilson FA, O'Scalaidhe SP, Goldman-Rakic PS. Functional synergism between putative gamma-aminobutyrate-containing neurons and pyramidal neurons in prefrontal cortex. *Proc Natl Acad Sci* 1994; **91**:4009–4013.
14 Marshansky S, Shumikhina S, Molotchnikoff S. Repetitive adaptation induces plasticity of spatial frequency tuning in cat primary visual cortex. *Neuroscience* 2011; **13**:355–365.
15 Kuhlman SJ, Tring E, Trachtenber JT. Fast-spiking interneurons have an initial orientation bias that is lost with vision. *Nat Neurosci* 2011; **14**: 1121–1123.
16 Ge R, Qian H, Wang J. Physiological synaptic signals initiate sequential spikes at soma of cortical pyramidal neuron. *Mol Brain* 2011; **4**:1.
17 González-Burgos G, Krimer LS, Povysheva NV, Barrionuevo G, Lewis DA. Functional properties of fast spiking interneurons and their synaptic connections with pyramidal cells in primate dorsolateral prefrontal cortex. *J Neurophysiol* 2005; **93**:942–953.
18 Fries P, Nikolic D, Singer W. The gamma cycle. *Trends Neurosci* 2007; **30**:309–316.
19 Gouwens NW, Zeberg H, Tsumoto K, Tateno T, Aihara K, Robinson HPC. Synchronization of firing in cortical fast-spiking interneurons at gamma frequencies: a phase-resetting analysis. *PLoS Comput Biol* 2010; **6**:e1000951.
20 Povysheva NV, González-Burgos G, Zaitsev AV, Kroner S, Barrionuevo G, Lewis DA, Krimer LS. Properties of excitatory synaptic responses in fast-spiking interneurons and pyramidal cells from monkey and rat prefrontal cortex. *Cereb Cortex* 2005; **16**:541–552.
21 Galarreta M, Hestrin S. Electrical and chemical synapses among parvalbumin fast-spiking GABAergic interneurons in adult mouse neocortex. *Proc Nat Acad Sci* 2002; **99**:12438–12443.
22 Hofer SB, Ko H, Pichler B, Vogelstein J, Ros H, Zeng H, *et al.* Differential connectivity and response dynamics of excitatory and inhibitory neurons in visual cortex. *Nat Neurosci* 2011; **14**:1045–1054.
23 McCormick DA, Connors BW, Lighthall JW, Prince DA. Comparative electrophysiology of pyramidal and sparsely spiny stellate neurons of the neocortex. *J Neurophysiol* 1985; **54**:782–806.
24 Chang Y, Luebke JI. Electrophysiological diversity of layer 5 pyramidal cells in the prefrontal cortex of the Rhesus monkey: in vitro slice studies. *J Neurophysiol* 2007; **98**:2622–2632.

6. Article intitulé: Electrophysiological and firing properties of neurons: categorizing soloists and choristers in primary visual cortex

Neuroscience Letters 604 (2015) 103–108

Contents lists available at ScienceDirect

Neuroscience Letters

journal homepage: www.elsevier.com/locate/neulet

Research paper

Electrophysiological and firing properties of neurons: Categorizing soloists and choristers in primary visual cortex

Lyes Bachatene[a,b], Vishal Bharmauria[a,b], Sarah Cattan[a,b], Nayan Chanauria[a,b], Jean Rouat[a,b], Stéphane Molotchnikoff[a,b,*]

[a] Laboratoire de Neurosciences de la vision, Département de Sciences Biologiques, Université de Montréal, Montréal, QC, Canada
[b] Neurosciences Computationnelles et Traitement Intelligent des Signaux NECOTIS, Université de Sherbrooke, Québec, Canada

HIGHLIGHTS

- Neurons in cats' V1 exhibit variability in correlation with the population rate.
- Population coupling highly depends on the neuronal firing rate.
- Thin spike cells highly correlate their firing with the population.
- Broad spike cells fire independently being more soloists.

ARTICLE INFO

Article history:
Received 8 June 2015
Received in revised form 30 July 2015
Accepted 31 July 2015
Available online 3 August 2015

Keywords:
Soloists
Choristers
Visual cortex
Thin spike neurons
Broad spike neurons
Visual processing
Firing rate

ABSTRACT

Visual processing in the cortex involves various aspects of neuronal properties such as morphological, electrophysiological and molecular. In particular, the neural firing pattern is an important indicator of dynamic circuitry within a neuronal population. Indeed, in microcircuits, neurons act as soloists or choristers wherein the characteristical activity of a 'soloist' differs from the firing pattern of a 'chorister'. Both cell types correlate their respective firing rate with the global populational activity in a unique way. In the present study, we sought to examine the relationship between the spike shape (thin spike neurons and broad spike neurons) of cortical neurons recorded from V1, their firing levels and their propensity to act as soloists or choristers. We found that thin spike neurons, which exhibited higher levels of firing, generally correlate their activity with the neuronal population (choristers). On the other hand, broad spike neurons showed lower levels of firing and demonstrated weak correlations with the assembly (soloists). A major consequence of the present study is: estimating the correlation of neural spike trains with their neighboring population is a predictive indicator of spike waveforms and firing level. Indeed, we found a continuum distribution of coupling strength ranging from weak correlation-strength (attributed to low-firing neurons) to high correlation-strength (attributed to high-firing neurons). The tendency to exhibit high- or low-firing is conducive to the spike shape of neurons. Our results offer new insights into visual processing by showing how high-firing rate neurons (mostly thin spike neurons) could modulate the neuronal responses within cell-assemblies.

1. Introduction

Sensory information is represented in the cortex by networks of co-activated neurons which coordinate their firing activity, thus forming functional assemblies [25]. Encoding stimulus attributes involves a variety of strategies considering the anatomical and functional divergence within neuronal populations. Indeed, based on their intrinsic electrophysiological properties, cortical cells are classified into different types such as regular-spiking (RS), fast-rhythmic-bursting (FRB), fast-spiking (FS) and intrinsically bursting (IB) neurons [35]. Despite the fact that neurons exhibit large panoply of firing properties, their correlated activities within assemblies efficiently code the stimulus features rather than the independent spiking of each involved neuron [25]. As a matter of fact, it is largely reported that neurons coding for similar attributes exhibit high levels of correlation and are thus functionally strongly

Abbreviations: CCG, cross-correlogram; HF, high firing; LF, low firing.

http://dx.doi.org/10.1016/j.neulet.2015.07.049
0304-3940/

connected to each other [1,7,12,20,34,39] yet, the debate remains controversial [28,29,32,38]. However, in spite of the stimulus-selective correlation aspect, each neuron may also show coupling with its neighboring local population [27] as if it belongs to a "neuronal orchestra" [15]. It was recently shown in the mouse primary visual cortex and monkey area V4 that, regardless of neuronal preferences, population coupling may lead to discrimination between the choristers (highly coupled) and soloists (weakly coupled) [27]. These two groups differ in many aspects. For instance, highly correlated neurons may receive stronger synaptic drive from neighboring cells [27]. In addition, noise correlation (R_{sc}) is higher for choristers than soloists in IT cortex [18]. Anatomical differences were also observed since the cortical laminar distribution for these types of units is distinct [18]. In mouse V1, population coupling varies between the narrow-spiking and regular-spiking neurons; however, this difference was reported to be smaller than the class-variability [27]. In the present investigation, we sought to examine the relationship between the cell-type (thin spike and broad spike neurons), the firing rate (high-firing and low-firing) and the population coupling of above classes in adult anesthetized cats (columnar-organized cortex). We found that thin spike neurons systematically exhibited higher firing levels than broad spike neurons. In addition, high-firing (HF) neurons displayed higher coupling strength than the low-firing (LF) neurons.

We report that within a sub-network, LF neurons (which were mostly broad spike neurons and weakly coupled) and HF neurons (mainly thin spike neurons and highly coupled) likely play distinct roles in information coding where high-firing neurons may orchestrate the sensory selectivity of the neighboring cells.

2. Materials and methods

2.1. Ethical approval

Animal surgery procedures and electrophysiological recordings followed the guidelines of the Canadian Council on Animal Care and were approved by the Institutional Animal Care and Use Committee of the University of Montreal. Animals were supplied by the Division of Animal Resources of the University of Montreal. The experiments were conducted in accordance with the Guide for Care and Use of Laboratory Animals of the National Institutes of Health (USA).

Details of animal surgery, electrophysiology, visual stimulation and isolation of neurons are described in Bachatene et al. [4].

2.2. Cross-correlation computations

Cross-correlogram shows the conditional probability of a spike at time $t_0 + t$ on the condition that there is a reference event (or reference spike, spike-by-spike analysis) at time t_0. The spike train of each neuron was cross-correlated with the population rate activity (the multi-unit activity) at its preferred orientation (Fig. 1A). Time axis is divided into bins. The first bin is defined as: XMin, XMin + Bin. The next bin is XMin + Bin, XMin + Bin × 2, *etc*. We calculated the distances from each spike to all spikes of the spike train as follows:

$$d[i] = t_s[i] - \mathrm{ref}[k]$$

where t_s[i] represents the spike train, and ref[k] is each timestamp.

Bin counts were then divided by the number of reference events to normalize the counts per bin into probabilities. 95% statistical threshold for the significance of the bins was used. Each bin-width was set at 1 ms and a Gaussian filter width of 3 bins was used. Probabilities were calculated from the counts/bin as follows:

$$P = \frac{N}{T} \times b$$

where N/T is the neuron frequency and b represents the bin size of the calculated firing of the neuron. T represents the total time interval and N the number of spikes within this interval.

The 95% confidence limit was calculated assuming that the expected bin count (C) has a Poisson distribution:

$$C = P \times N\mathrm{ref}$$

where Nref is the number of reference events.

The 95% confidence limit is calculated as follows:

$$\text{Low Conf.} = x \text{ such that } \mathrm{Prob}(S < x) = 0.005$$

$$\text{High Conf.} = y \text{ such that } \mathrm{Prob}(S > y) = 0.005$$

where S represents a random variable which has a Poisson distribution with parameter C.

Raw cross-correlograms were corrected by using a shift-predictor procedure in order to eliminate the putative significant peaks resulting from the coincident firing due to simultaneous visual drive during each trial [4,13].

3. Results

3.1. Coupling strength strategy

We performed electrophysiological recordings in primary visual cortex of adult anesthetized cats ($n = 8$) that were visually stimulated (drifting sine-wave grating patches covering the excitatory fields, spatial frequency = 0.24 cycle/°, temporal frequency = 1.0–2.0 Hz, contrast = 80%, orientations: from 0° to 157.5°, 25 trials, stimulus duration: 4.1 s [5]). Recordings were performed from multiple cortical sites using multi-channel electrodes. Spiking responses were sorted from the multi-unit activity. In addition to the distinct waveforms, the isolation of cells was based on the classical procedure, *i.e.*, principal component analysis, autocorrelograms and cluster separation (Mahalanobis distance and mean cluster distance) [5,8].

We cross-correlated the firing activity of each neuron with the firing of the global population of neurons (multi-unit activity) using the shift-corrected cross-correlation computation (see Section 2 for details). Fig. 1A shows the population coupling strategy: raster plots of three simultaneously recorded cells and their coupling strength indicated by the peak straddling zero in the corresponding correlograms along with the population rate (three superimposed cross-correlograms with the respective color code for each neuron) are displayed. In this example, the green cell exhibited larger correlation-strength than the blue and purple cells. The histogram distribution of all values for correlation-strengths is displayed in Fig. 1B. Note that the values of coupling strengths were normalized (minimum value corresponds to zero, maximum value corresponds to 1) due to the variability between all experiments ($n = 73$ neurons). The absence of a bimodal mode suggests that the coupling strength ranges from low to high values. However, differences were observed based on two parameters: the spike-type and the firing rate (see next Sections).

3.2. Spike-types and coupling strength

In total, 73 neurons were isolated and classified into two major types, namely thin spike neurons ($n = 30$) and broad spike neurons ($n = 43$). Spike-width was quantified as the interval between the

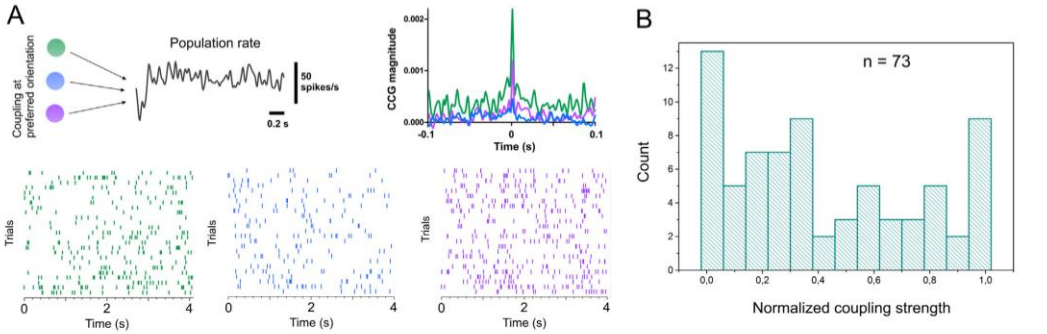

Fig. 1. Correlation strategy.
(A) Schematic representation of the correlation procedure between three recorded neurons and the populational rate. Raster plots of the spiking activity of the neurons and respective superimposed cross-correlograms are displayed. (B) Histogram distribution of the coupling strengths for all experiments ($n = 73$).

trough and peak of the average spike wave-shape of the neuron, allowing for the distinction between broad waveforms (spike-width $\geq$0.5 ms) and narrow waveforms (spike-width <0.5 ms) [4,9,22,31]. An example is shown in Fig. 2A where thin spike neurons and broad spike cells have distinct waveform with a trough-to-peak latency of 0.33 ms and 0.55 ms, respectively. Superimposed spike-waveforms of 20 cells are shown for each type in Fig. 2B. The bold traces represent the average waveforms. Fig. 2C illustrates the distribution of the thin spike neurons (black) and the broad spike neurons (orange) depending on their trough-to-peak interval (trough-to-peak interval <0.5 ms, mean = 0.30 ± 0.04 ms, for thin spike cells, trough-to-peak interval $\geq$0.5 ms, mean = 0.52 ± 0.04 ms, for broad spike cells [4,9,22,31]). Averaged spike-widths are displayed in Fig. 2D.

Fig. 2E illustrates the respective cross-correlation of a thin spike neuron and a broad spike neuron (the spike shapes are represented above each CCG) with the populational activity. Indeed, the correlation-strength indicated by the significant peaks in the cross-correlograms was notably different for the thin spike neurons (black CCG, CCG magnitude = 0.005) and the broad spike neurons (orange CCG, CCG magnitude = 0.0003). Fig. 2F and G display examples of cross-correlograms between the populational activity and the firing rate of thin spike cells (black) and broad spike cells (orange), respectively. This tendency was observed for all sampled neurons. The averaged values were 0.003 ± 0.0009 and 0.001 ± 0.0004 for thin spike cells and broad spike cells, respectively (t-test, $p < 0.05$, Fig. 2H).

3.3. Firing rate, spike-type and categorization of soloists and choristers

Correlating the spike trains of each neuron with the population rate generates two notable behaviors within the assembly: neurons acting as soloists show a weak correlation index whereas neurons acting as choristers exhibit strong correlation with the population activity. It has been suggested that soloists are distinct from choristers in many aspects such as the synaptic connectivity [27] and the laminar distribution [18]. We examined the relationship between the waveform type, the firing rate and the correlation-strength of the cells' firing with the population activity. Typical examples of response-frequency plots to optimal orientation are shown in Fig. 3A (same neurons as in Fig. 2F, G). The relationship between the firing rate and the presented oriented stimuli is displayed in Fig. 3B; polar plots of two neurons (thin and broad spikes) exhibit differences in their orientation tuning and firing rate. It may be worthwhile to underline that poorly tuned cells are often associated with thin spike neurons whereas highly tuned neurons are related to broad spike neurons [2,3,6,10,16,17,21,24,36].

Moreover, we found that thin spike cells presented higher levels of firing rate in comparison to broad spike cells (responses measured for optimal orientations, Fig. 3C, t-test, $p < 0.01$).

In addition, we sought to examine the relationship between the firing rate and the coupling strength. Fig. 3D illustrates these correlations for all experiments. We observed significantly higher correlations between the firing rate and the coupling activity as the R-squared ranged from 0.75 to 0.99.

4. Discussion

In the current study, we classified simultaneously recorded neurons from primary visual cortex of adult anesthetized cats into thin spike neurons and broad spike neurons and studied their firing rate patterns. These two parameters (spike waveforms and firing rate level) were then related to the coupling strength of neurons with the neighboring population. The firing activity of a neuron characterized as a 'chorister' is highly correlated with the firing rate of the global population. On the other hand, a 'soloist' tends to be more autonomous, exhibiting independent firing [23,27]. Here we found a systematic relationship between the cell-class, the firing pattern and the correlation-strength of neurons. Despite the large diversity of cell-types, cortical neurons coordinate their spiking activity forming functional sub-networks which, when co-activated encode the attributes of stimuli [25]. It is extensively reported that sensory neurons may exhibit different levels of correlation depending largely on their selectivity to specific sets of stimuli [1,7,12,20,34,39], though the debate persists [28,29,32,38].

It has been reported that the correlation properties are inherent characteristics of neurons [27]. Indeed, for both stimulation condition and spontaneous activity, soloists and choristers maintain their distinct firing-patterns such as carrying more general information for choristers than soloists [23,27]. On other hand, this correlation seems to be independent of neuronal sparseness and plays a key role in predicting visual search efficiency in humans [18].

Moreover, in rodent sensory cortex, it has been shown that soloists and choristers can be dissociated based on several features. Soloists were reported to be less functionally connected as they were driven less effectively by optogenetic activation [27]. Significant distinction in noise correlation, which represents the

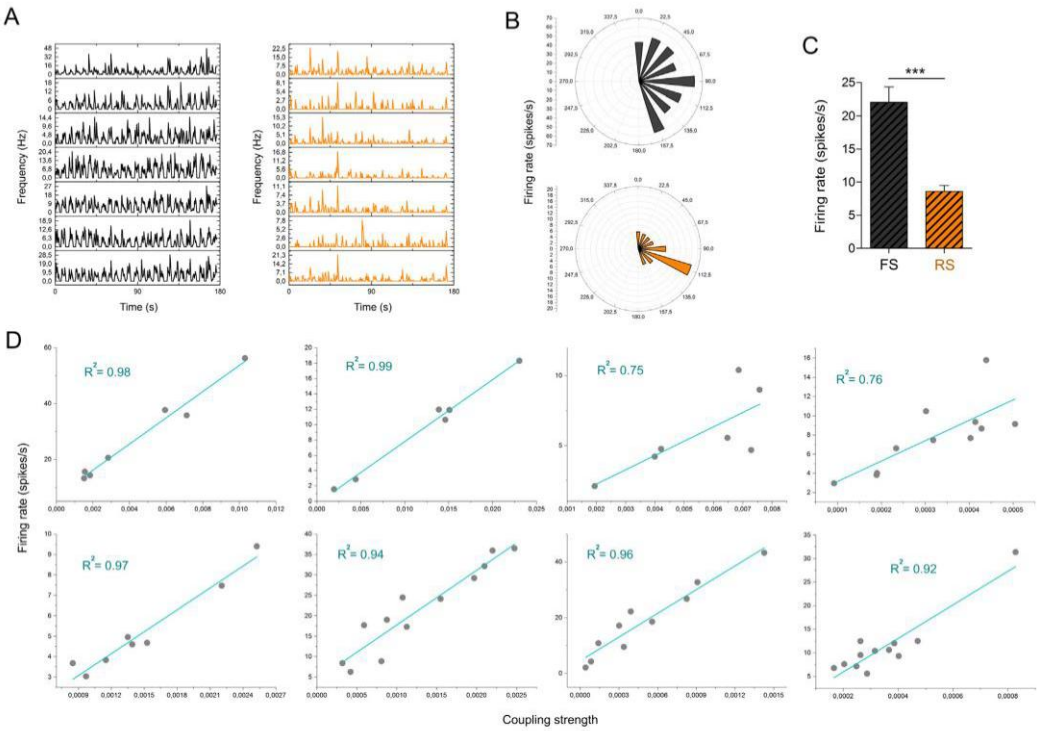

Fig. 3. Firing rate, spike-type and coupling strength.
(A) Frequency plots of typical examples of thin spike neurons (black) and broad spike neurons (orange). Note the differences on *Y*-axis scales. (B) Polar plots of two neurons showing the relationship between the stimulus and the firing rate. The broad spike neuron (orange) exhibit higher selectivity (sharply tuned). (C) Global statistics on the difference in firing rate levels between thin spike neurons and broad spike neurons. (D) Regression analyses between the firing rate and the correlation-strength for all experiments. *R*-squared values are indicated for each graphic (For interpretation of the references to color in this figure legend, the reader is referred to the web version of this article.).

correlation coefficient of spike count responses to the presentation of a stimulus [11], has also been reported; noise correlation (R_{sc}) was much higher for choristers than for soloists in IT cortex [18]. Laminar differences were observed in macaque IT where soloists are common at 0.2 and 1.2 mm depth, whereas choristers are rare in layer 4 and are located in non-granular output layers [18]. In the present investigation, we report that in cat's primary visual cortex, which exhibits a columnar organization, thin spike neurons exhibited higher firing levels and tend to differ in their coupling with their ensemble from broad spike neurons exhibiting lower firing levels and weaker population coupling. It has been reported that thin spike neurons and broad spike neurons exhibit different tuning properties [2,3,6,10,16,17,21,24,36]; thin spike cells being poorly tuned to orientation stimuli whereas broad spike cells being more highly tuned.

Furthermore, in cat's visual cortex, large number of excitatory neurons exhibit narrow spikes making the spike-width a non-valid parameter, therefore not permitting the distinction between pyramidal cells and inhibitory interneurons [26]. A recent study demonstrated that in cat V1, neurons show similar diversity in their spike-widths. In addition, neurons with a broad spike exhibit higher correlation levels between each other [31]. On the contrary, we found that correlating the spiking activity of each spike-waveform with the population activity shows the opposite trend: cells with a narrow spike-shape (also highly firing) exhibited greater coupling strengths than cells with a broad spike-shape. It is to be emphasized that on a cell–pair basis, the firing rates and peak magnitudes in CCG's are unrelated [14,30,33].

Complex circuitry mechanisms of individual neurons and the assemblies they form are involved in visual information processing [19]. Thus, measuring correlated spike-trains between neurons and the entire group predicts the spike shape and the firing rate pattern as the coupling level can be distinguishable between broad spike neurons (mainly LF neurons) and thin spike neurons (mainly HF neurons). Synchrony within a restricted space such as a cortical orientation domain can be accomplished by their specific relationships [37].

Combined with our recent finding which confers to the thin spike neurons higher gamma activity [8], these findings provide new insights into visual information processing. Indeed, within a cell-assembly comprising different cell-types, HF neurons may modulate the inputs and contribute to the selectivity of broad spike neurons in a recurrent "broad spike–thin spike" neuronal ensemble. A schematic model of a neuronal population is illustrated in Fig. 4 where a stimulus is coded by a cell-assembly; the HF neurons (black) are more correlated with the neuronal ensemble. This may occur to ensure an efficient firing of neurons preferring the presented stimulus. LF neurons (orange) are less coupled to the population but exhibit correlations with neighboring neurons preferring the same orientation.

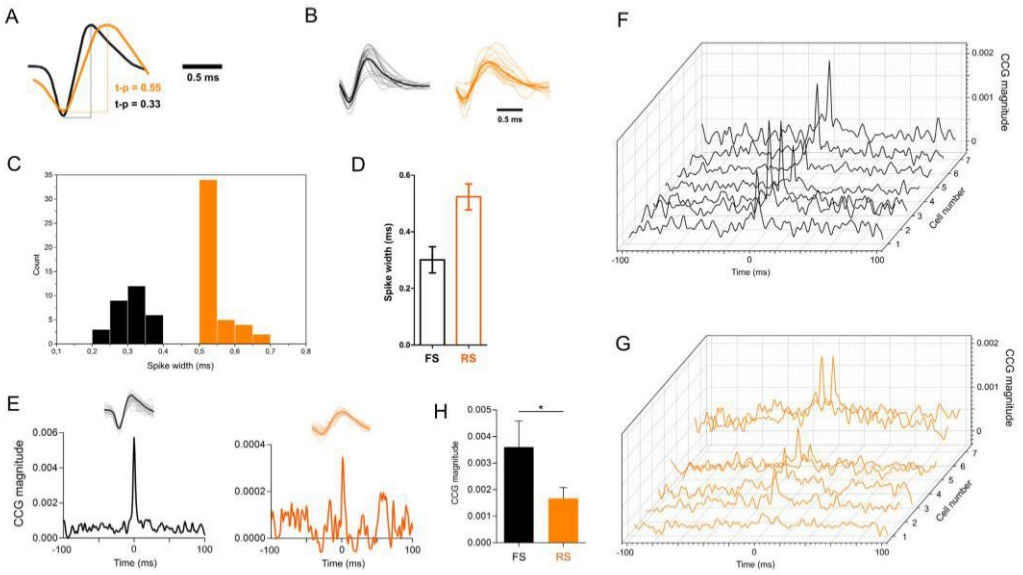

Fig. 2. Population coupling and types of neurons.
(A) Examples of two simultaneously recoded neurons showing the measurements of the spike-widths (trough-to-peak intervals). (B) Superimposed spike-waveforms of 20 cells from each type. The bold traces represent the average waveforms. (C) Histogram distribution of the trough-to-peak intervals for all neurons ($n = 73$). Orange and black histograms reflect the broad spike and the thin spike cells, respectively. (D) Averaged spike-widths for each cell-type. (E) Cross-correlograms between two neurons (the respective spike-waveforms are shown above each CCG) and the global spiking activity of the neuronal population. *X*-axis represents the time-window and *Y*-axis indicates the magnitude of the CCG. (F and G) Cross-correlograms between a group of thin spike cells (black) and the population rate (F), and between broad spike cells (orange) and the populational rate (G). (H) Global statistics on the correlation-strength for all neurons ($n = 73$) (For interpretation of the references to color in this figure legend, the reader is referred to the web version of this article.).

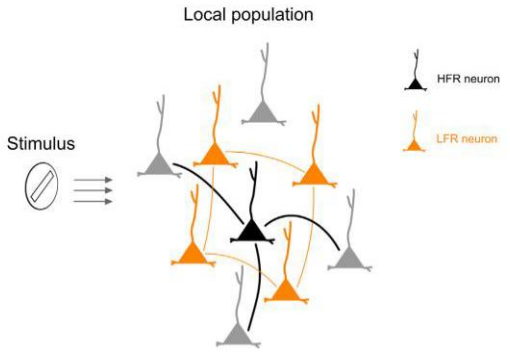

Fig. 4. Schematic model of a neuronal ensemble and the respective putative functional connections between thin spike neurons (HF neurons) and broad spike cells (LF neurons). (For interpretation of the references to color in the text, the reader is referred to the web version of this article.)

Conflict of interest

The authors have no conflicts of interest to declare.

Acknowledgements

Funding were supported by CRSNG (Conseil de Recherches en Sciences Naturelles et en Génie) and FRQ-NT (Fonds de recherche du Québec—Nature et technologies).

References

[1] K.D. Alloway, S.A. Roy, Conditional cross-correlation analysis of thalamocortical neurotransmission, Behav. Brain Res. 135 (2002) 191–196.
[2] B.V. Atallah, W. Bruns, M. Carandini, M. Scanziani, Parvalbumin-expressing interneurons linearly transform cortical responses to visual stimuli, Neuron 73 (2012) 159–170.
[3] R. Azouz, C.M. Gray, L.G. Nowak, D.A. McCormick, Physiological properties of inhibitory interneurons in cat striate cortex, Cereb. Cortex 7 (1997) 534–545.
[4] L. Bachatene, V. Bharmauria, S. Cattan, J. Rouat, S. Molotchnikoff, Modulation of functional connectivity following visual adaptation: homeostasis in V1, Brain Res. 1594 (2015) 136–153.
[5] L. Bachatene, V. Bharmauria, S. Cattan, J. Rouat, S. Molotchnikoff, Reprogramming of orientation columns in visual cortex: a domino effect, Sci. Rep. 5 (2015) 9436.
[6] L. Bachatene, V. Bharmauria, J. Rouat, S. Molotchnikoff, Adaptation-induced plasticity and spike waveforms in cat visual cortex, Neuroreport 23 (2012) 88–92.
[7] P. Bartho, H. Hirase, L. Monconduit, M. Zugaro, K.D. Harris, G. Buzsaki, Characterization of neocortical principal cells and interneurons by network interactions and extracellular features, J. Neurophysiol. 92 (2004) 600–608.
[8] V. Bharmauria, L. Bachatene, S. Cattan, N. Chanauria, J. Rouat, S. Molotchnikoff, Stimulus-dependent augmented gamma oscillatory activity between the functionally connected cortical neurons in the primary visual cortex, Eur. J. Neurosci. 41 (2015) 1587–1596.
[9] D.S. Bortone, S.R. Olsen, M. Scanziani, Translaminar inhibitory cells recruited by layer 6 corticothalamic neurons suppress visual cortex, Neuron 82 (2014) 474–485.
[10] J.A. Cardin, L.A. Palmer, D. Contreras, Stimulus feature selectivity in excitatory and inhibitory neurons in primary visual cortex, J. Neurosci. 27 (2007) 10333–10344.
[11] M.R. Cohen, A. Kohn, Measuring and interpreting neuronal correlations, Nat. Neurosci. 14 (2011) 811–819.
[12] J. Csicsvari, H. Hirase, A. Czurko, G. Buzsaki, Reliability and state dependence of pyramidal cell-interneuron synapses in the hippocampus: an ensemble approach in the behaving rat, Neuron 21 (1998) 179–189.
[13] Y. Dong, S. Mihalas, F. Qiu, R. von der Heydt, E. Niebur, Synchrony and the binding problem in macaque visual cortex, J. Vis. 8 (2008) 1–34.

[14] F. Duret, S. Shumikhina, S. Molotchnikoff, Neuron participation in a synchrony-encoding assembly, BMC Neurosci. 7 (2006) 72.
[15] A. Grinvald, A. Arieli, M. Tsodyks, T. Kenet, Neuronal assemblies: single cortical neurons are obedient members of a huge orchestra, Biopolymers 68 (2003) 422–436.
[16] S.B. Hofer, H. Ko, B. Pichler, J. Vogelstein, H. Ros, H. Zeng, E. Lein, N.A. Lesica, T.D. Mrsic-Flogel, Differential connectivity and response dynamics of excitatory and inhibitory neurons in visual cortex, Nat. Neurosci. 14 (2011) 1045–1052.
[17] H. Hu, J. Gan, P. Jonas, Interneurons, Fast-spiking, parvalbumin(+) GABAergic interneurons: from cellular design to microcircuit function, Science 345 (2014) 1255263.
[18] C.P. Hung, D. Cui, Y.P. Chen, C.P. Lin, M.R. Levine, Correlated activity supports efficient cortical processing, Front. Computat. Neurosci. 8 (2014) 171.
[19] H. Ko, Neuroscience. Functional organization of synaptic connections in the neocortex, Science 346 (2014) 555.
[20] H. Ko, S.B. Hofer, B. Pichler, K.A. Buchanan, P.J. Sjostrom, T.D. Mrsic-Flogel, Functional specificity of local synaptic connections in neocortical networks, Nature 473 (2011) 87–91.
[21] S.J. Kuhlman, E. Tring, J.T. Trachtenberg, Fast-spiking interneurons have an initial orientation bias that is lost with vision, Nat. Neurosci. 14 (2011) 1121–1123.
[22] Y.T. Li, B.H. Liu, X.L. Chou, L.I. Zhang, H.W. Tao, Strengthening of Direction Selectivity by Broadly Tuned and Spatiotemporally Slightly Offset Inhibition in Mouse Visual Cortex, Cereb. Cortex (2014), http://dx.doi.org/10.1093/cercor/bhu049 [Epub ahead of print].
[23] C.P. Lin, Y.P. Chen, C.P. Hung, Tuning and spontaneous spike time synchrony share a common structure in macaque inferior temporal cortex, J. Neurophysiol. 112 (2014) 856–869.
[24] D.A. McCormick, B.W. Connors, J.W. Lighthall, D.A. Prince, Comparative electrophysiology of pyramidal and sparsely spiny stellate neurons of the neocortex, J. Neurophysiol. 54 (1985) 782–806.
[25] J.E. Miller, I. Ayzenshtat, L. Carrillo-Reid, R. Yuste, Visual stimuli recruit intrinsically generated cortical ensembles, Proc. Natl. Acad. Sci. U. S. A. 111 (2014) E4053–E4061.
[26] L.G. Nowak, R. Azouz, M.V. Sanchez-Vives, C.M. Gray, D.A. McCormick, Electrophysiological classes of cat primary visual cortical neurons in vivo as revealed by quantitative analyses, J. Neurophysiol. 89 (2003) 1541–1566.
[27] M. Okun, N.A. Steinmetz, L. Cossell, M.F. Iacaruso, H. Ko, P. Bartho, T. Moore, S.B. Hofer, T.D. Mrsic-Flogel, M. Carandini, K.D. Harris, Diverse coupling of neurons to populations in sensory cortex, Nature 521 (2015) 511–515.
[28] B.J. Palanca, G.C. DeAngelis, Does neuronal synchrony underlie visual feature grouping? Neuron 46 (2005) 333–346.
[29] P.R. Roelfsema, V.A. Lamme, H. Spekreijse, Synchrony and covariation of firing rates in the primary visual cortex during contour grouping, Nat. Neurosci. 7 (2004) 982–991.
[30] E.T. Rolls, A. Treves, The neuronal encoding of information in the brain, Prog. Neurobiol. 95 (2011) 448–490.
[31] D.P. Schulz, M. Sahani, M. Carandini, Five key factors determining pairwise correlations in visual cortex, J. Neurophysiol. (jn 94) (2015) 02015.
[32] M.N. Shadlen, J.A. Movshon, Synchrony unbound: a critical evaluation of the temporal binding hypothesis, Neuron 24 (1999) 67–77.
[33] S. Shumikhina, J. Guay, F. Duret, S. Molotchnikoff, Contextual modulation of synchronization to random dots in the cat visual cortex, Exp. Brain Res. 158 (2004) 223–232.
[34] A. Stepanyants, J.A. Hirsch, L.M. Martinez, Z.F. Kisvarday, A.S. Ferecsko, D.B. Chklovskii, Local potential connectivity in cat primary visual cortex, Cereb. Cortex 18 (2008) 13–28.
[35] M. Steriade, Neocortical cell classes are flexible entities, Nat. Rev. Neurosci. 5 (2004) 121–134.
[36] H.A. Swadlow, Efferent neurons and suspected interneurons in binocular visual cortex of the awake rabbit: receptive fields and binocular properties, J. Neurophysiol. 59 (1988) 1162–1187.
[37] P. Tiesinga, T.J. Sejnowski, Cortical enlightenment: are attentional gamma oscillations driven by ING or PING? Neuron 63 (2009) 727–732.
[38] C. van der Togt, S. Kalitzin, H. Spekreijse, V.A. Lamme, H. Super, Synchrony dynamics in monkey V1 predict success in visual detection, Cereb. Cortex 16 (2006) 136–148.
[39] Y. Yoshimura, J.L. Dantzker, E.M. Callaway, Excitatory cortical neurons form fine-scale functional networks, Nature 433 (2005) 868–873.

7. Article intitulé: Fluoxetine and serotonin facilitate attractive-adaptation-induced orientation plasticity in adult cat visual cortex

EJN fens EUROPEAN JOURNAL OF NEUROSCIENCE

European Journal of Neuroscience, Vol. 38, pp. 2065–2077, 2013 doi:10.1111/ejn.12206

NEUROSYSTEMS

Fluoxetine and serotonin facilitate attractive-adaptation-induced orientation plasticity in adult cat visual cortex

Lyes Bachatene, Vishal Bharmauria, Sarah Cattan and Stéphane Molotchnikoff
Department of Biological Sciences, University of Montreal, Montreal, QC, Canada

Keywords: adaptation, fluoxetine, plasticity, serotonin, visual cortex

Abstract

Neurons in V1 display orientation selectivity by responding optimally to a preferred orientation edge when it is presented within their receptive fields. Orientation plasticity in striate cortex occurs either by ocular deprivation or by imposition of a non-preferred stimulus for several minutes. Adaptation of neurons to a non-optimal orientation induces shifts of tuning curves towards the adapting orientation (attractive shift) or away from it (repulsive shift). Here, we investigated the effects of the neurotransmitter serotonin and antidepressant fluoxetine (a selective serotonin reuptake inhibitor) on the modulation of adaptation-induced orientation plasticity. We show that serotonin and fluoxetine promote mostly attractive shifts. Attractive shifts augmented in magnitude towards adapter, whereas repulsive neurons reversed their behavior in the direction of the forced orientation. Furthermore, neurons which retained their original preferred orientation expressed plasticity by shifting their tuning curves after drug administration mostly towards adapter. Our data suggest a pre-eminent role of fluoxetine by inducing and facilitating short-term plasticity in V1.

Introduction

Neurons in the primary visual cortex are selective to stimulus properties such as orientation (Hubel & Wiesel, 1959, 1968). Cells respond optimally when the preferred stimulus is applied within their respective receptive fields. Properties that deviate from the preferred characteristics evoke weaker responses. Over a range of axes of orientation, it is common to obtain a typical Gaussian fit of the tuning curve that reveals the preferred orientation. Such curves are established during the critical period that follows birth (Chiu & Weliki, 2003; Tanaka *et al.*, 2009). Several laboratories have demonstrated that frequent or prolonged presentation of a non-preferred orientation induces modifications of the tuning curves of neurons (Dragoi *et al.*, 2000; Ghisovan *et al.*, 2009; Nemri *et al.*, 2009; Bachatene *et al.*, 2012). This presented non-preferred stimulus to which a neuron generally responds poorly is called an adapter and the process of stimulus presentation for a specific period is referred to as adaptation. In this framework, adaptation is a method that points towards the 'forced' application of a non-preferred orientation (Krekelberg *et al.*, 2006; Stroud *et al.*, 2012). After adaptation, the peak of a neuron's tuning curve shifts either towards the adapting orientation (attractive shifts) or away from it (repulsive shifts). Similar results have been obtained for other features, namely spatial frequency (Marshansky *et al.*, 2011), direction of motion (Kohn & Movshon, 2004) and speed (Movshon, 1975). Interestingly, the adaptation-induced plasticity occurs in the adult, and hence in a fully mature brain well beyond the critical period that follows birth. Investigations have concluded that visual plasticity can be restored after ocular deprivation by electrical stimulation of the locus coeruleus (Kasamatsu *et al.*, 1985), or can be modulated by several substances such as acetylcholine and noradrenaline (Bear & Singer, 1986), and L-threo-DOPS (Mataga *et al.*, 1992). Moreover, it has been shown that over- expression of the protein Lynx1 restricts plasticity in V1 by contributing to the stability of cortical networks in the presence of cholinergic innervations. Conversely, ablating Lynx1 improves cholinergic circuitries and may restore plasticity in mice (Morishita *et al.*, 2010). In monocular deprived adult rats, ocular dominance plasticity may be reinstated by a decline of both GABAergic transmission and expression of chondroitin sulfate proteoglycans (Harauzov *et al.*, 2010). Some authors have shown that down-regulation of chondroitin sulfate proteoglycans coupled with reverse lid-suturing in adult rats restores ocular dominance (Pizzorusso *et al.*, 2002, 2006). This is supported by an augmentation of both visual acuity and dendritic spine density (Pizzorusso *et al.*, 2006). However, in adult cat V1, the recovery from monocular deprivation is insufficiently re-established after administration of chondroitinase (Vorobyov *et al.*, 2013). Such physiological and molecular mechanisms of visual plasticity are of high therapeutic importance for visual system pathologies, e.g. amblyopia (Maya-Vetencourt & Origlia, 2012).

Recently, Maya-Vetencourt *et al.* (2008, 2011) have shown that in adult rats, ocular-dominance plasticity is restored after long-term treatment with the antidepressant fluoxetine. Furthermore, it has been shown that administration of fluoxetine to patients with ischemic stroke leads to an increase of motor recovery in comparison with placebo subjects (Chollet *et al.*, 2011). In line with the above published data, we sought to examine the effects of serotonin and fluoxetine on shifts of orientation tuning curves of neurons following adaptation in adult anesthetized cats. We show that serotonin

Received 2 January 2013, revised 26 February 2013, accepted 28 February 2013

and fluoxetine mostly potentiate attractive shifts, suggesting a facilitatory effect on orientation plasticity after adaptation.

Material and methods

Ethical approval

Electrophysiological recordings were performed on the primary visual cortex of nine adult domestic cats (*Felis catus*). Animal surgery procedures and electrophysiological recordings followed the guidelines of the Canadian Council on Animal Care and were approved by the Institutional Animal Care and Use Committee of the University of Montreal. Animals were supplied by the Division of Animal Resources of the University of Montreal.

Animals, anesthesia and surgical procedures

Adult cats (2.5–3.5 kg, age 12–24 months) of either sex, sedated with acepromazine maleate (1 mg/kg, i.m., Atravet; Wyeth-Ayerst, Guelph, ON, Canada) and atropine sulfate (0.04 mg/kg, i.m., ATRO-SA; Rafter, Calgary, AB, Canada), were anesthetized with ketamine hydrochloride (25 mg/kg, i.m., Rogarsetic; Pfizer, Kirkland, QC, Canada) maintained with 0.3% isoflurane (AErrane; Baxter, Toronto, ON, Canada). Lidocaine hydrochloride (2%, Xylocaine; AstraZeneca, Missis-sauga, ON, Canada) was injected subcutaneously as a local anesthetic during surgery. A tracheotomy was performed for artificial ventilation, and one forelimb vein was cannulated. Animals were then placed in a stereotaxic apparatus. Xylocaine gel (5%; Astra Pharma, Mississauga, ON, Canada) was applied on the pressure points. For the remaining preparations and recording, paralysis was induced with 40 mg and maintained with 10 mg/kg/h gallamine triethiodide (i.v., Flaxedil; Sigma Chemical, St. Louis, MO, USA) administered in 5% dextrose lactated Ringer's nutritive solution. General anesthesia was maintained by artificial ventilation with a mixture of N_2O/O_2 (70 : 30) supplemented with 0.5% isoflurane (AErrane; Baxter) for the duration of the experiment. Proper depth of anesthesia was ensured throughout the experiment by monitoring the EEG, the electrocardiogram and expired CO_2. In addition, heart rate remained unmodified after skin stimulation. End-tidal CO_2 partial pressure was kept constant between 25 and 30 mmHg. A heated pad was used to maintain a body temperature of 37.5 °C. Tribrissen (30 mg/kg/day, s.c.; Schering-Plough, Pointe-Claire, QC, Canada) and Duplocillin (0.1 mL/kg, i.m.; Intervet, Withby, ON, Canada) were administered to the animals to prevent bacterial infection. The pupils were dilated with atropine sulfate (1%, Isopto-Atropine; Alcon, Mississauga, ON, Canada) and the nictitating membranes were retracted with phenylephrine hydrochloride (2.5%, Mydfrin; Alcon). The loci of the area centrales were inferred from the positions of the blind spots, which were ophthalmoscopically focused and back projected onto a translucent screen. To verify the stability of the eye this procedure was repeated at the end of tests. Plano contact lenses with artificial pupils (5 mm diameter) were placed on the cat's eyes to prevent the cornea from drying (University of Montréal, PQ, Canada).

At the end of each experiment, the animals were killed via a lethal dose of pentobarbital sodium (100 mg/kg, Somnotol; MTC Pharmaceuticals, Cambridge, ON, Canada) by intravenous injection.

Electrophysiological recordings

Multi-unit activity in the primary visual cortex was carried out with tungsten microelectrodes (2–10 MΩ at 1 kHz; Frederick Haer & Co, Bowdoinham, ME, USA). Each set of electrodes, consisting of four microelectrodes in linear array (inter-electrode spacing 400 μm) enclosed in stainless steel tubing, was controlled by a separate micromanipulator. The signal from the microelectrodes was amplified, band-pass filtered (300 Hz–3 kHz), digitized and recorded with a 0.05-ms temporal resolution (Spike2, CED, Cambridge, UK). We recorded at an average of 400–500 μm cortical depth from two recording sites. Each recording site yielded up to eight neurons. Action potentials were sorted using a window discriminator for further off-line analyses. Multi-unit signals from one electrode usually included up to seven well-isolated single units. The spike sorting method was based on cluster classification in reduced space (Spike2, CED). The stability of each cell's activity across conditions was verified qualitatively by visual control of the cluster disposition and of the waveform shape. Auto-correlograms were systematically performed to ensure proper single-cell capture (deep at zero).

Visual stimulation (adaptation protocol) and drug administration

Stimulation was monocular (dominant eye, the opposite eye was shut). After clearly detectable activity was obtained, the multiunit receptive fields (RFs) were mapped as the minimum response fields (Barlow *et al.*, 1967) by using a hand-held ophthalmoscope. RF edges were determined by moving a light bar from the periphery towards the centre until a response was elicited. Eye–screen distance was 57 cm. These preliminary tests revealed qualitative properties such as dimensions, velocity preference, orientation and directional selectivity. Visual stimuli were generated with a VSG 2/5 graphic board (Cambridge Research Systems, Rochester, UK) and displayed on a 21-inch monitor (Sony GDM-F520 Trinitron, Tokyo, Japan) placed 57 cm from the cat's eyes, with 1024 × 768 pixels, running at 100 Hz frame refresh. Stimuli were drifting sine-wave grating patches (~2° to 5°) covering the excitatory RF (Maffei & Fiorentini, 1973).

Patch characteristics were set to evoke optimal responses: contrast at 80%, mean luminance at 40 cd/m^2, optimal spatial and temporal frequencies set within 0.1–0.5 cycles/degree and 1.0–2.0 Hz, respectively. The blank screen was uniformly gray (~ 35 cd/m^2). In all cases the above parameters were chosen with the aim of evoking maximal discharges. V1 neurons are known to respond well to sine wave drifting gratings (Bardy *et al.*, 2006). After manual RF characterization, nine oriented stimuli centered on the preferred orientation were selected and used for the rest of the experiment. With a 22.5° interval between orientations, tuning curves covered 180°. Test orientations were applied in random order. Each oriented stimulus was presented in blocks of 25 trials lasting 4.1 s each, with a random inter-trial interval (1.0–3.0 s) during which no stimuli were presented. Thus, a recording session lasted for 25–30 min. Peristimulus time histograms were recorded. Once control orientation tuning curves were characterized, an adapting non-preferred stimulus was presented continuously for 12 min. The adapting stimulus was a drifting grating whose orientation was randomly selected in the range 22.5–67.5° from the neuron's preferred orientation. It has been shown previously that larger gaps between optimal and adapting orientations are less efficient in inducing orientation shifts (Ghisovan *et al.*, 2009). All other stimulus parameters were kept constant, at control values, throughout the recordings. During this adaptation period no recordings were performed. Immediately after adaptation, orientation tuning curves was measured starting with the adapting and control preferred orientations to prevent an unlikely

premature recovery, as these two orientations were the center of interest, while the remaining orientations were recorded in random order. Following a recovery period of 60–90 min, another tuning curve measurement was performed.

After the recovery period, we applied topically on the cortical surface a custom-cut filter paper (1 × 1 mm) soaked in 10 mM serotonin or fluoxetine; we also used γ-aminobutyric acid (GABA) as a control test for drug diffusion as this drug suppresses all electrical activity (see Results).

Data analysis

Once single cells were sorted off-line from multi-unit spike trains accumulated during data acquisition, orientation tuning curves were constructed from the raw data. Because orientation tuning is best described by Gaussian-like functions, we fitted our raw data with the von Mises function (Swindale, 1998). This allowed us to determine with precision the preferred orientation of neurons and then measure shifts in orientation preference. The von Mises function is defined as $M(\theta) = A.e^{\,b[\cos(\theta-c)]+d}$, where A is the value of the function at the preferred orientation, c, and b is a width parameter. An additional parameter, d, represents the spontaneous firing rate of the cell (Swindale, 1998; Kohn & Movshon, 2004). The above calculations are necessary because tuning curves derived from raw data may be imperfect in determining the preferred orientation given that the interval between the stimulus orientations is relatively large, 22.5°. In the cat, over 90% of V1 neurons are well tuned to stimulus orientation (Bishop & Henry, 1972). It was, however, necessary to ensure that cells in our sample were properly tuned for orientation. We measured an orientation selectivity index (OSI) by dividing the firing rate at orthogonal orientations by the firing rate for the preferred orientation, and subtracting the result from 1 (Ramoa *et al.*, 2001; Liao *et al.*, 2004). The closer the OSI is to 1, the stronger the orientation selectivity. To compare the mean OSI between control, post-adaptation and post-drug administration, a one-way ANOVA statistical test was performed with a significance level of 95%. We also correlated the OSI of each neuron with the amplitude of shift and used linear regression with 95% confidence interval to verify the relation. Adaptation-induced shifts were measured as the distance between peak positions of the fitted tuning curves before and after conditioning. To assess the statistical significance of tuning shifts, curve fits were generated separately for each of the 25 trials, and the mean difference was tested by a paired t-test. Shifts in preferred orientation larger than 5° were statistically significant (paired sample two-tailed t-test, $P < 0.01$). Furthermore, paired two-tailed Student's tests were carried out to verify the significance of differences between experimental conditions. In addition to the amplitude of shifts, we computed the modulation of responses for orientation classes (original optimal, adapter, new optimal and a flank orientation before and after adaptation). We used a one-tailed Wilcoxon rank test with 95% confidence interval to compare the response amplitude before and after the tests. Thereafter, we compared the amplitude of response between two specific classes of orientations (prior to drug administration versus post-drug administration, see Fig. 6) using a two-way ANOVA statistical test (95% significance level). Moreover, the firing rate of spontaneous activity (firing rate of the neurons when a black screen was presented, no stimulus) was compared between control, post-adaptation, recovery and drug conditions and a one-way ANOVA statistical test was used to compare the mean firing response between these conditions with a 95% significance level. All statistical tests described in the results were computed using the numerical software GraphPad Prism version 5 (GraphPad Software Inc., La Jolla, CA, USA).

Results

The present experiments were aimed at investigating the effects of the neurotransmitter serotonin and antidepressant fluoxetine (a selective serotonin reuptake inhibitor, SSRI) on shifts of orientation tuning curves of neurons following adaptation on adult cats of either sex. No difference was observed between males and females in the results presented below. After a classical visual stimulation protocol to determine the Gaussian orientation tuning curves, we established the shifts of tunings of the recorded neurons after adaptation prior to drug application. Thereafter, we proceeded with drug testing on the same neurons. After the recovery period from the first adaptation, we administered serotonin or fluoxetine topically with a custom-cut filter paper soaked in 10 mM solution deposited on the surface of the primary visual cortex (adjacent to the recording electrode shaft). In addition, drug diffusion was assessed by recording responses from neighboring sites. Moreover, we used the potent inhibitory GABA (10^{-2} mM) to supplement our results regarding substance diffusion. Figure 1 illustrates the experiments aimed at showing that the drug's effect is limited to a tissue volume inferior to 400–500 μm. The general set-up is displayed in Fig. 1A. A typical example of multi-unit recordings is shown in Fig. 1B. It demonstrates that the diffusion of drugs was restricted to a volume inferior to ~ 400–500 μm. On the left, we show two electrodes positioned laterally (inter-electrode distance 400 μm), while on the right, the recording tips are vertically spaced along the electrode shank (inter-recording site distance 500 μm). The application of GABA next to electrode #2 (E2) reduced considerably the multi-neuronal activity while the electrical activity under electrode #1 (E1) remained unaffected. Similarly, in depth recordings (right side), the most superficial site (site 2) illustrates the firing decline, whereas 500 μm below, the multi-neuronal firing remains unmodified by serotonin. Although serotonin may decrease the general activity of neurons (Licata *et al.*, 1993; Zhong & Yan, 2011; Avesar & Gulledge, 2012), these cells maintain a tuning curve as one specific orientation evokes the maximal firing rate relative to other orientations. The experimental protocol is shown schematically in Fig. 1C. The test began by determining the orientation tuning curves by randomly presenting sine-wave gratings at eight orientations wherein the preferred orientation evokes the highest firing rate. In the next phase, a non-preferred orientation is applied uninterruptedly for 12 min to induce adaptation. This initial step, for most cells, ascertains the shift of the peak of the tuning curve for the unit under investigation. The recovery of the original tuning curve is achieved about 60–90 min after the cessation of first adaptation: consequently, the original tuning curve is reinstated. After the recovery period, the drug was topically applied. Immediately after administration of the substance, we carried out a second adaptation for the same duration (12 min) with the same non-preferred orientation (as the first adaptation), and the entire process was repeated.

The present paper describes data recorded from single unit analysis. Of 139 isolated neurons, 68 were tested with serotonin (four cells were eliminated and eight units were unclassified) and 71 neurons were investigated with fluoxetine (one unit was eliminated and 10 were unclassified). Neurons were eliminated when their firing activity was lost during the experiment, and as a consequence they could not be traced. Unclassified neurons refer to neurons for which the tuning curve could not be determined. We also calculated the OSI of each neuron as 1 – (firing rate at orthogonal orientation/firing

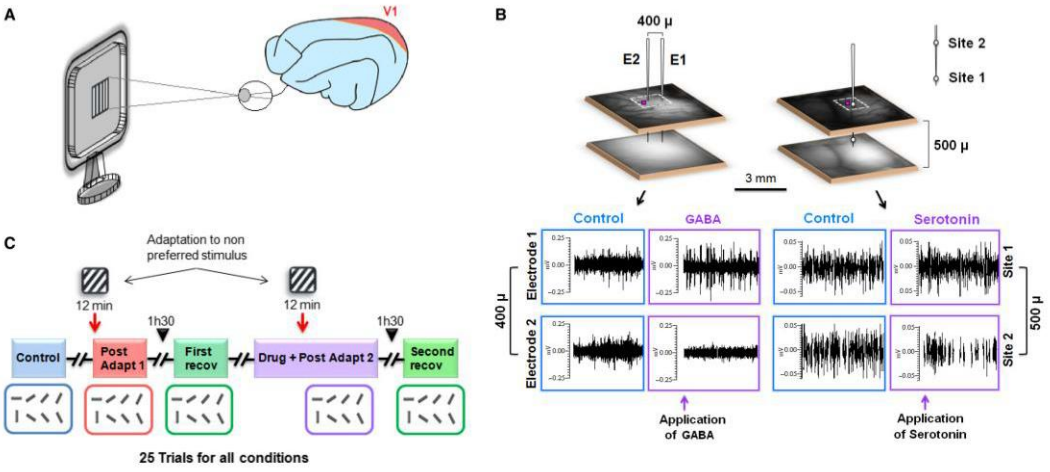

FIG. 1. Experimental procedures and drug diffusion. (A) Visual stimulation on adult cat striate cortex. (B) Electrophysiological recordings using multi electrodes (left cortex) and multisite electrode (right cortex); small square beside the electrode (E2 and site 2) represents the filter paper soaked with the drug. Below are shown the firing rates of multi-unit activity using GABA (left cortex) and serotonin (right cortex) for drug diffusion. (C) Experimental time course. All the orientations are randomly presented on the screen in 25 trials with arbitrary intervals.

rate at preferred orientation); the closer the OSI is to 1, the stronger the orientation-selectivity. We also correlated the orientation selectivity index with the amplitude of shift for each neuron. The mean OSI was superior to 0.7 for each condition ($OSI_{control}$ = 0.78, $OSI_{post\text{-}adaptation}$ = 0.73, $OSI_{post\text{-}drug\ administration}$ = 0.82), and no significant difference was observed between these conditions (one-way ANOVA: $F = 1.77$, $P = 0.17$, see Supporting Information Fig. S2A). Results from the correlation between the OSI and the amplitude of shifts showed no significant correlation after adaptation (linear regression: $F = 0.05$, $P = 0.81$) or after drug administration (linear regression: $F = 0.02$, $P = 0.88$).

Serotonin and fluoxetine facilitate adaptation-induced plasticity

Previous studies have shown that prolonged adaptation of 12 min to a non-preferred stimulus leads to shifts of peaks of orientation tuning curves towards the adapting orientation in most of cases (attractive shift) (Ghisovan *et al.*, 2008, 2009; Nemri *et al.*, 2009; Bachatene *et al.*, 2012). Figure 2A and B present an example of the effect of serotonin on the attractive shifts. In these figures, the spike waveform at every stage of the study is shown in rectangular boxes, i.e. the neuron was traced throughout all steps of the recording. The red triangle represents the adapting orientation in this and all subsequent figures. The upper two plots show the orientation tuning curve of a cell as derived from the raw data, i.e. spike counts. Horizontal orientation (optimal orientation = 1.65°, derived from Gaussian fits) evoked the highest firing rate specifying the preferred orientation of the neuron (blue curve). The adapting orientation (112.5°), applied uninterruptedly for 12 min, induced a new optimal orientation (red curve) at 46.82°. In this case, the amplitude of the attractive shift was 45.17°. The lower curves are obtained after Gaussian fits as derived from raw values (Control R^2 = 0.7, Adaptation R^2 = 0.9, Recovery R^2 = 0.9, Serotonin R^2 = 0.5). Following the recovery (green curve) of the original preferred orientation (1.31°), serotonin was applied over the cortex (see Fig. 1). The impact of the drug resulted in an increase of shift by 110.29° from 1.31° to 111.6° (Fig. 2B). Indeed, in the presence of serotonin, the new preferred orientation coincided with the adapter (shift increased from 45.17° to 110.29°).

Comparable results were obtained with fluoxetine (Fig. 2C and D, Control R^2 = 0.5, Adaptation R^2 = 0.6, Recovery R^2 = 0.8, Fluoxetine R^2 = 0.6). Prior to fluoxetine application, the attractive shift was 23.06° (original preferred: 65.98°, adapter set at 135°, following adaptation optimal axis = 89.04°). Fluoxetine administration increased the attractive shift to 106.13°, which displaced the peak of the tuning curve further towards the adapting orientation (Fig. 2D).

It is worth underlining that adaptation declines the responses evoked by the initial optimal orientation (Ghisovan *et al.*, 2008). Interestingly, in some cases the attractive translation is partial, i.e. the adaptation-induced shift failed to reach the adapter (Fig. 2A and C), particularly if the gaps separating adapting and the initial optimal orientations were too large. Following the adaptation procedure accompanied by serotonin or fluoxetine (Fig. 2B and D, respectively), the amplitude of the attractive shift increased (amplified shift effect) in the presence of the drug and attained that of the adapter, suggesting the effectiveness of both drugs in driving the peak of the tuning curve towards the adapter. The new optimal orientation coincided with the imposed orientation in 74% of neurons treated with serotonin, and in 73% of neurons treated with fluoxetine. No specific properties (cortical depth, firing rate or specific receptive field) were found for neurons which acquired a new preferred orientation similar to the adapter.

Refractory neurons

Twenty-two per cent of neurons that we term 'refractory' did not display any significant shift of their orientation tuning curves after first adaptation, i.e. they maintained their original preferred orientation following the first adaptation. In our experiments, a shift is considered significant if it is > 5° (shifts below to this threshold are insignificant, paired sample two-tailed *t*-test, $P > 0.01$, Ghisovan

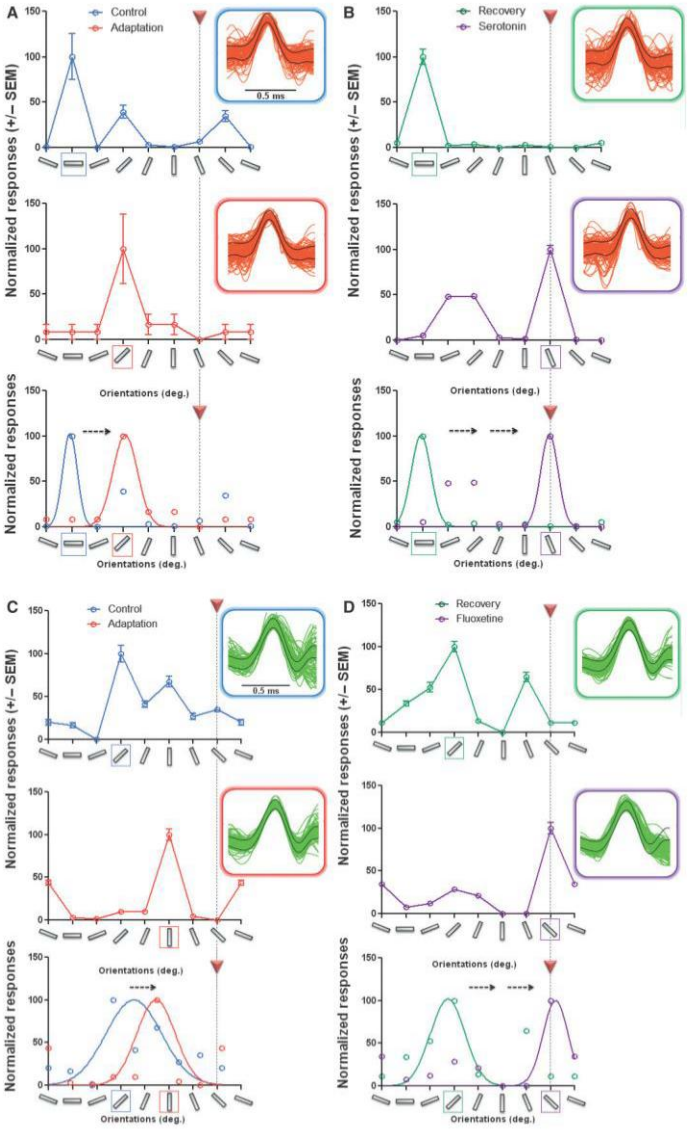

FIG. 2. Amplified attractive effect of serotonin and fluoxetine. (A) Raw data and Gaussian fit of normalized responses of one neuron for control (blue) and post-adaptation (red). Red triangle represents adapting orientation. Gaussian fits show shift of the tuning curve (attractive shift, 45.17°). (B) Raw data and Gaussian fit of normalized responses of the same neuron for recovery (green) and after the second adaptation during serotonin application (purple); the new attractive shift is 110.29°. Orange spikes represent waveforms of the same neuron for all conditions. (C, D) Same results for a different neuron, during fluoxetine administration (attractive shift post-adaptation 23.06°, amplified attractive shift during fluoxetine application 106.13°). Green spikes show the waveforms of the same cell.

et al., 2009). Thus, refractory neurons retained their original optimal orientation following an initial adaptation period to a non-preferred stimulus or showed a very small jitter of their peak inferior to 5°. Figure 3 illustrates that administration of serotonin (Fig. 3A and B, Control $R^2 = 0.9$, Adaptation $R^2 = 0.9$, Recovery $R^2 = 0.9$, Serotonin $R^2 = 0.8$) or fluoxetine (Fig. 3C and 3D, Control $R^2 = 0.8$, Adaptation $R^2 = 0.8$, Recovery $R^2 = 0.7$, Fluoxetine $R^2 = 0.9$) prompted a significant shift of the peaks in the post-adaptation

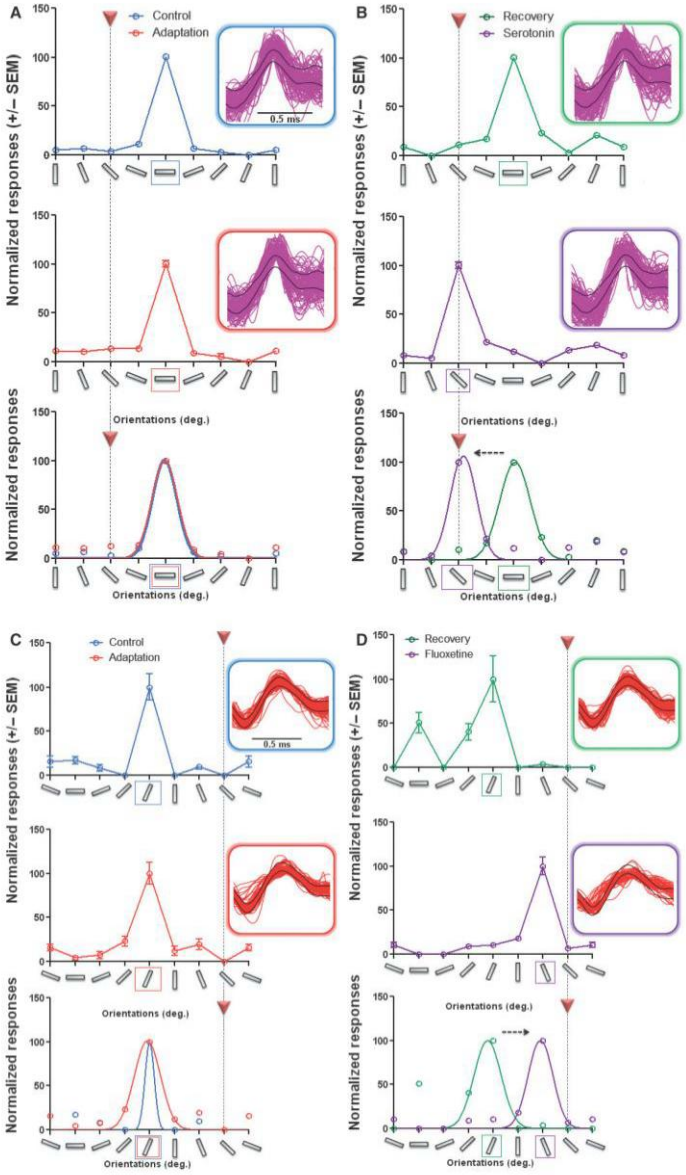

FIG. 3. Induction of attractive shift by the action of serotonin and fluoxetine. (A) Raw data and Gaussian fit of normalized responses of one neuron for control and post-adaptation conditions (blue and red curves, respectively). Red triangle represents the adapter. Gaussian fits below show a non-significant shift after the first adaptation. (B) Raw data and Gaussian fit of normalized responses of the same cell for recovery and second adaptation in the presence of serotonin (green and purple curves, respectively). Pink spikes represent waveforms of the same cell for the entire procedure. The tuning curve shifted toward the adapter in the presence of the drug. (C, D) Similar induction of an attractive shift for another neuron during fluoxetine administration. Red spikes represent waveforms of the same neuron.

period. In sections B and D, administration of serotonin (B) and fluoxetine (D) displaced the orientation tuning curves towards the adapting orientation (attractive shift 42.33° and 48.02°, respectively). In most refractory cells, shifts were attractive (91%, $n = 11$ for serotonin experiments, 93%, $n = 14$ for fluoxetine experiments) (see also Fig. 5).

Serotonin and fluoxetine reverse the repulsive shifts

Although 12 min of adaptation induces attractive shifts in about two-third of neurons, a fairly large number of units do exhibit repulsive shifts. In the present investigation, 32% of neurons ($n = 56$, serotonin experiments) and 25% of neurons ($n = 60$, fluoxetine experiments) responded with repulsive shifts after the first adaptation. In the following section, comparative effects of serotonin and fluoxetine are described, wherein the repulsive shifts post-first adaptation were reversed towards the adapter. Figure 4 illustrates such reversal of the orientation-selectivity (Control $R^2 = 0.8$, Adaptation $R^2 = 0.5$, Recovery $R^2 = 0.5$, Serotonin $R^2 = 0.6$). For instance, in Fig. 4A the first adaptation displaced the peak of the tuning curve by 79.32° away from the adapter (optimal orientation 119.7°, adapter set at 135° and new optimal orientation 40.38°). During serotonin application, a repeated adaptation resulted in optimal orientation corresponding to the adapter: 142.5° (Fig. 4B). Comparable results were recorded with fluoxetine (Control $R^2 = 0.5$, Adaptation $R^2 = 0.6$, Recovery $R^2 = 0.7$, Fluoxetine $R^2 = 0.8$). Indeed, Fig. 4C shows a repulsive shift (31.68° as obtained from Gaussian fits) after the first adaptation for the illustrated neuron (purple spike). Following the second adaptation in the presence of fluoxetine (Fig. 4D), we observed an attractive effect towards the imposed orientation (adapter set at 22.5°), and thus fluoxetine cancels the repulsive shift and induces an attractive change of the peak of the orientation tuning curve (attractive shift 8.25°, from Gaussian fit).

Modulations of shifts following serotonin and fluoxetine applications

Figure 5A and B display for every analysed cell the changes of shift magnitudes and displacement direction of orientation tuning curve peak induced by serotonin and fluoxetine. Cells are grouped into three major classes according to the direction of the shift following the first adaptation: from left to right these are repulsive to attractive, attractive to attractive (increase of attractive shift) and no shift to attractive, whereas the other two groups with very few neurons (six units for serotonin experiments in Fig. 5A, and ten units for fluoxetine experiments in Fig. 5B) did not display an attractive facilitatory effect. Drugs were applied after the first adaptation following recovery of the original orientation-selectivity. The shifts following the first adaptation are depicted by red circles, whereas shifts in the presence of serotonin or fluoxetine are indicated by purple squares (serotonin) and purple circles (fluoxetine). Paired two-tailed Student's tests were used to compare the amplitude of shifts after the first adaptation versus the second adaptation with administration of the drug. The effects of serotonin are displayed in Fig. 5A. Eighteen neurons (32%, $n = 56$) reacted with a repulsive shift after the first adaptation with an average amplitude shift of 25.4 ± 19.4°. Seventeen of these neurons reversed the initial repulsive shift towards the opposite direction: attractive, the average amplitude of the new shift was 24 ± 19.2° (paired two-tailed t-test: $t = 7.9$, $P < 0.0001$, see Fig. 5A, first column from left), and one neuron remained unaffected by the drug (see proportion of unaffected neurons). Twenty-seven neurons (48%, $n = 56$) reacted attractively as a result of the first adaptation. Twenty-three of these neurons responded with significant augmented shifts (averaged shift following the first adaptation 15.1 ± 9.6°, averaged shift with serotonin reached 33 ± 29.4°; paired two-tailed t-test: $t = 3.4$, $P = 0.002$, second column from left). Interestingly, 11 neurons (20%, $n = 56$) that retained their orientation-selectivity after the first adaptation (averaged shift amplitude = 2.2 ± 2.0°, i.e. not significant) exhibited a large attractive shift for 10 neurons (new averaged shift amplitude = 23 ± 17.1°, paired two-tailed t-test: $t = 3.8$, $P = 0.0039$), although one neuron remained unaffected. This suggests a facilitating role of serotonin in inducing attractive shifts. In addition to these three major classes, a few cells (3%, $n = 56$) reacted by shifting their peak from attractive to repulsive translation (fourth column from left) and four units (7%, $n = 56$) remained unaffected by the drug (right column). The horizontal bars underline the mean values of tuning shifts.

In Fig. 5B, on a cell-by-cell basis, we show the changes of shift magnitudes after the second adaptation while fluoxetine was applied to the cortex. The same global trend of results was obtained: the drug potentiates attractive shifts, i.e. repulsive displacement reversed to attractive shifts (25%, $n = 60$), attractive shifts remaining attractive although the increase is insignificant (averaged shift after the first adaptation equals 22 ± 11.1°, and the averaged shift after the second adaptation with fluoxetine administration is 27 ± 25.4°; paired two-tailed t-test: $t = 0.9$, $P = 0.37$). Thirteen cells failed to change their orientation-selectivity once the first adaptation was carried out, and these cells exhibited strong attractive displacements as fluoxetine was deposited (2.6 ± 1.3° shift after the first adaptation, this shift reached 23.5 ± 14.2° post-adaptation and fluoxetine administration; paired two-tailed t-test: $t = 4.9$, $P = 0.0003$).

Thus, these results suggest that serotonin and fluoxetine (an SSRI) (Manji *et al.*, 2001; Castrén, 2005; Kaneko *et al.*, 2007; Briscoe *et al.*, 2008) potentiate attractive shifts following adaptation, and as a consequence these drugs facilitate the emergence of responses to a new preferred orientation close to the adapter.

The results presented above show the important role of these two drugs in facilitating neuronal adaptation-induced plasticity within the primary visual cortex. Note that for the amplified effect of the drugs (attractive to attractive), tests were significant for serotonin (paired two-tailed t-test: $t = 3.4$, $P = 0.002$) with an increase in amplitude of shifts of more than 50%, whereas for fluoxetine, attractive shift modifications were not significant (paired two-tailed t-test: $t = 0.9$, $P = 0.37$), suggesting that the facilitatory effect is due to direct serotoninergic actions, while the smaller effect of fluoxetine would be due to an indirect path such as inhibition of serotonin reuptake, which is pronounced after chronic administration (Maya-Vetencourt *et al.*, 2008; Wang *et al.*, 2008). Indeed, in a recent investigation, it has been shown that the effect of fluoxetine on polysynaptic transmission is relatively small in comparison with the action of serotonin (Komlosi *et al.*, 2012).

Modulations of response magnitude following serotonin and fluoxetine applications

Figure 6A and B compare response modulations during serotonin and fluoxetine applications for the group of neurons that increased the attractive effect during drug administration. In addition to responses obtained at the flanks of the tuning curve, we focused these analyses on the evoked discharges in response to three orientations: original optimal orientation, the adapter and new optimal orientation. Colored squares (in accordance with the orientation classes) represent average changes in response amplitude relative to the baseline, which corresponds to the response magnitude recorded before testing. These control responses are normalized (100%) in the computations of Fig. 6. As indicated in the Methods, in the absence of drugs, we carried out an adaptation protocol to ensure that indeed the unit is shifting the peak of its orientation curve. One-tailed Wilcoxon rank tests (95% confidence interval) were computed to compare the response amplitude before and after adaptation for each orientation class. Two-way ANOVA (95% significance level)

was used to compare the amplitude of response between two specific classes of orientations: prior to drug administration versus post-drug administration. Blue squares show changes in response amplitude for the original optimal orientation (control). As expected from the previous results, this response amplitude decreased after adaptation. For serotonin and fluoxetine experiments, we found that this

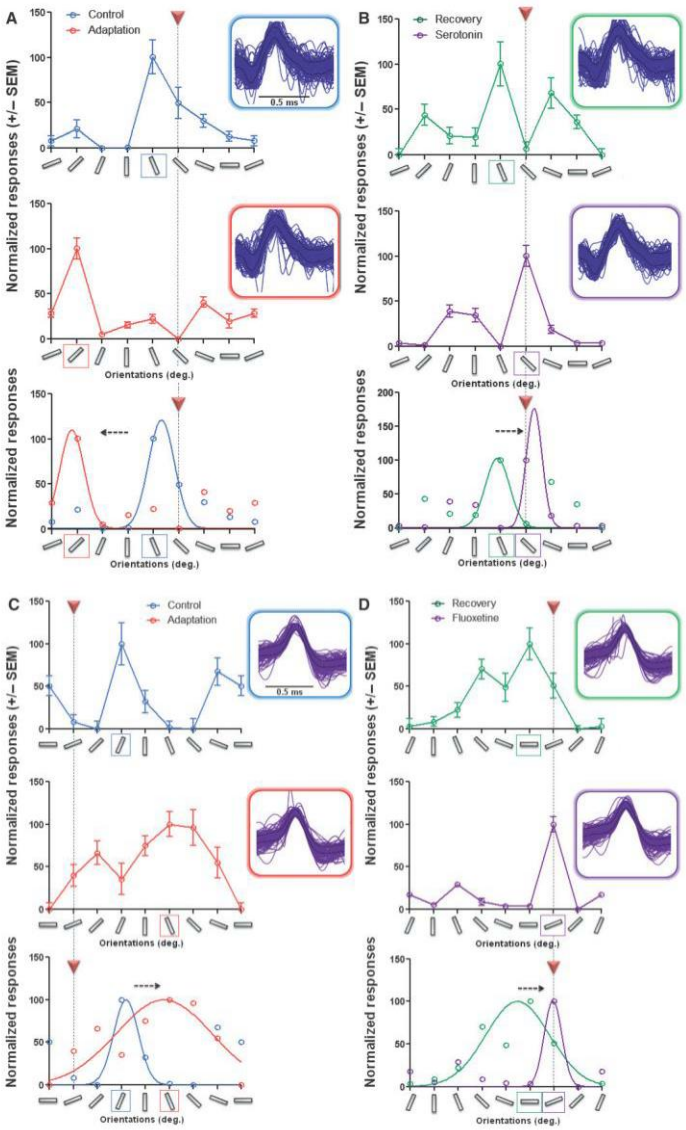

FIG. 4. Inversion of shift by serotonin and fluoxetine. (A) Raw data and Gaussian fit of normalized responses of one neuron for control (blue curve) and after the first adaptation process (red curve). The red triangle indicates the imposed orientation during adaptation. Note the shift of the tuning curve away from the adapter (repulsive shift). (B) Raw data and Gaussian fit of normalized responses of the same recorded cell for recovery (green curve) and after the second adaptation during serotonin deposition (purple curve). Blue spikes represent waveforms of the same neuron over all steps. The drug inversed the shift of the tuning curve towards the adapting orientation (see Gaussian fits below). (C, D) Same effect (inversion of repulsive shift) for a different presented neuron (purple spikes indicating the same cell for all conditions) in the presence of fluoxetine.

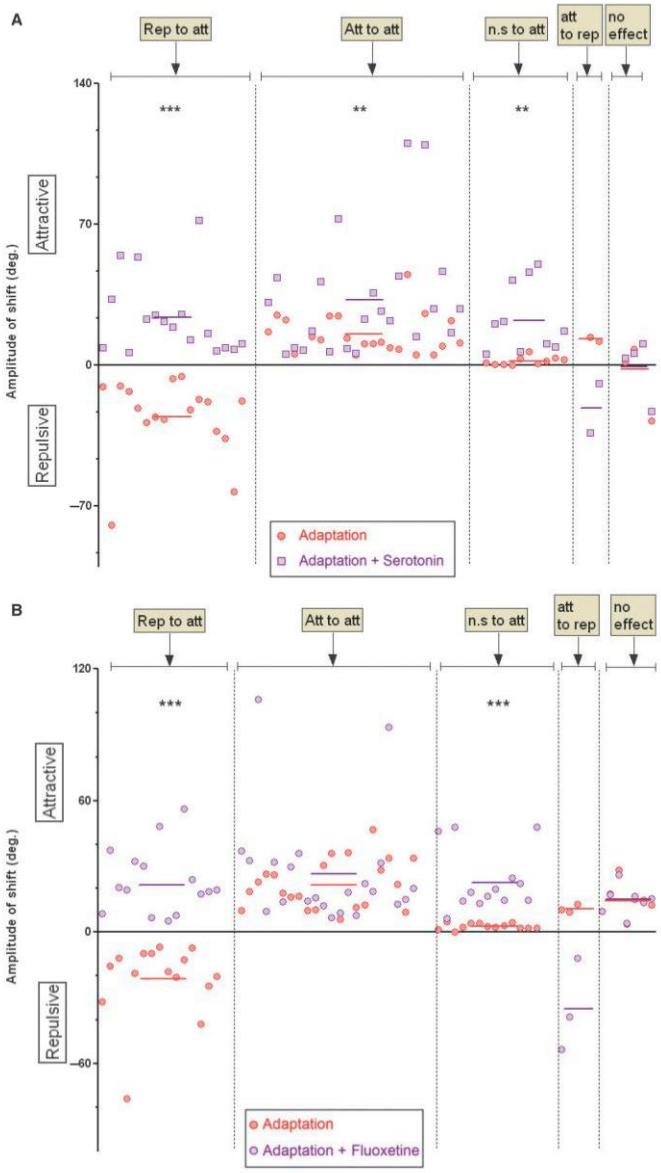

FIG. 5. Modulation of shift-magnitudes for every analysed neuron. (A) Global distribution of neurons for serotonin experiments. Red circles represent shifts of each neuron after the first adaptation, and purple squares represent shifts of the same neurons after the second adaptation during serotonin administration. Horizontal bars indicate the average shift of each group for both conditions. The lower side represents the repulsive side, i.e. the shifts away from the adapter, and the upper side represents the attractive side, i.e. the shifts towards the adapter. The first group (left) shows the reversal effect of serotonin from repulsive to attractive shift (for values see Results). The second group shows the amplified attractive effect. The third group represents refractory neurons; the drug induced an attractive shift (see Results). The fourth group represents a small proportion of neurons which reverse their shifts from attractive to repulsive (two neurons). The last group (right) shows the population of neurons which was not affected by serotonin (no effect). (B) Fluoxetine showed a similar tendency. Red circles show shifts of each analysed cell after the first adaptation, and purple circles represent shifts of the same cells after the second adaptation during fluoxetine administration, stars (***) indicate the significance level of the statistical test (see text).

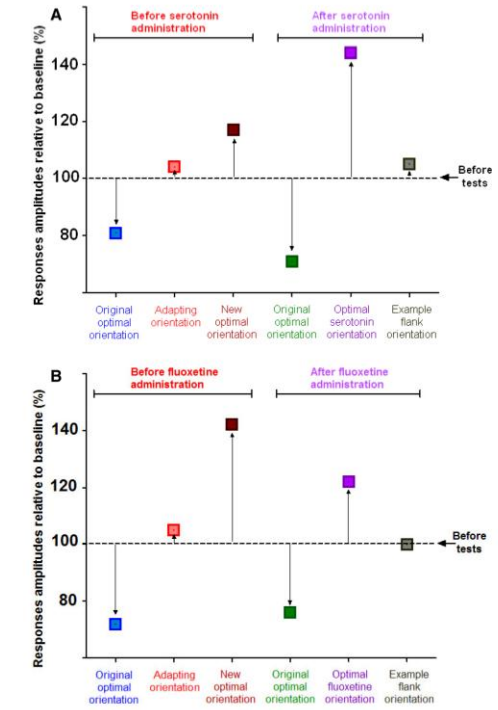

FIG. 6. Graph representing changes in response amplitudes for different orientations. (A) Graph of response amplitudes for serotonin experiments. Colored squares represent averaged changes in response amplitude following a specific stimulus (orientation) in several conditions relative to baseline (normalized firing rate before adaptation = 100%). Blue squares show the change in response amplitude for the original optimal orientation (control), which decreased after adaptation. Red squares show the change in response amplitude for the adapter, which increased post-adaptation. Brown squares show modifications in response amplitude for the new optimal orientation, which increased after adaptation. Green squares represent the new original optimal orientation, which decreased post-adaptation. Purple squares show the change in response amplitude for the preferred orientation during application of serotonin; the response amplitude increased. Gray squares illustrate an example of flank orientation; the response amplitude remained mainly similar. (B) Similar to A, for fluoxetine experiments.

original optimal response decreased in response magnitudes by −19% (Wilcoxon matched-paired signed rank test, $P = 0.020$) and −28% (Wilcoxon matched-paired signed rank test, $P = 0.004$) prior to their application, respectively. Red squares show mean response enhancements to the adapter: attractive shifts + 4.08% (Wilcoxon matched-paired signed rank test, $P = 0.46$) for serotonin experiments and + 5% (Wilcoxon matched-paired signed rank test, $P = 0.20$) for fluoxetine experiments. Brown squares indicate the average change in response amplitude for the new preferred orientation. These discharges increased by 17% (Wilcoxon matched-paired signed rank test, $P = 0.002$) after adaptation for serotonin experiments, and augmented by 42% (Wilcoxon matched-paired signed rank test, $P = 0.0003$) post-adaptation for fluoxetine experiments. The modulation of response magnitude during the drug administration is shown by the three colored squares of the right side in each figure. Green squares represent the original optimal orientation, and in a fashion similar to the first step (before drug administration) these responses declined by 29% (Wilcoxon matched-paired signed rank test, $P = 0.001$) for serotonin tests and 24% (Wilcoxon matched-paired signed rank test, $P = 0.0001$) for fluoxetine experiments. Purple squares represent modifications in firing amplitude for the new preferred orientation after application of serotonin (Fig. 6A) or fluoxetine (Fig. 6B). The magnitude of these responses increased by 44% (Wilcoxon matched-paired signed rank test, $P = 0.04$) for neurons administered with serotonin, and by 22% (Wilcoxon matched-paired signed rank test, $P = 0.0005$) for neurons administered with fluoxetine. Gray squares indicate flank orientations (67.5–90° from the optimal orientation); these weak responses fail to change following drug application. Thus, this suggests that the influence of

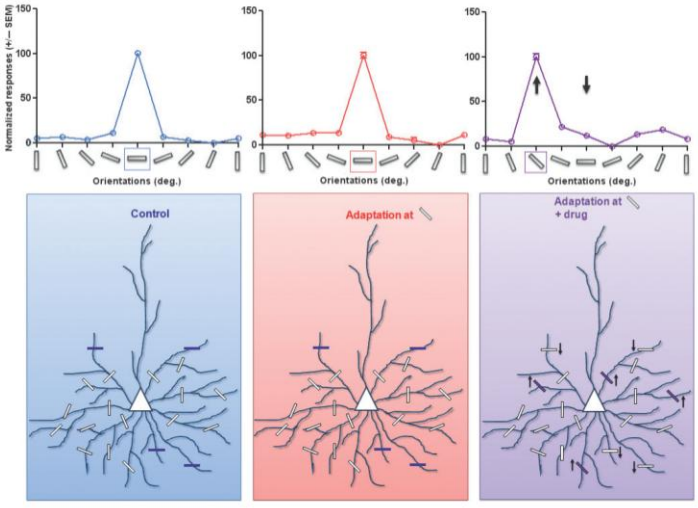

FIG. 7. Proposed model for adaptation and action of drug mechanisms. Example of a refractory neuron based on results with respective tuning curves for each condition: control (blue), post-adaptation (red) and post-administration of the drug (purple). White bars represent all the preferred orientations for each segment of the dendrite. After the first adaptation, the preferred orientation remained as for the control (horizontal). After the second adaptation during drug administration, the synaptic weight for the adapter increased and the synaptic weight for the original optimal decreased (push–pull).

serotonin as well as fluoxetine on response amplitude is limited to adapted and original orientations, i.e. it is not a global effect.

It is noticeable that the response magnitude of neurons is considerably modulated throughout the experiments for specific orientations (described above), but it is interesting that firing magnitudes of neurons post-drug administration adaptation (purple square) are not significantly changed in comparison with prior to drug administration (brown square) (two-way ANOVA test: $F = 1.33$, $P = 0.25$ for serotonin experiments, $F = 1.7$, $P = 0.30$ for fluoxetine experiments). In particular, no additional strengthening was observed. Hence, it is worth noting that the effect of both drugs is overwhelming on the shift magnitude rather than firing rates. It may be due to saturation of the discharge rates. It can be inferred that both drugs modulate the plasticity by affecting mostly the selectivity range of a neuron rather than its evoked firing. Furthermore, spontaneous activity remained unchanged after administration of the drug (one-way ANOVA: $F = 0.11$, $P = 0.95$, see Supporting Information Fig. S2B).

Discussion

The results described may be summarized as follows: the neurotransmitter serotonin and SSRI fluoxetine facilitate movement of the peak of orientation tuning curve in the direction of the adapter, thus producing attractive shifts. Indeed, in the absence of drugs, about 30% of cells displaced their optimal orientation in the repulsive direction, whereas in the presence of both drugs, the proportion of repulsive shifts is quite small: only a few cells exhibited repulsive direction. In addition, the magnitude of attractive shifts increased under the influence of both agents and particularly with serotonin. Interestingly, the firing rates were not increased in a significant fashion. The differential effects suggest that both drugs promote orientation-selectivity rather than the strength of the evoked discharges.

Comparative results

In previous studies, we have shown that successive adaptation enhances the firing rate of responses to the new optimal orientation. Consequently, the responses following the second adaptation (drug application) may be partially due to reiteration of the adaptation procedures and not entirely attributed to the presence of drugs. However, in these previous reports (Ghisovan *et al.*, 2008), shifts in the orientation tuning curves following the second adaptation were relatively small in magnitude (magnitude of shifts between the two adaptation periods were ~ 15.7–19.5° and ~ 15.6–13.6° for attractive and repulsive shifts, respectively). This contrasts strikingly with the present results. The average attractive shift was 24° under the influence of serotonin and 23.4° under the influence of fluoxetine in the case of reversal from repulsive to attractive displacements, whereas the shift increased on average to 33° with serotonin and 27° with fluoxetine for cells displaying an attractive shift after the first attempt. Furthermore, and notably during drug deposition, only very few neurons displayed repulsive shifts after adaptation: 5% for both serotonin and fluoxetine experiments. Without drugs, the proportion of repulsive shifts remained much higher: 16% (Ghisovan *et al.*, 2008). Neurons which maintained their original preferred orientation after the first adaptation protocol changed their refractory reaction under the influence of both drugs. Indeed, for neurons tested with serotonin, the average shift increased significantly (paired two-tailed *t*-test: $t = 3.8$, $P = 0.0039$), and for neurons tested with the antidepressant fluoxetine, neurons that were refractory after the first adaptation showed a significant shift (paired two-tailed *t*-test: $t = 4.9$, $P = 0.0003$) after the second adaptation during drug administration. Thus, serotonin and fluoxetine induce attractive shifts, promoting sensitization of refractory neurons to 'learn' the imposed stimulus. This suggests that the action of both substances is biasing the synaptic drive in favor of the adapter. It can be attained by changing the cellular threshold resulting in a higher firing rate of the neurons with a preferred orientation similar to that of the adapter. This could explain why the spontaneous activity remained unchanged. There seems to be a dual effect of the second adaptation: without drugs it is the response magnitude that is enhanced (to the adapter) while displacement of the peak of the orientation tuning curve remained to a large extent unmodified (see above). In the presence of drugs, it is the magnitude of the shifts that is augmented, with a strong bias towards attractive direction.

Interestingly, response magnitudes evoked by flank orientations are not significantly changed; the influence of drugs is restricted to the adapter and to the original preferred orientation.

Sensitization to the adapter

Both drugs were closely associated with reactivation of brain plasticity. Maya-Vetencourt *et al.* (2008) unambiguously showed in rats that long-term chronic treatment of fluoxetine (in drinking water) reduces GABAergic inhibition and simultaneously increases brain-derived neurotrophic factor (BDNF) expression, allowing the reinstatement of ocular dominance plasticity in adult rats. It appears that this antidepressant compound increases glutamatergic synaptic transmission. It has also been suggested that fluoxetine restructures branches of dendritic extremities (Chen *et al.*, 2011), has neurodevelopmental effects (Homberg *et al.*, 2010), and potentiates neuron maturation and synaptic plasticity (Wang *et al.*, 2008). In adult rats, serotonin reinstates the induction of *N*-methyl-D-aspartate (NMDA)-dependent long-term potentiation (Park *et al.*, 2012). Furthermore, an increase of serotonin transmission augments the BDNF-trkB signaling path, which in turn promotes processes of plasticity (Maya-Vetencourt *et al.*, 2011). In addition, it is suggested that the 5-HT_{1A} receptor is associated with epigenetic remodeling of chromatin structure, leading to reactivation of cortical plasticity (Maya-Vetencourt *et al.*, 2011).

As we deposited serotonin, it is very likely that we increased the amount of serotonin in the tissue volume open to synaptic transmission and corresponding receptors. If their model (Maya-Vetencourt *et al.*, 2011) is applied to our data, this would suggest that both drugs lead to new equilibrium of the synaptic inputs, which in turn allows functional modification of neuronal circuits (Jaffer *et al.*, 2012). Results suggest that both drugs act on most active synapses (Chen *et al.*, 2011). Application of the adapter certainly produces a surge of action potentials during a brief time-window and high probability of synchronizing inputs upon the recipient neurons (Ghisovan *et al.*, 2008). Hence our protocol implies that cells driven by the adapter for several minutes impact the dendritic membrane in such a way that clusters of dendritic spines prevail in pushing the cell to fire maximally in response to orientations close to the adapter. Furthermore, our data suggest that these modifications may occur in a relatively short period of time, compatible with the time course of molecular cascades described above. Because our results show that the responses are roughly limited to the orientations close to the adapter, they are reminiscent of the stimulus-selective response potentiation (SRP) described by Frenkel *et al.* (2006), which requires activation of NMDA receptors. In support of this, it has been shown that serotonin enhances responses to the NMDA receptors in adult rats (Reynolds *et al.*, 1988).

Serotonin and fluoxetine fail to influence firing rates

Several investigations have been reported on neuronal selectivity to orientation for different species such as cats (Carandini & Ferster, 2000; Kisvárday *et al.*, 2000) and rodents (Jia *et al.*, 2010). Combining high-speed two-photon imaging with electrophysiological recordings (Jia *et al.*, 2010) and functional mapping with electrophysiological recordings or optical imaging followed by three-dimensional anatomical reconstruction (Kisvárday *et al.*, 2000), it has been demonstrated that a single dendritic branch receives synaptic connections from neurons selective to different orientations (Kisvárday *et al.*, 2000; Jia *et al.*, 2010). Such a large range indicates that many or all orientations may be efficient in exciting a single cortical cell. Although dendritic branches show synaptic contacts associated with a particular axis of orientation, these studies demonstrate that various orientations are interspersed and represented throughout the dendritic tree (Kisvárday *et al.*, 2000; Jia *et al.*, 2010). Therefore, activating an alternative group of synapses shifts the optimal orientation but not necessarily the discharge rates. The firing rate that is the neuronal output is susceptible to saturation (Carandini & Ferster, 2000) and hence once available receptors are saturated then the maximal rate of action potential firing is reached and no further increase is possible. It is also possible that the restriction of the firing rates may be due to inhibition.

Because weak responses evoked by unpreferred orientation (flank orientations) are barely modified by both drugs, it appears that each drug's action is constrained almost to the initial optimal orientation (decline) and the new acquired orientation (facilitation). It has been suggested that this dual modulation is attributed to a push–pull mechanism (Palmer & Davis, 1981; Ferster, 1988, 1992; Tolhurst & Dean, 1990; Troyer *et al.*, 1998; Shapley *et al.*, 2003; Ghisovan *et al.*, 2009), which appears to be sensitive to SSRIs.

Proposed model

Based on our findings, we suggest a model for how adaptation mechanisms might occur in the primary visual cortex at the neuronal level and how serotonin and fluoxetine could regulate post-adaptation mechanisms. The model takes into consideration that the output of primary visual cortex neurons is due to synaptic weight distributions within the dendritic tree of a neuron for every orientation. As a consequence, the maximum discharge occurs for specific orientations that solicit predominantly the corresponding synaptic links. The adaptation process tends to reorganize this distribution such that neurons change their synaptic weight favoring the imposed orientation or in the direction opposite to it, as has been described previously.

Based on our results, we show in the proposed model (Fig. 7) an example of a refractory neuron (same neuron as in Fig. 3). As tuning curves overlapped pre- and post-adaptation, this could be attributed to the same synaptic equilibrium, which is not disturbed and maintained post-adaptation (here 0° is the optimal for control and post-adaptation, no shift). Interestingly, serotonin or fluoxetine appears to recalibrate the synaptic cross-influence by a push–pull mechanism, possibly associated with the corresponding decrease and increase of synaptic strengths for the original optimal orientation and the adapter, respectively, thus leading to a shift. This mechanism could involve specific receptors to induce this push–pull effect.

Plasticity within the primary visual cortex is a key property which can contribute to cerebral treatments or cognitive mechanisms such as memory or learning. We have shown that the neurotransmitter serotonin and antidepressant fluoxetine (an SSRI) promote attractive shifts to an imposed stimulus and facilitate neuronal property changes in learning process of a new feature, thus facilitating cerebral plasticity in primary visual cortex neurons. We have revealed a pre-eminent role of serotonin, which could be involved in a push–pull mechanism responsible for response modulations due to serotoninergic affinity to its receptors. Fluoxetine would act either by inhibiting serotoninergic recapture, or by direct actions on the changes of properties of specialized neurons for orientation in V1. Our experiments showed a predominant role of serotonin and fluoxetine by improving the "training" capacity of the refractory neurons, as well as a facilitation of plasticity for the repulsive neurons in relation to adaptation, by guiding the primary visual neurons to learn an unfamiliar feature of an image.

Supporting Information

Additional supporting information can be found in the online version of this article:
Fig. S1. Example tuning curves showing the local effect of the drug.
Fig. S2. Orientation selectivity index and spontaneous activity.

Acknowledgement

This study was supported by grants to S.M. (NSERC, FQRNT).

Abbreviations

5-HT, 5-hydroxytryptamine; BDNF, brain-derived neurotrophic factor; GABA, γ-aminobutyric acid; NMDA, *N*-methyl-D-aspartate; OSI, orientation selectivity index; RF, receptive field; SRP, stimulus-selective response potentiation; SSRI, selective serotonin reuptake inhibitor; trkB, tyrosine-related kinase B.

References

Avesar, D. & Gulledge, A.T. (2012) Selective serotonergic excitation of callosal projection neurons. *Front. Neural Circuits*, **6**, 12.
Bachatene, L., Bharmauria, V., Rouat, J. & Molotchnikoff, S. (2012) Adaptation-induced plasticity and spike waveforms in cat visual cortex. *NeuroReport*, **23**, 88–92.
Bardy, C., Huang, J.Y., Wang, C., FitzGibbon, T. & Dreher, B. (2006) "Simplification" of responses of complex cells in cat striate cortex: suppressive surrounds and "feedback" inactivation. *J. Physiol.*, **574**, 731–750.
Barlow, H.B., Blakemore, C. & Pettigrew, J.D. (1967) The neural mechanism of binocular depth discrimination. *J. Physiol.*, **193**, 327–342.
Bear, M.F. & Singer, W. (1986) Modulation of visual cortical plasticity by acetylcholine and noradrenaline. *Nature*, **320**, 172–176.
Bishop, P.O. & Henry, G.H. (1972) Striate neurons: receptive field concepts. *Invest. Ophthalmol.*, **11**, 346–354.
Briscoe, V.J., Ertl, A.C., Tate, D.B., Dawling, S. & Davis, S.N. (2008) Effects of a selective serotonin reuptake inhibitor, fluoxetine, on counterregulatory responses to hypoglycemia in healthy individuals. *Diabetes*, **57**, 2453–2460.
Carandini, M. & Ferster, D. (2000) Membrane potential and firing rate in cat primary visual cortex. *J. Neurosci.*, **20**, 470–484.
Castrén, E. (2005) Is mood chemistry? *Nat. Rev. Neurosci.*, **6**, 241–246.
Chen, J.L., Lin, W.C., Cha, J.W., So, P.T., Kubota, Y. & Nedivi, E. (2011) Structural basis for the role of inhibition in facilitating adult brain plasticity. *Nat. Neurosci.*, **14**, 587–594.
Chiu, C. & Weliki, M. (2003) The role of neural activity in the development of orientation selectivity. In Chalupa, L.M. & Werner, J. (Eds), *The Visual Neurosciences*. MIT Press, Cambridge, MA, pp. 117–125.
Chollet, F., Tardy, J., Albucher, J.F., Thalamas, C., Berard, E., Lamy, C., Bejot, Y., Deltour, S., Jaillard, A., Niclot, P., Guillon, B., Moulin, T., Marque, P., Pariente, J., Arnaud, C. & Loubinoux, I. (2011) Fluoxetine for motor recovery after acute ischaemic stroke (FLAME): a randomised placebo-controlled trial. *Lancet Neurol.*, **10**, 123–130.
Dragoi, V., Sharma, J. & Sur, M. (2000) Adaptation-induced plasticity of orientation tuning in adult visual cortex. *Neuron*, **28**, 287–298.

Ferster, D. (1988) Spatially opponent excitation and inhibition in simple cells of the cat visual cortex. *J. Neurosci.*, **8**, 1172–1180.
Ferster, D. (1992) The synaptic inputs to simple cells of the cat visual cortex. *Prog. Brain Res.*, **90**, 423–441.
Frenkel, M.Y., Sawtell, N.B., Diogo, A.C.M., Yoon, B., Neve, R.L. & Bear, M.F. (2006) Instructive effect of visual experience in mouse visual cortex. *Neuron*, **51**, 339–349.
Ghisovan, N., Nemri, A., Shumikhina, S. & Molotchnikoff, S. (2008) Visual cells remember earlier applied target: plasticity of orientation selectivity. *PLoS ONE*, **3**, e3689.
Ghisovan, N., Nemri, A., Shumikhina, S. & Molotchnikoff, S. (2009) Long adaptation reveals mostly attractive shifts of orientation tuning in cat primary visual cortex. *Neuroscience*, **164**, 1274–1283.
Harauzov, A., Spolidoro, M., DiCristo, G., De Pasquale, R., Cancedda, L., Pizzorusso, T., Viegi, A., Berardi, N. & Maffei, L. (2010) Reducing intracortical inhibition in the adult visual cortex promotes ocular dominance plasticity. *J. Neurosci.*, **30**, 361–371.
Homberg, J.R., Schubert, D. & Gaspar, P. (2010) New perspectives on the neurodevelopmental effects of SSRIs. *Trends Pharmacol. Sci.*, **31**, 60–65.
Hubel, D.H. & Wiesel, T.N. (1959) Receptive fields of single neurones in the cat's striate cortex. *J. Physiol.*, **148**, 574–591.
Hubel, D.H. & Wiesel, T.N. (1968) Receptive fields and functional architecture of monkey striate cortex. *J. Physiol.*, **195**, 215–243.
Jaffer, S., Vorobyov, V., Kind, P.C. & Sengpiel, F. (2012) Experience-dependent regulation of functional maps and synaptic protein expression in the cat visual cortex. *Eur. J. Neurosci.*, **35**, 1281–1294.
Jia, H., Rochefort, N.L., Chen, X. & Konnerth, A. (2010) Dendritic organization of sensory input to cortical neurons *in vivo*. *Nature*, **464**, 1307–1312.
Kaneko, Y., Kashiwa, A., Ito, T., Ishii, S., Umino, A. & Nishikawa, T. (2007) Selective serotonin reuptake inhibitors, fluoxetine and paroxetine, attenuate the expression of the established behavioral sensitization induced by methamphetamine. *Neuropsychopharmacol.*, **32**, 658–664.
Kasamatsu, T., Watabe, K., Heggelund, P. & Scholler, E. (1985) Plasticity in cat visual cortex restored by electrical stimulation of the locus coeruleus. *Neurosci. Res.*, **2**, 365–386.
Kisvárday, Z.F., Crook, J.M., Buzás, P. & Eysel, U.T. (2000) Combined physiological–anatomical approaches to study lateral inhibition. *J. Neurosci. Meth.*, **103**, 91–106.
Kohn, A. & Movshon, J.A. (2004) Adaptation changes the direction tuning of macaque MT neurons. *Nat. Neurosci.*, **7**, 764–772.
Komlosi, G., Molnar, G., Rozsa, M., Olah, S., Barzo, P. & Tamas, G. (2012) Fluoxetine (prozac) and serotonin act on excitatory synaptic transmission to suppress single layer 2/3 pyramidal neuron-triggered cell assemblies in the human prefrontal cortex. *J. Neurosci.*, **32**, 16369–16378.
Krekelberg, B., Van Wezel, R.J. & Albright, T.D. (2006) Adaptation in macaque MT reduces perceived speed and improves speed discrimination. *J. Neurophysiol.*, **95**, 255–270.
Liao, D.S., Krahe, T.E., Prusky, G.T., Medina, A.E. & Ramoa, A.S. (2004) Recovery of cortical binocularity and orientation selectivity after the critical period for ocular dominance plasticity. *J. Neurophysiol.*, **92**, 2113–2121.
Licata, F., Li Volsi, G., Maugeri, G., Ciranna, L. & Santangelo, F. (1993) Serotonin-evoked modifications of the neuronal firing rate in the superior vestibular nucleus: a microiontophoretic study in the rat. *Neuroscience*, **52**, 941–949.
Maffei, L. & Fiorentini, A. (1973) The visual cortex as a spatial frequency analyser. *Vision Res.*, **13**, 1255–1267.
Manji, H.K., Drevets, W.C. & Charney, D.S. (2001) The cellular neurobiology of depression. *Nat. Med.*, **7**, 541–547.
Marshansky, S., Shumikhina, S. & Molotchnikoff, S. (2011) Repetitive adaptation induces plasticity of spatial frequency tuning in cat primary visual cortex. *Neuroscience*, **172**, 355–365.
Mataga, N., Imamura, K. & Watanabe, Y. (1992) L-threo-3,4-dihydroxyphenylserine enhanced ocular dominance plasticity in adult cats. *Neurosci. Lett.*, **142**, 115–118.
Maya-Vetencourt, J.F. & Origlia, N. (2012) Visual cortex plasticity: a complex interplay of genetic and environmental influences. *Neural Plast.*, **2012**, 631965.
Maya-Vetencourt, J.F., Sale, A., Viegi, A., Baroncelli, L., De Pasquale, R., O'Leary, O.F., Castrén, E. & Maffei, L. (2008) The antidepressant fluoxetine restores plasticity in the adult visual cortex. *Science*, **320**, 385–388.
Maya-Vetencourt, J.F., Tiraboschi, E., Spolidoro, M., Castrén, E. & Maffei, L. (2011) Serotonin triggers a transient epigenetic mechanism that reinstates adult visual cortex plasticity in rats. *Eur. J. Neurosci.*, **33**, 49–57.
Morishita, H., Miwa, J.M., Heintz, N. & Hensch, T.K. (2010) Lynx1, a cholinergic brake, limits plasticity in adult visual cortex. *Science*, **330**, 1238–1240.
Movshon, J.A. (1975) The velocity tuning of single units in cat striate cortex. *J. Physiol.*, **249**, 445–468.
Nemri, A., Ghisovan, N., Shumikhina, S. & Molotchnikoff, S. (2009) Adaptive behavior of neighboring neurons during adaptation-induced plasticity of orientation tuning in VI. *BMC Neurosci.*, **10**, 147.
Palmer, L.A. & Davis, T.L. (1981) Receptive-field structure in cat striate cortex. *J. Neurophysiol.*, **46**, 260–276.
Park, S.W., Jang, H.J., Cho, K.H., Kim, M.J., Yoon, S.H. & Rhie, D.J. (2012) Developmental switch of the serotonergic role in the induction of synaptic long-term potentiation in the rat visual cortex. *Korean J. Physiol. Pha.*, **16**, 65–70.
Pizzorusso, T., Medini, P., Berardi, N., Chierzi, S., Fawcett, J.W. & Maffei, L. (2002) Reactivation of ocular dominance plasticity in the adult visual cortex. *Science*, **298**, 1248–1251.
Pizzorusso, T., Medini, P., Landi, S., Baldini, S., Berardi, N. & Maffei, L. (2006) Structural and functional recovery from early monocular deprivation in adult rats. *Proc. Natl. Acad. Sci. USA*, **103**, 8517–8522.
Ramoa, A.S., Mower, A.F., Liao, D. & Jafri, S.I.A. (2001) Suppression of cortical NMDA receptor function prevents development of orientation selectivity in the primary visual cortex. *J. Neurosci.*, **21**, 4299–4309.
Reynolds, J.N., Baskys, A. & Carlen, P.L. (1988) The effects of serotonin on *N*-methyl-D-aspartate and synaptically evoked depolarizations in rat neocortical neurons. *Brain Res.*, **456**, 286–292.
Shapley, R., Hawken, M. & Ringach, D.L. (2003) Dynamics of orientation selectivity in the primary visual cortex and the importance of cortical inhibition. *Neuron*, **38**, 689–699.
Stroud, A.C., Ledue, E.E. & Crowder, N.A. (2012) Orientation specificity of contrast adaptation in mouse primary visual cortex. *J. Neurophysiol.*, **108**, 1381–1391.
Swindale, N.V. (1998) Orientation tuning curves: empirical description and estimation of parameters. *Biol. Cybern.*, **78**, 45–56.
Tanaka, S., Tani, T., Ribot, J., O'Hashi, K. & Imamura, K. (2009) A postnatal critical period for orientation plasticity in the cat visual cortex. *PLoS ONE*, **4**, e5380.
Tolhurst, D.J. & Dean, A.F. (1990) The effects of contrast on the linearity of spatial summation of simple cells in the cat's striate cortex. *Exp. Brain Res.*, **79**, 582–588.
Troyer, T.W., Krukowski, A.E., Priebe, N.J. & Miller, K.D. (1998) Contrast-invariant orientation tuning in cat visual cortex: thalamocortical input tuning and correlation-based intracortical connectivity. *J. Neurosci.*, **18**, 5908–5927.
Vorobyov, V., Kwok, J.C., Fawcett, J.W. & Sengpiel, F. (2013) Effects of digesting chondroitin sulfate proteoglycans on plasticity in cat primary visual cortex. *J. Neurosci.*, **33**, 234–243.
Wang, J.W., David, D.J., Monckton, J.E., Battaglia, F. & Hen, R. (2008) Chronic fluoxetine stimulates maturation and synaptic plasticity of adult-born hippocampal granule cells. *J. Neurosci.*, **28**, 1374–1384.
Zhong, P. & Yan, Z. (2011) Differential regulation of the excitability of prefrontal cortical fast-spiking interneurons and pyramidal neurons by serotonin and fluoxetine. *PLoS ONE*, **6**, e16970.

8. Discussion générale

8.1 Chapitre A : réorganisation corticale, mécanismes

L'une des propriétés stables des neurones dans le cortex strié est la sélectivité à l'orientation. Depuis les travaux majeurs de Hubel et Wiesel (1962), nous savons que les neurones de V1 déchargent à la présentation d'un stimulus particulier au sein de leur champ récepteur. Si l'on insère une électrode de manière oblique dans le cortex, les réponses neuronales optimales vont varier de façon méthodique (environ 16.5 degrés pour chaque 0.09 mm de cortex). Une organisation si systématique implique donc qu'en ayant une colonne de référence, nous pouvons prédire la séquence d'orientation qui suit. Ceci repose sur le fait que l'organisation corticale est en effet la conséquence d'une architecture de connexions neuronales bien déterminée, par exemple, les neurones du corps genouillé latéral sont alignés et connectés avec une cellule du cortex visuel (Jin et al., 2011 ; Henry et al., 1973). Cette ségrégation donne cette notion de sélectivité à l'orientation.

Des études ont montré cependant que cette organisation en colonnes est variable (Horton and Adams, 2005 ; Kaas et al., 1989 ; Swindale et al., 2000), les réponses neuronales au stimulus optimal initial peuvent diminuer laissant place à l'émergence d'un nouveau stimulus préféré acquis à la suite d'une adaptation visuelle (Dragoi et al., 2000 ; Dragoi et al., 2001 ; Ghisovan et al., 2009 ; Ghisovan et al., 2008 ; Kohn, 2007 ; Kohn and Movshon, 2004 ; Krekelberg et al., 2006 ; Hietanem et al., 2007). Cette nouvelle sélectivité acquise par des neurones d'une colonne stimulée peut poser un problème d'une surreprésentation du nouveau stimulus acquis et le manque de représentation du stimulus initial (perte de ses réponses). Pour éviter cette situation, une question fondamentale se pose alors : est-ce que les neurones appartenant aux

colonnes voisines (qui n'ont donc pas été adaptés) changent leur sélectivité ? En d'autres mots, est-ce que l'hyper-colonne subit une altération (une réorganisation) complète avec l'émergence d'un nouvel *état* du cortex ?

Notre hypothèse est qu'effectivement ces neurones doivent changer leur sélectivité dans le but de compenser les modifications des neurones de la colonne adaptée. Une façon simple de vérifier cette hypothèse : nous avons testé des sites d'enregistrement multiples avec une procédure d'adaptation effectuée sur un seul site qui sert de référence. Nos résultats ont montré que la réorganisation corticale ne serait pas strictement anatomique mais serait un processus fonctionnel qui dépend des conditions de stimulation. Ces données ont des implications multiples sur les phénomènes de plasticité corticale :

1. La sélectivité à l'orientation dans le cortex visuel est une organisation qui ne dépend pas de facteurs anatomiques basés sur les connexions neuronales acquises après la naissance. L'architecture des colonnes d'orientation semble plutôt être une formation labile qui dépend des conditions de stimulation qui excitent les neurones voisins. Ces domaines subissent un « remapping » continu.
2. Les domaines d'orientation seraient donc une architecture fonctionnelle et non anatomique. Cette architecture serait basée sur la ségrégation parallèle des entrées émanant de la rétine en premier lieu, puis du corps genouillé latéral.

Les colonnes d'orientation ont longtemps été considérées comme des organisations anatomiques et structurelles établies au cours de la période post-natale, et immuables après la fin de la période critique liée au premières années d'apprentissage (Crair et al., 1998). À

titre d'exemple, une expérience a été menée sur des chatons (durant leur période critique), les neurones visuels de ces animaux qui s'étaient développés dans un environnement strié (une orientation dominante) ont montré des représentations importantes de l'orientation imposée (Sengpiel et al., 1999). En effet, leurs cartes de préférence à l'orientation ont exhibé une dominance de la couleur correspondant au stimulus d'exposition (Figure 7). Cependant, à l'âge adulte, Il a également été montré qu'il était possible d'engendrer un changement d'orientation préférée suite à une courte exposition à une orientation non-optimale pour les neurones du cortex visuel primaire chez le chat (Dragoi et al., 2000, Godde et al., 2002 ; Ghisovan et al., 2009, Bachatene et al., 2013) (Figure 7).

Cette plasticité de la perception visuelle à l'orientation induite par apprentissage visuel est un processus dépendant de la durée d'adaptation, une longue adaptation induit des déplacements de courbes de syntonisation à l'orientation plus importants (Ghisovan et al., 2009). Cette dépendance s'observe également pour le type de déplacement, en effet, une courte durée d'adaptation induit des déplacements répulsifs (la nouvelle orientation optimale acquise s'éloigne de l'orientation imposée) alors qu'une longue adaptation favorise une augmentation de réponse à l'adaptante, il y a facilitation de l'effet d'apprentissage ; la diminution de réponse pour certaines orientations s'accompagne d'une augmentation de réponse pour d'autres orientations. La sélectivité à l'orientation dans V1 peut donc être réorganisée activement selon les propriétés du stimulus adaptant.

Figure 7 - Plasticité des cartes de sélectivité à l'orientation durant la période post-natale et durant l'âge adulte. En période post-natale (à gauche), l'exposition de chatons à des environnements striés avec une orientation dominante conduit à la surexposition de cette orientation dans les cartes de sélectivité à l'orientation enregistrées en imagerie optique (cartes de gauche et milieu) en comparaison à des chatons exposés à des environnement normaux où toutes les orientations sont représentées de façon égale dans la carte de sélectivité (Sengpiel et al., 1999). Durant l'âge adulte (à droite), il y a également une restructuration des cartes de sélectivité à l'orientation à la suite d'une période d'adaptation visuelle à une orientation spécifique (Godde et al., 2002).

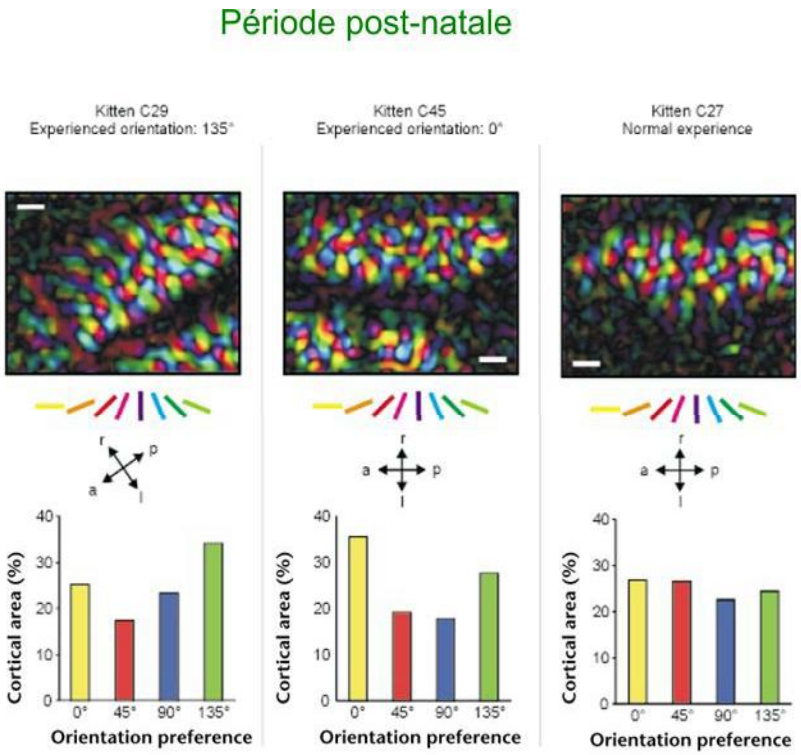

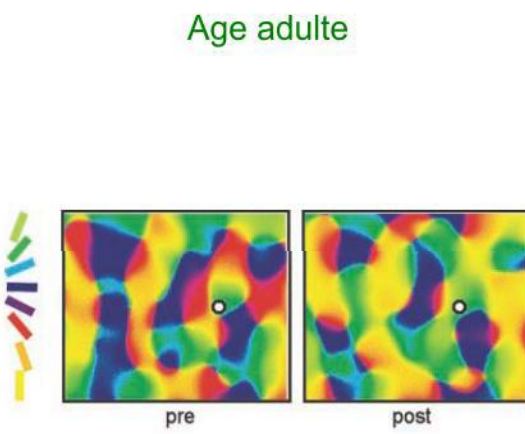

Sengpiel et al., 1999

Godde et al., 2002

Les résultats de cette étude sont consolidés par diverses investigations. Chez la souris, il a été démontré qu'une seule branche dendritique reçoit diverses entrées sur une distance spatiale assez courte, ces entrées codent pour différents stimuli orientés (Jia et al., 2010), les relations de connectivité mutuelle sont donc importantes. Nous croyons que durant les phénomènes de plasticité neuronale, l'impact du stimulus imposé se fait sur le seuil d'excitabilité et de décharge des neurones, augmentant principalement les efficacités synaptiques sur l'arbre dendritique et, par conséquent, permettant l'émergence d'un nouveau stimulus optimal avec une perte du taux de réponses au stimulus initial. Si un tel modèle était admis pour le chat, un stimulus serait dominant, ce qui conduirait le neurone à augmenter sa force synaptique au-delà de son seuil d'excitabilité et lui conférerait sa sélectivité à l'orientation optimale.

Les neurones du cortex visuel primaire reçoivent des entrées poly-synaptiques des cellules avoisinantes mais également de réseaux de neurones de sites corticaux distaux. De ce fait, il y a de nombreuses connexions parallèles (feed-forward) et connexions rétroactives (feedback) (Ringach, 2004 ; Gilbert and Wiesel, 1989). Chez le chat en particulier, le cortex visuel primaire partage de nombreuses connexions réciproques avec le cortex visuel secondaire (aire 18) (Bullier et al., 1988). Il a été démontré par des enregistrements intracellulaires qu'un seul neurone cortical reçoit de multiples entrées synaptiques (Monier et al., 2003). Donc, la diversité des combinaisons des entrées peut être reflétée par les patrons de connectivité intra-corticaux, permettant des propriétés changeables (Monier et al., 2003). Il est à prévoir que lorsque les effets de l'adaptation sont observés du point de vue de la balance entre les entrées, plus spécifiquement le gradient entre les poids synaptiques excitateurs et inhibiteurs, les neurones sont plus susceptibles d'acquérir un nouveau stimulus optimal. En effet, le stimulus

imposé conduit à des efférences qui, au niveau cortical, peuvent redistribuer les poids synaptiques du réseau de neurones en changeant le ratio excitation-inhibition.

Il faut souligner également qu'à cause des réseaux intra-corticaux sous-jacents, un neurone particulier qui modifie sa sélectivité influence d'autres neurones voisins avec lesquels il est connecté de façon directe ou indirecte. Ces interconnexions et leurs changements contribuent à la plasticité de la sélectivité à l'orientation du réseau cortical entier. Ces changements typiques ont été observés dans d'autres systèmes sensoriels tels que le système auditif (Froemke et al., 2007). Les résultats de ces études sur les changements de propriétés neuronales suggèrent fortement que la sélectivité à l'orientation dans le système visuel est une caractéristique malléable, et qui est ajustée par des neurones spécifiques. Les changements du réseau de neurones global dépendent des changements des neurones testés par l'entrainement visuel. Les colonnes d'orientation transcendent l'aspect anatomique et sont donc des unités fonctionnelles plastiques.

8.2 Chapitre B : connectivité neuronale

La connectivité fonctionnelle est étudiée en calculant la probabilité que deux neurones soient connectés ensemble et que l'un projette sur l'autre. Pour estimer cette probabilité, des corrélations croisées sont calculées entre les deux neurones en utilisant comme référence temporelle pour les décharges du neurone cible les décharges du neurone référence qui sont les plus proches dans le temps. Ensuite un algorithme qui combine ces corrélations dans un corrélogramme est utilisé (Perkel et al., 1967). Il s'agit d'un calcul du coefficient dont la valeur est une probabilité que le neurone projette (ou se connecte de façon fonctionnelle) sur un autre neurone. Cet algorithme est basé sur les valeurs des deux bins maximales du point de référence 0 (de chaque côté du corrélogramme croisé) dans un laps de temps de plus ou moins 5 millisecondes autour du zéro. Ces calculs sont d'une importante indication des projections neuronales entre un neurone pris comme référence et un second comme neurone cible, puisqu'elles sont le reflet de la modulation de la connectivité neuronale (Reid, 2012). Le présent travail a donc pour but d'expliquer l'effet de l'adaptation visuelle sur la dynamique de cette connectivité. Par la suite nous avons construit des matrices de connectivité basées sur les coefficients de probabilité à partir des corrélogrammes croisés pour un groupe de neurones dont la sélectivité à l'orientation est également similaire pré et post-adaptation.

8.2.1 Analyse par corrélation croisée

Ce type de calcul est utilisé dans les expérimentations électrophysiologiques dans le but de révéler des relations fonctionnelles entre les trains de décharge de neurones enregistrés simultanément (Perkel et al., 1967). C'est une stratégie fonctionnelle qui permet de révéler les

interactions plus ou moins directes des neurones impliqués dans les connexions cortico-thalamiques ou cortico-corticales.

Le calcul de corrélogrammes croisés sont basés sur les décharges d'un neurone cible (à une fenêtre temporelle spécifique) en relation avec les décharges d'un neurone référence.

L'axe temporel est divisé en fragments (bins), les distances entre chaque potentiel d'action et tous les potentiels d'action du train de décharge sont calculées. Afin d'y extraire les probabilités, les taux de décharge des fragments sont divisés par le nombre d'événements référence.

En récapitulatif, le principe de cet algorithme tel que postulé par Perkel et al., (1967) repose sur les coïncidences des trains de potentiels d'action de deux neurones sur un laps de temps relativement court pouvant s'interpréter par des projections synaptiques directes (3 à 5 millisecondes). Si un neurone (N1) projette sur un deuxième neurone (N2), le potentiel d'action de N1 pourrait conduire à l'apparition d'un potentiel d'action dans N2 avec un délai temporel suffisamment court pour pouvoir déduire dans l'histogramme de corrélation croisée un patron de connectivité fonctionnelle entre les deux neurones. Ainsi, nous pouvons examiner le nombre de potentiels d'action produits dans N2, en fonction du temps, en utilisant le temps d'émission des potentiels d'action dans N1 comme référence.

Par ailleurs, N1 et N2 pourraient décharger en même temps et synchroniser leur activité au temps zéro de l'échelle temporelle de l'histogramme de corrélation croisée, cela pourrait être dû à un input afférent commun aux deux neurones et un pic central se manifesterait donc dans l'histogramme. Ce pic correspond à l'augmentation de probabilité de décharge des deux neurones en même temps (augmentation de probabilité de synchronie).

Ainsi, en utilisant cet algorithme, les relations fonctionnelles entre diverses cellules neuronales peuvent être révélées. Chez le primate, il a été démontré qu'il existe des interactions entre les neurones ganglionnaires rétiniens et les neurones thalamiques du corps genouillé latéral: un neurone rétinien conduit à 80% des potentiels d'action d'un neurone thalamique (Sincich et al., 2007).

La présence de pics positifs, décalés par rapport au zéro de l'histogramme de corrélation croisée a notamment permis d'expliquer les projections thalamo-corticales, par exemple qu'il y avait un rapport entre les zones On et OFF des neurones thalamiques et leurs projections spécifiques aux sous-régions corticales (Alonso et al., 2001) et au type de cellules du cortex visuel. Par exemple, il existerait environ un rapport de 30 pour 1 concernant les connexions entre les neurones du CGL et ceux des cellules simples du cortex visuel primaire, c'est-à-dire qu'une cellule simple connecte une trentaine de neurones thalamiques (Alonso et al., 2001).

Il a été démontré dans l'aire MT du macaque que la corrélation croisée des décharges neuronales entre paires est majoritairement de période courte entre 10 et 100 ms (Bair et al., 2001), aussi, différents laps de temps variant de 3 à 10 ms sont fréquemment utilisés dans ces analyses afin de mettre en évidence les relations inter-neuronales (Bartho et al., 2004). Ces périodes correspondent à l'apparition des pics dans les corrélogrammes.

Une synchronie de décharge reflète une forme typique du corrélogramme croisé avec un pic central (à 0 dans l'échelle temporelle) et est associée à un input commun vers les deux neurones cibles (Denman and Contreras, 2013).

Figure 8 – Corrélation croisée : connexions fonctionnelles. La détermination de la corrélation de décharges de deux neurones nous permet de considérer une projection fonctionnelle du neurone A au neurone B lorsque le pic apparait d'un côté ou l'autre du zéro de l'échelle temporelle (offset) ou une afférence commune lorsque un pic central apparait (zero-spanning). Notons que les corrélogrammes sont plus évidents à une échelle de mesure plus petite (0.2 s pour les corrélogrammes du haut, 0.025 s pour les corrélogrammes du bas).

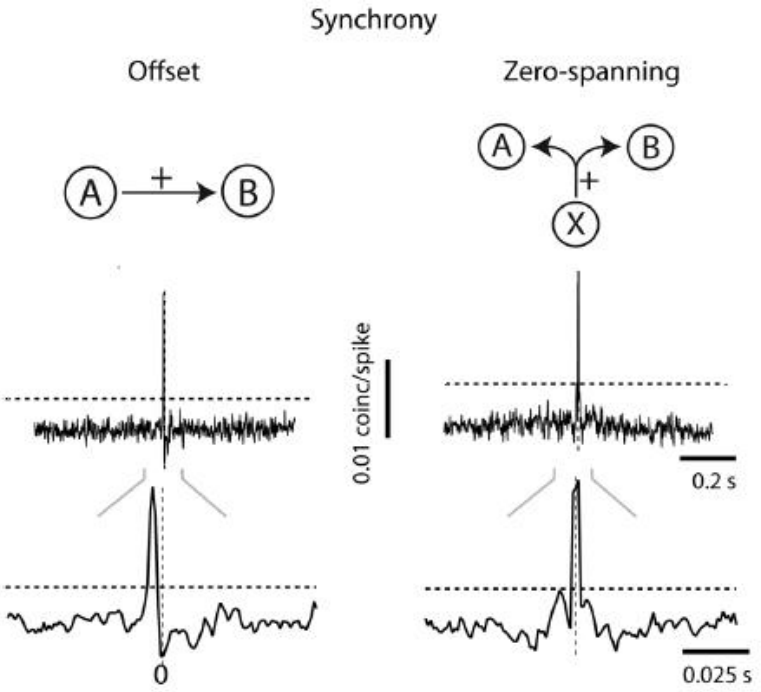

Denman and Contreras, 2013

Dans nos résultats, les phénomènes de synchronie de décharges sont très rares. La forme commune la plus représentée est une forme caractéristique avec des pics décalés par rapport au centre du corrélogramme croisé, de telles formes sont attribuées à des projections monosynaptiques entre neurones (Denman and Contreras, 2013). En plus de fournir les projections fonctionnelles entre les cellules, l'analyse par corrélation croisée évalue la force de cette connectivité par un index de significativité (coefficient de probabilité) dans la

compréhension des variations des assemblées neuronales en réponse à une expérience (Bock et al., 2011).

Nous avons par ailleurs exploré la relation entre la modulation de connectivité neuronale et le taux de décharge des neurones impliqués, comme montré précédemment (Duret et al., 2006; Ghisovan et al., 2008, Rolls and Treves, 2011), aucune corrélation significative n'a été observée entre les coefficients de probabilité et le taux de décharge des neurones.

8.2.2 Connectivité neuronale et sélectivité à l'orientation

Au sein du cortex visuel primaire, les neurones sont dispersés dans des domaines corticaux et sont connectés latéralement et verticalement, les connexions horizontales sont caractérisées comme des longues projections entre neurones ayant des propriétés de sélectivité similaires (Das and Gilbert., 1995, Sompolinsky et al.,1990), les connexions verticales sont décrites comme étant des entrées aux couches II/III de la couche IV (Yoshimura et al., 2000, Stratford et al., 1996) qui elle-même reçoit des entrées du corps genouillé latéral (Alonso et al., 1996). Les connexions neuronales corticales sont très spécifiques, elles dépendent principalement des propriétés de réponses des neurones (Alonso, 2002). Par exemple, dans le cortex visuel du macaque, il a été démontré que la corrélation variait selon les conditions de stimulation et qu'elle était plus importante entre les neurones ayant des propriétés homogènes de sélectivité à la direction (Bair et al., 2001). Il a également été montré que dans le cortex visuel de la souris, la similarité de l'activité neuronale à une propriété spécifique du stimulus affecte les probabilités de connexion (Ko et al., 2011). Ces recherches mettent en évidence le fait que les propriétés des stimuli influencent les relations temporelles entre neurones (Gray et

al., 1990 ; Bharmauria et al., 2015). Néanmoins, la dynamique de connectivité à la suite de phénomènes de plasticité est un domaine à explorer. En se basant sur nos résultats, nous avons conclu que l'adaptation visuelle tend à rééquilibrer les forces de connectivité entre différents microcircuits neuronaux mais conserve un «état» global stable, ceci est en parfaite concordance avec de récentes recherches stipulant que l'adaptation contribue à une homéostasie de population neuronale (Benucci et al., 2013). De plus, l'adaptation visuelle pourrait fournir une « fenêtre d'opportunité » aux neurones afin de modifier la balance excitation-inhibition dans le but de réorganiser l'activité corticale du réseau auquel ils appartiennent (Stanley, 2013).

Pour conclure, l'adaptation visuelle influence la sélectivité neuronale et conduit à de rapides changements au sein des microcircuits neuronaux en termes de projections intercellulaires. Le code neuronal s'adapte donc aux changements de conditions de stimulation. Les neurones du cortex visuel primaire coordonnent leurs décharges en constituant des assemblées neuronales (Lee and Reid, 2011; Kampa et al., 2011; Wallace and Kerr, 2010 ; Bharmauria et al., 2015) en réponse aux stimuli externes, il est donc capital de poursuivre les investigations dans la compréhension des mécanismes de traitement de l'information visuelle.

Le traitement visuel dans le cerveau dépend fortement de la connectivité fonctionnelle des neurones afin d'établir des circuits neuronaux fonctionnels dans le cortex visuel. Des connexions spécifiques sont mises en place entre des neurones sélectifs à des stimuli particuliers au sein d'assemblées neuronales qui traitent l'information visuelle (Yoshimura et al., 2005). Ces assemblées neuronales fonctionnelles recrutées lorsqu'activées encodent les attributs des stimuli visuels (Miller et al., 2014) et sont cruciales pour la perception. Il a été démontré que les neurones qui codent pour les mêmes propriétés du stimulus montrent des

hauts niveaux de connectivité fonctionnelle (Yoshimura et al., 2005; Alloway and Roy, 2002 ; Ko et al., 2011). Dans la section précédente, nous avons traité de la modulation de la connectivité fonctionnelle entre paires neuronales partageant la même sélectivité neuronale pré- et post-plasticité et avons montré que l'adaptation visuelle impacte sur les forces de connexions entre ces paires. Dans la présente section, une autre stratégie a été adoptée : contrairement au précédent travail qui se basait sur un spectre d'orientation réduit (cellules qui partageant les mêmes orientations optimales initiales et ayant acquis les mêmes nouvelles propriétés), cette section se base sur une stratégie de sommation des poids de connectivité au sein de réseaux neuronaux sur un spectre d'orientation plus large. Nos hypothèses de base étant :

- Que la somme des forces de connexion soit différente après adaptation visuelle. Auquel cas, quels sont les paramètres qui nous permettraient d'expliquer ces différences (cellules particulières, forme des spikes…).
- Que la somme des forces de connexion soit maintenue, ce qui correspondrait à l'hypothèse de plasticité homéostatique décrite à des niveaux différents (physiologique, moléculaire, génétique) (Surmeier and Foehring, 2004 ; Turrigiano, 2012 ; Turrigiano, 1999).

La stratégie de corrélation croisée a été utilisée dans le but de calculer les poids synaptiques qui sont le reflet des connexions fonctionnelles. De plus, un deuxième aspect d'homéostasie a été traité dans ce chapitre, il s'agit de comprendre comment les cartes d'orientation variaient après une adaptation visuelle. Pour cela, un protocole d'imagerie optique intrinsèque a été utilisé (Cattan et al., 2014). En complément aux techniques d'électrophysiologie classique, l'imagerie optique permet d'enregistrer l'activité de populations de cellules. C'est une technique non-invasive qui se base sur les effets indirects de l'activité électrique des neurones,

par exemple en mesurant les augmentations de débits sanguins qui sont quasi-simultanées à l'activation de groupes de neurones. Lorsqu'une cellule émet des potentiels d'action, il y a une augmentation de la consommation en glucose, couplée par une augmentation de la circulation sanguine. De la même manière que la conservation des poids de connectivité citée précédemment, nous avons montré que les cartes d'orientation changeaient de conformation (distribution des pixels correspondant à chaque orientation optimale) mais qu'il y a conservation de la proportion de chaque orientation optimale dans les cartes. Autrement dit, les cartes d'orientation se modifient à la manière de la reprogrammation expliquée dans le chapitre A. La conformation en colonnes se maintient.

Nous avons donc là un couplage « Sélectivité – Connectivité » qui est en parfaite concordance avec le concept de plasticité homéostatique. En effet, un processus homéostatique est établi dans le but de stabiliser la force globale des connexions initialement mesurée au sein d'un réseau de neurones. Cette activité régulatrice est considérée comme une activité complémentaire à la plasticité Hebbienne où l'on observe des changements de poids synaptiques dans le but d'acquérir de nouvelles propriétés. Ceci vient expliquer le titre de la présente thèse : l'homéodynamie, une parfaite osmose entre la dynamique cérébrale de la plasticité et l'homéostasie biologiquement nécessaire. Les systèmes sensoriels sont continuellement affectés par les attributs des stimuli externes (Patterson et al., 2014). Le système visuel est fortement altéré par l'expérience visuelle; les propriétés des neurones et de leurs circuits subissent d'importants changements durant la période de développement (Hensch, 2005 ; Sengpiel et al., 1999). On sait aujourd'hui que ces changements peuvent persister (moindrement que durant le développement) à un âge adulte en réponse à diverses stratégies telles que la privation monoculaire (He et al., 2006, Shibata et al., 2012), des lésions

rétiniennes ou corticales (Keck et al., 2011) ou encore une expérience sensorielle (entrainement visuel par exemple) (Bachatene et al., 2012 ; Dragoi et al., 2000 ; Ghisovan et al., 2009 ; Cattan et al., 2014 ; Kohn and Movshon, 2004 ; Nemri et al., 2009 ; Patterson et al., 2013). Nous savons que la stimulation visuelle contribue au recrutement de groupes fonctionnels de neurones (Miller et al., 2014), en conséquence, les changements de propriétés d'un groupe neuronal peuvent affecter les propriétés de l'information fournie aux assemblées neuronales sous-jacentes (Cattan et al., 2014 ; Patterson et al., 2014).

8.2.3 La dynamique de connectivité neuronale

Le traitement des informations cérébrales est intimement lié à la dynamique des circuits neuronaux. Les neurones des couches 2/3 du cortex visuel primaire sont interconnectés spécifiquement, ce qui permet l'émergence de circuits neuronaux indépendants au sein de cette architecture (Yoshimura et al., 2005). Nous avons observé au cours de ce chapitre que la plasticité induite par l'expérience changeait les forces de connectivité fonctionnelle mais, en contrepartie, il y a une stabilisation des sommes des poids de connectivité. Ceci est en parfaite concordance avec le concept de plasticité homéostatique décrit dans plusieurs travaux (Turrigiano, 1999 ; Hebb, 1949 ; Shatz, 1990). Cette activité régulatrice est considérée comme un complément à la plasticité de Hebb qui s'opère dans le but de changer les propriétés neuronales en fonction de l'expérience (Turrigiano, 1999 ; Hebb, 1949 ; Shatz, 1990). Par exemple, chez des animaux jeunes, l'adaptation à un stimulus particulier mène à un développement spécifique des cartes d'orientation. L'exposition de ces animaux à un environnement orienté de façon stricte permet l'obtention de cartes corticales où le caractère

du stimulus imposé (axe d'orientation) est plus fortement représenté que les autres orientations (Sengpiel et al., 1999). Plusieurs travaux ont également montré que la plasticité induite par adaptation peut être réalisée à l'âge adulte, et ce; concernant plusieurs attributs du stimulus : orientation, fréquence spatiale, contraste, mouvement, direction (Bachatene et al., 2012 ; Dragoi et al., 2000 ; Ghisovan et al., 2009 ; Kohn and Movshon, 2004 ; Nemri et al., 2009 ; Marshansky et al., 2011). Ces modifications de sélectivité qui s'accompagnent de modifications de connectivité sont cruciales au codage neuronal, il a été observé par exemple que la synchronie entre les activités neuronales était modulée durant les ondes gamma du cerveau et que ceci améliore l'encodage de l'information visuelle (Wang et al., 2011 ; Hansen and Dragoi, 2011). De nouvelles assemblées neuronales fonctionnelles sont formées avec un maintien de forte connectivité entre les neurones partageant les mêmes propriétés (Ko et al., 2011 ; Ko et al., 2013). La plasticité homéostatique a donc pour but de prévenir d'une augmentation excessive ou insuffisante des niveaux de décharges neuronales durant une potentialisation à long terme (LTP) ou une dépression à long terme (LTD), toutes deux sont déterminantes pour les changements de force de connectivité et par conséquent les modifications de propriétés optimales des neurones (Burrone et al., 2002 ; Turrigiano and Nelson, 2004).

Un autre scénario est à envisager : le changement de l'équilibre excitation-inhibition (E-I) conduisant à des effets notables sur l'activité de décharge des neurones et le traitement de l'information (Turrigiano, 2012 ; Nelson and Turrigiano, 2008). Un maintien de cette balance du ratio E-I pourrait ainsi prévenir des excès d'augmentation ou de diminution des forces globales de connectivité (Turrigiano, 2012). Le cortex s'adapte et réorganise ses connexions

en fonction des nouveaux stimuli acquis afin de permettre un taux de décharge et de connectivité stables pour un remodelage ultérieur.

8.3 Chapitre C : Propriétés électrophysiologiques des neurones

8.3.1 Plasticité et types neuronaux

Les neurones du cortex visuel primaire se différencient anatomiquement de par leurs formes (neurones pyramidaux et neurones étoilés). En électrophysiologie, il est également possible de différencier deux types majeurs de formes de décharges des neurones : des potentiels d'action à décharge régulière, et des potentiels d'action à décharge rapide, tous deux correspondant respectivement à des neurones pyramidaux et à des interneurones (Ison et al., 2011; Wilson et al., 1994) chez la souris notamment. Ce paramètre (dissociation des formes de potentiels d'action) n'étant pas totalement valide chez le chat (Nowak et al., 2003). Il est bien connu que l'apprentissage visuel par adaptation contribue à des changements au niveau de la sélectivité des neurones (Ghisovan et al., 2008; Ghisovan et al., 2009; Bachatene et al., 2013; Patterson et al., 2013, Dragoi et al., 2000). Notre but était donc de déterminer s'il existe une relation entre les différences observées dans les changements de sélectivité des neurones suite à l'adaptation visuelle et ces deux types cellulaires. Nous avons donc isolé des neurones de l'aire V1 de chats adultes anesthésiés et analysé les réponses neuronales de chaque unité, puis nous les avons classés selon leur type de décharge dans le but de conclure s'il y a une quelconque corrélation entre ces deux facteurs (type neuronal et changement de sélectivité post-adaptation).

L'analyse des courbes d'orientation de tous les neurones isolés permet de déterminer l'orientation préférentielle de chaque cellule pré-adaptation (contrôle), ainsi que l'orientation préférentielle après une période d'adaptation visuelle (12 minutes), en effet, un stimulus non préféré au départ est imposé dans le but d'induire un apprentissage et une plasticité neuronale à l'orientation. Les cellules voient donc leur courbe de syntonisation glisser après adaptation, un déplacement attractif de la courbe tend à la coïncider avec le stimulus imposé ou du moins s'y rapprocher, un déplacement répulsif au contraire éloigne la courbe du stimulus imposé. Dans ces deux cas, une nouvelle orientation devient optimale. Les neurones peuvent également conserver leur orientation préférentielle après la période d'adaptation et n'expriment aucun déplacement de leur courbe (*neurones réfractaires*). De plus, un critère nous permet de distinguer des neurones à décharge régulière et des neurones à décharge rapide, souvent associés aux neurones pyramidaux et aux interneurones, respectivement au niveau du cortex. Nous avons donc investigué dans cette étude les différences observées en termes de déplacement de courbe d'orientation pour ces deux classes de neurones.

Les interneurones possèdent une bande passante plus large (Kuhlman et al., 2011; Hofer et al., 2011), ils sont sélectifs à un spectre d'orientation plus important, chaque entrée contribue donc aux réponses cellulaires avec approximativement le même taux de décharge, considérant que l'adaptation visuelle affecte majoritairement l'orientation de départ et l'orientation imposée (ou la nouvelle orientation acquise, si différente de l'orientation imposée), après adaptation visuelle les autres entrées des interneurones tendent à maintenir leur fort taux de décharge, ce qui explique un déplacement de courbe plus petit pour cette classe de neurones. D'autre part, les neurones pyramidaux à décharge régulière ont des courbes plus pointues (sélectivité plus importante), ceci est dû à une combinaison d'entrées inhibitrices (Fries et al., 2007). Donc,

l'effet de déséquilibre excitation-inhibition produit par l'adaptation visuelle résulte en un déplacement des courbes d'orientation plus important, à cause du moindre taux de décharge des entrées voisines, d'autant plus que l'adaptation visuelle tend à agir sur le stimulus optimal de départ et sur le nouveau stimulus acquis (effet push-pull, Ghisovan et al., 2009). Nous avons conclu cette étude par un effet d'interaction des neurones pyramidaux et des interneurones en formant des sous-circuits avec des populations neuronales sélectives à l'orientation, les cellules pyramidales mettent en place cette sélectivité qui serait régulée par les interneurones. Au sein des systèmes sensoriels, la balance excitation-inhibition joue un rôle capital dans les phénomènes de plasticité cérébrale.

8.3.2 Un orchestre neuronal ?

L'information sensorielle est représentée dans le cortex par des réseaux de neurones coactifs qui coordonnent leur activité de décharge (Miller et al., 2014). L'encodage des attributs des stimuli implique une large variété de stratégies considérant les divergences anatomiques et fonctionnelles au sein des populations de neurones. En effet, en se basant sur les propriétés électrophysiologiques intrinsèques des neurones corticaux, ceux-ci sont classés en différents types tels que les neurones à décharge régulière, les neurones à rythme rapide en bursts de décharge, les neurones à haute fréquence de décharge et les neurones à décharge rapide intrinsèque (Steriade, 2004). En dépit de ces variations des propriétés de décharge des neurones, leurs activités corrélées au sein d'assemblées neuronales codent efficacement les attributs des stimuli visuels, il a été démontré que cette activité était plus efficace que l'activité indépendante de chaque cellule neuronale (Miller et al., 2014). Comme vu précédemment, les

neurones codant pour des attributs similaires exhibent entre eux des taux plus élevés de connectivité fonctionnelle.

En dehors de cet aspect de corrélation lié aux attributs du stimulus visuel, chaque neurone peut également montrer une corrélation (couplage) de son activité de décharge avec l'activité de décharge de l'assemblée neuronale avoisinante (Okun et al., 2015), un peu comme faisant partie d'un orchestre neuronal (Grinvald et al., 2003). Il a été démontré que dans le cortex visuel primaire de la souris ainsi que dans l'aire V4 du singe, deux groupes de neurones qui se différencient de par leur stratégie de couplage populationnel, exhibaient des différences dans plusieurs aspects. Les neurones hautement couplés (choristes) reçoivent des entrées synaptiques des cellules voisines plus forts qui ceux reçus par les neurones solistes (Okun et al., 2015). Aussi, des différences anatomiques ont été constatées au niveau de la distribution laminaire de ces deux groupes de neurones (Hung et al., 2014). Les auteurs de ces études ont montré une légère différence entre les solistes et les choristes en termes de forme du potentiel d'action (donc fréquence de décharge), néanmoins ces différences n'étaient pas significatives dû à la grande variabilité des résultats (Okun et al., 2015).

Chez le chat adulte dont le cortex visuel est organisé en colonnes, nous avons investigué la relation entre le type de potentiel d'action (spikes réguliers de forme normale et spikes rapides de forme plus allongée), la fréquence de décharge (décharge normale ou haute fréquence) et la corrélation (couplage) de l'activité de chaque neurone avec l'activité de la population neuronale avoisinante. Nous avons trouvé une relation systématique entre ces paramètres : premièrement, les neurones à potentiel d'action de forme régulière avaient une fréquence de décharge moindre par rapport aux neurones à potentiel d'action au décours temporel plus long (forme plus allongée). Deuxièmement, les neurones à forte décharge exhibaient de plus hauts

niveaux de couplage populationnel par rapport aux neurones à décharge régulière. Ces résultats mettent en évidence le fait que dans un réseau de neurones, ces deux types de neurones pourraient jouer des rôles distincts dans le codage de l'information, où les neurones à haute fréquence de décharge orchestrent la sélectivité sensorielle des neurones voisins.

Dans la présente étude, nous avons classé des neurones visuels en fonction d'une propriété électrophysiologique bien connue : la forme du potentiel d'action. Ce paramètre est notamment utilisé chez des espèces telles que la souris de par les différences anatomiques et fonctionnelles observées pour chaque forme du potentiel d'action.

Après cette classification, nous avons examiné les propriétés de décharge de chacun de ces deux types neuronaux puis investigué leur couplage populationnel (corrélation de l'activité de chaque neurone avec celle du groupe neuronal avoisinant).

La corrélation de l'activité neuronale semble être une caractéristique inhérente des neurones (Okun et al., 2015). En effet, le couplage populationnel des choristes et des solistes semble être maintenu en présence de stimuli (réponses évoquées) et en son absence (activité spontanée) (Lin et al., 2014; Okun et al., 2015).

Dans le cortex sensoriel du rongeur, il a été démontré que les solistes et les choristes peuvent être dissociés selon certains paramètres : les solistes sont moins fonctionnellement connectés étant moins optogénétiquement activés (Okun et al., 2015). Des différences au niveau de la localisation laminaire ont été également rapportées dans le cortex inféro-temporal du singe : les solistes sont plus communément présents entre 0.2 et 1.2 mm de profondeur corticale, alors que les choristes sont rares dans la couche 4 et sont localisés dans les couches non-granulaires (Hung et al., 2014).

Dans notre étude, nous montrons que dans un cortex organisé en colonnes (cortex visuel primaire du chat adulte), les neurones à potentiel d'action de forme allongée et ceux à potentiel d'action de forme régulière montrent des distinctions en termes de taux de décharge et de coupage populationnel : les solistes ayant un moins fort taux de décharge et une moindre corrélation (couplage populationnel). Ces différences ne peuvent pas être attribuées aux propriétés excitatrices et inhibitrices des cellules pyramidales et des interneurones (ces derniers sont considérés excitateurs et inhibiteurs, respectivement chez la souris) chez le chat car un bon nombre de neurones excitateurs montrent des formes allongées de potentiels d'action. La forme du potentiel d'action n'est donc pas un paramètre valide de distinction entre les neurones pyramidaux excitateurs et les interneurones inhibiteurs chez le chat (Nowak et al., 2003). Nous avons montré qu'un large spectre de couplage populationnel variant de plus petites valeurs à de plus grandes valeurs donne une tendance de corrélations distinctes entre des neurones à potentiel d'action régulier (et à fréquence de décharge régulière) et des neurones à potentiel d'action de forme allongée (et à fréquence de décharge rapide). Les mécanismes complexes de neurones individuels et des assemblées qu'ils forment sont impliqués dans le traitement de l'information. Il est donc important d'identifier des paramètres pouvant élucider certaines relations entre le codage de l'information et les propriétés électrophysiologiques des neurones. En conséquence de cette étude, les calculs des corrélations des réponses de chaque neurone avec l'assemblée neuronale à laquelle il appartient pourraient être un bon indicateur de prédiction du type de forme du potentiel d'action et du taux de décharge du neurone et vice versa. Les corrélations qui constituent la synchronisation neuronale dans un espace anatomique restreint comme la colonne d'orientation du cortex visuel, peuvent donc être accomplies par des neurones choristes et

d'autres neurones solistes. Combinés avec nos récents résultats d'une étude qui confère aux neurones à forte décharge une activité gamma importante (Bharmauria et al., 2015), ces résultats donnent de nouvelles perspectives sur l'orchestration du traitement de l'information où les neurones à forte décharge accentuent la sélectivité des neurones voisins.

8.4 Chapitre D : effets des antidépresseurs

Cette partie a pour but d'examiner l'un des neurotransmetteurs les plus importants dans le cerveau, tant au niveau de ses fonctions de codage sensoriel qu'au niveau de manifestation du comportement. Il s'agit de la sérotonine, liée à de grandes pathologies associées à un dysfonctionnement du système sérotoninergique telles que la dépression. En effet, un faible taux de sérotonine pouvant conduire à un état dépressif, l'utilisation d'inhibiteurs sélectifs de la recapture de la sérotonine (ISRS) tels que la fluoxétine (agissent sur les mécanismes de recapture de la sérotonine dans le but d'en augmenter sa quantité) permet de réduire les effets de la dépression. Dans ce chapitre, nous intégrons notre modèle de plasticité des neurones du cortex visuel en présence de sérotonine ou de fluoxétine (élévation du niveau sérotoninergique) afin d'y déterminer les mécanismes de modulation des traitements corticaux.

Plusieurs études ont été menées sur le rôle régulateur de la sérotonine et la fluoxétine dans le cortex visuel du rongeur. Les deux substances utilisées dans notre étude ont été associées dans la réactivation de la plasticité cérébrale. Il a notamment été montré qu'un traitement chronique de fluoxétine sur des rats réduit l'inhibition GABAèrgique et augmente l'expression du facteur de croissance BDNF, ceci a pour conséquence la récupération de la plasticité de dominance

oculaire chez ces sujets adultes (Maya-vetencourt et al., 2008). Il a été également suggéré que la fluoxétine restructure les branches des extrémités dendritiques (Chen et al., 2011). Des expériences sur des enregistrements intracellulaires ont révélé un effet dépolarisant entrainant une activité de décharge (Tanaka and North, 1993). De plus, un niveau élevé de transmission sérotoninergique augmente des cascades de signalisation du BDNF résultant par une potentialisation de la plasticité (Maya-vetencourt et al., 2011).

Il parait évident que le nombre important de récepteurs sérotoninergiques se reflète dans l'action excitatrice ou inhibitrice de la sérotonine à divers niveaux corticaux et dans ses fonctions complexes dans la régulation des circuits corticaux. Cette grande divergence de récepteurs peut également expliquer des différences observées au cours du développement. En effet, dans le cortex préfrontal, il a été montré que la sérotonine engendrait une action généralement excitatrice après trois semaines suivant la naissance puis devenait majoritairement inhibitrice (Zhang, 2003).

8.4.1 Sérotonine et inhibition

Le rôle régulateur de la sérotonine dans les circuits corticaux implique des études in vitro et in vivo, tant sur le plan de la modulation des courants synaptiques, sur la modulation des taux de décharges, et sur les changements de propriétés neuronales (ce dernier sera traité plus en détail plus bas). En effet, il a été démontré chez le rongeur, au niveau du cortex visuel, que l'induction, de façon pharmacologique, de la diminution du système sérotoninergique entraine une potentialisation à long terme (Edagawa et al., 2001) et qu'au niveau de l'hippocampe (structure du système limbique jouant un rôle majeur dans la mémoire et la

navigation spatiale), il y a ralentissement de la potentialisation à long terme (Mnie-Filali et al., 2006). Il semble donc que l'effet de la sérotonine est d'induire une inhibition de la LTP, un scénario qui pourrait s'agencer avec nos travaux de recherche et notre modèle d'organisation dendritique proposé (modèle où chaque neurone est sensible à un stimulus de façon plus ou moins importante, selon des seuils de sensibilité au sein de l'arbre dendritique).

De façon intéressante, il a également été démontré une corrélation entre l'âge des animaux testés (chats) et l'effet d'induction de LTP ou de LTD. En effet, en contrepartie de cette inhibition de la potentialisation à long terme, il a été montré que certains récepteurs sérotoninergiques étaient responsables de fluctuations entre LTP et LTD et que ces fluctuations dépendaient de l'âge (Kojic et al., 2000).

8.4.2 En lien avec notre modèle de plasticité

Qu'en est-il de l'effet de la sérotonine et de la fluoxétine lorsque l'administration de celles-ci est couplée à une période d'apprentissage visuel ? Dans de précédentes études, il a été démontré qu'à la suite d'un processus d'adaptation visuelle successif, on observe une augmentation du taux de décharge de la nouvelle orientation optimale acquise. Une hypothèse peut donc émerger : les effets obtenus suite à l'application des drogues pourraient être dus partiellement à la seconde phase d'adaptation. Néanmoins, dans ces études précédemment publiées (Ghisovan et al., 2008), l'amplitude des déplacements des courbes n'était pas affectée, de plus la proportion de déplacements répulsifs dans ces études était de 16% à la suite d'une adaptation visuelle successive, dans notre cas, seuls 5% de déplacements répulsifs ont été observés (dans le cas des deux drogues).

Analogiquement aux modèles cités plus haut, nos résultats suggèrent que l'action des deux drogues est limitée à des synapses actives (Chen et al., 2011), cette action conduit à un nouvel équilibre des entrées synaptiques qui par conséquent aboutit à des modifications fonctionnelles des circuits neuronaux (Jaffer et al., 2012).

En combinant l'imagerie par double photon et des enregistrements électrophysiologiques (Jia et al., 2010), ainsi que des protocoles de reconstruction anatomique en trois dimensions (Kisvarday et al., 2000), il a été démontré qu'une seule branche dendritique reçoit des connexions synaptiques de différents neurones sélectifs à différentes orientations, et que par conséquent les orientations sont représentées et dispersées au sein de l'arbre dendritique d'un seul neurone (Jia et al., 2010; Kisvarday et al., 2000), ce qui peut être en accord avec certaines courbes d'orientations où il n'y a pas absence totale de décharge aux orientations non optimales. Nos résultats ont montré que l'effet des drogues est limité à deux orientations d'intérêt (diminution de l'orientation originale optimale et augmentation de la nouvelle orientation optimale acquise), nous avons donc proposé un modèle basé sur les distributions des pondérations synaptiques (poids synaptiques) au sein d'un même neurone comme l'ont suggéré les études citées précédemment. Après l'administration de la drogue, il y a rééquilibre des forces synaptiques en faveur de l'orientation imposée, tandis que la drogue éloigne les décharges à l'orientation originale optimale du seuil d'excitation et n'affecte pas les orientations des flancs de la courbe.

En conclusion, la plasticité dans le cortex visuel primaire joue un rôle majeur dans le traitement cérébral et les mécanismes cognitifs tels que l'apprentissage ou la mémoire. Nous avons montré que la sérotonine et l'antidépresseur qui est la fluoxétine facilitent l'apprentissage par adaptation visuelle en potentialisant les réponses aux stimuli imposés.

8.5 Considérations méthodologiques : Stabilité des cartes d'orientation

Les changements de sélectivité neuronale des domaines d'orientation du cortex visuel pourraient être attribués à des fluctuations spontanées des niveaux du taux de décharge. Même si cette hypothèse n'est pas totalement négligeable, nombre d'études ont montré que lorsque les conditions de stimulation de changent pas (pas de plasticité induite), il y a une stabilité des cartes d'orientation ainsi que des propriétés des neurones individuels (Chapman et al., 1996 ; Gödecke et al., 1997 ; Shtoyerman et al., 2000). De plus, les changements de sélectivité observés ont été limités à deux orientations optimales d'intérêt : l'orientation de base et la nouvelle orientation optimale acquise post-adaptation. Le taux de décharge varie de façon systématique entre sa diminution pour le stimulus optimal initial et son augmentation pour le stimulus appris. Ce patron de fluctuation ne peut être attribué à des fluctuations spontanées d'excitabilité.

Dans nos études portant sur l'imagerie optique intrinsèque, des algorithmes de traitement d'images ont été utilisés afin d'attribuer un code couleur à chaque stimulus présenté et d'en extraire les cartes d'orientation de la zone corticale désirée. Il est toutefois important de souligner que des tests ont été effectués afin de s'assurer de la stabilité des cartes corticales afin d'attribuer les modifications observées à l'effet de l'apprentissage visuel. Nous avons mesuré l'intensité lumineuse des images analysées et avons observé qu'elle n'était pas significativement différente entre les chats ou entre les différentes sessions d'enregistrement. Les images obtenues en imagerie optique sont toujours bruitées et nécessitent un traitement pour séparer le signal du bruit. Le bruit est inhérent à toute technique de mesure, il peut être

réduit mais en aucun cas supprimé. Le problème est donc de savoir si nous avons bien un signal à l'intérieur de ce bruit. Nous pensons que c'est le cas car :

- Les cartes présentent clairement des zones organisées à l'intérieur d'un pourtour aux orientations aléatoires. En aucun cas du bruit ne pourrait engendrer un patron aussi régulier.
- Les domaines d'orientation changent systématiquement après une période d'adaptation, ce qui n'est pas le cas si aucune adaptation n'est réalisée entre deux cartes. Nous avons également constaté que les domaines d'orientations, bien que reconnaissables entre différentes cartes changeaient légèrement de position. Nous pensons que cela est peut-être dû au bruit étant donné que les connexions neuronales changent légèrement au cours du temps ? Nous pensons que comparer les proportions de pixels dans chaque orientation est statistiquement justifié car bien que les bords des domaines d'orientations changent entre plusieurs cartes contrôle, les domaines restent grossièrement à la même place. Sur les 90000 pixels que contient au minimum une image, l'erreur parait acceptable.

9. Conclusion

Cette thèse de doctorat a contribué à l'avancement de la compréhension des changements opérant dans les assemblées neuronales du cortex visuel primaire ainsi que la dynamique des changements de neurones isolés individuellement sur plusieurs aspects : la sélectivité neuronale, la connectivité neuronale, la relation entre ces deux aspects et les propriétés électrophysiologiques des neurones, ainsi que les effets des antidépresseurs sur ce modèle de plasticité.

En effet, en plus du modèle de plasticité neuronale liée aux colonnes de dominance oculaire, notre modèle de plasticité lié à la dynamique de modulation des cartes d'orientation nous a permis de déduire les stratégies de changement de sélectivité et de connectivité neuronales et ce, à petite (électrophysiologie) et grande échelle (imagerie cérébrale).

Il n'en demeure pas moins que plusieurs aspects notamment génétiques et moléculaires pourraient consolider les mécanismes sous-jacents qui contrôlent cette plasticité neuronale. Les avancées technologiques permettront certainement d'élucider ces diverses questions

L'interaction entre la génétique et l'expérience sensorielle devient donc cruciale pour l'aboutissement à un cerveau modèle qui serait l'identité de chacun. L'une des meilleures métaphores vient sans doute de l'auteur du livre « le cerveau sur mesure », comme si chacun portait un cerveau qui lui allait à la perfection.

Nos recherches et les nombreuses études faites sur la plasticité cérébrale permettent notamment d'élaborer des stratégies de récupération de certains troubles mnésiques, ou encore de certaines pathologies telles que l'amblyopie (Figure 9, Maya-vetencourt and Origlia, 2012).

En effet, les effets de l'apprentissage visuel ou l'administration de certaines substances comme nous l'avons montré contribue à la facilitation d'encodage des stimuli, des recherches plus poussées sur la diminution de l'inhibition et ainsi la restauration de la plasticité juvénile peuvent aider à la guérison de nombreuses pathologies cérébrales.

Figure 9 - Récapitulatif des diverses stratégies de restauration de la plasticité corticale. Stratégies potentielles du traitement de l'amblyopie chez l'adulte (déficience visuelle) : l'activité physique, l'enrichissement environnemental par stimulation, la thérapie diététique, le traitement pharmacologique, et la privation oculaire temporaire peuvent réduire les taux d'inhibition et augmenter les niveaux de BDNF, par conséquent la plasticité cérébrale augmente. Dans notre cas, la stimulation visuelle et le traitement pharmacologique facilitent les effets d'apprentissage visuel.

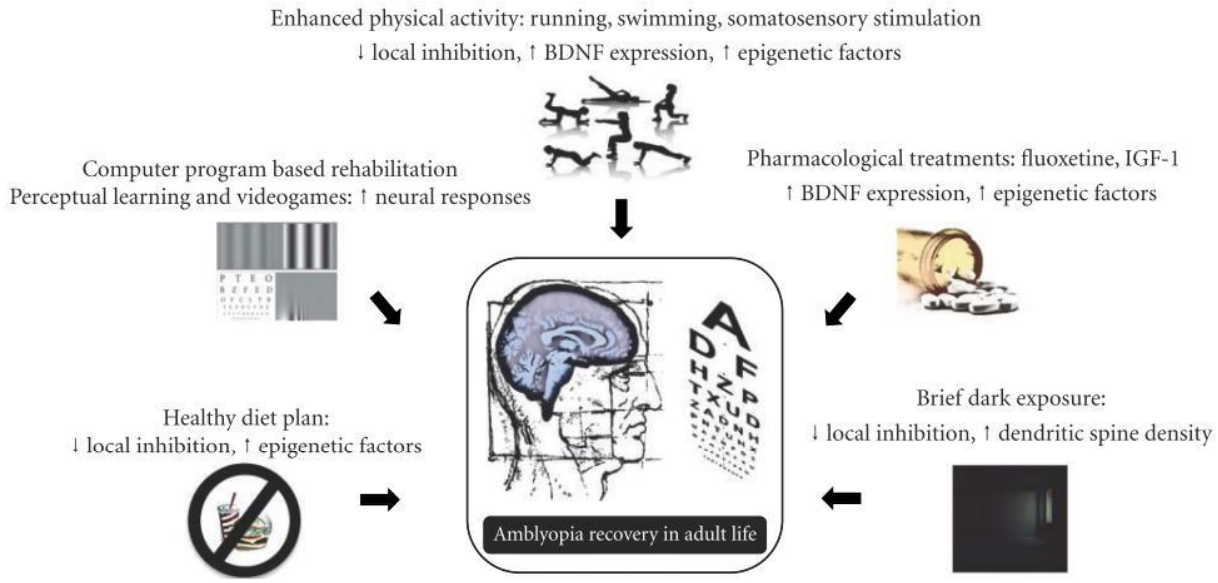

Maya-vetencourt and Origlia, 2012

Bibliographie

Alloway, K. D. & Roy, S. A. (2002) Conditional cross-correlation analysis of thalamocortical neurotransmission. Behav Brain Res. 135, 191-196.

Alonso, J. M. (2002) Neural connections and receptive field properties in the primary visual cortex. The Neuroscientist: a review journal bringing neurobiology, neurology and psychiatry 8, 443-456.

Alonso, J. M., Usrey, W. M. & Reid, R. C. (1996) Precisely correlated firing in cells of the lateral geniculate nucleus. Nature 383, 815-819, doi:10.1038/383815a0.

Alonso, J. M., Usrey, W. M., Reid, R. C. (2001) Rules of connectivity between geniculate cells and simple cells in cat primary visual cortex. J Neurosci 21: 4002-4015.

Bachatene L, Bharmauria V, Rouat J, Molotchnikoff S (2012a) Adaptation-induced Plasticity and Spike Waveforms in Cat Visual Cortex. Neuroreport. 23: 88-92.

Bachatene L, Bharmauria V and Molotchnikoff S (2012b). Adaptation and Neuronal Network in Visual Cortex, Visual Cortex - Current Status and Perspectives, ISBN: 978-953-51-0760-6, InTech, DOI: 10.5772/46011.

Bachatene, L., Bharmauria, V., Cattan, S. & Molotchnikoff, S. (2013) Fluoxetine and serotonin facilitate attractive-adaptation-induced orientation plasticity in adult cat visual cortex. Eur J Neurosci. 38, 2065-2077, doi:10.1111/ejn.12206.

Bair, W., Zohary, E. & Newsome, W. T. (2001) Correlated firing in macaque visual area MT: time scales and relationship to behavior. The Journal of neuroscience : the official journal of the Society for Neuroscience 21, 1676-1697.

Bartho, P. et al. (2004) Characterization of neocortical principal cells and interneurons by network interactions and extracellular features. J Neurophysiol. 92, 600-608, doi:10.1152/jn.01170.2003.

Benucci, A., Saleem, A. B. & Carandini, M. (2013) Adaptation maintains population homeostasis in primary visual cortex. Nature neuroscience 16, 724-729, doi:10.1038/nn.3382.

Bharmauria, V., Bachatene, L., Cattan, S., Chanauria, N., Rouat, J., & Molotchnikoff, S. (2015). Stimulus-dependent augmented gamma oscillatory activity between the functionally connected cortical neurons in the primary visual cortex. *Eur J Neurosci*. doi: 10.1111/ejn.12912

Bharmauria, V., Bachatene, L., Cattan, S., Brodeur, S., Chanauria, N., Rouat, J., & Molotchnikoff, S. (2015). Network-selectivity and stimulus-discrimination in the primary visual cortex: cell-assembly dynamics. *Eur J Neurosci*. doi: 10.1111/ejn.13101

Bishop PO, Henry GH (1972) Striate Neurons: Receptive Field Concepts. Invest Ophthalmol. 11: 346-354.

Bock, D. D. et al. (2011) Network anatomy and in vivo physiology of visual cortical neurons. Nature 471, 177-182, doi:10.1038/nature09802.

Bonhoeffer T & Grinvald A (1993). The layout of iso-orientation domains in area 18 of cat visual cortex: optical imaging reveals a pinwheel-like organization. J Neurosci 13, 4157-4180.

Born RT & Bradley DC (2005). Structure and Function of Visual Area MT. Annu Rev Neurosci 28, 157-189.

Braddick OJ, O'Brien JM, Wattam-Bell J, Atkinson J, Hartley T & Turner R (2001). Brain areas sensitive to coherent visual motion. Perception 30, 61-72.

Bullier, J., McCourt, M. E., & Henry, G. H. (1988). Physiological studies on the feedback connection to the striate cortex from cortical areas 18 and 19 of the cat. *Exp Brain Res, 70*(1), 90-98.

Burrone, J., O'Byrne, M., & Murthy, V. N. (2002). Multiple forms of synaptic plasticity triggered by selective suppression of activity in individual neurons. *Nature, 420*(6914), 414-418. doi: 10.1038/nature01242

Casagrande VA, Xu X (2004) Parallel visual pathways: a comparative perspective. The Visual Neurosciences. pp. 494-506 Cambridge, MA: MIT Press.

Cattan, S., Bachatene, L., Bharmauria, V., Jeyabalaratnam, J., Milleret, C., & Molotchnikoff, S. (2014). Comparative analysis of orientation maps in areas 17 and 18 of the cat primary visual cortex following adaptation. *Eur J Neurosci, 40*(3), 2554-2563. doi: 10.1111/ejn.12616

Chapman B, Stryker MP, Bonhoeffer T. (1996). Development of orientation preference maps in ferret primary visual cortex. *J Neurosci.* 16(20):6443-53.

Chen, J.L., Lin, W.C., Cha, J.W., So, P.T., Kubota, Y. & Nedivi, E. (2011) Structural basis for the role of inhibition in facilitating adult brain plasticity. Nat. Neurosci., 14 , 587 – 594.

Chiu C, Weliki M. (2003) The role of neural activity in the development of orientation selectivity. The visual neurosciences. 117–125 Cambridge, MA: MIT Press.

Chollet, F., Tardy, J., Albucher, J.F., Thalamas, C., Berard, E., Lamy, C., Bejot, Y., Deltour, S., Jaillard, A., Niclot, P., Guillon, B., Moulin, T., Marque, P., Pariente, J., Arnaud, C. & Loubinoux, I. (2011) Fluoxetine for motor recovery after acute ischaemic stroke (FLAME): a randomised placebo-controlled trial. Lancet Neurol., 10 , 123 – 130.

Cowan DO & Drisko RL (1976). Elements of Organic Photochemistry, Plenum Press

Crair MC, Gillespie DC & Stryker MP (1998). The role of visual experience in the development of columns in cat visual cortex. Science 279, 566-570.

Csicsvari, J., Hirase, H., Czurko, A. & Buzsaki, G. (1998) Reliability and state dependence of pyramidal cell-interneuron synapses in the hippocampus: an ensemble approach in the behaving rat. Neuron 21, 179-189.

Das, A. & Gilbert, C. D. (1995) Long-range horizontal connections and their role in cortical reorganization revealed by optical recording of cat primary visual cortex. Nature 375, 780-784, doi:10.1038/375780a0.

De Weerd P, Vandenbussche E, De Bruyn B, Orban GA (1990) Illusory Contour Orientation Discrimination in the Cat. Behav Brain Res. 39: 1-17.

Denman, D. J. & Contreras, D. (2013) The Structure of Pairwise Correlation in Mouse Primary Visual Cortex Reveals Functional Organization in the Absence of an Orientation Map. Cereb Cortex, doi:10.1093/cercor/bht128.

Dragoi V, Rivadulla C, Sur M (2001) Foci of Orientation Plasticity in Visual Cortex. Nature. 411: 80-86.

Dragoi V, Sharma J, Sur M (2000) Adaptation-induced Plasticity of Orientation Tuning in Adult Visual Cortex. Neuron. 28: 287-298.

Duret, F., Shumikhina, S. & Molotchnikoff, S. (2006) Neuron participation in a synchrony-encoding assembly. BMC neuroscience 7,72, doi:10.1186/1471-2202-7-72.

Edagawa Y, Saito H, Abe K. (2001) Endogenous serotonin contributes to a developmental decrease in long-term potentiation in the rat visual cortex. J Neurosci 21:1532-7.

Essen DC & Zeki SM (1978). The Topographic Organization of Rhesus Monkey Prestriate Cortex. J Physiol 277, 193-226.

Fagiolini M, Hensch TK. (2000) Inhibitory threshold for critical-period activation in primary visual cortex. Nature 404:183-6.

Felleman DJ, Van Essen DC (1991) Distributed Hierarchical Processing in the Primate Cerebral Cortex. Cereb Cortex. 1: 1-47.

Fries P, Nikolic D, Singer W. (2007) The gamma cycle. Trends Neurosci;30:309–316.

Froemke, R. C., Merzenich, M. M., & Schreiner, C. E. (2007). A synaptic memory trace for cortical receptive field plasticity. *Nature, 450*(7168), 425-429. doi: 10.1038/nature06289

Fujisawa S, Amarasingham A, Harrison MT, Buzsaki G. (2008) Behavior-dependent short-term assembly dynamics in the medial prefrontal cortex. Nat Neurosci. 11, 823-833.

Furmanski CS, Schluppeck D, Engel SA. (2004) Learning strengthens the response of primary visual cortex to simple patterns. Curr Biol 14:573-8.

Ghisovan N, Nemri A, Shumikhina S, Molotchnikoff S (2008) Visual Cells Remember Earlier Applied Target: Plasticity of Orientation Selectivity. PLoS One. 3: e3689.

Ghisovan N, Nemri A, Shumikhina S, Molotchnikoff S (2009) Long Adaptation Reveals Mostly Attractive Shifts of Orientation Tuning in Cat Primary Visual Cortex. Neuroscience.164: 1274-1283.

Gilbert CD, Wiesel TN (1979) Morphology and Intracortical Projections of Functionally Characterised Neurones in the Cat Visual Cortex. Nature. 280: 120-125.

Gilbert, C. D., & Wiesel, T. N. (1989). Columnar specificity of intrinsic horizontal and corticocortical connections in cat visual cortex. *J Neurosci, 9*(7), 2432-2442.

Godde B, Leonhardt R, Cords SM, Dinse HR. (2002) Plasticity of orientation preference maps in the visual cortex of adult cats. Proc Natl Acad Sci U S A. 99, 6352-6357.

Gödecke I, Kim DS, Bonhoeffer T, Singer W. (1997). Development of orientation preference maps in area 18 of kitten visual cortex. *Eur J Neurosci*. 9(8):1754-62.

González-Burgos G, Krimer LS, Povysheva NV, Barrionuevo G, Lewis DA (2005) Functional Properties of Fast Spiking Interneurons and their Synaptic Connections with Pyramidal Cells in Primate Dorsolateral Prefrontal Cortex. J Neurophysiol. 93: 942-953.

Gray, C. M., Engel, A. K., Konig, P. & Singer, W. (1990) Stimulus-Dependent Neuronal Oscillations in Cat Visual Cortex: Receptive Field Properties and Feature Dependence. The European journal of neuroscience 2, 607-619.

Grinvald, A., Arieli, A., Tsodyks, M., & Kenet, T. (2003). Neuronal assemblies: single cortical neurons are obedient members of a huge orchestra. *Biopolymers, 68*(3), 422-436. doi: 10.1002/bip.10273

Hansen, B. J., & Dragoi, V. (2011). Adaptation-induced synchronization in laminar cortical circuits. *Proc Natl Acad Sci U S A, 108*(26), 10720-10725. doi: 10.1073/pnas.1102017108

Harauzov, A., Spolidoro, M., DiCristo, G., De Pasquale, R., Cancedda, L., Pizzorusso, T., Viegi, A., Berardi, N. & Maffei, L. (2010) Reducing intra-cortical inhibition in the adult visual cortex promotes ocular dominance plasticity. J. Neurosci., 30 , 361 – 371.

Hata, Y., Tsumoto, T., Sato, H. & Tamura, H. (1991) Horizontal interactions between visual cortical neurones studied by cross-correlation analysis in the cat. J. Physiol. 441, 593-614.

He HY, Hodos W, Quinlan EM. (2006) Visual deprivation reactivates rapid ocular dominance plasticity in adult visual cortex. J Neurosci. 26, 2951-2955.

Hebb, D.O. (1949) The Organization of Behavior: A Neuropsychological Theory. New York: Wiley and Sons.

Henry, G. H., Bishop, P. O., Tupper, R. M., & Dreher, B. (1973). Orientation specificity and response variability of cells in the striate cortex. *Vision Res, 13*(9), 1771-1779.

Hensch, T. K. (2005). Critical period plasticity in local cortical circuits. *Nat Rev Neurosci, 6*(11), 877-888. doi: 10.1038/nrn1787

Hensch TK, Fagiolini M, Mataga N, Stryker MP, Baekkeskov S, et al. (1998) Local GABA circuit control of experience-dependent plasticity in developing visual cortex. Science 282:1504-8.

Hietanen, M. A., Crowder, N. A., Price, N. S., & Ibbotson, M. R. (2007). Influence of adapting speed on speed and contrast coding in the primary visual cortex of the cat. *J Physiol, 584*(Pt 2), 451-462. doi: 10.1113/jphysiol.2007.131631

Hishida R, Kamatani D, Kitaura H, Kudoh M, Shibuki K. (2007) Functional local connections with differential activity-dependence and critical periods surrounding the primary auditory cortex in rat cerebral slices. Neuroimage 34:679-93.

Hofer SB, Ko H, Pichler B, Vogelstein J, Ros H, Zeng H, et al. (2011) Differential connectivity and response dynamics of excitatory and inhibitory neurons in visual cortex. Nat Neurosci; 14:1045–1054.

Horton, J. C., & Adams, D. L. (2005). The cortical column: a structure without a function. *Philos Trans R Soc Lond B Biol Sci, 360*(1456), 837-862. doi: 10.1098/rstb.2005.1623

Huang ZJ, Kirkwood A, Pizzorusso T, Porciatti V, Morales B, et al. (1999) BDNF regulates the maturation of inhibition and the critical period of plasticity in mouse visual cortex. Cell 98:739-55.

Hubel DH, Wiesel TN (1959) Receptive Fields of Single Neurons in the Cat's Striate Cortex. J Physiol. 148: 574-591.

Hubel DH, Wiesel TN (1962) Receptive Fields, Binocular Interaction and Functional Architecture in the Cat's Visual Cortex. J Physiol.160: 106-154.

Hubel DH, Wiesel TN (1963a) Shape and Arrangement of Columns in Cat's Striate Cortex. J Physiol. 165: 559-568.

Hubel DH, Wiesel TN (1968) Receptive Fields and Functional Architecture of Monkey Striate Cortex. J Physiol. 195: 215-243.

Hubel DH, Wiesel TN (1963b) Receptive Fields of Cells in Striate Cortex of Very Young Visually Inexperienced Kittens. J Neurophysiol. 26: 994-1002.

Hubel DH & Wiesel TN (1974). Sequence regularity and geometry of orientation columns in the monkey striate cortex. J Comp Neurol 158, 267-293.

Hung, C. P., Cui, D., Chen, Y. P., Lin, C. P., & Levine, M. R. (2014). Correlated activity supports efficient cortical processing. *Front Comput Neurosci, 8*, 171. doi: 10.3389/fncom.2014.00171

Hyde KL, Lerch J, Norton A, Forgeard M, Winner E, et al. (2009) Musical training shapes structural brain development. J Neurosci 29:3019-25.

Ison MJ, Mormann F, Cerf M, Koch C, Fried I, Quiroga RQ (2011) Selectivity of Pyramidal Cells and Interneurons in the Human Medial Temporal Lobe. J Neurophysiol. 106: 1713-1721.

Issa NP, Trepel C & Stryker MP (2000). Spatial Frequency Maps in Cat Visual Cortex. J Neurosci 20, 8504-8514.

Jaffer, S., Vorobyov, V., Kind, P.C. & Sengpiel, F. (2012) Experience-dependent regulation of functional maps and synaptic protein expression inthe cat visual cortex. Eur. J. Neurosci., 35 , 1281 – 1294.

Jia, H., Rochefort, N.L., Chen, X. & Konnerth, A. (2010) Dendritic organization of sensory input to cortical neurons in vivo. Nature, 464 , 1307 – 1312.

Jin, J., Wang, Y., Swadlow, H. A., & Alonso, J. M. (2011). Population receptive fields of ON and OFF thalamic inputs to an orientation column in visual cortex. *Nat Neurosci, 14*(2), 232-238. doi: 10.1038/nn.2729

Kaas, J. H., Krubitzer, L. A., & Johanson, K. L. (1989). Cortical connections of areas 17 (V-I) and 18 (V-II) of squirrels. *J Comp Neurol, 281*(3), 426-446. doi: 10.1002/cne.902810308

Kampa, B. M., Roth, M. M., Gobel, W. & Helmchen, F. (2011) Representation of visual scenes by local neuronal populations in layer 2/3 of mouse visual cortex. Frontiers in neural circuits 5, 18, doi:10.3389/fncir.2011.00018.

Kaschube M, Schnabel M, Löwel S, Coppola DM, White LE, Wolf F (2010) Universality in the Evolution of Orientation Columns in the Visual Cortex. Science. 330: 1113-1116.

Keck, T., Scheuss, V., Jacobsen, R. I., Wierenga, C. J., Eysel, U. T., Bonhoeffer, T., & Hubener, M. (2011). Loss of sensory input causes rapid structural changes of inhibitory neurons in adult mouse visual cortex. *Neuron, 71*(5), 869-882. doi: 10.1016/j.neuron.2011.06.034

Kisvarday, Z.F., Crook, J.M., Buzas, P. & Eysel, U.T. (2000) Combinedphysiological – anatomical approaches to study lateral inhibition. J. Neurosci. Meth., 103 , 91 – 106.

Ko, H., Cossell, L., Baragli, C., Antolik, J., Clopath, C., Hofer, S. B., & Mrsic-Flogel, T. D. (2013). The emergence of functional microcircuits in visual cortex. *Nature, 496*(7443), 96-100. doi: 10.1038/nature12015

Ko, H., Hofer, S. B., Pichler, B., Buchanan, K. A., Sjostrom, P. J., & Mrsic-Flogel, T. D. (2011). Functional specificity of local synaptic connections in neocortical networks. *Nature, 473*(7345), 87-91. doi: 10.1038/nature09880

Kohn, A. (2007). Visual adaptation: physiology, mechanisms, and functional benefits. *J Neurophysiol, 97*(5), 3155-3164. doi: 10.1152/jn.00086.2007

Kohn A, Movshon JA. (2003) Neuronal adaptation to visual motion in area MT of the Macaque. Neuron; 39:681–691.

Kohn, A., & Movshon, J. A. (2004). Adaptation changes the direction tuning of macaque MT neurons. *Nat Neurosci, 7*(7), 764-772. doi: 10.1038/nn1267

Kojic L, Dyck RH, Gu Q, Douglas RM, Matsubara J, et al. (2000) Columnar distribution of serotonin-dependent plasticity within kitten striate cortex. Proc Natl Acad Sci U S A 97:1841-4.

Konig P, Engel AK, Roelfsema PR, Singer W. (1995) How precise is neuronal synchronization? Neural Comput. 7, 469-485.

Krekelberg, B., van Wezel, R. J., & Albright, T. D. (2006). Adaptation in macaque MT reduces perceived speed and improves speed discrimination. *J Neurophysiol, 95*(1), 255-270. doi: 10.1152/jn.00750.2005

Kuhlman SJ, Tring E, Trachtenber JT. (2011) Fast-spiking interneurons have an initial orientation bias that is lost with vision. Nat Neurosci; 14:1121–1123.

Kujovic M, Zilles K, Malikovic A, Schleicher A, Mohlberg H, Rottschy C, Eickhoff SB, Amunts K (2012) Cytoarchitectonic Mapping of the Human Dorsal Extrastriate Cortex. Brain Struct Funct. [Epub ahead of print]

Lee, W. C. & Reid, R. C. (2011) Specificity and randomness: structure-function relationships in neural circuits. Current opinion in neurobiology 21, 801-807, doi:10.1016/j.conb.2011.07.004.

Lin, C. P., Chen, Y. P., & Hung, C. P. (2014). Tuning and spontaneous spike time synchrony share a common structure in macaque inferior temporal cortex. *J Neurophysiol, 112*(4), 856-869. doi: 10.1152/jn.00485.2013

Lin CS, Friedlander MJ, Sherman SM (1979) Morphology of Physiologically Identified Neurons in the Visual Cortex of the Cat. Brain Res. 172: 344-348.

Lledo PM, Alonso M, Grubb MS. (2006) Adult neurogenesis and functional plasticity in neuronal circuits. Nat Rev Neurosci 7:179-93.

Markram H, Toledo-Rodriguez M, Wang Y, Gupta A, Silberberg G, Wu C (2004) Interneurons of the Neocortical Inhibitory System. Nat Rev Neurosci. 5: 793-807.

Marshansky S, Shumikhina S, Molotchnikoff S (2011) Repetitive Adaptation Induces Plasticity of Spatial Frequency Tuning in Cat Primary Visual Cortex. Neuroscience. 172: 355-365.

Martinez LM, Wang Q, Reid RC, Pillai C, Alonso JM, Sommer FT, Hirsch JA (2005) Receptive Field Structure Varies with Layer in the Primary Visual Cortex. Nat Neurosci. 8: 372-379.

Maya-Vetencourt, J. F., & Origlia, N. (2012). Visual cortex plasticity: a complex interplay of genetic and environmental influences. *Neural Plast, 2012*, 631965. doi: 10.1155/2012/631965

Maya Vetencourt, J. F., Sale, A., Viegi, A., Baroncelli, L., De Pasquale, R., O'Leary, O. F., Castrén, E., & Maffei, L. (2008) The antidepressant fluoxetine restores plasticity in the adult visual cortex. Science, 320(5874), 385-388.

Maya Vetencourt, J.F., Tiraboschi, E., Spolidoro, M., Castrén, E., & Maffei, L. (2011) Serotonin triggers a transient epigenetic mechanism that reinstates adult visual cortex plasticity in rats. Eur J Neurosci, 33, 49–57.

Maya-Vetencourt, J.F. & Origlia, N. (2012) Visual cortex plasticity: a complex interplay of genetic and environmental in fl uences. Neural Plast., 2012 , 631965.

Miller, J. E., Ayzenshtat, I., Carrillo-Reid, L., & Yuste, R. (2014). Visual stimuli recruit intrinsically generated cortical ensembles. *Proc Natl Acad Sci U S A, 111*(38), E4053-4061. doi: 10.1073/pnas.1406077111

Mnie-Filali O, El Mansari M, Espana A, Sanchez C, Haddjeri N. (2006) Allosteric modulation of the effects of the 5-HT reuptake inhibitor escitalopram on the rat hippocampal synaptic plasticity. Neurosci Lett 395:23-7.

Monier, C., Chavane, F., Baudot, P., Graham, L. J., & Fregnac, Y. (2003). Orientation and direction selectivity of synaptic inputs in visual cortical neurons: a diversity of combinations produces spike tuning. *Neuron, 37*(4), 663-680.

Moran J & Desimone R (1985). Selective attention gates visual processing in the extrastriate cortex. Science 229, 782-784.

Movshon JA (1975) The Velocity Tuning of Single Units in Cat Striate Cortex. J Physiol. 249: 445-468.

Nauhaus, I., Benucci, A., Carandini, M., & Ringach, D. L. (2008). Neuronal selectivity and local map structure in visual cortex. *Neuron, 57*(5), 673-679. doi: 10.1016/j.neuron.2008.01.020

Nelson, S. B., & Turrigiano, G. G. (2008). Strength through diversity. *Neuron, 60*(3), 477-482. doi: 10.1016/j.neuron.2008.10.020

Nemri A, Ghisovan N, Shumikhina S, Molotchnikoff S (2009) Adaptive Behavior of Neighboring Neurons During Adaptation-induced Plasticity of Orientation Tuning in VI. BMC Neurosci. 10: 147.

Nowak, L. G., Azouz, R., Sanchez-Vives, M. V., Gray, C. M. and McCormick, D. A. (2003) Electrophysiological classes of cat primary visual cortical neurons in vivo as revealed by quantitative analyses. Journal of Neurophysiology 89, 1541-1566.

Ohki K, Chung S, Ch'ng YH, Kara P, Reid RC (2005) Functional Imaging with Cellular Resolution Reveals Precise Micro-architecture in Visual Cortex. Nature. 433: 597-603.

Okun, M., Steinmetz, N. A., Cossell, L., Iacaruso, M. F., Ko, H., Bartho, P., . . . Harris, K. D. (2015). Diverse coupling of neurons to populations in sensory cortex. *Nature, 521*(7553), 511-515. doi: 10.1038/nature14273

Patterson, C. A., Wissig, S. C. & Kohn, A. (2013) Distinct effects of brief and prolonged adaptation on orientation tuning in primary visual cortex. J Neurosci. 33, 532-543, doi:10.1523/JNEUROSCI.3345-12.2013.

Patterson, C. A., Wissig, S. C., & Kohn, A. (2014). Adaptation disrupts motion integration in the primate dorsal stream. *Neuron, 81*(3), 674-686. doi: 10.1016/j.neuron.2013.11.022

Perkel DH, Gerstein GL, Moore GP (1967) Neuronal Spike Trains and Stochastic Point Processes. I. The Single Spike Train. Biophys J. 7: 391-418.

Peters A (1984) Identified neurons in visual cortex.Trends in Neurosci. 7 :375–378

Povysheva NV, Gonzalez-Burgos G, Zaitsev AV, Kröner S, Barrionuevo G, Lewis DA, Krimer LS (2006) Properties of Excitatory Synaptic Responses in Fast-spiking Interneurons and Pyramidal Cells From Monkey and Rat Prefrontal Cortex. Cereb Cortex. 16: 541-552.

Purves D, Augustine GJ, Fitzpatrick D, Hall WC, LaMantia AS, McNamara JO, Williams SM. Neuroscience, (2004) Sinauer Associates, Inc. Publishers, Sunderland, Massachusetts U.S.A.

Reid, R. C. (2012). From functional architecture to functional connectomics. *Neuron, 75*(2), 209-217. doi: 10.1016/j.neuron.2012.06.031

Ringach, D. L. (2004). Haphazard wiring of simple receptive fields and orientation columns in visual cortex. *J Neurophysiol, 92*(1), 468-476. doi: 10.1152/jn.01202.2003

Rolls, E. T. & Treves, A. (2011) The neuronal encoding of information in the brain. Progress in neurobiology 95, 448-490, doi:10.1016/j.pneurobio.2011.08.002.

Sale A, Maya Vetencourt JF, Medini P, Cenni MC, Baroncelli L, et al. (2007) Environmental enrichment in adulthood promotes amblyopia recovery through a reduction of intracortical inhibition. Nat Neurosci 10:679-81.

Sincich, L. C., Adams, D. L., Economides, J. R., Horton, J. C. (2007) Transmission of spike trains at the retinogeniculate synapse. J Neurosci 27: 2683-2692.

Sengpiel, F., Stawinski, P., & Bonhoeffer, T. (1999). Influence of experience on orientation maps in cat visual cortex. *Nat Neurosci, 2*(8), 727-732. doi: 10.1038/11192

Shatz, C. J. (1990). Impulse activity and the patterning of connections during CNS development. *Neuron, 5*(6), 745-756.

Shibata, K., Kawato, M., Watanabe, T., & Sasaki, Y. (2012). Monocular deprivation boosts long-term visual plasticity. *Curr Biol, 22*(9), R291-292. doi: 10.1016/j.cub.2012.03.010

Shtoyerman E, Arieli A, Slovin H, Vanzetta I, Grinvald A. (2000). Long-term optical imaging and spectroscopy reveal mechanisms underlying the intrinsic signal and stability of cortical maps in V1 of behaving monkeys. J Neurosci. 20(21):8111-21.

Sompolinsky, H., Golomb, D. & Kleinfeld, D. (1990) Global processing of visual stimuli in a neural network of coupled oscillators. Proc Natl Acad Sci U S A. 87, 7200-7204.

Southwell DG, Froemke RC, Alvarez-Buylla A, Stryker MP, Gandhi SP (2010) Cortical Plasticity Induced by Inhibitory Neuron Transplantation. Science. 327: 1145-1148.

Stanley, G. B. (2013) Reading and writing the neural code. Nature neuroscience 16, 259-263, doi:10.1038/nn.3330.

Stepanyants A, Hirsch JA, Martinez LM, Kisvarday ZF, Ferecsko AS, Chklovskii DB.(2008) Local potential connectivity in cat primary visual cortex. Cereb Cortex 18, 13-28.

Steriade, M. (2004). Neocortical cell classes are flexible entities. *Nat Rev Neurosci, 5*(2), 121-134. doi: 10.1038/nrn1325

Stratford, K. J., Tarczy-Hornoch, K., Martin, K. A., Bannister, N. J. & Jack, J. J. (1996) Excitatory synaptic inputs to spiny stellate cells in cat visual cortex. Nature 382, 258-261, doi:10.1038/382258a0.

Surmeier, D. J., & Foehring, R. (2004). A mechanism for homeostatic plasticity. *Nat Neurosci, 7*(7), 691-692. doi: 10.1038/nn0704-691

Swindale, N. V., Shoham, D., Grinvald, A., Bonhoeffer, T., & Hubener, M. (2000). Visual cortex maps are optimized for uniform coverage. *Nat Neurosci, 3*(8), 822-826. doi: 10.1038/77731

Tagawa Y, Kanold PO, Majdan M, Shatz CJ. (2005) Multiple periods of functional ocular dominance plasticity in mouse visual cortex. Nat Neurosci. 8, 380-388.

Tanaka E, North RA. (1993) Actions of 5-hydroxytryptamine on neurons of the rat cingulate cortex. J Neurophysiol 69:1749-57.

Tanaka S, Tani T, Ribot J, O'Hashi K, Imamura K (2009) A Postnatal Critical Period for Orientation Plasticity in the Cat Visual Cortex. PLoS One. 4: e5380.

Turrigiano, G. (2012). Homeostatic synaptic plasticity: local and global mechanisms for stabilizing neuronal function. *Cold Spring Harb Perspect Biol, 4*(1), a005736. doi: 10.1101/cshperspect.a005736

Turrigiano, G. G. (1999). Homeostatic plasticity in neuronal networks: the more things change, the more they stay the same. *Trends Neurosci, 22*(5), 221-227.

Turrigiano, G. G., & Nelson, S. B. (2004). Homeostatic plasticity in the developing nervous system. *Nat Rev Neurosci, 5*(2), 97-107. doi: 10.1038/nrn1327

Tyler CJ, Dunlop SA, Lund RD, Harman AM, Dann JF, Beazley LD, Lund JS (1998) Anatomical Comparison of the Macaque and Marsupial Visual Cortex: Common Features That May Reflect Retention of Essential Cortical Elements. J Comp Neurol. 400: 449-468.

Van Hooser SD (2007) Similarity and Diversity in Visual Cortex: Is There a Unifying Theory of Cortical Computation? Neuroscientist. 13: 639-656.

Wallace, D. J. & Kerr, J. N. (2010) Chasing the cell assembly. Current opinion in neurobiology, doi:10.1016/j.conb.2010.05.003.

Wang, Y., Iliescu, B. F., Ma, J., Josic, K., & Dragoi, V. (2011). Adaptive changes in neuronal synchronization in macaque V4. *J Neurosci, 31*(37), 13204-13213. doi: 10.1523/JNEUROSCI.6227-10.2011

Wilson FA, O'Scalaidhe SP, Goldman-Rakic PS (1994) Functional Synergism Between Putative Gamma-Aminobutyrate-Containing Neurons and Pyramidal Neurons in Prefrontal Cortex. Proc Natl Acad Sci U S A. 91: 4009-4013.

Yoshimura, Y., Dantzker, J. L., & Callaway, E. M. (2005). Excitatory cortical neurons form fine-scale functional networks. *Nature, 433*(7028), 868-873. doi: 10.1038/nature03252

Yoshimura, Y., Sato, H., Imamura, K. & Watanabe, Y. (2000) Properties of horizontal and vertical inputs to pyramidal cells in the superficial layers of the cat visual cortex. J Neurosci. 20, 1931-1940.

Zhang ZW. (2003) Serotonin induces tonic firing in layer V pyramidal neurons of rat prefrontal cortex during postnatal development. J Neurosci 23:3373-84.

Curriculum Vitae

ÉDUCATION :

2004-2008 : B.Sc. (Biochimie)
Département de Biochimie, Université de Mouloud Mammeri (Algérie)

2011-2012 : M.Sc. (Neurophysiologie – Neuropharmacologie)
Laboratoire de Neurosciences du système visuel
Département de Sciences Biologiques, Université de Montréal

2012-2015 : Ph.D. (Neurophysiologie – Circuits neuronaux)
Laboratoire de Neurosciences du système visuel
Département de Sciences Biologiques, Université de Montréal

À partir de Mai 2016 : Postdoctorat (Couplage neurovasculaire – IRMf)
Centre de recherche du CHUS
Département de radiologie diagnostique
Faculté de médecine et des sciences de la santé
Université de Sherbrooke

BOURSES ET PRIX D'EXCELLENCE REÇUS :

1. Bourse doctorale d'excellence (Fonds de recherche du Québec - Nature et technologies) 40000$ (Mai 2013 – Avril 2015)
2. Bourse d'excellence de la Faculté des Études Supérieures et Postdoctorales - 8000$ (Mai 2015)

3. Bourse d'excellence CERNEC : 8000$ (Année 2011) (Centre de recherche en Neurophysiologie et Cognition)
4. Bourse de passage accéléré au doctorat : 7000$ (Année 2012) Faculté des Études Supérieures et Postdoctorales)
5. Bourse de Doctorat : 7000$ (Année 2013) (Faculté des Études Supérieures et Postdoctorales)
6. Bourse d'excellence des fonds de bourse des sciences biologiques : 1700$ (Année 2012)
7. Prix d'excellence du public de la meilleure présentation orale : 500$ (Année 2012) Journée scientifique de l'école d'Optométrie (Groupe de Recherche en Sciences de la Vision)
8. Bourse d'études du GRSV (École d'Optometrie) : 300$ (Année 2012)
9. Prix Concordia University pour la meilleure présentation affichée (Centre de recherche en neuropsychologie et cognition) 250$ (Mars 2014)
10. Prix de la meilleure présentation orale (Groupe de recherche en Neurosciences Computationnelles et Traitement Intelligent des Signaux - 250$ (avril 2014)
11. Prix de publication d'un article (Revue des étudiants des cycles supérieurs de l'UdeM) - 250$ (2014)
12. Prix NeuroQam pour la meilleure présentation affichée (Centre de recherche en neuropsychologie et cognition) 250$ (Mars 2015)
13. Prix d'excellence de la meilleure présentation orale : 100$ (Année 2013) Journée scientifique du département des sciences biologiques, UdeM.

EXPÉRIENCES EN ENSEIGNEMENT :

Septembre-décembre 2014 **Chargé de cours,** Département de Sciences Biologiques
Physiologie animale comparée
Université de Montréal

Janvier-Avril 2011-2015 **Auxiliaire d'enseignement chef,** Département de Sciences Biologiques
Physiologie nerveuse et musculaire
Université de Montréal

Janvier-Avril 2011-2015 **Auxiliaire d'enseignement chef,** Département de Sciences Biologiques
Principes de Physiologie animale
Université de Montréal

Janvier-Avril 2011-2015 **Auxiliaire d'enseignement chef,** Département de Sciences Biologiques
Respiration, circulation et excrétion
Université de Montréal

Septembre-décembre 2011-2015 **Auxiliaire d'enseignement chef,** Département de Sciences Biologiques
Physiologie animale comparée 1
Université de Montréal

Septembre-décembre 2011-2015 **Auxiliaire d'enseignement chef,** Département de Sciences Biologiques
Physiologie animale comparée 2
Université de Montréal

PUBLICATIONS:

1. Bharmauria V, **Bachatene L**, Cattan S, Chanauria N, Rouat J, Molotchnikoff S. High noise correlation between the functionally connected neurons in emergent V1 microcircuits. *Exp Brain Res.* 2015 Nov 2. (Epub ahead of print)

2. Bharmauria V, **Bachatene L**, Cattan S, Brodeur S, Chanauria N, Rouat J, Molotchnikoff S. Network-selectivity and stimulus-discrimination in the primary visual cortex: cell-assembly dynamics. *Eur J Neurosci.* 2015 Oct 15. doi: 10.1111/ejn.13101. (Epub ahead of print)
3. **Bachatene L**, Bharmauria V, Cattan S, Chanauria N, Rouat J, Molotchnikoff S. Summation of connectivity strengths in the visual cortex reveals stability of neuronal microcircuits after plasticity. *BMC Neurosci.* 2015 Oct 9;16:64. doi: 10.1186/s12868-015-0203-1.
4. **Bachatene L**, Bharmauria V, Cattan S, Chanauria N, Rouat J, Molotchnikoff S. Electrophysiological and firing properties of neurons: Categorizing soloists and choristers in primary visual cortex. *Neurosci Lett.* 2015 Sep 14;604:103-8. doi: 10.1016/j.neulet.2015.07.049. Epub 2015 Aug 3.
5. Bharmauria V, **Bachatene L**, Cattan S, Chanauria N, Rouat J, Molotchnikoff S. Stimulus-dependent augmented gamma oscillatory activity between the functionally connected cortical neurons in the primary visual cortex. *Eur J Neurosci.* 2015 Jun;41(12):1587-96. doi: 10.1111/ejn.12912. Epub 2015 Apr 30.
6. **Bachatene L**, Bharmauria V, Cattan S, Rouat J, Molotchnikoff S. Reprogramming of orientation columns in visual cortex: a domino effect. *Nature Sci. Rep.* 2015 Mar 24;5:9436. doi: 10.1038/srep09436.
7. **Bachatene L**, Bharmauria V, Cattan S, Rouat J, Molotchnikoff S. Modulation of functional connectivity following visual adaptation: homeostasis in V1. *Brain Res.* 2015 Jan 12;1594:136-53. doi: 10.1016/j.brainres.2014.10.054. Epub 2014 Oct 31.
8. Cattan S, **Bachatene L**, Bharmauria V, Jeyabalaratnam J, Milleret C, Molotchnikoff S. Comparative analysis of orientation maps in areas 17 and 18 of the cat primary visual cortex following adaptation. *Eur J Neurosci.* 2014 Aug;40(3):2554-63. doi: 10.1111/ejn.12616. Epub 2014 May 15.
9. Bharmauria V, **Bachatene L**, Cattan S, Rouat J, Molotchnikoff S. Synergistic activity between primary visual neurons. *Neuroscience.* 2014 May 30;268:255-64. doi: 10.1016/j.neuroscience.2014.03.027. Epub 2014 Mar 21.
10. Jeyabalaratnam J, Bharmauria V, **Bachatene L**, Cattan S, Angers A, Molotchnikoff S. Adaptation shifts preferred orientation of tuning curve in the mouse visual cortex. *PLoS One.* 2013 May 23;8(5):e64294. doi: 10.1371/journal.pone.0064294. Print 2013.
11. **Bachatene L**, Bharmauria V, Cattan S, Molotchnikoff S. Fluoxetine and serotonin facilitate attractive-adaptation-induced orientation plasticity in adult cat visual cortex. *Eur J Neurosci.* 2013 Jul;38(1):2065-77. doi: 10.1111/ejn.12206. Epub 2013 Apr 15.
12. **Bachatene L**, Bharmauria V, Rouat J, Molotchnikoff S. Adaptation-induced plasticity and spike waveforms in cat visual cortex. *Neuroreport.* 2012 Jan 25;23(2):88-92. doi: 10.1097/WNR.0b013e32834e7e71.

Articles soumis

13. Cattan S, **Bachatene L**, Bharmauria V, Chanauria N, Ribot J, Milleret C, Molotchnikoff S. Pinwheel centers exhibit more plasticity than iso-orientation domains in the cat primary visual cortex. *Nature Sci. Rep.* (SREP-15-33431).
14. Bharmauria V, **Bachatene L**, Cattan S, Chanauria N, Etindele Sosso FA, Molotchnikoff S. Interplay of orientation selectivity and the power of low- and high-gamma bands in the cat primary visual cortex. *Neuroreport* (NR-S-15-00827).

CHAPITRES DE LIVRE ET RAPPORTS SCIENTIFIQUES:

1. **Bachatene L**, Bharmauria V, Molotchnikoff S (2012). Adaptation and Neuronal Network in Visual Cortex, InTech, DOI: 10.5772/46011

2. **Bachatene L**. Les antidépresseurs augmentent la plasticité cérébrale
   Article de recherche, Sciences de la santé

3. **Bachatene L**. L'antidépresseur Prozac facilite la plasticité du cortex visuel. Article de vulgarisation, Revue des étudiants des cycles supérieurs

SUPERVISION D'ÉTUDIANTS :

• Supervision d'étudiants de 1er cycle : Mai 2015 – ce jour

Titre du projet : Effets de la kétamine sur la plasticité du cortex visuel

• Supervision d'étudiants de 1er cycle : jan 2014 – jul 2014

Titre du projet 1: Examens des propriétés neuronales du cortex visuel de la souris suite à une adaptation visuelle

Titre du projet 2 : Changements de sélectivité neuronale après apprentissage hors des champs récepteurs chez les souris adultes.

• Supervision d'étudiants de 1er cycle : jan 2013 – jul 2013

Titre du projet : Effets des antidépresseurs sur la quantité de MAPK dans le cortex visuel primaire de la souris.

• Supervision d'étudiants de 1er cycle : jan 2012 – jul 2012

Titre du projet 1: Apprentissage visuel chez la souris adulte

Titre du projet 2 : Effet de la sérotonine sur les cascades moléculaires de la plasticité corticale chez la souris.

• Supervision d'étudiants de 1er cycle : jan 2011 – jul 2011

Titre du projet : Cascades moléculaires associées à la plasticité du cortex visuel primaire chez la souris adulte.

MEMBERSHIP ET ACTIVITÉS ADMINISTRATIVES:

1. Membre du Comité Scientifique du Réseau de Recherche en Santé de la Vision

2. Membre du comité d'évaluation de bourses de stages de recherche (Réseau de Recherche en Santé de la Vision) Mai 2014

3. Membre du comité d'évaluation des candidats pour le poste de professeur en écophysiologie animale (Département des Sciences Biologiques, Université de Montréal) Avr 2012

4. Membre du comité d'évaluation du prix « Réseau Vision » Déc 2012

5. Membre de Society for Neuroscience (SfN)

6. Membre du centre de recherche en neuropsychologie et cognition (CERNEC)

7. Membre du groupe Neurosciences Computationnelles et Traitement Intelligent des Signaux (NECOTIS, Université de Sherbrooke)

ACTIVITÉS LIÉES À LA RECHERCHE:

Révision sur invitation de 5 chapitres d'un livre : Visual Cortex ISBN: 978-953-51-0760-6 (2012)

Révision d’un article de recherche : journal Brain Research (Sept 2014, Manuscript Number: BRES-D-14-01252)

Révision d’un article de recherche : journal Cellular and Molecular Life Sciences (Nov 2015, Manuscript Number: CMLS-D-15-01023)